Selecting and Scaling Earthquake Ground Motions for Performing Response-History Analyses

NEHRP Consultants Joint Venture
A partnership of the Applied Technology Council and the
Consortium of Universities for Research in Earthquake Engineering

nehrp

NIST
National Institute of
Standards and Technology
U.S. Department of Commerce

Disclaimers

Cover photo – Illustration of example Conditional Spectrum for the Palo Alto, California site, anchored for 2% in 50 year motions at $T = 2.6s$.

NIST GCR 11-917-15

Selecting and Scaling Earthquake Ground Motions for Performing Response-History Analyses

Participants

National Institute of Standards and Technology

John (Jack) R. Hayes, Jr., Director, National Earthquake Hazards Reduction Program
Steven L. McCabe, Deputy Director, National Earthquake Hazards Reduction Program
Kevin K. F. Wong, Project Manager

NEHRP Consultants Joint Venture

Applied Technology Council
201 Redwood Shores Parkway, Suite 240
Redwood City, California 94065
www.ATCouncil.org

Consortium of Universities for
Research in Earthquake Engineering
1301 S. 46th Street, Building 420
Richmond, California 94804
www.CUREE.org

Joint Venture Management Committee

James R. Harris
Robert Reitherman
Christopher Rojahn
Andrew Whittaker

Joint Venture Program Committee

Jon A. Heintz (Program Manager)
Michael Constantinou
C.B. Crouse
James R. Harris
William T. Holmes
Jack Moehle
Andrew Whittaker

Project Technical Committee

Andrew Whittaker (Project Director)
Gail M. Atkinson
Jack W. Baker
Jonathan Bray
Damian N. Grant
Ronald Hamburger
Curt Haselton
Paul Somerville

Project Review Panel

John Egan
Robert Kennedy
Charles Kircher
Nicolas Luco
Robin McGuire
Jack Moehle
Michael Willford

Project Manager

Ayse Hortacsu

Working Group Members

Norman Abrahamson
Ana Luz Acevedo-Cabrera
Riccardo Diaferia
Connor Hayden
Ting Lin

FEMA Representative

Helmut Krawinkler

Preface

The NEHRP Consultants Joint Venture is a partnership between the Applied Technology Council (ATC) and the Consortium of Universities for Research in Earthquake Engineering (CUREE). In 2007, the National Institute of Standards and Technology (NIST) awarded a National Earthquake Hazards Reduction Program (NEHRP) "Earthquake Structural and Engineering Research" contract (SB1341-07-CQ-0019) to the NEHRP Consultants Joint Venture to conduct a variety of tasks, including Task Order 69220 entitled "Improved Procedures for Selecting and Scaling Earthquake Ground Motions for Performing Response-History Analysis."

The primary objective of this task was to develop guidance for selecting, generating, and scaling earthquake ground motions for effective use in performing response-history analyses for use in performance-based seismic engineering. The need for such guidance was identified in the ATC-57 report, *The Missing Piece: Improving Seismic Design and Construction Practices* (ATC, 2003), which defines a roadmap for the NIST problem-focused research and development program in earthquake engineering.

Following a thorough study of the state of the practice with regard to selecting and scaling ground motions for nonlinear response-history analysis of buildings, the project team developed a list of key challenges facing design professionals tasked with selecting and scaling earthquake ground motions. Based on the findings identified, and considering the potential for impacting design practice in the near-term, the following topics were chosen for study: (1) selection of ground motions based on the Conditional Spectrum; (2) response-spectrum matching; and (3) near-fault ground motions and fault-rupture directivity. To encourage consensus and consistency in the state of the practice going forward, recommendations related to selecting and scaling ground motions for design and performance assessment of low- and medium-rise buildings, and a discussion on best practices for applying the current rules in building codes and standards, are provided.

The NEHRP Consultants Joint Venture is indebted to the leadership of Andrew Whittaker, Project Director, and to the members of the project team for their efforts in developing this report. The Project Technical Committee, consisting of Gail Atkinson, Jack Baker, Jonathan Bray, Damian Grant, Ronald Hamburger, Curt Haselton, and Paul Somerville, performed, monitored, and guided the technical work on the project. The Working Groups, including Norman Abrahamson, Ana Luz

Table of Contents

List of Figures

List of Tables

Chapter 1

Introduction

Seismic provisions in current model building codes and standards include rules for design of structures using nonlinear response-history analysis, which are based, in large part, on recommendations for analysis of seismically isolated structures from more than 20 years ago. Unfortunately, there is currently no consensus in the earthquake engineering community on how to appropriately select and scale earthquake ground motions for code-based design and seismic performance assessment of buildings using nonlinear response-history analysis.

This report provides guidance to design professionals on selection and scaling of ground motions for the purpose of nonlinear response-history analysis. Gaps in the current knowledge related to selecting and scaling ground motions for seismic design and performance assessment are identified, and relevant provisions in current and recent ASCE/SEI Standards are explained and clarified.

1.1 Project Motivation

Present practice for selecting and scaling of earthquake ground motions for linear and nonlinear response-history analysis of buildings is based largely on engineering judgment from years ago, which was dominated by the limited availability of efficient computer programs to perform such analyses and the associated computational expense. Advances in computational power and availability of improved numerical models and robust numerical platforms have made nonlinear response-history analysis possible for design offices with low to moderate computational power. In addition, the advent of the first generation methods for performance-based seismic engineering (PBSE) in the mid-1990s has sped the development of tools for performing nonlinear response-history analysis and encouraged their use by design professionals.

The ATC-57 report, *The Missing Piece: Improving Seismic Design and Construction Practices* (ATC, 2003), which defines a roadmap for the NIST problem-focused research and development program in earthquake engineering, cited the ongoing transfer of research knowledge into practice as one significant need in support of performance-based seismic engineering. In 2008, the National Earthquake Hazard Reduction Program (NEHRP) sponsored a workshop including leading practitioners and researchers from around the United States to develop a comprehensive list of research needs to foster full development and implementation of PBSE. Following the workshop, the Building Seismic Safety Council (BSSC) developed the NIST

GCR 09-917-2 report, *Research Required to Support Full Implementation of Performance-Based Seismic Design* (NIST, 2009), which outlines and prioritizes major areas of research that are needed. In this report, the need for improving procedures for selecting and scaling ground motions for response-history analysis was identified as a high priority.

1.2   Project Objectives and Scope

The objective of this work is to improve guidance for selecting, generating, and scaling earthquake ground motions for performing response-history analysis of low- and medium-rise buildings. Both code-based design and seismic performance assessment are addressed. Following a thorough study of the state of the practice with regard to selecting and scaling ground motions for nonlinear response-history analysis of buildings, the project team developed a list of key challenges facing design professionals tasked with selecting and scaling earthquake ground motions. Based on the findings identified and considering the potential for impacting design practice in the near-term the following topics were chosen for study: (1) selection of ground motions based on the Conditional Spectrum; (2) response-spectrum matching; and (3) near-fault ground motions and fault-rupture directivity.

1.3   Report Organization and Content

This report presents findings, conclusions, and recommendations on ground motion selection and scaling. The resulting recommendations are based on review of available research and current practice and focused analytical studies targeted to investigate selected issues. The remaining chapters of this report are organized as follows:

Chapter 2 describes alternate purposes for selecting and scaling ground motions.

Chapter 3 describes the state of practice in response-history analysis, with emphasis on selection and scaling of ground motions, as presented in alternate codes and standards.

Chapter 4 provides the motivation, conclusions, and recommendations from the focused analytical studies.

Chapter 5 provides discussions on the application of ground motion selection and scaling procedures presented in current and recent ASCE/SEI Standards, and on alternate target spectra, key conclusions of problem-focused studies, and recommendations for future work.

Appendix A provides additional information on ground motion selection based on the Conditional Spectrum.

Appendix B provides additional information on response-spectrum matching.

Appendix C provides additional information on near-fault pulse motions.

Appendix D provides a summary of key issues identified in ground motion selection and scaling that helped determine the scope of the problem-focused studies that were undertaken.

A glossary of important terms, references cited, and a list of all project participants are provided at the end of this report.

Chapter 2
Goals of Response-History Analysis

2.1   Introduction

Ground motions are selected and scaled to enable response-history analysis that supports either design or performance assessment. The analyst must have a clear understanding of the goals of analysis before choosing procedures to select and scale ground motions.

For example, in order to predict average (or mean) story drift responses in a building for a given intensity of shaking (e.g., ground motion with a 2% probability of exceedance in 50 years), matching ground motions to a target spectrum may be an appropriate approach because spectrum matching reduces the variability (jaggedness) observed in acceleration spectra for individual ground motions and leads to higher confidence in the predictions of average responses for a given number of ground motion inputs. However, if the goal is to assess the probability of shear failure in a force-controlled shear wall, which requires prediction of both the mean value of demand and its variability, spectrum matching would be inappropriate because it suppresses the record-to-record variability inherent in recorded ground motions.

This chapter discusses alternate purposes for response-history analysis, summarizes three types of assessment that use response-history analysis, and discusses how different response parameters and considerations of variability can affect how ground motions are selected and scaled.

2.2   Use of Response-History Analysis

Nonlinear response-history analysis is performed for a number of reasons, including: (1) designing new buildings, especially those equipped with seismic isolators or energy dissipation devices; (2) designing seismic upgrades of existing buildings per ASCE/SEI 41-06, *Seismic Rehabilitation of Existing Buildings* (ASCE, 2007); (3) designing non-conforming framing systems in new buildings per ASCE/SEI 41-06; and (4) assessing performance of new and existing buildings per ATC-58-1, *Seismic Performance Assessment of Buildings* (ATC, 2011).

2.2.1   Goals of Design and Performance Assessment

The goals of response-history analysis will generally be different for design and performance assessment. Building codes and their reference standards dictate how most new buildings are designed and detailed in the United States. The commentary

to these codes and standards identify the target minimum seismic performance of new buildings. For example, Table C.1.3.1b in the commentary to Chapter 1 of ASCE/SEI 7-10, *Minimum Design Loads for Buildings and Other Structures* (ASCE, 2010), identifies the expected seismic performance of a standard occupancy building as a 10 percent or less probability of total or partial collapse, conditioned on (or given) the occurrence of Maximum Considered Earthquake (MCE) shaking.

The 90% draft of ATC-58-1, *Seismic Performance Assessment of Buildings* (ATC, 2011) is the state-of-the-art in seismic performance assessment of existing and new buildings. This guideline does not recommend a minimum level of seismic performance but rather seeks to provide the techniques and tools needed to compute unbiased estimates of the response of structural and nonstructural components, and distributions of loss.

2.2.2   Evaluation of Goals

Performance goals can be evaluated either explicitly or indirectly. For seismic performance assessment per ATC-58-1, estimates of response, probability of collapse, and loss are computed explicitly, with appropriate considerations of variability in ground motion, soil conditions, and modeling of the soil-structure system.

For design of new buildings per ASCE/SEI 7-10, the performance goal of a 10 or less percent probability of a total or partial collapse given MCE shaking is evaluated indirectly. For Equivalent Lateral Force (ELF) or static analysis, values of the response modification factor, R, and displacement amplification factor, C_d, are used to establish design forces for a given framing system, where some of these values have been calibrated using results of hundreds of nonlinear response-history analyses of archetype buildings and properly accounting for uncertainties (see Appendix F of FEMA P-695, *Quantification of Building Seismic Performance Factors* (FEMA, 2009)) and all others are based on judgment (see ATC-19, *Structural Response Modification Factors* (ATC, 1995)).

For nonlinear response-history analysis in support of design per Section 16.2 of ASCE/SEI 7-10, simple acceptance criteria are used to ensure stable, predictable response of the framing system under MCE shaking: average (mean) member deformations in response to design earthquake shaking (intensity equal to two-thirds of MCE intensity) cannot exceed two-thirds of a value that results in loss of gravity-load resistance or in deterioration of member strength to less than the 67 percent of the peak value, and story drifts cannot exceed limiting prescriptive values that are much smaller than those typically associated with collapse (see Sections 12.12.1 and 16.2.4.3 of ASCE/SEI 7-10). By providing a substantial margin against failure at the component level, and limiting story drifts to small values, it is expected that the performance goal will be achieved without explicit consideration of the uncertainties

in the calculations (e.g., analysis or record-to-record variability, and modeling of soil and structure). As such, the performance goal of ASCE/SEI 7-10 is achieved indirectly even if nonlinear response-history analysis is used.

2.3 Types of Performance Assessment

ATC-58-1 identifies three types of performance assessment: intensity, scenario, and time-based. The best method for selecting and scaling ground motions will depend on the type of assessment being performed. Each type of assessment is introduced below.

2.3.1 Intensity-Based Assessments

Intensity-based assessments are the most common of the three types and compute the response of a building and its components for a specified intensity of ground shaking. Response can take the form of parameters such as component force, component deformation, story drift, or global estimates of loss (repair, business interruption, casualties). Best estimates and distributions of loss can be computed but different procedures for selecting and scaling the ground motions are needed. Code-based design involves an intensity-based assessment of a mathematical model but with a focus on mean or average responses.

For an intensity-based assessment, the ground motion intensity is defined typically as a 5% damped elastic spectral acceleration at a period (i.e., $S_a(T)$). This definition is statistically meaningful, and used in this report, because seismic hazard curves are generated for $S_a(T)$. An alternate definition is a 5%-damped elastic acceleration response spectrum, which could be one specified by a standard such as ASCE/SEI 7.

2.3.2 Scenario-Based Assessments

A scenario-based assessment computes the response of a building to a user-specified earthquake event, which is typically defined by earthquake magnitude and the distance between the earthquake source and the building site.

The typical product of a scenario-based assessment is the average response and its variability, where response is defined above. For this type of assessment, the variability in response will be influenced by variability in site conditions, ground motion prediction equations, ground motions used for analysis, and mathematical models. The scenario-based assessment approach is not discussed in much detail in this report.

2.3.3 Risk-Based Assessments

A risk-based (referred to as time-based assessment in ATC-58-1) assessment provides information on response over a user-specified period of time (e.g., annual rates or 1 year, or design life of a building, 50 to 100 years). This is the most

comprehensive type of assessment and involves a number of intensity-based assessments over the range of ground motion levels of interest. The predicted responses for each intensity-based assessment are then combined (integrated) with the ground motion hazard curve to predict the annual rates of exceedance.

2.4 Response Parameters

There are many response parameters of potential interest to an analyst. Values of demand computed for a chosen parameter will depend on the frequency content of the ground motion input. The best method for selecting and scaling ground motions, and the range of period used for scaling to a target spectrum, will therefore vary as a function of the analyst's choice of parameters. Below is a list of commonly used response quantities, along with notes in parentheses.

- Peak transient drift in each story

- Maximum peak transient drift in all stories (commonly first-mode dominated, but also related to both higher-modes and lower frequencies that lie above first mode)

- Floor accelerations (often higher-mode dominated)

- Floor spectra

- Component inelastic deformations

- Element forces for force-controlled components (often higher-mode dominated)

- Residual story drift

- Behavioral mode of structural response (e.g., frame side sway, where plastic hinges form in beam ends and at the base of each column, or soft story; mode of response can differ between records scaled to the same intensity)

As noted previously, response can take the form of discrete values (best estimates or means) or distributions. Explicit consideration of variability in response will be important in many cases, including calculation of collapse probabilities and understanding possible differences in failure modes of components (e.g., shear versus flexure) and systems (e.g., frame side sway versus soft story, or ductile versus brittle).

If distributions of response are required, the ground motion scaling method must address and account for record-to-record variability. A much larger number of ground motion histories will be needed for analysis if distributions of response are required, or if collapse probabilities are to be calculated, than if best estimates of response are sought. The calculation of distributions of response must also address other uncertainties or variability in the assessment, but a discussion of those uncertainties is beyond the scope of this report.

Chapter 3

State of Practice

3.1   Introduction

The primary purpose of this chapter is to summarize the state of practice as represented by mandatory language in the following selected resources:

- seismic standards for new buildings, ASCE/SEI 7, *Minimum Design Loads for Buildings and Other Structures* (ASCE, 2006 and 2010),

- seismic standards for existing buildings, ASCE/SEI 41-06, *Seismic Rehabilitation of Existing Buildings* (ASCE, 2007),

- seismically isolated and conventional bridges, *Guide to Specifications for Seismic Isolation Design* and *LRFD Bridge Design Specifications* (AASHTO, 2010a and b),

- nuclear facilities, ASCE/SEI 43-05, *Seismic Design Criteria for Structures, Systems, and Components in Nuclear Facilities* (ASCE, 2005),

- liquefied natural gas facilities, *Seismic Design Guidelines and Data Submittal Requirements for LNG Facilities* (FERC, 2007),

- dams, FEMA 65, *Federal Guidelines for Dam Safety* (FEMA, 2005),

- civil works, EC1110-2-600, *Selection of Design Earthquakes and Associated Ground Motions* (U.S. Army Corps of Engineers, 2009), and

- Department of Defense facilities, UFC 3-310-04, *Seismic Design for Buildings* (Department of Defense, 2004, 2007, and 2010).

The presentation of mandatory language in each standard in Sections 3.2 through 3.10 is preceded by a summary statement of the expected performance of the structure designed to that standard followed by a description of how results of analysis are used for design, and observations. The mandatory language presented in ASCE/SEI Standard 7 is presented for two editions of the standard because a number of standards make reference to ASCE/SEI Standard 7-05.

Section 3.11 lists key challenges facing design professionals tasked with selecting and scaling ground motions in accordance with current standards and a provides a segue into Chapter 4 that lists gaps in the knowledge and summarizes the problem-focused studies performed in this project.

3.2   New Buildings, ASCE/SEI Standard 7-05

3.2.1   Performance Expectations

The performance expectations for buildings and other structures designed per ASCE/SEI 7-05, *Minimum Design Loads for Buildings and Other Structures* (ASCE, 2006), are a function of Occupancy Category. For structures belonging to Occupancy Categories I and II, the expectations are the following: (1) a low probability of collapse in maximum considered earthquake (MCE) shaking with a return period of 2475 years subject to a deterministic cap; (2) a low probability of damage sufficient to cause life loss for shaking with an intensity equal to 67% of MCE shaking; and (3) a high probability that components and systems essential to protecting life safety, including fire sprinklers, emergency lighting and exit lighting, would be functional after shaking with an intensity of 67% of MCE shaking. For structures belonging to Occupancy Category III, the performance expectations of collapse and life loss require lower probabilities than Occupancy Category I and II structures, and higher probability for functionality of life-safety systems than structures in Occupancy Categories I and II. For Occupancy Category IV structures, the performance expectations are a very low probability of collapse for MCE shaking, a low probability of life-safety risk for MCE shaking, and a high probability of functionality following shaking lower than MCE. The probability is not quantified in any of these cases.

Sets of earthquake ground motions generated per the rules of ASCE/SEI 7-05 are expected to be appropriate for predicting response at levels of system displacement and component deformation beyond yield.

3.2.2   Rules for Selecting and Scaling Ground Motions

Section 16.1.3 of ASCE/SEI 7-05 provides rules for selecting and scaling ground motions. A minimum of three appropriate ground motions must be used for analysis.

For analysis of two-dimensional building frames, Section 16.1.3.1 writes

> "Each ground motion shall consist of a horizontal acceleration history, selected from an actual recorded event. Appropriate acceleration histories shall be obtained from records of events having magnitudes, fault distance, and source mechanisms that are consistent with those that control the maximum considered earthquake. Where the required number of appropriate recorded ground motion records are not available, appropriate simulated ground motion records shall be used to make up the total number required. The ground motions shall be scaled such that the average value of the 5 percent damped response spectra for the suite of motions is not less than the design response spectrum for the site for periods ranging from $0.2T$ to $1.5T$ where T is the fundamental period of the structure in the fundamental mode for the direction of response being analyzed."

For analysis of three-dimensional building frames, Section 16.1.3.2 writes

> "…ground motions shall consist of pairs of appropriate horizontal ground motion components that shall be selected and scaled from individual recorded events. Appropriate ground motions shall be selected from events having magnitudes, fault distance, and source mechanisms that are consistent with those that control the maximum considered earthquake. Where the required number of appropriate recorded ground motion pairs are not available, appropriate simulated ground motion pairs shall be used to make up the total number required. For each pair of horizontal ground motion components, a square root of the sum of the squares (SRSS) spectrum shall be constructed by taking the SRSS of the 5 percent damped response spectra for the scaled components (where an identical scale factor is applied to both components of a pair). Each pair of motions shall be scaled such that for a period between $0.2T$ and $1.5T$, the average of the SRSS spectra from all horizontal component pairs does not fall below 1.3 times the corresponding ordinate of the design response spectrum …by more than 10 percent."

3.2.3 Calculation of Demands for Component Checking

Section 16.2.4 of ASCE/SEI 7-05 describes how individual member forces, member inelastic deformations, and story drifts are computed for design using the results of nonlinear dynamic analysis. Peak response quantities are computed for each analysis. If seven or more ground motions (for two-dimensional analysis) or ground motion pairs (for three-dimensional analysis) are used for analysis, the arithmetic mean of the peak response is used for component and story checking. If fewer than seven analyses are performed, the maximum value of the peak response quantities is used for component and story checking.

3.2.4 Observations

The rules for scaling motions for 2D (planar) and 3D analysis of building frames are based on guidance written in the late 1980s and presented in Chapter 23 of the 1991 Uniform Building Code (ICC, 1991) for analysis of seismically isolated buildings for which the translational periods along the horizontal axes are the same.

The period range of $0.2T$ to $1.5T$, where T is the fundamental translational period of the structure, is intended to account for an increase in period due to inelastic action (increasing the fundamental period to an effective value of $1.5T$) and the second mode translational period, which often falls between one-quarter and one-third of the fundamental period if the building framing is regular. The period range was set for planar analysis and taken as appropriate for 3D analysis, which assumes the fundamental translational period along each axis to be similar. The period range is inappropriate if the framing systems along each principal horizontal axis of the

building are substantially different and uncoupled, for example, shear walls along one axis and moment frames along the other.

The SRSS combination of orthogonal horizontal spectral ordinates can also be traced to rules for seismic isolation design written in the early 1990s. The SRSS rule $(=\sqrt{S_x^2(T_i) + S_y^2(T_i)})$ has no solid technical basis because the design spectrum for horizontal shaking is a geometric mean spectrum $(=\sqrt{S_x(T_i) \times S_y(T_i)})$. The rule was adopted because it had been used for modal combinations of component and global response in prior editions of ASCE/SEI 7.

The use of either three (or more) or seven (or more) sets of ground motions for analysis can also be traced to rules written for seismic isolation design in the 1980s and 1990s. If 3 sets of analyses were performed, the maximum value of the three peak responses is used for component checking, with due attention being paid to the sign of the action. If seven sets of analyses are performed, the average value of the seven peak responses is used for component checking. Although the mandatory language permits the use of 4, 5, 6, 8, and more sets of ground motions, there is no practical advantage to be gained using other than three or seven sets of ground motions. Both sets of rules are intended to provide a reasonable estimate of mean global and local responses as judged by the expert design professionals that drafted the standard. However, the rules have no technical basis. The minimum number of analyses to estimate the mean response with a high degree of confidence is a function of the goodness of fit of the scaled motion to the target spectral shape, the expected dispersion in the response, the required degree of confidence, and the required level of accuracy. Huang et al. (2008b) provided an equation that can be used to estimate the required number of sets of ground motions without consideration of spectral shape. More than seven sets of motions are required to estimate the mean response with high confidence and high accuracy, given the dispersion in response near the onset of failure. Many tens of sets of motions are required to estimate fractiles on component and system response, for example, the 84th percentile deformation on a component.

3.3   New Buildings, ASCE/SEI Standard 7-10

3.3.1 Performance Expectations

The performance expectation for Occupancy Category I and II buildings and other structures designed per the 2010 edition of ASCE/SEI 7 is a high probability (99%) of no collapse over the design life (assumed 50 years), if sited outside the deterministic near-fault region. If these structures are sited inside the deterministic region, the probability of collapse is greater than 1%. Performance expectations for all Occupancy (Risk) Categories are provided in Table C.1.3.1b of ASCE/SEI 7-10 and are not repeated here. Identical to ASCE/SEI 7-05, sets of earthquake ground motions generated per the rules of ASCE/SEI 7-10 are expected to be appropriate for

predicting response at levels of system displacement and component deformation beyond yield.

3.3.2 Rules for Selecting and Scaling Ground Motions

Section 16.1.3 of ASCE/SEI 7-10 provides the rules for selecting and scaling ground motions. A minimum of three appropriate ground motions must be used for analysis.

An important difference between ASCE/SEI 7-05 and ASCE/SEI 7-10 is the definition of the response spectrum for horizontal shaking. In ASCE/SEI 7-05, the spectrum is the geometric mean of the two horizontal components. In ASCE/SEI 7-10, the spectrum is defined as the maximum rotated component, where the ratio of maximum to geometric mean spectral demand can be taken as 1.1 at 0.2 second and 1.3 at 1.0 second. Huang et al. (2008a, 2010) provide the technical basis for these multipliers.

Section 16.1.3.1 provides the rules for analysis of two-dimensional frames. The wording is identical to the corresponding section in ASCE/SEI 7-05 and is not repeated here.

For analysis of three-dimensional building frames, Section 16.1.3.2 writes

"…ground motions shall consist of pairs of appropriate horizontal ground motion components that shall be selected and scaled from individual recorded events. Appropriate ground motions shall be selected from events having magnitudes, fault distance, and source mechanisms that are consistent with those that control the maximum considered earthquake. Where the required number of appropriate recorded ground motion pairs are not available, appropriate simulated ground motion pairs shall be used to make up the total number required. For each pair of horizontal ground motion components, a square root of the sum of the squares (SRSS) spectrum shall be constructed by taking the SRSS of the 5-percent-damped response spectra for the scaled components (where an identical scale factor is applied to both components of a pair). Each pair of motions shall be scaled such that for a period between $0.2T$ and $1.5T$, the average of the SRSS spectra from all horizontal component pairs does not fall below the corresponding ordinate of the response spectrum used for design...

At sites within 3 miles (5 km) of the active fault that controls the hazard, each pair of components shall be rotated to the fault-normal and fault-parallel directions of the causative fault and shall be scaled so that the average of the fault-normal components is not less than the MCE_R response spectrum for the period range of $0.2T$ to $1.5T$."

3.3.3 Calculation of Demands for Component Checking

Section 16.2.4 describes how individual member forces, member inelastic deformations, and story drifts are computed for design using the results on nonlinear dynamic analysis. The rules are identical to those in ASCE/SEI 7-05, which are summarized above, and not repeated here.

3.3.4 Observations

The rules for selecting and scaling ground motions for 2D (planar) analysis are essentially identical to those in ASCE/SEI 7-05, with the exception being the characterization of the design response spectrum for horizontal shaking: a geometric mean (or geomean) spectrum in the 2005 edition and a maximum direction spectrum in the 2010 edition. The maximum direction spectrum is used for 2D analysis because the probability of collapse will be underestimated if response along the perpendicular building axis is ignored and the geometric mean spectrum is used as the basis of the 2D analysis.

The maximum direction horizontal shaking spectrum is used as the basis for 3D response-history analysis, with one horizontal component being more intense than the other, which is consistent with the findings of Huang et al. (2009, 2010). Each pair of ground motion records is selected and amplitude scaled so that one component is consistent with the maximum direction spectrum, the spectral ordinates of the other component are less than those of the geometric mean spectrum, and the pair of scaled components recovers the geometric mean spectrum.

Although the geomean spectrum is used as the basis for 3D analysis, the mandatory language of ASCE/SEI 7-10 does not recover the geomean spectrum. Consider first a geomean spectrum with an ordinate at a period of 1.0 second of 0.4g, with the ordinate of one component equal to 0.32g and the other component equal to 0.50g. Assume the maximum direction ordinate is 0.52g ($= 1.3 \times 0.40$). The SRSS rule of ASCE/SEI 7-10 recovers 0.59g. Consider second a geomean spectrum with an ordinate at a period of 1.0 second of 0.4g, with the ordinate of each component equal to 0.4g. Assume the maximum direction ordinate is 0.52g ($= 1.3 \times 0.40$). The SRSS rule of ASCE/SEI 7-10 recovers 0.56g. Consider third a near-fault, geomean spectrum with an ordinate at a period of 1.0 second of 0.6g, with the ordinate of one component equal to 0.30g and the other component equal to 1.2g. Assume the maximum direction ordinate is 0.78g ($= 1.3 \times 0.60$). The SRSS rule of ASCE/SEI 7-10 recovers 1.23g.

Studies past (e.g., Somerville et al., 1997; Abrahamson, 2000) and more recent (e.g., Howard et al., 2005; Beyer and Bommer, 2006; Huang et al., 2008a, 2009) have shown that forward-directivity ground motion components in the near-fault region are often more intense in the fault-normal direction than the fault-parallel direction.

(At site-to-source distances greater than 5 km, Huang et al. (2009) showed that the orientation of the more intense component, the so-called maximum direction component, is effectively random with respect to the strike of the fault.) The rule for sites within 3 miles (5 km) of the active fault that controls the seismic hazard seeks to ensure the averaged fault-normal spectral demand recovers the maximum direction spectrum, although Huang et al. (2008a) note the multiplier on geomean spectral demand in the intermediate period range of 1.3 underestimates the best estimate factor in the forward-directivity region. As written, there is a disconnection between the rules for sites within and beyond the 3-mile threshold, namely, for distances less than 3 miles the target spectrum is the risk-targeted MCE spectrum, and for distances greater than 3 miles the target spectrum is the risk-targeted design spectrum. For consistency, the risk-targeted design spectrum should be used for all site-to-source distances.

3.4 Existing Buildings, ASCE/SEI Standard 41-06

3.4.1 Performance Expectations

The resource documents for ASCE/SEI Standard 41-06, *Seismic Rehabilitation of Existing Buildings*, (ASCE, 2007) are the *NEHRP Guidelines for the Seismic Rehabilitation of Buildings*, FEMA 273, (FEMA, 1997a), *NEHRP Commentary on the Guidelines for the Seismic Rehabilitation of Buildings*, FEMA 274, (FEMA, 1997b), and FEMA 356, *Prestandard and Commentary for the Seismic Rehabilitation of Buildings*, (FEMA, 2000). Unlike ASCE/SEI Standard 7, ASCE 41-06 does not provide specific performance expectations. Rather, the user of the standard selects the appropriate (or possible) levels of performance for the existing building. Identical to ASCE/SEI 7-05, sets of earthquake ground motions generated per the rules of ASCE 41-06 are expected to be appropriate for predicting response at levels of system displacement and component deformation ranging from elastic response through the onset of collapse.

3.4.2 Rules for Selecting and Scaling Ground Motions

Section 1.6.2.2 of ASCE/SEI 41-06 describes how acceleration time series are to be generated for seismic performance assessment, namely,

"Time history analysis shall be performed with no fewer than three data sets (each containing two horizontal components or, if vertical motion is to be considered, two horizontal components and one vertical component) of ground motion time histories that shall be selected and scaled from no fewer than three recorded events. Time histories shall have magnitude, fault distances, and source mechanisms that are consistent with those that control the design earthquake ground motion. Where three recorded ground-motion time history sets having these characteristics are not available, simulated time history data sets having

equivalent duration and spectral content shall be used to make up the total number required. For each data set, the square root sum of the squares (SRSS) of the 5%-damped site-specific spectra of the scaled horizontal components shall be constructed. The data sets shall be scaled such that the average value of the SRSS spectra does not fall below 1.3 times the 5%-damped spectrum for the design earthquake for periods between $0.2T$ and $1.5T$ (where T is the fundamental period of the building)."

Section C3.3.4.2.3 of ASCE/SEI 41-06 identifies correlation between horizontal components of ground motion as an issue to be considered in the selection and scaling process, and points the reader to U.S. Nuclear Regulatory Commission Regulatory Guide 1.92 (USNRC, 1976) for details.

3.4.3 Calculation of Demands for Component Checking

Section 3.3.4.3, Nonlinear Dynamic Procedure, Determination of Forces and Deformations, points to Section 3.3.2.2.4, Linear Dynamic Procedure, Time-History Method, for guidance on calculation of forces and deformations. Similar to ASCE/SEI 7-05, ASCE/SEI 41-06 writes

"Response parameters shall be calculated for each time-history analysis. If fewer than seven time-history analyses are performed, the maximum response of the parameter of interest shall be used for design. If seven or more time-history analyses are performed, the average value of each response parameter shall be permitted to be used for design."

3.4.4 Observations

The ASCE/SEI 41-06 rules for selecting and scaling ground motions, and for calculating demands for component checking, are essentially identical to those of ASCE/SEI 7-05, with the only key difference being the guidance provided on correlation of horizontal components of ground motion. Explicit consideration of the correlation of horizontal components of ground motion by design professionals is rare.

The correlation between a pair of ground-motion time series is measured using a correlation coefficient, ρ, defined as:

$$\rho = \frac{E\left\{\left(X_1 - m_1\right)\left(X_2 - m_2\right)\right\}}{s_1 s_2}$$

where X_1 (X_2) is the ground acceleration for component 1 (2) of a pair of orthogonal horizontal ground-motion time series; m_1 and s_1 (m_2 and s_2) are the mean and standard deviation of X_1 (X_2), respectively; and $E\{\ \}$ is the expectation operator. For

a given acceleration time series with n data points, m_1 and s_1 (m_2 and s_2) are computed using the following equations:

$$m = \frac{1}{n}\sum_{i=1}^{n}x(t_i)$$

$$s = \sqrt{\frac{1}{n-1}\sum_{i=1}^{n}\left(x(t_i)-m\right)^2}$$

where $x(t_i)$ is the acceleration at a time instant t_i.

An upper bound of 0.3 is required on the correlation coefficient of two orthogonal horizontal ground-motion time series used for analysis in consensus standards ASCE 4-98 (ASCE, 2000) and ASCE/SEI Standard 43-05 (ASCE, 2005). The technical basis for this is provided in the results of Hadjian (1981). Huang et al. (2010) extended the studies of Hadjian using larger sets of ground motions than those available in the 1980s and investigated the distributions of three correlation coefficients of orthogonal horizontal ground-motion time series. The results support the upper bound of 0.3 on the correlation coefficient between two orthogonal horizontal ground acceleration time series.

3.5   New Bridges, AASHTO LRFD Bridge Design Specification

3.5.1 Performance Expectations

The performance expectations for bridges in the United States vary by the importance of the bridge, which is affected by whether the bridge forms part of a lifeline. Lifeline bridges such as the new San Francisco-Oakland Bay Bridge are expected to be operational (i.e., little damage) after very rare earthquake shaking. Significant damage is acceptable in non-important bridges during rare earthquake shaking.

3.5.2 Rules for Selecting and Scaling Ground Motions

The AASHTO *LRFD Bridge Design Specifications* (AASHTO, 2010b) document includes mandatory language and commentary related to "…step-by-step time-history method of analysis used for either elastic or inelastic analysis…" Article 4.7.4.3b of the *Specification* writes

> "Developed time histories shall have characteristics that are representative of the seismic environment of the site and the local site conditions.
>
> Response-spectrum-compatible time histories shall be used as developed from representative recorded motions. Analytical techniques used for spectrum matching shall be demonstrated to be capable of achieving seismologically realistic time series that are similar to the time series of the initial time histories selected for spectrum matching.

Where recorded time histories are used, they shall be scaled to the approximate level of the design response spectrum in the period range of significance. Each time history shall be modified to be response-spectrum-compatible using the time-domain procedure.

At least three response-spectrum-compatible time histories shall be used for each component of motion in representing the design earthquake (ground motions having a seven percent probability of exceedance in 75 yr). All three orthogonal components (*x*, *y* and *z*) of design motion shall be input simultaneously when conducting a nonlinear time-history analysis. The design actions shall be taken as the maximum response calculated for the three ground motions in each principal direction.

If a minimum of seven time histories are used for each component of motion, the design actions may be taken as the mean response calculated for each principal direction.

For near-field sites (*D* < 6 mi), the recorded horizontal components of motion that are selected should represent a near-field condition and should be transformed into principal components before making them response-spectrum-compatible. The major principal component should then be used to represent motion in the fault-normal direction and the minor principal component should be used to represent motion in the fault-parallel direction."

The commentary to Article 4.7.4.3.4b provides additional information regarding appropriate characteristics for the seismic environment, such as tectonic setting, earthquake magnitude, type of faulting, source-to-site distance, local soil conditions and expected ground-motion characteristics, such as strong motion duration, spectral shape, near-fault characteristics. Hazard disaggregation is identified as a way to establish dominant earthquake magnitudes and site-to-source distances. The commentary also provides some guidance on time-domain response-spectrum matching, noting that the spectra for the seed motions for spectrum matching should be similar in shape to the target spectra.

The AASHTO *Guide Specifications for Seismic Isolation Design* (AASHTO, 2010a) includes requirements for response-history analysis in Article 7.4, Time-History Method. The analyst is pointed to Article 4.7.3.4 of the LRFD *Bridge Design Specifications* for guidance on selecting and scaling ground motions.

3.5.3   Calculation of Demands for Component Checking

Article 4.7.3.4 of the *LRFD Bridge Design Specification* provides rules for computing demands for component checking, which are essentially identical to those

described previously for ASCE/SEI 7-05 and ASCE/SEI 7-10. The rules for calculating component demands in seismically isolated bridges are identical.

3.5.4 Observations

The observations provided above on ASCE/SEI 7-05 and ASCE/SEI 7-10 for selecting and scaling ground motions and acceptance criteria for component checking apply to the AASHTO *LRFD Bridge Design Specifications* and the *Guide Specifications for Seismic Isolation Design*. Three noteworthy differences between the AASHTO and ASCE/SEI 7-10 provisions on the topic of selecting and scaling ground motions are the explicit language in the AASHTO specification related to response-spectrum matching and consideration of vertical excitation, and the site-to-source distance (6 miles versus 3 miles) below which components of ground motion must be rotated into the fault-normal and fault-parallel directions.

3.6 Nuclear Facilities, ASCE/SEI Standard 43-05

3.6.1 Performance Expectations

Nuclear facilities process, handle, and store radioactive materials in a form or quantity that pose potential nuclear hazard to staff at the facilities, the environment, and the public at large. Performance standards for nuclear structures are therefore more demanding (stringent) than for buildings and bridges. Performance goals are presented in a probabilistic format in ASCE/SEI 43-05, *Seismic Design Criteria for Structures, Systems, and Components in Nuclear Facilities,* (ASCE, 2005). These goals differ by Seismic Design Category (SDC, 1 through 5) and Limit State (A through D). A category is assigned to each structure, system, and component depending on the severity of the adverse radiological and toxicological effects of the hazards resulting from a structural failure. A building whose failure would have no adverse effects would be assigned to SDC 1 (and be designed per ASCE/SEI Standard 7). A new nuclear reactor building or nuclear material processing facility would be assigned to SDC 5. The four limit states are A (incipient collapse), B (moderate permanent deformation), C (limited permanent deformation), and D (essentially elastic).

For design of new nuclear power plants, the structure, systems, and components are assigned to SDC 5 and essentially elastic response is targeted for earthquake hazard with a mean annual frequency of exceedance of 0.0001. Further, the designer must demonstrate that the mean annual frequency of the First Onset of Significant Inelastic Deformation is 0.00001. The reference risk is much lower than the reference hazard.

3.6.2 Rules for Selecting and Scaling Ground Motions

Section 2.3 of ASCE/SEI 43-05 defines design response spectra (DRS) for site response analysis:

"… the free surface at the top of the soil profile is the most common location at which the DRS is to be determined. … Prior to performing the site response evaluations, the characteristic earthquakes (magnitudes and distances) at frequencies of 1 Hz and 10 Hz associated with the UHRS [Uniform Hazard Response Spectrum] at the control location [typically the bedrock outcrop] shall be obtained. The selection of these bounding frequencies is considered appropriate for the relatively stiff structures typical of nuclear facilities. The spectral shapes associated with these characteristic events shall then be scaled to the UHRS at 1 Hz and 10 Hz, respectively. If the envelope spectrum associated with these two scaled spectra does not fall more than 10% below the UHRS at any frequency in the frequency range of interest, site response evaluations can be performed for these two bedrock spectra…"

Section 2.4 of ASCE/SEI 43-05 provides criteria for developing acceleration time series for analysis of nuclear facilities. These criteria will form the backbone of the forthcoming edition of ASCE Standard 4, *Seismic Analysis of Safety-Related Nuclear Structures*. The criteria are:

"Ground motions that are generated to "match" or "envelop" given design response spectral shapes defined in Section 2.2 shall comply with steps (a) through (f) below. The general objective is to generate a modified recorded or synthetic accelerogram that achieves approximately a mean-based fit to the target spectrum; that is, the average ratio of the spectral acceleration calculated from the accelerogram to the target, where the ratio is calculated frequency by frequency, is only slightly greater than one. The aim is to achieve an accelerogram that does not have significant gaps in the Fourier amplitude spectrum, but which is not biased high with respect to the target. Records biased high with respect to a spectral target may overdrive (overestimate damping and stiffness reduction) a site soil column or structure when nonlinear effects are important.

(a) The time history shall have a sufficiently small time increment and sufficiently long duration. Records shall have a Nyquist frequency of at least 50Hz (e.g., a time increment of at most 0.010s) and a total duration of at least 20s. If frequencies higher than 50Hz are of interest, the time increment of the record must be suitably reduced to provide a Nyquist frequency ($N_y = 1/(2\Delta t)$ where Δt = time increment) above the maximum frequency of interest. The total duration of the record can be increased by zero packing to satisfy these frequency criteria.

(b) Spectral accelerations at 5% damping shall be computed at a minimum of 100 points per frequency decade, uniformly spaced over the log frequency scale from 0.1Hz to 50Hz or the Nyquist frequency. If the target response spectrum is defined in the frequency range from 0.2Hz to 25Hz, the

comparison of the synthetic motion response spectrum with the target spectrum shall be made at each frequency computed in this frequency range.

(c) The computed 5%-damped response spectrum of the accelerogram (if one synthetic motion is used for analysis) or of the average of all accelerograms (if a suite of motions is used for analysis) shall not fall more than 10% below the target spectrum at any one frequency. To prevent spectra in large frequency windows from falling below the target spectrum, the spectra within a frequency window of no larger than ± 10% centered on the frequency shall be allowed to fall below the target spectrum. This corresponds to spectra at no more than nine adjacent frequency points defined in (b) above from falling below the target spectrum.

(d) In lieu of the power spectral density requirement of ASCE 4, the computed 5%-damped response spectrum of the synthetic ground motion (if one synthetic motion is used for analysis) or the mean of the 5%-damped response spectra (if a suite of motions is used for analysis) shall not exceed the target spectrum at any frequency by more than 30% (a factor of 1.3) in the frequency range between 0.2Hz and 25Hz. If the spectrum for the accelerogram exceeds the target spectrum by more than 30% at any frequency in this frequency range, the power spectral density of the accelerogram needs to be computed and shown to not have significant gaps in energy at any frequency over this frequency range.

(e) Because of the high variability in time domain characteristics of recorded earthquakes of similar magnitudes and at similar distances, strict time domain criteria are not recommended. However, synthetic motions defined as described above shall have strong motion durations (defined by the 5% to 75% Arias intensity), and ratios V/A and AD/V^2 (A, V, and D are the peak ground acceleration, ground velocity, and ground displacement, respectively), which are generally consistent with characteristic values for the magnitude and distance of the appropriate controlling events defined for the UHRS [Uniform Hazard Response Spectrum].

(f) To be considered statistically independent, the directional correlation coefficients between pairs of records shall not exceed a value of 0.30. Simply shifting the starting time of a given accelerogram does not constitute the establishment of a different accelerogram. If uncoupled response of the structure is expected, then only one time history is required. Then, the seismic analysis for each direction can be performed separately and then combined by the square root of the sum of the squares (SRSS).

Synthetic, recorded, or modified recorded earthquake ground motion time histories may be used for linear seismic analyses. Actual recorded earthquake ground motion or modified recorded ground motion shall be used for nonlinear seismic analyses. For nonlinear analyses, it is desirable to utilize actual recorded

earthquake ground motion. However, to meet the requirements of steps (a) through (f) above, as many as 30 recorded earthquake motions would be required. As a result, it is acceptable to use modified recorded earthquake accelerograms that shall meet steps (a) through (f). A modified recorded accelerogram is a time-history record of acceleration versus time that has been produced from an actual recorded earthquake time history. However, the Fourier amplitudes are scaled such that the resulting response spectrum envelops the target response spectrum in the manner described above. The Fourier phasing from the recorded earthquake time history is preserved in a modified recorded earthquake accelerogram.

The selection of recorded or modified recorded accelerograms is based on the identification of dominant magnitude-distance pairs that impact the site DRS. The accelerograms used for nonlinear seismic calculations shall be selected from the appropriate magnitude/distance (*M/D*) bins. It may be necessary to produce different accelerograms that characterize the seismic hazard at appropriate low (about 1Hz) and high (10Hz) frequency. Alternatively, the accelerograms may be selected to match the dominant *M/D* pairs at the peak velocity and acceleration segments of the design spectrum. If behavior at the peak displacement frequency range is of interest, additional accelerograms may be selected whose controlling event is appropriate at these frequencies. If recorded accelerograms are used directly as input to the nonlinear analyses, the suite of time histories shall meet the requirements of steps (a) through (f) above. If modified recorded time histories are generated to match the target spectrum, it is important to ensure that the phase spectra of the motions are generated from recorded motions in the appropriate *M/D* bins. In addition, the strong motion duration (as defined as the duration from the 5% to 75% Arias intensity) shall fall within the range appropriate for the *M/D* bin. In accepting the suite of motions, the range in variation in rise time of the Arias intensity shall be considered, such that all do not have the same rise time characteristics."

3.6.3 Calculation of Demands for Component Checking

A minimum of one set of earthquake histories is required for response-history analysis per ASCE/SEI 43-05. This set (or more) of ground motions is defined at a rock outcrop at depth and propagated through lower bound, best estimate, and upper bound soil columns to compute demands on structural components and in-structure (floor) spectra for design of secondary systems. Although unproven at this time, it is assumed that the maximum peak responses from analysis using the three soil columns represent demand at the 80th percentile level. For checking the adequacy of structural components in nuclear reactor structures, maximum peak component demands are compared against component design capacities (nominal values

multiplied by strength reduction factors) established by materials standards such as ACI 349 (ACI, 2006) without reduction for inelastic response (i.e., $R = F_\mu = 1$).

3.6.4 Observations

The ASCE/SEI 43-05 rules for selecting and scaling ground motions are more onerous than those described previously for buildings and bridges and most can be traced to the 1998 edition and prior editions of ASCE 4-98 (ASCE, 2000).

Scenario spectra, similar in concept to the Conditional Mean Spectrum, are introduced in Section 2.3, and are used with the selection and scaling procedures of Section 2.4, to generate ground motions for nonlinear response-history analysis.

3.7   Liquefied Natural Gas Facilities, FERC Guidelines

3.7.1 Performance Expectations

The Federal Energy Regulatory Commission drafted *Seismic Design Guidelines and Data Submittal Requirements for LNG Facilities* (FERC, 2007), yet the draft document has not been finalized. Similar to ASCE/SEI 43-05, the FERC guidelines classify structures, systems and components into Seismic Categories (SC) I, II and III. The guidelines are drawn from rules and procedures provided in ASCE/SEI 7-05, ASCE 4-98, Appendix E of API 650, *Welded Tanks for Oil Storage* (API, 2008), and NFPA 59A, *Standard for the Production, Storage and Handling of Liquefied Natural Gas* (NFPA, 2009).

Liquefied natural gas (LNG) storage containers and the impounding systems, system components required to isolate the LNG container and maintain it in a safe shutdown condition, and safety-critical systems are classified as SC I. Structures, systems, and components not included in SC I that are required to maintain safe plant operation should be classified as SC II. All other components are classified as SC III.

The performance expectations for components of LNG facilities vary by seismic category. For SC I structures components and systems are expected to remain operable after an Operating Basis Earthquake (OBE) and there should be no loss of containment capability of the primary LNG container and it should be possible to isolate and then maintain the container during and after a Safe Shutdown Earthquake (SSE). SC II structures should satisfy the performance goals of the 2006 IBC, *International Building Code* (ICC, 2006), for essential facilities. Structures, components and systems assigned to SC III should meet the performance goals of the 2006 IBC for non-essential facilities.

3.7.2 Rules for Selecting and Scaling Ground Motions

Guidance for selecting and scaling ground motions is included in Section 6.1 of the draft FERC guidelines under the heading of site response analysis, namely, "base

ground motions should be selected and scaled in accordance with Chapter 21 of ASCE 7-05," which is summarized in Section 3.2 of this report.

3.7.3 Calculation of Demands for Component Checking

Section 4 of the draft FERC *Guidelines* provides acceptance criteria for component checking. The procedures vary by seismic category.

For SC I structures, checks are performed for OBE and SSE shaking. Allowable stresses and capacities with traditional seismic increases are used for OBE checking. Inelastic reduction factors can be applied to demands computed for SSE shaking.

SC II structures should meet the requirements of ASCE/SEI 7-05 for Occupancy Category IV structures. An importance factor of 1.5 is applied to demands computed for structures, systems and components.

Seismic Category III structures, systems, and components are required to satisfy the requirements of ASCE/SEI 7-05 for Occupancy Category II structures, with importance factors set equal to 1.0.

3.7.4 Observations

There are no observations unique to the FERC Guidelines; see the relevant observations in prior sections.

3.8   Dams, Federal Guidelines for Dam Safety, FEMA 65

3.8.1 Performance Expectations

Section V of FEMA 65, *Federal Guidelines for Dam Safety* (FEMA, 2005), provides qualitative criteria for evaluating the seismic adequacy of dams. The performance expectations for a dam are project-specific and related to the seismic hazard at the site (high, significant, low) and the acceptable level of damage and economic loss in the event of very rare earthquake shaking.

Section II of the Guidelines identify the intensity of earthquake shaking using a number of terms, including, Maximum Credible Earthquake (MCE), Maximum Design Earthquake (MDE), Safety Evaluation Earthquake (SEE), and Operating Basis Earthquake (OBE). The MCE is established by deterministic seismic hazard analysis. Depending on the acceptable level of damage, the MDE, which is identical to the SEE, can be established by deterministic seismic hazard analysis (and set equal to the MCE), probabilistic seismic hazard analysis, or a combination of both. The OBE is intended to represent the ground shaking that is expected within the service life of the structure and is typically established by probabilistic seismic hazard analysis.

Dams should be capable of withstanding the MDE without catastrophic failure that may, for example, involve uncontrolled release of water. Severe damage or significant economic loss may be acceptable. For OBE shaking, little or no damage, and no interruption of service are permitted.

3.8.2 Rules for Selecting and Scaling Ground Motions

Section III Part D of FEMA 65 provides criteria for developing acceleration time series for analysis of dams. The criteria are:

"*1. General.* When acceleration time histories (also referred to as accelerograms) of ground motions are required for the dynamic analysis of a structure, they should be developed to be consistent with the design response spectrum, as well as have an appropriate strong motion duration for the particular design earthquake. In addition, whenever possible, the acceleration time histories should be representative of the design or safety evaluation earthquake in all the following aspects: earthquake magnitude, distance from source-to-site, fault rupture mechanisms (fault type, focal depth), transmission path properties, and regional and geological conditions. Since it is not always possible to find empirical records that satisfy all of the above criteria, it is often necessary to modify existing records or develop synthetic records that meet most of these requirements.

2. Approaches to Developing Time Histories. There are two general approaches to developing acceleration time histories: selecting a suite of recorded motions and synthetically developing or modifying one or more motions. These approaches are discussed below. For either approach, when modeling near-source earthquake ground motions (i.e., minimum source site distance less than 10 km), it is desirable that the motions include a strong intermediate- to long-period pulse to model this particular characteristic of ground motion often observed in the near field and generally accepted to be responsible for significant damage. Of specific importance at distances less than 10 km are the effects of directivity in developing fault-normal and fault-parallel components (Somerville et al., 1997).

a. Selecting Recorded Motions

(1) Typically, in selecting recorded motions, it is necessary to select a suite of time histories (typically 3 or more) such that, in aggregate, valleys of individual spectra that fall below the design (or "target") response spectrum are compensated by peaks of other spectra and the exceedance of the design response spectrum by individual spectral peaks is not excessive (preferably at least within the bandwidth of interest for structure specific analysis). For nonlinear analyses, it is desirable to have additional time histories because of the importance of

phasing (pulse sequencing) to nonlinear response. In the past, when using selected recorded motions, simple scaling of acceleration time histories was frequently performed to enhance spectral fit. However, scaling should be done with caution. The ramifications of significant scaling of acceleration time-histories on velocity, displacement, and energy can be profound.

(2) The advantage of selecting recorded motions is that each accelerogram is an actual recording; thus, the structure is analyzed for motions that are presumably most representative of what the structure could experience. The disadvantages are: multiple dynamic analyses are needed for the suite of accelerograms selected; although a suite of accelerograms is selected, there will typically be some exceedances of the smooth design spectrum by individual spectrum peaks; and although a reasonably good spectral fit may be achieved for one horizontal component, when the same simple scaling factors are applied to the other horizontal components and the vertical components for the records selected, the spectral fit is usually not as good for the other components.

b. Synthetically Developing or Modifying Motions

(1) Techniques. A number of techniques and computer programs have been developed to either completely synthesize an accelerogram or modify a recorded accelerogram so that the response spectrum of the resultant waveform closely matches the design or target spectrum. Recent advances have used either (a) frequency-domain techniques with an amplitude spectrum based upon band-limited white noise and a simple, idealized source spectrum combined with the phase spectra of an existing record; or (b) kinematic models that produce three components of motion using complex source and propagation characteristics. Such motions have the character of recorded motions since the modeling procedures are intended to simulate the earthquake rupture and wave propagation process. Recent research suggests dynamic and three-dimensional models may be important in estimating engineering ground motions in the future.

(2) Comments. The natural appearance and duration of strong motion can be maintained using these techniques. A good fit to the target spectrum may or may not be possible with a single component of motion. However, for nonlinear applications, it is particularly desirable to have multiple accelerograms because different accelerograms may have different phasing (pulse sequencing) characteristics of importance to nonlinear response yet have essentially identical response spectra. For near-field situations, the characteristics of the motions should reproduce the coherent velocity pulses ("fling") commonly observed in near-field recordings.

(3) Advantages and Disadvantages. The advantages of synthetic techniques for developing time-histories are: the natural appearance and strong motion duration can be maintained in the accelerograms; three component motions (two horizontal and one vertical) each providing a good spectral match can be developed; and the process is relatively efficient. The disadvantage is that the motions are not "real" motions. Real motions generally do not exhibit smooth spectra. Although a good fit to a design spectrum can be attained with a single accelerogram, it may be desirable to fit the spectrum using more than one accelerogram. Such motions have the character of recorded motions since the modeling procedures are intended to simulate the earthquake rupture and wave propagation process.

3. Application. Ground motion parameters should be specified in a manner that is consistent with the analyses to be performed. Where ground motions are specified at one location (e.g., a rock outcrop) and are used in the analysis at a different location (e.g., at the base of a soil layer), the motions need to be adjusted accordingly. Where magnitude and distance are used in empirical procedures, it is important to verify that distance-attenuation definitions in the procedure are consistent with those inferred for the site of interest…."

3.8.3 Calculation of Demands for Component Checking

Section V presents qualitative criteria for evaluating the structural adequacy of concrete and embankment dams for earthquake loading.

For concrete dams, stresses and strains are computed by dynamic analysis, either linear or nonlinear. No guidance is provided on how to estimate demands for component checking if multiple response-history analyses are performed (e.g., peak maximum value of three analyses, average maximum value of seven analyses). Compressive stresses resulting from gravity and earthquake dynamic loadings are combined and compared with the dynamic compressive strength of concrete. The dynamic tensile strength of concrete can be exceeded, with evaluation of impacts based on "sound engineering judgment." The results of dynamic analysis are used to check against sliding and overturning.

For embankment dams, dynamic analysis is performed to check for global stability and to estimate deformations.

3.8.4 Observations

The FEMA 65 guidance and commentary on selecting and scaling earthquake ground motions is more detailed than that presented in the documents discussed previously with the exception of ASCE/SEI 43-05 (Section 3.6).

3.9 Civil Works, U.S. Army Corps of Engineers, EC1110-2-6000

3.9.1 Performance Expectations

In 2009, the U.S. Army Corps of Engineers (USACE) drafted guidance for the selection and scaling of earthquake ground motions for the seismic analysis and design and evaluation of civil works structures, *Selection of Design Earthquakes and Associated Ground Motions*, EC 1110-2-6000.

Section 2-2 of the document defines design earthquakes and ground motions. Similar to FEMA 65, shaking is defined using Operating Basis Earthquake (OBE) and Maximum Design Earthquake (MDE).

The OBE is defined as an earthquake ground motion that can be reasonably expected during the service life of the structure: a 50-percent probability of exceedance. For a 100-year service life, this corresponds to a return period of 144 years. The required performance for OBE shaking is that the "project functions with little or no damage, and without interruption of function." The shaking intensity of the OBE is determined by probabilistic seismic hazard analysis.

The MDE is the maximum level of ground motion for which a structure is designed or evaluated. The required performance is that the "project function without catastrophic failure, such as uncontrolled release of a reservoir, although severe damage or economic loss may be tolerated." For critical structures (defined as structures whose failure during or immediately following an earthquake could result in loss of life), the MDE is set equal to the Maximum Credible Earthquake, which is defined as the ground motion resulting from the maximum earthquake in the vicinity of the site, is determined by deterministic seismic hazard analysis. For non-critical structures, the intensity of the MDE is less than that of the Maximum Credible Earthquake, and is chosen to provide "economical designs meeting appropriate safety standards." In some cases the MDE is defined by an acceleration response spectrum with ordinates that have a 10% probability of exceedance in 100 years (or a return period of 950 years).

3.9.2 Rules for Selecting and Scaling Ground Motions

Chapter 6 of EC 1110-2-6000 provides guidance on selecting and scaling earthquake ground motions. Ground motions for analysis and design can be: (1) recorded in past earthquakes; (2) simulated; or (3) recorded in past earthquakes and then modified. The averaged ordinates of the response spectra for a set of acceleration time series should equal or exceed the ordinates of the design response spectrum for "each design earthquake for which time histories are required." Design response spectra can be defined: (1) deterministically for a constant number of standard deviations above the median demand for a user-specified combination of magnitude, distance,

and other factors; (2) probabilistically using a uniform hazard spectrum; or (3) using a conditional mean (or scenario) spectrum.

Section 6-1 notes that design ground motions should have appropriate characteristics, with consideration given to strong motion duration and as appropriate, the features of near-fault ground motion including directivity, directionality, and velocity pulses.

Section 6-2 identifies resources to aid in the selection of seed ground motions: strong motion databases (6-2a), collections of simulations of ground motions suitable for the Central and Eastern United States (6-2b), on-demand ground motion simulations from the United States Geological Survey (6-2c), and site-specific time series developed from ground-motion simulations (6-2d).

Section 6-3 provides detailed guidance on the development of acceleration time series to fit a user-specified design response spectrum. There are two high-level approaches for developing sets of ground motions that match on average a design response spectrum: (1) scaling recorded or simulated ground motions; and (2) spectrum-matching using time- or frequency-domain approaches. Either approach is described as generally acceptable. The period range used for scaling requires the designer or analyst to decide on the period range of significance for the structure. Supplemental information on each high-level approach is presented below.

3.9.2.1 Scaling Recorded or Simulated Ground Motions

Section 6-3b(1) provides guidance on the number of time series required for response-history analysis:

> "..increasing the number of time histories can achieve a closer average fit of the spectra of the time histories after scaling the spectra to the level of the design response spectrum. Increased numbers of time histories will also result in increased confidence in the determination of the mean response and increased information on the variability of response of the structure to the design-level motions. At least three time-history records should be used for linear dynamic analysis; and at least five time-history records should be used for nonlinear dynamic analysis. If the structure response is found to be significantly sensitive to the time history characteristics for the records selected, then the number of time histories should be increased. As defined herein, a time history "record" may consist of a single horizontal component or a horizontal and vertical component for two-dimensional analysis, or may consist of two horizontal components or two horizontal components and a vertical component for a three-dimensional analysis where the two horizontal components (and the vertical component if used) are applied simultaneously in the analysis."

Sections 6-3b(2) and 6-3b(3) discuss the required degree of fit of the spectra of the scaled ground motions to the design response spectrum:

"..In developing the match of the spectra of a set of time histories to the design spectrum, a first step is to scale each record to the level of the design spectrum. A quantitative measure of the overall fit of the spectrum of a time history record to a design or target spectrum is the mean squared error (MSE) of the differences (summed over a discrete set of periods) between the spectral accelerations of the record and the design spectrum, computed using logarithms of spectral acceleration and period. Thus a scaling factor can be determined for each record that minimizes the MSE over a user-defined period range of significance. Although scaling to minimize the MSE of a record is desirable, it is not necessarily required as long as criteria for the fit of the average spectrum of the time histories to the design spectrum is satisfied. Recommended criteria for the fit is that the average spectrum should not be below the design response spectrum by more than 10 percent at any spectral period over the period range of significance, and the average of the ratios of the average spectrum to the design spectrum over the same period range should not be less than 1.0. Note that because the selected records are individually scaled by constant factors in the simple scaling approach, there is no need to reevaluate the baseline correction after scaling. It is only necessary to satisfy the spectrum fit requirements…

Additional considerations [are provided] for degree of fit when two or three components of motion are used in analysis. If analyses are to be made for two orthogonal horizontal components, it is preferable that the same scaling factor be used for both components of the time histories to preserve the as-recorded relationship between the components. An initial scaling factor based on minimizing the MSE can be determined in a similar manner as described above for a single horizontal component, however, the scaling factor is applied to the geometric mean of the two horizontal components. The time histories for at least one horizontal component of motion should meet the fit criteria stated in paragraph (2) above. If the criteria are not met for the other component of motion, alternatives to be considered by the principal design engineer and the structural or geotechnical analyst include (a) accepting a lesser degree of fit for the other component if there is a principal direction of response and the component meeting the fit requirement is used for that component; (b) increasing the scaling factors so that the fit criteria are met by both components; and (c) using different scaling factors for the other component so that the fit criteria are met by both components. Each of these approaches is considered to be an acceptable approach. The vertical component is usually scaled by the same factor used for the horizontal components. If the vertical component is important to the response of the structure, the response spectra of the vertical components

of the records should be evaluated for reasonableness by comparing the spectra with a design vertical spectrum…If necessary to achieve a spectral fit, vertical components can be scaled by different factors than used for horizontal components."

Section 6-3(b)4 discusses the amplitude of factors used to scale recorded ground motions. No limits are provided on the factors and the guidance notes "… the magnitude of the scaling factor is of secondary importance as long as the time history sets after scaling have characteristics that correspond with those developed for the design ground motion…"

The number of periods (or frequencies) for calculation of response spectra is discussed in Section 6-3(b)5. The analyst is tasked with establishing appropriate criteria to ensure a "… pronounced valley in a spectrum of an acceleration time series will not be present at any frequency between frequencies at which spectra are calculated. A typical criterion is that response spectra should be calculated at equally spaced log frequencies with the spacing of frequencies corresponding to 100 frequencies per decade …"

3.9.2.2 Ground Motions Matched to a Spectrum

Two methods of spectrum matching are described: time domain and frequency domain. Both methods are described as "… capable of producing design time histories that not only have spectra that are a close match to a design response spectrum, but also preserve the basic character of the original time histories with respect to the amplitude and frequency content of the time series over the time history duration."

Section 6-3(c)2 provides guidance for selecting seed motions for spectrum matching. The use of seed motions that have the same general shape as the design response spectrum is recommended because "… it will generally be easier to obtain a good match and also to produce time histories after matching that better preserve the time-domain appearance of the original time histories…"

The required number of time series, aggregate fit of the spectra to the design response spectrum and other guidance is provided in Section 6-3(c)3:

"…The number of time histories is important for both simple-scaled time history sets and spectrum-matched sets. However, for linear elastic analysis, it is expected that structural response will vary much less among spectrum-matched time histories than for simple-scaled time histories because of the close fit of the time history spectra with the design spectra. Thus, at the discretion of the principal design engineer and structural analyst, the number of time histories could potentially be relaxed for spectrum-matched time histories used for linear

elastic analyses. For nonlinear analysis and determination of inelastic response, the variation of inelastic response may also be less for spectrum-matched time histories than for simple-scaled histories. However, it is recommended that the number of time histories used for nonlinear analysis be the same for simple-scaling and spectrum-matching methods. Although less dispersion in responses would be expected for spectrum-matched time history sets than for simple-scaled time history sets, the potential influence of time history characteristics other than the elastic response spectrum characteristics suggests that it is prudent to not relax the criteria for number of records for the spectrum matching method when nonlinear analyses are performed. The aggregate fit to be achieved between the spectra of the time history records and the design spectrum should also be the same for simple-scaled and spectrum-matched time histories. The fit may be much easier to achieve with the spectrum matching method because of the close match usually obtained between time history spectra and design spectra with this method. It is recommended to use approximately 100 points per log period or frequency cycle for spectrum matching to avoid spectral peaks and valleys between computation periods."

3.9.3 Calculation of Demands for Component Checking

The focus of the USACE guidelines is selecting and scaling ground motions for the broad range of civil works, including structures, constructed by the Army Corps of Engineers. No guidance is provided on the calculation of local and global demands for the purpose of design.

3.9.4 Observations

The USACE guidelines are the most comprehensive of those used in design practice at the time of this writing. The high-level rules for scaling motions are more detailed than those available for buildings and bridges and similar in detail to those being proposed for new build safety-related nuclear structures in the updated version of ASCE Standard 4-98, *Seismic Analysis of Safety-Related Nuclear Structures* (ASCE, 2000), currently being developed. Comprehensive guidance and examples are provided for both scaled recorded ground motions and spectrally matched ground motions. Importantly, and different from most other standards, simulated ground motions are discussed in some detail, the conditional mean spectrum (Baker and Cornell, 2006) is introduced, and guidance is provided on scaling vertical components of ground motion.

3.10 Defense Facilities, Department of Defense, UFC 3-310-04

3.10.1 Performance Expectations

The United Facilities Criteria (UFC) 3-310-04, *Seismic Design for Buildings* (Department of Defense, 2004, 2007, 2010) is used for the seismic design of Army,

Navy, and Air Force buildings. The UFC draws heavily from the 2003 IBC, *International Building Code* (ICC, 2003), which in turn draws from the 2002 edition of ASCE/SEI 7. Guidance is provided in the UFC for new structural framing systems, and nonstructural components and systems. Limited guidance is provided for seismic evaluation and retrofit of existing Department of Defense (DoD) buildings.

The UFC documents changes to 2003 IBC for conventional Department of Defense (DoD) buildings in Appendix B, DoD buildings considered essential because of their mission or need for participation in post-earthquake recovery efforts Appendix D, and DoD buildings considered as national strategic assets in Appendix E. Performance expectations for each class of building are different as described below.

The performance objective for conventional DoD buildings (Seismic Use Group I, equivalent to ASCE/SEI 7 Occupancy Categories I and II) is that of the 2003 IBC and the 2002 edition of ASCE/SEI 7, namely, a small but not quantified probability of collapse in MCE shaking, which is achieved by design for life safety for an intensity of shaking equal to 67% of MCE shaking. Similar to ASCE/SEI 7, MCE shaking is defined by an acceleration response spectrum with a 2% probability of exceedance in 50 years, with ordinates capped by a deterministic spectrum.

The performance objectives for essential DoD buildings (Seismic Use Group III, equivalent to ASCE/SEI 7 Occupancy Category IV) are life safety for the MCE and immediate occupancy for shaking with a probability of exceedance of 10% in 50 years.

The performance objective for national strategic assets (Seismic Use Group IV, equivalent to ASCE/SEI 7 Occupancy Category V) is that structure be designed to "…ensure that their superstructures and installed mission-critical nonstructural elements remain elastic, and their installed equipment remains operational, for MCE ground motions." The effects of vertical earthquake shaking must be considered explicitly for Seismic Use Group IV structures.

3.10.2 Rules for Selecting and Scaling Ground Motions

Guidance on selecting and scaling ground motions for DoD buildings is provided in Appendix B, Section 1615.2.1 of the UFC:

> "At least five recorded or simulated horizontal acceleration time histories shall be selected from events having magnitudes and fault distances that are consistent with those that control the MCE. Each selected time history shall be scaled so that its response spectrum is, on average, approximately at the level of the MCE rock response spectrum [the required location for generating an MCE] over the structural period range of significance to the structural response. For structures

with first mode participation factors less than 0.75, an acceptable period range is $0.2T$ to $2.0T$ (T = fundamental period). For other structures, and for all base isolated structures, an acceptable period range is $0.5T$ to $2.0T$."

Procedures for selecting and scaling the vertical component of ground motion are not provided. Appendix E, Section E-15.1.5 states "For the ground motion component associated with the vertical axis of the structure, applied forces shall be determined using a linear acceleration response spectrum."

3.10.3 Calculation of Demands for Component Checking

Demands for component checking are determined using the procedures set forth in the 2003 IBC and 2002 edition of ASCE/SEI Standard 7, namely, if seven or more ground motions are used for analysis, the arithmetic mean of the peak responses is used for component and story checking. If fewer than seven analyses are performed, the maximum value of the peak response quantities is used for component and story checking.

3.10.4 Observations

The UFC provides limited guidance on selecting and scaling ground motions, with rules being adapted from those presented in the 2003 IBC and 2002 edition of ASCE/SEI 7. Many of the observations made on the 2005 edition of ASCE/SEI 7 apply to the 2002 edition but are not repeated here. The basis for extending the upper limit on the period range for scaling from $1.5T$ in ASCE/SEI 7 to $2.0T$ is unclear.

3.11   Key Concerns Facing Design Professionals

The review of current practice as outlined in Sections 3.2 through 3.10 enabled the development of the following list of key concerns facing design professionals tasked with selecting and scaling ground motions using current codes and standards of practice:

1. What are appropriate target spectra for design and performance assessment (uniform hazard, uniform risk, conditional mean, or conditional)?

2. How many sets of records are required for design or performance assessment performed using nonlinear response-history analysis (3, 5, 7, 11, or more)?

3. How should vertical components of ground motion be selected and scaled?

4. How should ground motions be selected and scaled using conditional spectra and conditional mean spectra?

5. What are the advantages, disadvantages, and limitations of response-spectrum matching?

6. How is fault-rupture directivity to be treated in terms of seismic hazard calculations; how many pulse-type motions should be included in a near-fault record set; and how should pulse-type motions be scaled to a target spectrum?

Chapter 4

Problem-Focused Studies

4.1   Introduction

This chapter summarizes the approach taken in conducting problem-focused studies and the conclusions and recommendations drawn from them. The studies were conducted to address key concerns facing design professionals tasked with selecting and scaling ground motions using current codes and standards of practice.

Study topics were selected with the goal of substantially impacting design practice in the short term, with consideration given to the level of effort and time available in the project. Three topics were chosen for study as part of this project as listed below:

1.   Selection of ground motions based on the Conditional Spectrum,

2.   Response-spectrum matching, and

3.   Near-fault ground motions and fault-rupture directivity.

Topics 1, 2, and 3 are summarized in Sections 4.2, 4.3, and 4.4, respectively, and discussed in detail in Appendices A, B, and C, respectively. The conclusions and recommendations brought forward from these Appendices into this chapter represent the consensus view of the project team. The topics are summarized in the body of this report with each section containing three sub-sections: motivation, discussion, and conclusions and recommendations.

Additional key issues were reviewed and documented in Appendix D. These included considerations for selecting and scaling ground motions in the Central and Eastern United States, characteristics of ground motions in active crustal regions and subduction regions, current practice and recent developments in the use of physics-based simulations, and considerations for site, basin, and basin-edge effects.

4.2   Study on Ground Motion Selection Based on the Conditional Spectrum

4.2.1   Motivation

The Conditional Mean Spectrum (Baker and Cornell, 2006b; Baker, 2011) and the related Conditional Spectrum (Jayaram et al., 2011) are alternatives to the Uniform Hazard Spectrum (McGuire, 2004) that can be used as targets for ground motion selection. The Uniform Hazard Spectrum (UHS) is constructed by enveloping the spectral amplitudes at all periods that are exceeded with a given probability,

computed using probabilistic seismic hazard analysis (Cornell, 1968; Kramer, 1996; McGuire, 2004). However, those spectral values at each period are unlikely to all occur in a single ground motion, as has been noted for many years (e.g., Bommer et al., 2000; Naeim and Lew, 1995; Reiter, 1990).

Conditional spectra instead condition the spectrum calculation on spectral acceleration at a single period, and then compute associated spectral acceleration values at all other periods. This conditional calculation assures that ground motions selected to match that spectrum have appropriate properties for naturally occurring ground motions that would occur at the site of interest. A notable feature of this approach is that structural response estimates for multi-mode or nonlinear systems obtained from this approach are usually lower than comparable estimates from a comparable UHS. Resources for computing this spectrum (both how-to guides and electronic tools for providing calculated spectra) are available as noted below and in Appendix A.

While this alternative spectrum approach is attractive for several reasons, there are gaps in the knowledge of how to best use it. It requires hazard disaggregation information to compute, making it a site-specific calculation. However, the USGS now provides a tool to directly download a Conditional Mean Spectrum (CMS) for a given site, so the spectrum is relatively easy to obtain. The CMS is also a period-specific spectrum and is conditioned on spectral acceleration at a user-specified period. The choice of that period may not be obvious, and the response spectrum changes if the conditioning period changes (unlike the UHS). The shape of the spectrum also changes as the spectral amplitude changes (even when the site and period are fixed).

The CMS was initially proposed with an emphasis on the mean spectrum and less attention was paid to the variability in the spectrum. This was in part because there was no simple way to select ground motions that matched a specified variability. Recently an approach has been developed to select ground motions that match both a conditional mean and conditional variability (Jayaram et al., 2011). The approach has been named the Conditional Spectrum (Abrahamson and Al Atik, 2010) and the source code for that algorithm can be found at www.stanford.edu/~bakerjw/gm_selection.html.

The Conditional Spectrum (CS) can be applied to multi-component excitation. One straightforward way of doing this is to use a multi-component definition of the response spectrum, such as "RotD50" or "RotD100" (Boore, 2010). These are measures of multi-component ground motions, as examined by computing response spectra of individual components at various orientations. RotD50 denotes the median spectral value and RotD100 is the largest value over all rotation angles. Conditional values of, for example, RotD100, can be calculated given the target value of

RotD100 at a given period. It is also possible to compute a CS for a given orientation, by conditioning on a spectral value of the ground motion in a different orientation. The computations are the same, and the only additional information required is correlations of spectral values across components. Baker and Cornell (2006a), among others, provide this information. Gulerce and Abrahamson (2010) have implemented this concept to compute vertical response spectra conditional on a specified horizontal spectral acceleration value. Huang et al. (2010) have examined correlations of maximum component response spectra and have determined that they are comparable to existing models for average (i.e., geometric mean or GMRotI50) response spectra. This means that, in conjunction with existing models to predict means and standard deviations of maximum component spectral acceleration, one can construct a CS for maximum component response spectrum.

The most widely used period when implementing Conditional Spectrum is the first-mode elastic period of the structure, but other periods are plausible. Questions regarding the choice of period often arise, for example, when considering multi-component excitation of a building with different modal periods in two horizontal directions. The study documented in Appendix A evaluated this issue in depth and demonstrated that if the analysis goal is a risk-based assessment (involving dynamic analysis at a number of intensities of shaking), the results obtained are invariant to the choice of conditioning period if the CS is used as the target spectrum. In contrast, a situation where analysis results vary with the choice of conditioning period is an intensity-based assessment conditioned on S_a at a single period.

4.2.2 Discussion

This study considered the sensitivity of drift hazard calculations to the choice of conditioning period when the CS is used as a target for ground motion selection and scaling. Drifts and accelerations in ductile reinforced concrete frame structures of varying configurations were studied, and risk-based assessments were performed for each several times, using ground motions selected and scaled to match Conditional Spectra, where the conditioning period used for these calculations was varied. For each case, the risk-based analysis results were similar. The similarity of the results stems from the fact that careful record selection ensures that distributions of response spectra at all periods are nominally comparable, so the distribution of resulting structural responses should also be comparable (to the extent that elastic response spectra describe the relationship between the ground motions and structural responses).

A few caveats regarding the above observations are notable. First, while the assessment results are not sensitive to the choice of a conditioning period, choosing a spectral acceleration-conditioning period that is a good predictor of the structural response parameter of interest (i.e., for which record-to-record variability in elastic

response for a given S_a amplitude is small) will reduce the number of dynamic analyses required to get a stable analysis result. Second, risk-based assessments require a significant number of dynamic analyses. The results in this study were obtained using 40 dynamic analyses at each of 10 spectral acceleration amplitudes, and reducing the number of analyses will reduce the robustness of the results.

An important issue regarding conditioning period arises for intensity-based assessments, where the goal is to compute the structural response associated with an S_a value at a given period having a specified amplitude (e.g., for a building-code-type check). In this case, the response prediction will change depending upon the choice of conditioning period. This comes from the fact that the choice of intensity measure is an inherent part of the problem statement, and changing the intensity measure changes the question that is being asked. Resolution of this issue is not simple, but lies in identifying a performance check that, when passed, confirms satisfactory reliability of the structural system (as determined from a risk-based assessment).

4.2.3 Conclusions and Recommendations

The key conclusions of this study are:

1. Structural response results obtained from ground motions matching a CS target will usually be less than or equal to corresponding response results from ground motions matching a UHS with the same spectral acceleration at the CS conditioning period.

2. When performing a risk-based assessment and matching a CS (including variability) the results will be the same no matter which conditioning period is used for CS calculations. This is because CS-based ground motions will be consistent with ground-motion hazard at all spectral periods (not just the conditioning period).

3. Fewer ground motions are needed to obtain a stable risk-based-assessment result if a good conditioning period is used (i.e., one that results in small record-to-record variability in structural responses among analyses using ground motions having the same spectral acceleration at the conditioning period).

4. A significant number of ground motions (and associated response history analyses) are required to estimate full distributions of response for risk-based assessments. The studies herein used 40 ground motions per intensity level, at 10 intensity levels; these numbers could perhaps be reduced somewhat, but it has not been demonstrated that robust results can be obtained using a significantly smaller number of analyses.

5. If one is performing an intensity-based assessment and matching a CS or CMS, the answer will depend to some degree on the choice of conditioning period.

The key recommendations from this study are:

1. The CMS provides a defensible target spectrum for intensity-based response-history analysis, and so should be allowed as an alternative target spectrum in ASCE/SEI 7 Chapter 16. The conditioning period for the CMS impacts response-history analysis results, and so guidance should be provided with regard to how an analyst should choose conditioning periods to satisfy the intent of the standard. A tentative recommendation is to build one spectrum conditioned on the first mode period and add an additional spectrum at a shorter period, such that the envelope of the two approximately match the UHS over a range of periods. This approach has some precedence in other consensus documents (e.g., ASCE/SEI 43-05). The greater analysis effort associated with considering multiple target spectra will somewhat negate the benefit of the reduced conservatism that will result from avoiding use of the UHS, but this is an optional approach and thus no additional effort is required unless an analyst chooses it.

2. The CS is a recommended target spectrum for risk-based assessments and collapse fragility functions, based upon its ability to successfully meet the stated objective of those procedures.

3. For the risk-based procedure in ATC-58-1, the currently stated choice of T_1 as a conditioning period is appropriate (though not critical), and a single period can be used for predicting drift- and acceleration-sensitive responses. The recommended CS calculation procedures and ground-motion selection algorithms are referenced in this report.

4.3 Study on Response-Spectrum Matching

4.3.1 Motivation

Response-spectrum matching is a process in which a real recorded earthquake ground motion is modified in some manner such that its response spectrum matches a desired target spectrum across a range of periods and possibly multiple damping values. In the context of spectrum matching, the input ground motion is referred to as the "seed" motion. The spectrum-matching process modifies the frequency content of a seed motion. The principal advantage of using spectrum-matched records is that the record-to-record variability of the input is substantially reduced, which also reduces the variability in the output or response. An additional advantage is that it is possible to enhance some of the frequencies within the record while suppressing others, which is useful if modifying records for use in a region such as the Central and Eastern United States where appropriate strong motion recordings are unavailable. Due to decreased variability, it is possible to obtain stable estimates of the mean response using fewer structural analyses (Shome et al., 1998; Watson-Lamprey and

Abrahamson, 2006; Hancock et al., 2008). On the other hand, since the variability is artificially reduced, spectrum-matched records can only be used to estimate mean (or median) response and not the distribution of response. Furthermore, several authors (Carballo and Cornell, 2000; Bazzurro and Luco, 2006; Huang et al., 2008b) identified a systematic unconservative bias in the estimation of mean nonlinear response using matched records, although this conclusion is not supported consistently in the literature (Hancock et al., 2008; Heo et al., 2011).

There is little guidance available to users of spectrum-matching software as to what constitutes an acceptable modification to an initial seed ground motion, and how to assess if a ground motion may be considered realistic for use in response-history analysis. Given that the objective of response-history analysis is to obtain unbiased estimates of peak structural response quantities, matched motions should be considered acceptable on the basis of their effect on nonlinear structural response, and not based on whether every cycle of the original motion has been preserved intact. On the other hand, in lieu of specific studies on the effect of matching on nonlinear response, the engineering seismologist or analyst can only draw conclusions about acceptability based on visual observations of how much the record has changed in the time domain. In typical applications, this is done by a qualitative visual check on one or more of the acceleration, velocity, or displacement ground motion histories, and the Husid plot (Husid, 1973), which shows the growth of Arias Intensity (Arias, 1970) over time (e.g., see recommendations in Hancock et al., 2006).

One particular non-stationary characteristic of seed ground motions that would ideally be preserved in spectrum matching is the presence of pulses in the velocity history. As discussed in Appendices C and D, velocity pulses are often observed in ground motions recorded in the near-fault region, and therefore it is desirable to generate spectrum-compatible records that include these characteristics. Spectrum matching cannot be relied upon to generate pulses in a signal, and therefore the objective would be to select a seed record that already contains the desired non-stationary characteristics, and to ensure that these characteristics are preserved after matching. The elastic response spectrum of a record containing a velocity pulse tends to have higher spectral ordinates at periods centered on the period of the pulse (see Shahi and Baker (2011) among others) and therefore the utility of spectrum matching will depend on the choice of target spectrum.

To investigate the issues discussed above, two studies were carried out, which are summarized in the following sub-sections, together with key results.

4.3.2 Discussion

4.3.2.1 Precision and Accuracy Using Spectrum Matching

The first study investigated whether bias is introduced, and to what extent the dispersion is reduced, when spectrum-matched records are used for response-history analysis. The analyses were also used to assess whether robust limits on the amount of change introduced to a seed ground motion by spectrum matching could be established.

The study used two building models and seed ground motions from the Pacific Earthquake Engineering Research (PEER) Center's Ground Motion Selection and Modification (GMSM) study (Haselton et al., 2009). The demand parameters that were monitored were maximum story drift ratio, peak acceleration at the roof level, and a floor spectral acceleration ordinate for which results are not provided in this report but the conclusions were broadly similar to those for peak floor acceleration.

These models and demand parameters were selected both to allow comparison with the PEER GMSM work, and because a high-level point of comparison had been developed for maximum story drift as part of that work that could also serve as a benchmark for the results of this work. The point of comparison estimates were developed based on regression analyses on the results of hundreds of response-history analyses, and were considered to be the best available estimates of the true response, based on current knowledge of seismology and structural engineering. Similar high-level estimates were not available for the other two parameters. Therefore the point of comparison for these parameters was taken as the median response from 40 response-history analyses, using ground motions selected per the algorithm of Jayaram et al. (2011), preserving the mean and standard deviation of the Conditional Spectrum. This approach gave good agreement with the high-level point of comparison estimate of maximum story drift, and this provided confidence that a robust benchmark was being used.

Several suites of ground motions (generally with 28 motions per suite) were used for the analyses, considering the following variations: (1) using linearly scaled seed motions vs. spectrum-matched motions; (2) spectrum matching carried out over different period ranges and damping values; (3) selecting seed motions with different methods; and (4) using different target spectrum for matching. Spectrum matching was carried out with RspMatch2005 software (Hancock et al., 2006).

Using the results of a subset of these analyses, a number of scalar measures of change introduced to a seed motion by spectrum matching were investigated, to see if large changes tended to produce biased responses from the response-history analyses. No consistent and statistically significant relationships were observed between the change parameters and the responses, suggesting that ground motions with large

changes introduced by spectrum matching should not necessarily be rejected on this basis alone. The non-stationary characteristics of the seed ground motion are completely modified by the matching process in some isolated cases and the impact of these isolated cases may not have been picked up by the regression analyses.

4.3.2.2 Effect of Response-Spectrum Matching on Velocity Pulses

The second study investigated whether velocity pulses could be preserved in spectrum matching. A single earthquake scenario was considered with two possible pulse periods. Seed ground motions identified by the method of Baker (2007b) as containing a velocity pulse with a period within 10% of the scenario pulse period were selected from the PEER NGA database (http://peer.berkeley.edu/nga/).

For each pulse period, three separate target spectra for spectrum matching were developed: (1) a spectrum for the scenario using the median from a ground motion prediction equation, amplified by a narrow-band adjustment from Shahi and Baker (2011) at periods centered around the pulse period; (2) a median spectrum amplified by a broadband adjustment across a wide range of periods from Somerville et al. (1997) and Abrahamson (2000); and (3) a median spectrum without amplification. Spectrum matching was carried out on each of the records to each of these target spectra. In the third case, the velocity pulse was extracted from the seed motion using the method of Baker (2007b) before spectrum matching was carried out, and then added back into the ground motion following spectrum matching.

For each case, the pulse was extracted from the original seed motion and the spectrum-matched motion, and its characteristics were compared. Mixed results were obtained. In some cases, the "pulse indicator" of Baker (2007b) indicated that the final record should not be considered pulse-type, because too much energy had been added to the rest of the signal, and therefore the pulse did not dominate the final record as it did the original seed motion. In other cases, the final motion still contained a pulse, but its period was lengthened, or its phasing had been changed from the original motion.

In general, it was found that the first and third target spectra described above gave the most useful results (i.e., the most pulses preserved in the final sets of ground motions). This result was somewhat expected, as the second target incorporates an adjustment across a wide range of periods, and therefore represents the averaged effect of pulses with a range of periods. Individual records have velocity pulses at a single period only if they exist in the record and therefore the ordinates of their response spectra tend to be higher around this period. Artificially manipulating the ground-motion history to match a smoothed spectrum that did not have this higher spectral demand would require that either the pulse is reduced in effect, or that

significant energy content is added to the rest of the signal to increase the spectral demand at other periods.

4.3.3   Conclusions and Recommendations

The key conclusions of this study are:

1. The use of spectrum-matched ground motions for nonlinear response-history analysis does not produce an unconservative (low) bias in response.

2. Matching ground motions to a CMS rather than a UHS did not significantly bias the estimates of maximum story drift.

3. No reduction in the minimum number of ground motion records used for nonlinear response-history analysis should be permitted if the motions are spectrum matched.

4. The period range to be used for spectrum matching depends on the choice of seed motions, the expected degree of inelastic response, and the demand parameter(s) being investigated.

5. Ground motions with large changes in amplitude and frequency content introduced by spectrum matching should not necessarily be rejected from a ground motion set.

The key recommendations from this study are:

1. The best target spectrum for matching depends on the application being considered. The UHS may be appropriate if conservative estimates of building response are acceptable and it is unclear if multiple modes contribute substantially to the response parameters of interest. Otherwise the CMS should be used as the target.

2. Spectrum-matched motions should not be used to estimate percentile values of response other than the median (or other measures of central tendency).

3. The upper bound on the period range for spectrum matching should be increased to $3T_1$ for analysis of taller flexible moment frames responding well beyond yield.

4. Target spectra for matching motions with velocity pulses should include a narrow-band adjustment for the pulse, namely, an increase in spectral response conditioned on a specified pulse period.

5. Spectrum matching of two-component ground motions should be carried out consistently with the definition of the target spectrum (e.g., geomean or maximum rotated). For maximum rotated spectral response in the near-fault region, the orientation of the maximum response is reasonably well defined and the two components can be spectrum matched independently, that is, one

component matched to a maximum (or perhaps fault-normal) spectrum and the other to a minimum (or perhaps fault-parallel) spectrum.

4.4 Study on Near-Fault Pulse Motions

4.4.1 Motivation

Earthquake ground motions recorded at short site-to-source distances, say, less than 10 km, can have significantly different characteristics than those recorded at distances greater than 25 km; see Appendix C. Sites in this near-fault region may experience shaking described as forward directivity (FD) when rupture occurs towards the site (e.g., Somerville et al., 1997). Double-sided velocity pulses are often observed in the fault-normal component of these near-fault motions. Single-sided velocity pulses are often observed in the fault-parallel component (the fling step) of these motions associated with permanent offset along the fault. Near-fault motions do not necessarily contain velocity pulses.

In this study, a new definition of pulse-type motions is offered and near-fault earthquake records are classified accordingly. A proposal for the number of pulse-type motions to be included in a record set is made on the basis of regression analysis of strong-motion data recorded in the near-fault region.

4.4.2 Discussion

4.4.2.1 Near-Fault Motion Classification

Pulse motions differ from non-pulse, termed ordinary, ground motions through their intense, compact signal in the velocity-time series. Most of the energy in a pulse motion is concentrated in one or two cycles of the velocity-time series. Pulse motions often produce high spectral demand at longer periods than do ordinary motions. To distinguish pulse motions from ordinary ground motions in the near-fault region, a classification scheme was developed to identify early-arriving, high-intensity, two-sided velocity pulses, which is different from those proposed by Shahi and Baker (2011) and Bray and Rodriguez-Marek (2004).

Ground motion data were obtained from the PEER NGA flatfile (http://peer.berkeley.edu/nga/) used to develop the NGA ground motion prediction equations (Chiou et al., 2008). This study only considered records with moment magnitudes greater than or equal to 6.0 and closest source-to-site distances of less than 30 km. The resulting ground motion data set contained 390 records from 35 earthquakes. All motions were low-pass filtered to focus on the characteristics of the velocity-time series near the period of the most significant velocity pulse in the record as defined by the period with the maximum ratio of 5%-damped spectral velocity in its maximum recorded component to the median spectral velocity estimated using the NGA ground motion prediction equation of Abrahamson and

Silva (2008) for the corresponding combination of magnitude and distance. The filtered velocity-time series was then rotated to identify the record's maximum component as defined by the component with the highest peak-to-peak velocity (PPV).

The classification scheme differentiated pulse motions from non-pulse motions through a weighting scheme that emphasized characteristics such as the rate of change of the record's normalized cumulative squared velocity and the number of significant pulses. The classification of records also involved subjective evaluation because not all the nuances of a record are captured by even the most highly sophisticated classification schemes. Once the pulse motions were identified, the Isochrone Directivity Predictor (IDP) of Spudich and Chiou (2008), the maximum peak ground velocity (PGV) ratio of the two orthogonal components, and the orientation of the maximum PPV pulse to the strike of the fault were used to differentiate FD pulse motions from other pulse-type motions.

Using the proposed classification scheme, of the 390 records considered, 54 records were classified as FD pulse motions, 34 records were classified as pulse motions that could not be explained by forward directivity, and 30 records were considered questionable as to whether they were pulse-type motions or not. The remaining 272 records and the 30 questionable records were classified as non-pulse (ordinary) motions. Thus, 88 records were classified as pulse motions, with the majority of these pulse motions being classified as FD pulse motions. These pulse motions have pulse periods of at least 0.5 second. The characteristics of the pulse motions are provided in Appendix C.

4.4.2.2 Proportion of Pulse Motions in a Record Set

The disaggregation of the seismic hazard at a site provides the controlling magnitude, site-to-source distance, and the number of log standard deviations by which the predicted value exceeds the median, ε. Pulse-type motions are more likely to be observed when the spectral acceleration at the selected hazard level is associated with $\varepsilon \geq 1$. The probability depends greatly on site-to-source distance, with the probability of occurrence of pulse motions decreasing with increasing site-to-source distance.

A probability model was developed to understand the dependence of the proportion (or percentage) of pulse motions on ε and distance, and is presented in Appendix C. This relationship could be used to estimate the number of ground motion records in a set that should have pulse-type characteristics.

4.4.2.3 Selection and Scaling of Pulse Motions

Once an appropriate number of pulse motions is estimated with the relationship provided above, records could be selected from the records provided in Appendix C. Pulse motions are provided in two period bins: 0.7 to 2.2 seconds, and 2.2 to 6.0 seconds.

It remains unclear how a pair of pulse-type motions should be scaled to a target spectrum such as a Uniform Hazard Spectrum or a Conditional Mean Spectrum. The scaling procedure will be dependent on the type of target spectrum and whether that spectrum accounts explicitly for forward-directivity effects. However, regardless of the procedure used to scale a pair of pulse-type motions and the choice of target spectrum, the velocity-time series of the scaled and seed motions should be compared to ensure that the non-stationary aspects of the seed motion are preserved.

The maximum component of the two horizontal components of pulse motions is most likely to occur within $\pm 30^{\circ}$ of the fault-normal orientation for small site-to-source distances and large earthquake magnitudes, confirming the observations of others, including Huang et al. (2008a).

4.4.3 Conclusions and Recommendations

The key conclusions of this study are:

1. In the near-fault region, rupture of a fault towards a site can produce pulse-type motions in which much of the seismic energy is concentrated in one or two intense cycles in the velocity-time series. The characteristics and damage potential of these pulse-type motions are substantially different from those of ordinary ground motions. These conclusions are consistent with the results of prior studies by others, including Bertero et al. (1978), Mahin and Bertero (1981), Somerville et al. (1997), Krawinkler et al. (2003), and Baker (2007b).

2. Scaling procedures developed for ordinary motions may not be appropriate for pulse-type motions.

3. Pulse-type motions are more likely to occur when $\varepsilon \geq 1$ and the site-to-source distance is small.

The key recommendations from this study are:

1. The appropriate proportion or percentage of pulse-type motions in a record set could be estimated using the predictive equation presented in Appendix C.

2. Seed pulse-type motions could be selected from the records provided in Appendix C.

3. For small site-to-source distances, a pair of scaled pulse-type motions should have its maximum component oriented within $\pm 30^o$ of the fault-normal orientation.

Chapter 5
Recommendations for Design Practice

5.1 Introduction

This chapter provides recommendations for selecting and scaling ground motions for design and performance assessment of low- and medium-rise buildings, a discussion of how to best apply the rules of ASCE/SEI 7-05 and ASCE/SEI 7-10, and recommendations for future research. Commentary is embedded in each section of the chapter.

Response-history analysis of a building model involves the following steps:

1. Identify the goal(s) of the analysis,

2. Build an appropriate mathematical model of the building,

3. Select a target spectrum (or spectra) for analysis,

4. Select and scale earthquake ground motions consistent with the target spectrum (spectra), and

5. Perform analysis and interpret the results.

This chapter addresses steps 3 and 4 and reflects on steps 1, 2, and 5.

5.2 Response-History Analysis

The first step requires the analyst to identify the goal(s) of the analysis, namely, design or performance-assessment, calculation of mean values of response parameters (e.g., component deformation, component force) or distributions of response parameters. As discussed in Chapter 2, this decision will dictate the choice of target spectrum, how the ground motions are selected and scaled, and how the results of the analysis are assembled and interpreted.

Construction of a mathematical model of a building requires a priori knowledge of the likely degree of its inelastic response for the chosen intensity of shaking so that appropriate component models are used. For example, if limited inelastic response is expected, simple bilinear component hysteretic models may be adequate. Conversely, if component deformations are likely close to values associated with failure, and story drifts are close to those values at which collapse is possible,

component hysteretic models must address deterioration of strength and stiffness and second-order effects must be considered explicitly. Further, if the effects of vertical shaking may be important, all beams, columns, and slabs should be included in the model and masses should be distributed appropriately across the footprint of each floor. The use of a poor mathematical model will produce erroneous results regardless of the attention paid to the selection and scaling of the ground motions. The validity of the analysis results may depend on where the motions are applied to the model (ground level or underside of basement) and if soil-structure-interaction materially affects the ground motion inputs, both of which require site-specific calculations.

After analysis is performed, response data must be interpreted with user-specified acceptance criteria. Data are typically assembled and checked component by component, which is usually conservative because failure of discrete components does not necessarily lead to unacceptable building performance. However, there is no consensus on how to judge response at a level higher than components, except using loss-calculation tools such as those being developed as part of the ATC-58-1 project. This topic is beyond the scope of this project.

Assuming acceptance checking is performed at the component level, and seven sets of motions are used for analysis, the forces and deformations at the critical cross sections in each component are grouped together for assessment. In many cases for design, the average value (arithmetic mean) of the seven responses (e.g., inelastic rotation at a joint) is compared with an acceptable value (e.g., a 16th percentile estimate of capacity) and if the demand is less than the capacity then the component passes. For analyses generating little inelastic action in building components, this process is reasonable, especially if dispersion in the response is of no concern. However, if distributions of component response parameters are required, as might be needed to assess or design force-controlled components such as columns, many more than 7 sets of motions must be generated and analyzed.

Where intensities are sufficient for a proportion of ground motions to cause collapse, many more than seven sets of motions will be required to compute the probability of collapse with reasonable confidence.

The treatment of responses generated by analysis using near-fault motions warrants discussion. Buildings sited close to major active faults will likely experience forward-directivity ground motions that include velocity pulses. The set of ground motions generated for nonlinear response-history analysis should include one or more records with velocity pulses in each horizontal component. If the period of one or more of these pulses aligns approximately with the period of the building, large component and system responses may result, and the component responses might distribute bi-modally, with one (lower) mode characterizing response to the non-

pulse-type motions, and one (higher) mode characterizing response to the pulse-type motions. There is no consensus on how to compare such a distribution of response with a discrete acceptance criterion. This topic is also beyond the scope of this project but warrants careful study in the future.

5.3 Selecting Target Spectra for Selecting and Scaling Ground Motions

5.3.1 Ground Motion Intensity Measures

There are many ground motion intensity measures and this section identifies only a few. The simplest measures, such as peak ground acceleration, peak ground velocity, and peak ground displacement, provide little information on the damage potential of an earthquake ground motion for a specific building. Relatively simple but improved measures are based on the response of an elastic single-degree-of-freedom system, including spectral acceleration, velocity, and displacement. More complex (and rarely-used) measures include inelastic response of a single-degree-of-freedom system and vector-based (multiple) intensity measures (e.g., elastic spectral accelerations at two periods, inelastic spectral displacement at the first-mode period, and elastic spectral displacement at the second-mode period).

The most widely used intensity measure is 5%-damped spectral acceleration, S_a, and this report focuses on it, although it has many limitations and cannot characterize the nonlinear response of a building. Other ground motion properties will tangibly affect structural response, including spectral shape, strong motion duration (important for deteriorating systems and collapse calculations), and presence of velocity pulses.

Three definitions of horizontal spectral acceleration are identified here. One of these is for analysis of two-dimensional (planar) frames, and two are for analysis of three-dimensional frames: (1) arbitrary component; (2) geometric mean; and (3) maximum direction. The procedures used to select and scale motions must be consistent with whichever definition is chosen (Baker and Cornell, 2006b). Spectral acceleration of an arbitrary component, computed from analysis of single horizontal components of ground motion, could be used for planar analysis of frames, but modern ground motion prediction equations do not exist for this definition in the Western United States. Geometric mean spectral acceleration has been widely used in hazard calculations for more than two decades although until recently few structural earthquake engineers understood the definition and how to apply it. For a pair of horizontal ground motions, the geometric mean spectral acceleration is calculated, period-by-period, as the square root of the product of the two spectral accelerations. (An alternate definition for geometric mean, GMRotI50, was proposed by Boore (2010) to provide an orientation independent definition of geometric mean spectral acceleration. That definition is not discussed here.) The third definition, maximum

direction spectral acceleration (see Huang et al. 2008a and 2010) is the greatest unidirectional acceleration value for any possible orientation of a pair of horizontal ground motions. Huang et al. (2009) demonstrated the following: (1) for intermediate and longer periods the orientation of maximum shaking is relatively similar for a wide range of periods; and (2) for short periods (i.e., 0.1 seconds), the orientation of maximum shaking varies significantly by period.

5.3.2 Probabilistic Seismic Hazard Analysis

The three types of target spectrum described in following subsections are constructed typically using probabilistic seismic hazard analysis (Cornell, 1968; Kramer, 1996; McGuire, 2004). Such analysis employs ground motion prediction equations that relate earthquake-scenario information (e.g., a magnitude, M, and distance, R, pair) and site information (e.g., $V_{s,30}$ or a qualitative description of the soil column) to the ground motion intensity levels that are expected at the building site. For a given ground motion scenario, ground motion prediction equations provide an estimate of the median expected ground motion intensity and the variability in the prediction (typically in terms of a logarithmic standard deviation, σ_{LN}). In the Western United States, the median intensity for horizontal shaking is generally the geometric mean of the two horizontal components at a given period, $S_{a,gm}(T)$.

As an example, consider a 20-story building located in Palo Alto, California, 10 km from the San Andreas Fault, on a site having a soil shear wave velocity in the upper 30 meters of $V_{s,30} = 400$ m/s. Assume the building has a fixed-base first-mode period, T_1, of 2.6 seconds, and its performance is to be assessed for shaking with a 2% probability of exceedance in 50 years (or a return period of 2475 years).

Probabilistic seismic hazard analysis (PSHA) considers all possible earthquake scenarios on contributing faults near a site to compute exceedance probabilities of spectral quantities. In practice, this is typically computed using the tool provided by the United States Geological Survey (http://earthquake.usgs.gov/hazards) or with tools that provide more flexibility to the user, such as OpenSHA (http://opensha.org/) or proprietary software.

Each probabilistic seismic hazard analysis calculation results in a hazard curve for a specified period of interest. Figure 5-1a presents a seismic hazard curve for the Palo Alto site, computed for the building period of 2.6 seconds and $V_{s,30} = 400$ m/s. This figure shows $S_{a,gm}$ (2.6s) = 0.45g for the 2% in 50 year ground motion. Figure 5-1b shows the disaggregation for this ground motion intensity at the Palo Alto site. Based on this disaggregation, the controlling earthquake scenario has magnitude 7.8 and $R = 11$ km. The disaggregation includes a value of 1.3 for ε, the number of log standard deviations by which the predicted value exceeds the median.
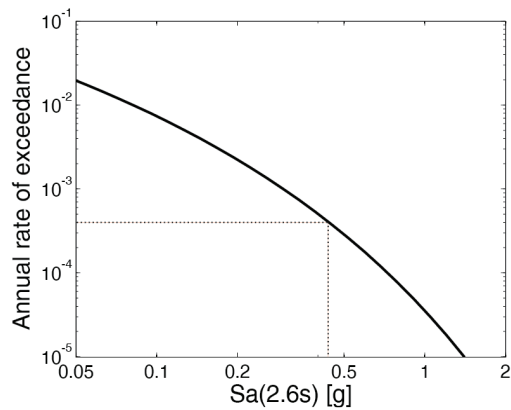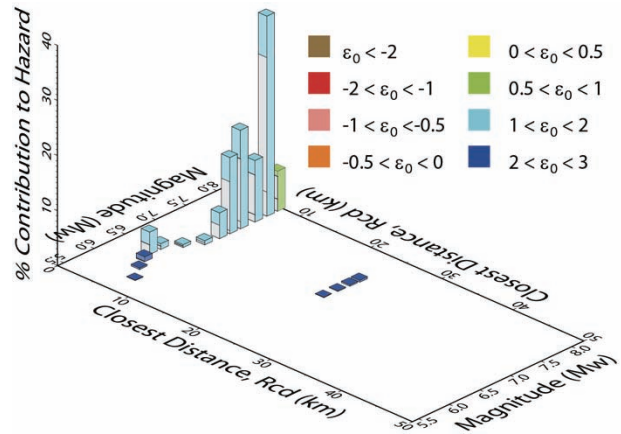
a) Seismic hazard curve   b) Disaggregation data from USGS

Figure 5-1   Example seismic hazard analysis for Palo Alto site for 2% in 50-year shaking.

Site soil effects can be included generically in PSHA if the ground motion prediction equations accept $V_{s,30}$ as an input parameter. The example above used this approach. Other ways of addressing site effects are discussed below.

Three viable target spectra are discussed in Sections 5.3.3 (Uniform Hazard Spectrum), 5.3.4 (Conditional Mean Spectrum), and 5.3.5 (Conditional Spectrum). User-specified target spectra (e.g., an 84th percentile acceleration response spectrum computed using a ground motion predictive equation for a user specified combination of magnitude and distance) are not discussed.

5.3.3 Uniform Hazard Spectrum

The Uniform Hazard Spectrum (UHS) has been used as the target spectrum in design practice for the past two decades. Figure 5-2 shows an example UHS for the Palo Alto site for a 2% probability of exceedance in 50 years; linear and log-log scales are provided in panels a and b, respectively. The previously mentioned geometric mean spectral acceleration at $T = 2.6$ seconds of 0.45g is shown in the figure.

The UHS is created by PSHA at many periods in the range of interest (2.6 seconds was chosen in Figure 5-2a, selecting a frequency of exceedance for the hazard, (say 0.0004), calculating the value of spectral acceleration (or other quantity) at each period for which PSHA was performed, and plotting spectral acceleration versus period. The hazard calculations are performed period by period, without consideration of hazard at adjacent periods. The UHS is a conservative target spectrum for seismic analysis of buildings, especially for very rare levels of ground motion (e.g., Bommer et al., 2000; Naeim and Lew, 1995; Reiter, 1990), where it is most unlikely that high amplitude spectral values are observed at all periods in a single ground motion set.
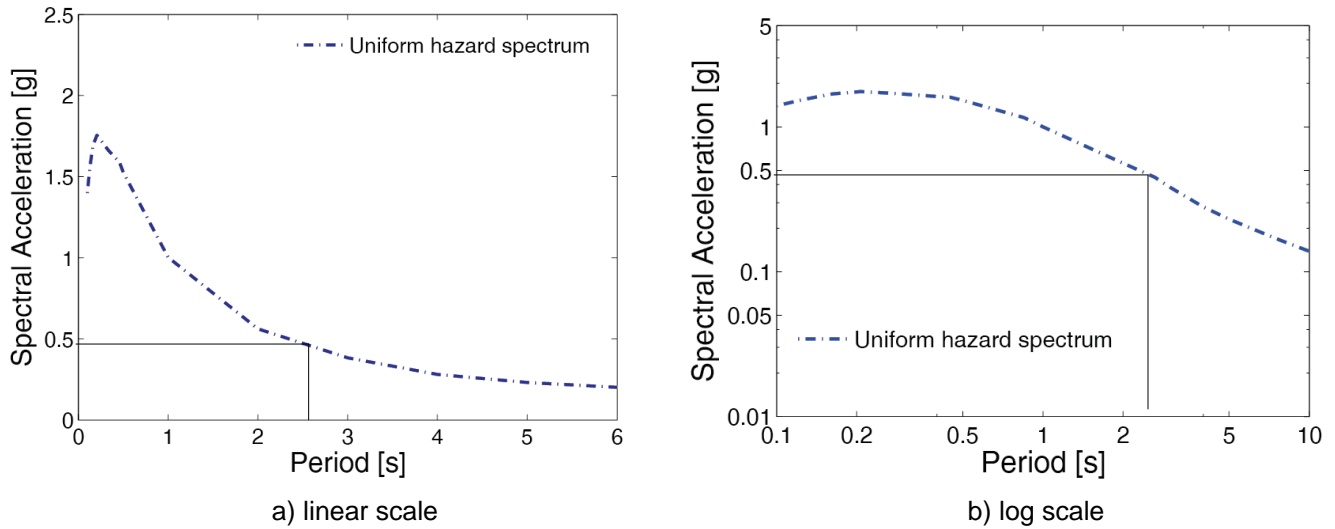
Figure 5-2   Example 2% in 50-year Uniform Hazard Spectrum for the Palo Alto site.

If not included explicitly in the PSHA, site soil effects can be included in a UHS one of two ways:

1. Develop a UHS for a rock outcrop at depth and then perform site response analysis using an appropriately validated site response program (e.g., DeepSoil (Hashash and Park, 2001) and SHAKE (Schnabel et al., 1972; Idriss and Sun, 1992) to predict the ground motion intensity at the ground surface (or at the basement of the building if the ground motions are input at the basement level).

2. Develop a UHS for rock outcrop at depth, and then use site amplification factors to predict the ground motion intensity at the ground surface free field (e.g., the site factors in Tables 11.4-1 and 11.4-2 of ASCE/SEI 7-10). Note that these factors are likely only appropriate for the Western United States, apply over a period range to a generic soil classification, and cannot capture the spectral signature of a specific site.

5.3.4   Conditional Mean Spectrum

The CMS conditions the entire spectrum on spectral acceleration at a single user-specified period and then computes the mean values of spectral acceleration at all other periods. This conditional calculation ensures that ground motions modified to match the spectrum have properties of recorded ground motions. The CMS calculation requires hazard disaggregation information, making it site-specific. The appropriate conditioning period may not be immediately obvious and the CMS changes with conditioning period, unlike the UHS. Further, the spectrum changes shape as the peak spectral value is changed, even when the site and period are not changed. Multiple conditioning periods could be used to generate a family of CMS for either design or performance assessment (Somerville and Thio, 2011).

Baker and Cornell (2006) provide the equations required to generate a CMS and these are not repeated here. Figure 5-3 provides example Conditional Mean Spectra anchored at a period of 2.6 seconds (the fundamental period of the 20-story example building) and three other periods ($T_2 = 0.45$s, $T_3 = 0.85$s, and $2 \times T_1 = 5$s). The associated UHS is also shown. For each CMS, the spectral ordinate at conditioning period is equal to that of the UHS, but all other ordinates are less, period by period, than those of the UHS.
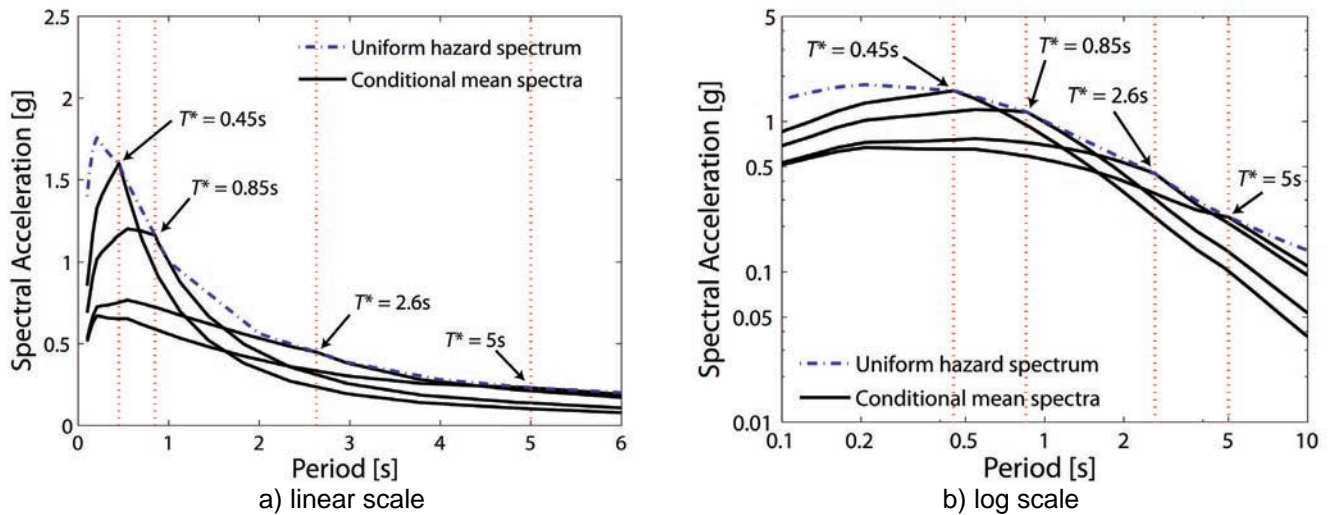
Figure 5-3   Example Conditional Mean Spectra for the Palo Alto site anchored for 2% in 50-year motion at $T = 0.45$s, 0.85s, 2.6s, and 5s.

5.3.5 Conditional Spectrum

The CMS was proposed initially in 2006 with an emphasis on mean demands and less attention was paid to the variability in the spectral demand. At that time there was no simple way to select ground motions that matched a specified variability. As noted in Chapter 4 an approach has been proposed by Jayaram et al. (2011) to select ground motions that match both a conditional mean and conditional variability. Abrahamson and Al Atik (2010) coined the term Conditional Spectrum (CS) to describe the augmentation of the CMS considering variability. The CS is an alternative target spectrum.

Figure 5-4 provides an example of a ground motion set selected and scaled based on the CS for the 20-story example building (anchored at 2.6 seconds).

The Conditional Spectrum can also be applied to multi-component excitation. One straightforward way of doing this would be to use a multi-component definition of the response spectrum, such as RotD50 or RotD100 (Boore, 2010).

a) linear scale

b) log scale
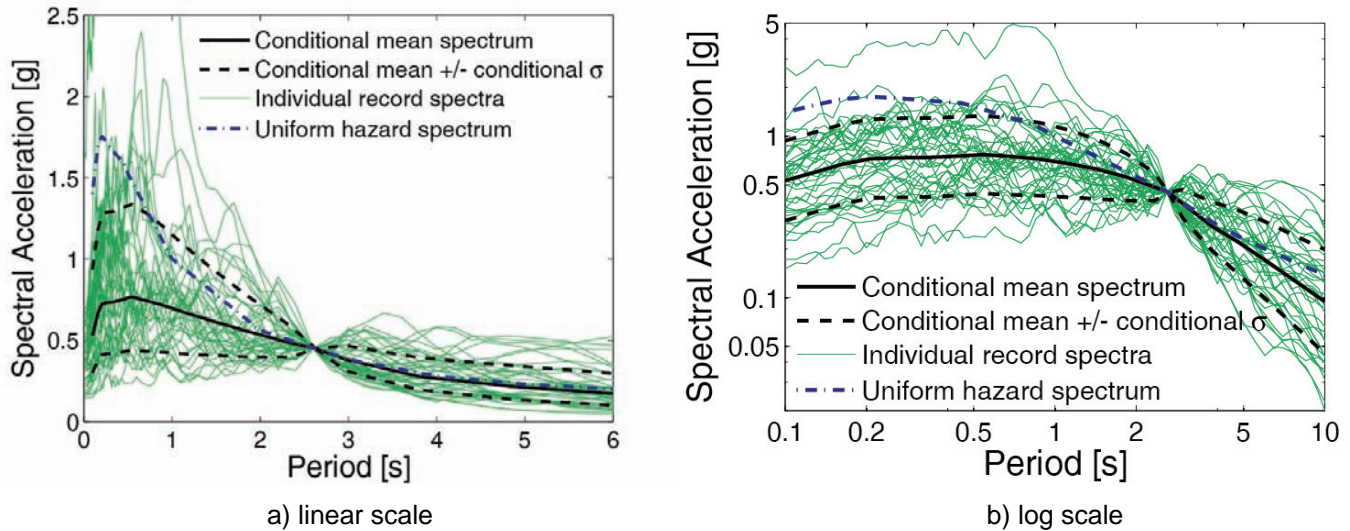
Figure 5-4   Example Conditional Spectrum for the Palo Alto site, anchored for 2% in 50-year motions at $T = 2.6$s.

5.3.6   Recommendations for Selecting a Target Spectrum for Bi-Directional Horizontal Shaking

Recommendations for the choice of target spectrum for three-dimensional analysis (i.e., requiring two horizontal components of ground motion as input) are provided in this subsection. Not all possible cases are addressed.

The recommendations assume that component deformation and story drift in low- to medium-rise buildings are due primarily to first mode response. In the presentation below, the building is assumed to have principal horizontal directions X and Y, uncoupled first mode periods of T_{1X} and T_{1Y}, respectively, an averaged first mode period $\overline{T} = 0.5(T_{1X} + T_{1Y})$, and a ratio $\lambda = T_{1X,Y} / \overline{T}$; the conditioning period is denoted T^*.

Near-fault and forward-directivity effects (including velocity pulses) should be included explicitly in hazard calculations (Shahi and Baker, 2011) and in the target spectrum, be it UHS, CMS, or CS. A narrow-banded representation of directivity effects should be used in the CMS and CS.

If the goal of response-history analysis is predicting the mean (average) deformation response of components and drift response of stories, and $0.67 \le \lambda \le 1.50$, the conditional mean spectrum with $T^* = \overline{T}$ should be used as the target spectrum. The recommended range is based on judgment. Otherwise, use either the UHS, or CMS conditioned on both T_{1X} and T_{1Y} and envelope results. Note that mean responses of components and stories computed using the UHS will generally be conservative (biased high). The use of UHS may lead to underpredictions of building response if applied at the base of a nonlinear soil column or at the boundary of a nonlinear soil

domain because more intense bedrock shaking across a broad range of frequencies may fail the 1D or 2D soil domain, thereby limiting the intensity of shaking experienced by the building.

If the goal of response-history analysis is predicting the mean (average) acceleration response of floors, where higher mode effects are expected to contribute significantly, use the UHS as the target spectrum. The mean responses computed using the UHS will generally be biased high.

If the goal of response-history analysis is predicting the distribution of component deformation response, drift response of stories, and acceleration of floor plates, use the conditional spectrum with $T^* = \bar{T}$ as the target spectrum. This is the goal of many intensity-based assessments and time (risk)-based assessment per the ATC-58-1 project. (Note that other sources of variability, such as modeling uncertainty, should also be addressed in an analysis targeting distributions of response. Although the choice of conditioning period is not critical for the CS, $\bar{T}$ is used as a default.)

As can be noted from the above recommendations, there is no single target spectrum that is best for all cases. The choice of a target spectrum will depend on the number of analyses the user is willing to perform and how the results of the analysis will be interpreted. This report has sought to clarify how to make this choice for a given situation rather than suggesting a single target spectrum that would not be appropriate in some situations.

5.4   Selecting Horizontal Ground Motions for Scaling

Recommendations are provided for selecting pairs of seed ground motions for use at distant and near-fault sites. Seed pairs should be selected from a bin of recorded motions such as the PEER NGA database (http://peer.berkeley.edu/peer_ground_motion_database), COSMOS (http://db.cosmos-eq.org/scripts/default.plx), or K-NET (http://www.k-net.bosai.go.jp). A bin of ground motion records containing pulses is presented in Appendix C. The seismic hazard at the site should be disaggregated before selecting seed motions.

Physics-based simulations of ground motions as described in Appendix D can also be used for large magnitude earthquakes at short site-to-source distances because there may be a lack of appropriate recordings, even in worldwide databases.

5.4.1 Distant Sites

The most important factor in selecting ground motions for scaling to a target spectrum is spectral shape over the period range of interest (currently $0.2T_1$ to $1.5T_1$ in ASCE/SEI 7-10). Secondary considerations are the earthquake magnitude, site-to-

source distance, and ε that dominate the hazard curve at period $\bar{T}$, and local site conditions. Selecting a pair of motions whose geometric mean spectral shape is similar to the target spectrum minimizes the need for scaling and modification. Magnitude and distance will affect strong motion duration, which may be important for buildings with components that will degrade under cyclic loading. If the mathematical model used for analysis cannot capture cyclic degradation, there is little need to consider strong motion duration in the selection process.

5.4.2 Near-Fault Sites

The two most important factors in selecting ground motions for scaling to a target spectrum are spectral shape and presence of velocity pulses. Selecting a pair of motions whose geometric mean spectral shape is similar to the target spectrum minimizes the need for scaling and modification. Velocity pulses are present in many near-fault ground motion recordings, especially in the forward-directivity region. Alavi and Krawinkler (2000), Somerville et al. (2004), Mavroedis and Papageorgiou (2003), Bray and Rodriguez-Marek (2004), Fu and Menun (2004), Baker (2007b), Shahi and Baker (2011) have all observed a relationship between pulse period and earthquake magnitude. An alternate relationship is proposed in Appendix C. Disaggregation of the seismic hazard curve will identify the combinations of earthquake magnitude, site-to-source distance and ε that dominate the hazard around period $\bar{T}$. This triplet can aid the selection of pulse periods and thus seed ground motions for later scaling.

5.5   Scaling Seed Ground Motions to a Target Spectrum

This section provides recommendations for scaling pairs of horizontal ground motions to each type of spectrum, noting that the UHS and CMS are used when mean or average estimates of responses are sought, and the CS is used when distributions of response are sought.

A period range or interval must be specified when scaling ground motions consistent with a UHS or CMS. The recommended interval is $(0.2T_{1,min}, 3T_{1,max})$ for moment-frame buildings and $(0.2T_{1,min}, 2T_{1,max})$ for shear-wall or braced frame buildings, where $T_{1,min}$ ($T_{1,max}$) is the lesser (greater) of the first mode translational periods along the two horizontal axes of the building. No period range is required with the CS.

Response-spectrum matching of a pair of horizontal ground motions is acceptable if the target spectrum is either a UHS or a CMS, if the scaled pair of motions will not include velocity pulses, and if the goal of the analysis is to calculate mean responses and not distributions of responses. Seed ground motions for spectrum matching should be selected per Section 5.4. Ground motions should be matched in pairs (Grant, 2011).

The number of sets of ground motions (2 horizontal components or 3 components) required for response-history analysis is dependent on factors that include:

- whether mean values or distributions of responses are required,

- the expected degree of inelastic response (e.g., none through collapse),

- the number of modes contributing significantly to the response quantities (e.g., story drift or floor acceleration) of interest,

- whether seed motions are selected randomly (not recommended per Section 5.4) or with explicit consideration of spectral shape,

- the quality and detail of the mathematical model of the building and the soil domain, and

- the required accuracy of the estimated values of mean and variance.

Many more sets of motions are required to estimate stable values of variance than mean. In general, the greater the mean inelastic response, the greater the record-to-record variability in the response, and the greater the number of sets of motions required for stable estimates of means and variances. More sets of motions are required if many modes contribute to response. (For example, only one motion is required to estimate the maximum elastic response of a single degree of freedom system.) The greater the required accuracy of the means (and variances if sought), the greater will be the required number of sets of ground motions. Importantly, if the mathematical model of the building is incapable of predicting cyclic component behaviors over the expected range of inelastic response, responses computed using any number (3, 7, 11, 30+) of sets of ground motions will be inaccurate.

As described in Chapter 3, design practice per ASCE/SEI 7-05 and ASCE/SEI 7-10, requires the use of a minimum of three sets of ground motions for response-history analysis. If three sets are used, peak maximum responses are used for component checking. If seven sets are used for analysis, average maximum responses can be used for component checking. Assuming seed motions are selected with explicit consideration of spectral shape and the mathematical model can trace cyclic component behaviors accurately over the expected ranges of inelastic response, no less than seven sets of ground motions should be used to estimate values of mean response and no less than 30 sets of motions should be used to estimate distributions of responses. Calculations of the probability of collapse of a building or the construction of collapse fragility curves for loss calculations per ATC-58-1 should use no less than 30 sets of ground motions because the variability in response will be great.

5.6   Other Important Factors

5.6.1 Vertical Ground Motion

Vertical ground shaking can damage some types of buildings and should be considered in these cases. Buildings with long-span floors, floors supporting sensitive equipment, industrial facilities supporting massive equipment (e.g., boilers), and long cantilevers are candidates for analysis including vertical shaking. Vertical ground motions have traditionally been generated in two ways: (1) scaling to a target UHS for vertical shaking similar to that described previously in this report; and (2) scaling the amplitude of the seed vertical component by the same amplitude scaling factor used for the pair of horizontal motions. The target spectrum for (1) can be computed by either probabilistic seismic hazard analysis using ground motion prediction equations for vertical shaking, or multiplying the ordinates of the UHS for horizontal shaking by empirically based vertical-to-horizontal ratios that may be period-dependent.

A new approach, consistent with the CS introduced previously, is to compute a vertical spectrum conditioned on a target horizontal spectral value. This calculation is performed similarly to the CS except a period-dependent vertical-to-horizontal correlation coefficient is used instead of a horizontal-to-horizontal correlation coefficient. Gulerce and Abrahamson (2011) have operationalized this new procedure. The ordinates of target vertical spectra obtained with this procedure are generally much lower than those obtained using a uniform hazard calculation or by applying empirical vertical-to-horizontal ratios to a horizontal UHS. For those cases where vertical shaking governs a design or dominates a performance assessment, ground motions should be scaled to either a vertical UHS or a vertical CS or CMS, where the conditioning period is related to modal properties in the vertical direction.

5.6.2 Ground Motion Input to a Mathematical Model

Guidelines for Performance-Based Seismic Design of Tall Buildings (PEER, 2009) and NIST GCR 11-917-14, *Soil-Foundation-Structure Interaction for Buildings Structures* (NIST, 2011) both recommend inclusion of subterranean building levels in the mathematical model. Time-domain nonlinear response-history analysis of the soil-structure system can be performed per Figure 5-5a and input motions for this analysis would be applied at a rock outcrop below the building. Two other options are shown in Figures 5-5b and c. The coarser model of the two is shown in Figure 5-5b wherein the ground motions, either free-field surface motions or foundation input motions, are applied at the underside of the basement. A better model, although poorer than that of Figure 5-5a but computationally more efficient, is shown in Figure 5-5c wherein the soil domain in the vicinity of the building is modeled with springs and dashpots and identical horizontal ground motions, either free-field

surface motions or foundation input motions, are input at each basement level in the building.

(a) Complete system   (b) Model for service-level earthquake   (c) Model for maximum-considered earthquake
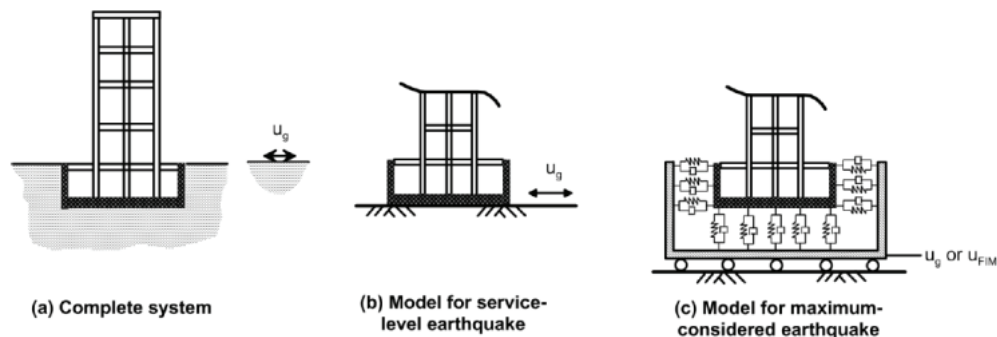
Figure 5-5   Illustration of ground motion input methods to the base of a structural model (from NIST, 2011).

5.6.3 Orientation of Components of Ground Motion

There is little and inconsistent guidance in codes and standards on how horizontal components of ground motion are to be oriented with respect to the principal horizontal axes of a building. Although not part of the scope of this project, the choice is related to the proximity of the building to the causative fault and some discussion is warranted.

5.6.3.1 Distant Sites

Section 12.5.3 of ASCE/SEI 7-10 specifies that the "orthogonal pairs of ground motion acceleration histories" should be "applied simultaneously" but provides no direction on how pairs of motions should be oriented. *Recommendations for the Seismic Design of High-Rise Buildings* (CTBUH, 2008) states that motions should be oriented randomly and there is no need to apply individual pairs of motions in multiple orientations. PEER *Guidelines* (PEER, 2009) require the components to be applied along the principal directions of the building but does not specify how the ground motion components should be oriented before they are applied to the structural model (e.g., randomly or oriented according to a maximum direction).

There is no systematic directional dependence to ground motion at distant sites (e.g., Huang et al., 2009). A pair of scaled horizontal motions can be oriented randomly with respect to a horizontal axis of a building (regardless of whether a maximum direction spectrum or a geometric mean spectrum is used to scale the horizontal ground motions) or applied as the seed motions were recorded with respect to the strike of the causative fault (i.e., if the seed motions were recorded in the fault-normal and fault-parallel directions, apply the corresponding scaled motions in the same directions). Each pair of motions need to be applied to the model in only one orientation.

5.6.3.2 Near-Fault Sites

For near-fault sites, the scaled motions need to be applied in the same orientations as the corresponding seed motions were recorded with respect to the strike of the causative fault.

5.7   Selecting and Scaling Ground Motions per ASCE/SEI Standard 7

This section provides recommendations for best applying the rules on ground motion selection and scaling provided in two editions of ASCE/SEI Standard 7. The text seeks to clarify the application of these rules but not change the rules.

5.7.1   Recommendations for ASCE/SEI 7-05

The ASCE/SEI 7-05 rules governing selection and scaling of pairs of horizontal ground motions require the specification of a target spectrum and a period range for scaling.

The intensity measure used to define the acceleration response spectrum is not defined in ASCE/SEI 7-05 in terms of a specific direction of horizontal response (e.g., average or maximum direction of response in the horizontal plane), but may be assumed to represent average response in the horizontal direction. The Maximum Considered Earthquake (MCE) ground motion maps in Chapter 22 of ASCE/SEI 7-05 were developed by the USGS using empirical ground motion relations that characterize geometric mean response for sites in the Western United States, and theoretical ground motion relations that characterize arbitrary (random) response for sites in the Central and Eastern United States.

The target spectrum of ASCE/SEI 7-05 is defined as 1.3 times the design spectrum for comparison with the square root of the sum of the squares (SRSS) combination of the two horizontal components of selected earthquake records over the period range of interest. The factor of 1.3 implicitly acknowledges that the design spectrum is based on average horizontal response, and that the SRSS combination of horizontal components produces spectral response that is inherently higher than average response (e.g., by as much as 1.4 times the average when the two horizontal components have the same value of response spectral acceleration at the period of interest). The intent of ASCE/SEI 7-05 is to scale records such that the response spectra of the scaled records are, on average, about equal to, but not less than, the design spectrum over the period range of interest.

The period range for scaling is $0.2T$ to $1.5T$, where T is the first mode period. The upper limit on the period range of $1.5T$ is intended to account for period elongation due to inelastic action, and $0.2T$ is intended to capture higher modes of response. ASCE/SEI 7-05 is silent as to how this scaling range should be modified if the first

mode periods along the horizontal translational axis are both uncoupled and substantially different. In this case, to capture second mode response and period lengthening in each principal direction of response, the range should be taken as (150% of the greater first mode period, 20% of the smaller first mode period). For example, if the first mode periods along the two horizontal axes are 3 seconds and 1.5 seconds, the period range for scaling shall be 4.5 seconds and 0.3 seconds, respectively.

5.7.1.1 Sites Distant to Active Faults

ASCE/SEI 7-05 requires selection of pairs of ground motions from individual recorded events having magnitude, site-to-source distance, and source mechanisms that are consistent with those that control the ground motions at the site. Where the required number of recorded ground motions is not available, ASCE/SEI 7-05 permits the use of simulated ground motion records. Although typically considered during record selection, ASCE/SEI 7-05 does not require selected ground motion records to be obtained from sites with the same site geologic conditions (i.e., soil type) as that of the site of interest.

All these parameters (magnitude, site-to-source distance, source mechanism, and site geology), as well as regional geology (e.g., basins), affect the amplitude, frequency content, and duration of earthquake ground motion and the level and shape of the motion's response spectrum. Spectral shape, although not mentioned in ASCE/SEI 7-05, is important because the scaling procedure of ASCE/SEI 7-05 is facilitated when the shape of the SRSS spectra for each pair of horizontal component ground motions in the set of 3 or more is similar to the shape of the target spectrum in the period range of $0.2T$ to $1.5T$.

Two procedures that are widely used to scale ground motions per ASCE/SEI 7-05 are amplitude scaling and amplitude scaling and modification of frequency content. The amplitude scaling procedure consists of applying a constant scale factor to all acceleration ordinates of each pair of horizontal components (different scale factors may be selected for each pair). The scale factors are selected to best achieve agreement between the average SRSS spectrum and the target spectrum over the period range of $0.2T$ to $1.5T$. The combination of amplitude scaling and frequency-content modification (commonly referred to as spectrum matching) consists of modifying the frequency content of each horizontal component after amplitude scaling has been applied. Constant amplitude scaling will usually result in an average SRSS spectrum that is not as close a match to the target spectrum as the average SRSS spectrum obtained from the spectrum-matching procedure. Variability in the spectral demand is lost if records are matched to the spectrum but some is retained if the records are amplitude scaled, although whether sufficient variability is maintained with amplitude scaling is not known. Thus, the use of spectrum-matched

records will provide more accurate estimates of the mean or average structural response, but the amplitude scaling method will provide greater variability in the response.

Spectrum matching or frequency-content modification using either time- or frequency-domain procedures is acceptable. However, frequency-domain procedures, consisting of modifying the real and imaginary parts of the record's Fourier Transform by the same factor to preserve the phase angle at a given frequency, sometimes produce records that have a sine-wave appearance over certain portions of the duration, which is generally in the low amplitude segments at the beginning and end of the record. This phenomenon is less often observed in records that are spectrum matched with time-domain procedures, but in either case it is rarely observed when the initial fit between the response spectrum of the record (after amplitude scaling) and the design spectrum are reasonably close over the period range of $0.2T$ to $1.5T$.

Section 16.1.3.2 of ASCE/SEI 7-05 defines the precision required for scaling ground motions, namely, the average SRSS spectrum of the ensemble of horizontal component SRSS spectra does not fall below the target spectrum by more than 10% over the period range of $0.2T$ to $1.5T$, that is, the average SRSS spectrum must be at least 117% ($0.9 \times 130\%$) of the design spectrum in this period band. Conventional practice is to scale each pair of ground motions to meet this criterion. This approach is easily accomplished with the spectrum-matching procedure, but regardless of the approach or scaling procedure, the usual goal is to have the average SRSS be at the level of the target spectrum over the period range, with few (if any) narrow period bands where the average SRSS spectrum is at the minimum acceptable (117%) level.

5.7.1.2 Sites Close to Active Faults

Sites close to active faults, say 15 km for faults capable of generating earthquakes of magnitude 7.25 and 20 km for faults capable of generating magnitude-8 earthquakes, will likely experience the effects of near-fault shaking. For these sites, a correction to the design spectrum is warranted, if current or past ground motion prediction equations are used for the seismic hazard computations. The design spectrum should be adjusted upwards to account for average directivity effects by applying the first of the correction factors proposed by Somerville et al. (1997), or some fraction thereof, in the analysis. If Next Generation Attenuation (NGA) relationships (Power et al., 2008) are used for the hazard analysis, the fraction noted above will likely range between 0.5 and 1.0 because NGA database of recorded strong motions is still deficient in earthquake records from large magnitude events (greater than magnitude 7.5) at small site-to-source distances. The correction is trivial for deterministic analysis and more complicated for probabilistic analysis because the possible location of the epicenter of each fault must be considered a random variable and the

period-dependent correction factors will differ for each simulation in the analysis (Abrahamson, 2000).

Recordings of large magnitude earthquakes at small site-to-source distance will generally exhibit larger spectral demand normal to the causative fault (fault normal, FN) than parallel to the fault (fault parallel, FP) at periods greater than 0.5 second, when the fault rupture propagates toward the recording station, a phenomenon called forward directivity. Disaggregation of the seismic hazard at the site into dominant magnitude-distance pairs is a key to proper selection of seed motions. Pairs of ground motions selected for scaling at sites in the near-fault region should be recorded for similar magnitude earthquakes as indicated by the disaggregation and at similar site-to-source distances, so as to ensure an appropriate difference in the FN and FP spectral demands and strong motion duration in the seed motions. Records from distant sites should not be used as seed motions for near-fault sites.

The scaling process is identical for near-fault and distant sites once the seed motions are selected.

5.7.2 Recommendations for ASCE/SEI 7-10

The key differences between the procedures in ASCE/SEI 7-05 and ASCE/SEI 7-10 are the definition of the intensity measure and the target spectrum.

The intensity measure used to define response spectral acceleration in ASCE/SEI 7-10 is in the "maximum direction" of response (i.e., maximum response in the horizontal plane at the period of interest). The Risk-Adjusted Maximum Considered Earthquake (MCE_R) ground-motion maps in Chapter 22 of ASCE/SEI 7-10 were developed by the USGS using factors (e.g., 1.1 at short-periods and 1.3 at a period of 1 second) to convert values of geometric mean or random ground motions to values representing maximum response in the horizontal plane.

The target spectrum of ASCE/SEI 7-10 is now defined as 1.0 times the design spectrum for comparison with the SRSS combination of the two horizontal components of selected earthquake records over the same period range of interest, namely, 0.2T to 1.5T. The factor of 1.0 factor recognizes that the design spectrum is now based on maximum response in the horizontal plane, and that the SRSS combination of horizontal components produces spectral response that is approximately equal to maximum response. The intent of ASCE/SEI 7-10 design requirements is to scale records such that the maximum responses in the horizontal plane of the scaled records are, on average, about equal to, but not less than, the design spectrum over the period range. Further, although the definition of the response spectral intensity parameter has changed (from average to maximum response in the horizontal plane), a set of records scaled in accordance with

ASCE/SEI 7-10 should have approximately the same intensity as the same set scaled in accordance with ASCE/SEI 7-05.

5.8   Recommendations for Future Study

This report provides guidance to design professionals on selection and scaling of ground motions for the purpose of nonlinear response-history analysis. Three problem-focused studies were undertaken as part of this project to inform the guidance and recommendations provided above. In addition, gaps in the current knowledge related to selecting and scaling ground motions for seismic design and performance assessment were identified. Some of the key gaps are listed below. Closing these and other gaps will require close collaboration of engineering seismologists, geotechnical engineers, structural engineers and loss modelers. The key gaps identify the need for:

- A technical basis for the number of sets of ground motions necessary to compute mean values of responses and distributions of responses,

- Incorporation of forward directivity in probabilistic seismic hazard analysis and target spectra,

- Characteristics of ground motions in a record set that include velocity pulses,

- Scaling a pair of motions containing single-sided pulses (fling step) and double-sided pulses to a target spectrum,

- Assessing the adequacy of a design where the distributions of responses are bi-modal and not lognormal or normal,

- Assessing the adequacy of a design if one or more analyses indicates collapse,

- Extending the conditional spectra approaches to address two horizontal components of ground motion and multiple modes along each horizontal axis,

- Increased number of seed sets of strong ground motions in the Central and Eastern United States (to be augmented by physics-based simulations), and

- Increased number of ground motions from small site-to-source distances.

Appendix A
Ground Motion Selection Based on Conditional Spectra

A.1   Introduction

This appendix presents a study of the impact of conditioning period on structural analysis results obtained from ground motions selected using Conditional Spectrum concepts. The Conditional Spectrum calculation has potentially important applications to ground motion selection for performance-based engineering, as it provides a quantitative means to model the distribution of response spectra associated with ground motions having a target spectral acceleration at a single conditioning period. Calculation of this spectrum is now fairly well documented, and algorithms for selecting ground motions to match this spectrum are also available (Jayaram et al., 2011). One unresolved issue is how best to condition this target spectrum for cases where the structure of interest is sensitive to excitation at multiple periods due to nonlinearity and multi-mode effects. In such cases, there is not yet consensus regarding what period to condition on when computing the Conditional Spectrum.

As will be discussed below, a key distinction when studying this issue is whether one is performing a time-based or intensity-based assessment. If one is performing a time-based assessment (i.e., computing the annual frequency of an engineering demand parameter exceeding a value, y) then it is found that if the Conditional Spectrum is used as the ground motion selection target, the resulting structural reliabilities are comparable regardless of the conditioning period used for seismic hazard analysis and ground motion selection. On the other hand, if one is performing an intensity-based assessment (i.e., computing the mean or the distribution of an engineering demand parameter associated with a given $S_a(T^*)$), then the answer will vary depending upon the conditioning period, T^*, that is chosen. This is because changing the conditioning period effectively changes the question that is being asked (i.e., "what is the response given a ground motion intensity level?" where the ground motion intensity definition is changing). The difference in conclusions for these two analysis cases will be important for the conclusions at the end of this appendix.

In this appendix, seismic hazard analysis, ground motion selection, and nonlinear dynamic structural analysis are performed to assess the performance of a 20-story concrete frame building. This analysis is performed using widely varying conditioning periods and the results are studied for each case. Additional similar results for 11 other structures having a range of heights and periods were performed

to illustrate the generality of the observations presented here. The results supporting these calculations are documented by Lin (2012). A variety of structures were analyzed, yet they are all two-dimensional models of frame structures. While the generality of these models is limited, the discussion of the analysis approach is general and is likely to be applicable to a broader range of structural models.

A.2   Background

Recent work has illustrated that scaling up arbitrarily selected ground motions to a specified spectral acceleration, S_a, level at period T can produce overly conservative structural responses, because a single extreme $S_a(T)$ level of interest for engineering analysis does not imply occurrence of equally extreme S_a levels at all periods (e.g., Baker and Cornell, 2006b). The Conditional Mean Spectrum (CMS) and Conditional Spectrum (CS) have been developed to describe the expected response spectrum associated with a ground motion having a specified $S_a(T)$ level (Baker and Cornell, 2006b; Baker, 2011; Lin et al., 2011). The Conditional Mean Spectrum for a rare (i.e., positive ε) $S_a(T)$ level has a relative peak at T and tapers back towards the median spectrum at other periods. The Conditional Spectrum differs from the Conditional Mean Spectrum only in that it also considers the variability in response spectra at periods other than the conditioning period (which by definition has no variability).

The Conditional Spectrum approach for selecting and scaling ground motions requires the user to specify a conditioning period (denoted here as T^*) that is then used to compute corresponding distributions of spectral values at all other periods, and ground motions can then be selected to match these spectral values. These motions can then be used as inputs to dynamic structural analysis to compute engineering demand parameters (EDP). When calculating maximum interstory drift in buildings (also referred to as maximum story drift), T^* is often chosen to be the building's elastic first-mode period, T_1. This is done because $S_a(T_1)$ is often a "good" predictor of that engineering demand parameter, so scaling ground motions based on this parameter can lead to reduced scatter in resulting response predictions and thus minimizes the required number of dynamic analyses (Shome et al., 1998).

There are two common practical situations, however, where the application and implications of using the Conditional Spectrum concept is not yet easily applied. The first case is for prediction of engineering demand parameters that are not dominated by the first-mode structural response due to contributions from higher modes, such as peak floor accelerations, or to longer periods associated with reduced-stiffness nonlinear response such as the onset of collapse (Haselton and Baker, 2006). The second case is for selection of ground motions prior to identification of a single conditioning period, because the structure is not yet designed or because multiple designs having multiple periods are being considered. In both of these situations, one

is faced with the possibility of using a Conditional Spectrum not conditioned on S_a at the period that most efficiently predicts structural response. Even in cases where one does know an effective conditioning period for computing the CMS or CS, the question still arises as to whether a comparable-intensity S_a at some other conditioning period might produce a larger level of engineering demand parameters than the primary spectrum being considered.

The hypothesis of this appendix is that if the analysis objective is to compute the annual rate of the structure experiencing EDP > y, and if the ground motions are selected to have proper conditional mean and conditional variability, then the resulting answer is relatively insensitive to the choice of conditioning period. There are still benefits to selecting a "good" conditioning period, as will also be discussed, but the primary focus is on the robustness of the specific above-mentioned calculation to variations in conditioning period. While some researchers have previously suggested that the choice of conditioning period may not be critical to estimating reliability (e.g., Abrahamson and Yunatci, 2010; Shome and Luco, 2010), those authors did not perform a full reliability assessment using nonlinear dynamic analyses, and did not consider spectral variability at periods other than the conditioning period. To demonstrate empirical evidence for the hypothesis, repeated time-based assessments of drift hazard (i.e., rate of EDP > y) using nonlinear dynamic analysis are performed.

A.3   Demonstration Analysis

To illustrate the effect of conditioning period, two parallel performance assessments are performed to predict the annual rate of exceeding various levels of maximum interstory drift ratio (MIDR), using ground motions selected to match Conditional Spectra conditioned on two periods. Next, the effect of repeating the procedure using other conditioning periods and a comparison to an assessment with ground motions selected to match a Uniform Hazard Spectrum or Conditional Mean Spectrum will be considered.

Eleven additional structures have been analyzed using the same procedure. In addition to the MIDR results, comparable results for the rate of exceeding peak floor accelerations and individual-story drifts and accelerations have also been computed. Those additional results are documented by Lin (2012), to show the generality of the results.

A.3.1 Building Site and Structural Model

The structure being studied is located in Palo Alto, California, approximately 10 km from the San Andreas Fault. The structure utilized in this study is a 20-story reinforced concrete special moment frame with the perimeter frame designed to resist lateral forces. This building was designed for work on the FEMA P-695 report

(FEMA, 2009a), and is denoted Building 1020 in that study. It is modeled in OpenSEES (2011), with strength deterioration (both cyclic and in-cycle) and stiffness deterioration that is believed to reasonably capture the responses up to the point of dynamic-instability collapse. The first three elastic modal periods are 2.6s, 0.85s, and 0.45s. The building was designed per IBC 2003, *International Building Code* (ICC, 2003), for a site with a slightly lower design ground motion level than the site being utilized in this study (by approximately 20%). This building serves as a testbed to evaluate the ability to robustly estimate the annual rate of some engineering demand parameters exceeding various thresholds. This calculation is not trivial, as the building's MIDR is affected by multiple modes excited at multiple periods, and experiences effective period lengthening as it behaves nonlinearly up to the collapse level for high intensity ground motions.

A.3.2 Seismic Hazard Analysis and Ground Motion Selection

Seismic hazard analyses to obtain ground motion hazard curves for spectral accelerations at four periods (0.45s, 0.85s, 2.6s, and 5s) were performed, corresponding to the first three modal periods of the building and a lengthened period that may be a good predictor of nonlinear response. For each spectral period and amplitude of interest, the rate of exceeding that amplitude and a disaggregation distribution providing the causal magnitudes, distances and ε values associated with spectral accelerations of that amplitude were obtained. Figure A-1 illustrates a typical hazard curve and disaggregation result. All of these data come from the U.S. Geological Survey online tools (USGS, 2008). Ten rates of exceedance are considered for each conditioning period, ranging from 0.023 to 0.00005 per year (i.e., 50% in 30 years to 1% in 200 years probability of exceedance), as those are the exceedance rates for which the USGS provides the needed hazard and disaggregation information. Hazard curves and disaggregation results are not provided for exactly the conditioning periods used here, so interpolation between hazard results at adjacent periods is utilized in some cases.

Using the hazard curve and disaggregation information for a particular conditioning period, the Conditional Spectrum calculation is used to compute the mean and standard deviation of logarithmic response spectral values at all other periods, conditioned on an amplitude of $S_a(T^*)$. The mean and standard deviation of $\ln S_a$ are given by the following equations (Baker and Cornell, 2005).

$$\mu_{\ln S_a(T_i)|\ln S_a(T^*)} = \mu_{\ln S_a}\left(M,R,T_i\right) + \rho\left(T_i,T^*\right)\varepsilon\left(T^*\right)\sigma_{\ln S_a}\left(T_i\right) \qquad \text{(A-1)}$$

$$\sigma_{S_a(T_i)|S_a(T^*)} = \sigma_{\ln S_a}\left(T_i\right)\sqrt{1-\rho^2\left(T_i,T^*\right)} \qquad \text{(A-2)}$$

where $\mu_{\ln S_a}\left(M,R,T_i\right)$ and $\sigma_{\ln S_a}\left(T_i\right)$ are the predicted mean and standard deviation from a ground motion prediction model (Campbell and Bozorgnia (2008) in this case), $\rho(T_i,T^*)$ is the correlation between the spectral values at period T_i and the

conditioning period T^* (obtained from Baker and Jayaram 2008), and M, R and $\varepsilon(T^*)$ come from the disaggregation distributions described in the previous section.
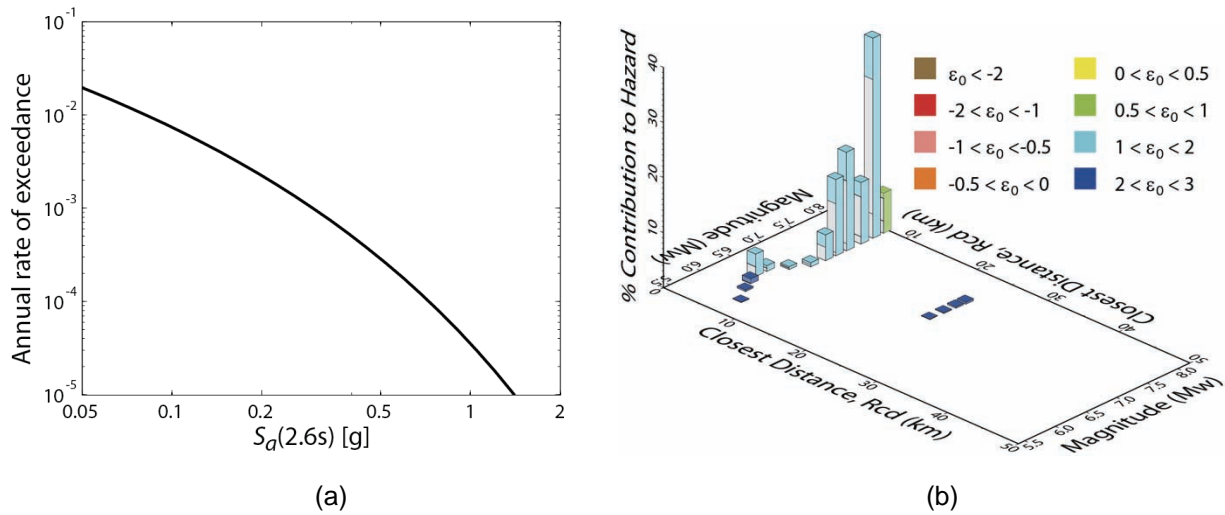
Figure A-1   Plots showing: (a) Hazard curve for S_a(2.6s) for the example site in Palo Alto; (b) example disaggregation results, providing the distribution of magnitude, distance and ε values associated with occurrence of a given $S_a(T^*)$ level, adapted from USGS (2008).

In this case the M, R and $\varepsilon(T^*)$ values used are the mean values from disaggregation at the given S_a (T^*) level; this is an approximation relative to the use of the full distributions of potential M, R and $\varepsilon(T^*)$ values. This approximation is known to be reasonably accurate in predicting conditional mean spectra at this site, but to slightly underestimate conditional standard deviations (Lin et al., 2011) - an issue that will be discussed later.

The mean spectra associated with several amplitudes for S_a(0.85s) and S_a(2.6s) are shown in Figure A-2. Note the increasing "peaked-ness" of the spectra at the conditioning period as the amplitude at that period increases. This is because the Conditional Spectrum accounts for the fact that those high-amplitude values are larger-than-mean values for the earthquake causing the ground motion (i.e., they are "positive ε") and that the spectral values at other periods are unlikely to be comparably high.
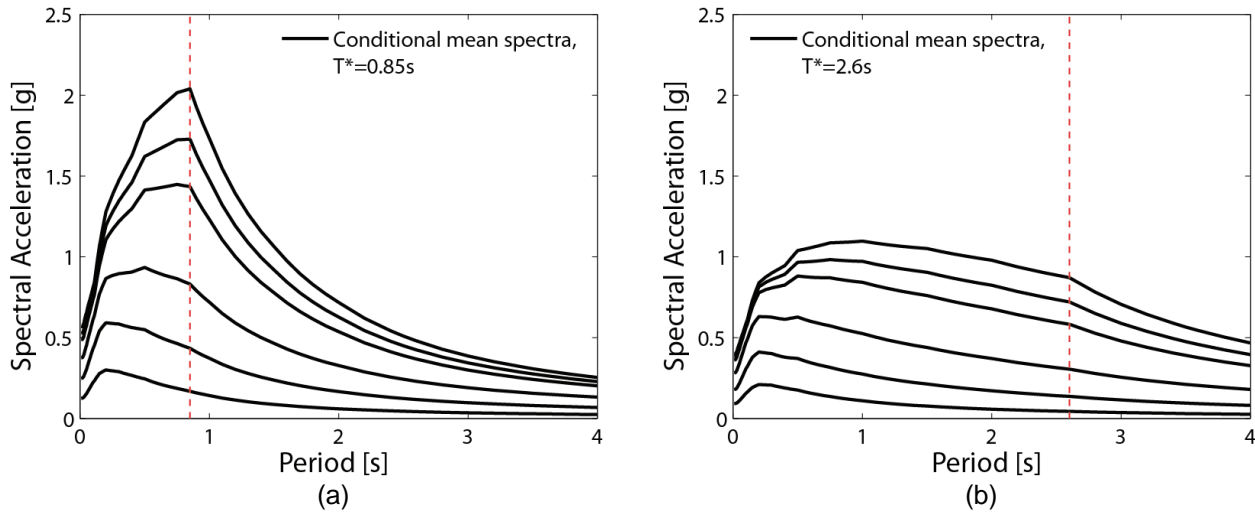
Figure A-2   Conditional Mean Spectra at six rates of exceedance for the example site: (a) conditioned on S_a(0.85s); and (b) conditioned on S_a(2.6s).

For each conditioning period and spectral amplitude, forty recorded ground motions were selected and scaled such that their spectra matched the target mean and standard deviations computed using Equations A-1 and A-2. Figure A-3 shows the target spectra and selected ground motions' spectra for 0.85s and 2.6s conditioning periods, at S_a amplitudes with 2% probability of exceedance in 50 years. Ground motions were selected from the PEER NGA database (Chiou et al., 2008). No further constraints were placed on the ground motion selection (e.g., magnitudes and distances) other than limiting scale factors to less than four, with the primary selection focus being on the match of the ground motion spectra to the target spectra. This was done because the structure response parameter of interest in this case is thought to be most closely related to spectral values. Also, earthquake magnitude and distance affect this structural response primarily as they relate to spectral values (which are accounted for carefully) rather than other ground motion parameters such as duration. More details regarding the ground motion selection algorithm and its implications are provided by Jayaram et al. (2011).

A.3.3   Structural Analysis and Drift Hazard

With the selected ground motions (40 motions at each of 10 intensity levels, for a given conditioning period), dynamic analysis of the structure described above was performed. Results are shown in Figure A-4 for the ground motions selected conditioned on two periods. Some analyses resulted in collapse of the building, and Figure A-5 shows the collapse data for each choice of T^*.
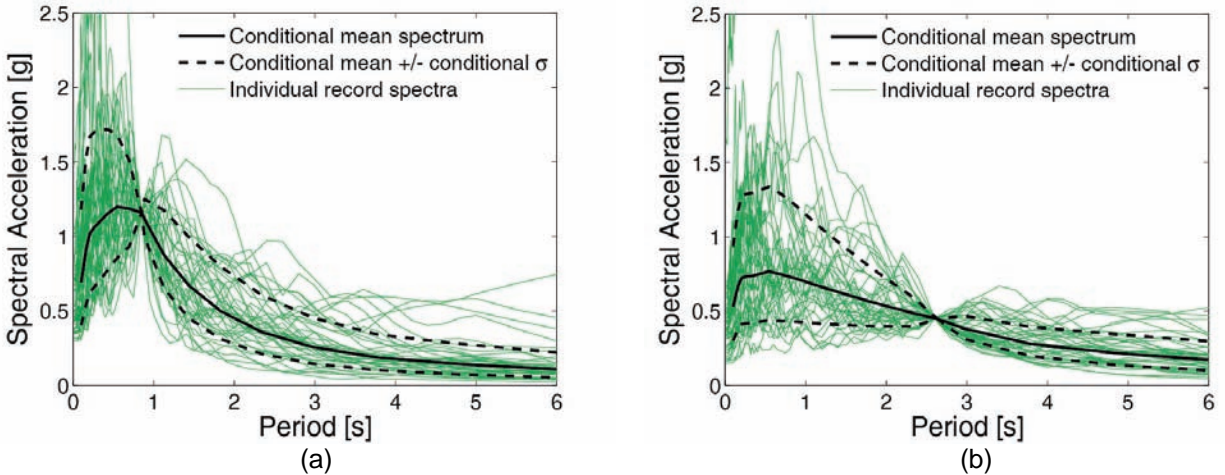
Figure A-3   Conditional Spectra for a site at Palo Alto, California, with spectral acceleration at the conditioning period having a 2% probability of exceedance in 50 years: (a) conditioned on $S_a(0.85s) = 1.2$ g; and (b) conditioned on $S_a(2.6s) = 0.45g$.

Before proceeding to use the data in the primary calculation of interest here, two notable observations can be made. First, $S_a(2.6s)$ appears to be a more efficient predictor of MIDR than $S_a(0.85s)$, as indicated by the average log standard deviations for a given S_a of 0.33 and 0.44, respectively (a difference that is visually apparent in the scatter of the Figure A-4 data). Second, the median MIDR given $S_a(T^*)$ with a 2% in 50 years exceedance probability is not the same in both cases. For the $S_a(0.85s)=1.2g$ case, the median MIDR = 1.6%. For the $S_a(2.6s)=0.45g$ case, the median MIDR = 2.3%. These two values are indicated with red lines in Figure A-4a and b, respectively. These median values are in some sense similar to the values that would be of interest in an MCE-based building code check in United States practice, and here it is clear that the result depends upon the chosen conditioning period. The primary interest here, however, is on the annual rate of exceeding an MIDR level.
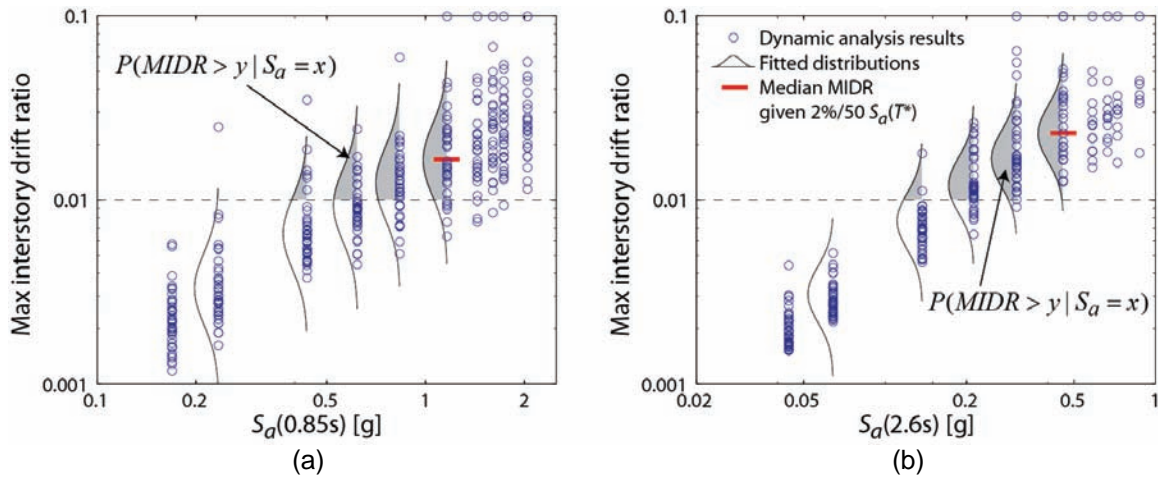
Figure A-4   Maximum interstory drift ratios from dynamic structural analysis, for ground motions selected conditioned on :(a) $S_a(0.85s)$; and (b) $S_a(2.6s)$.
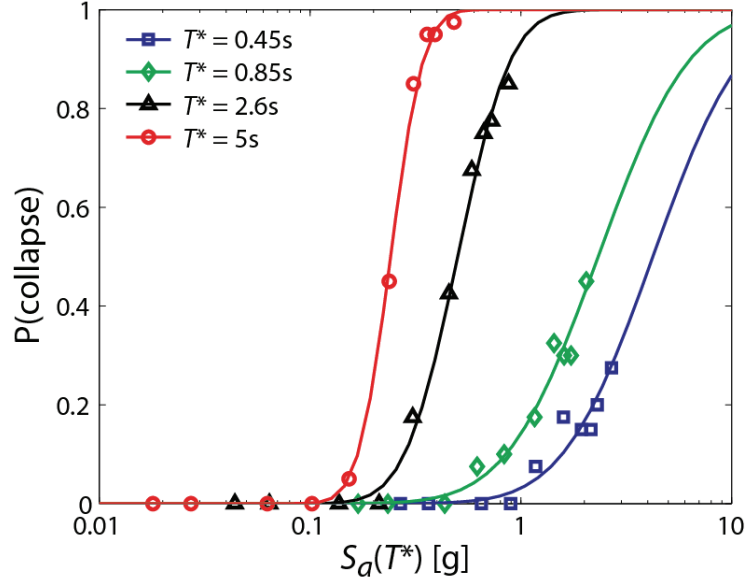
Figure A-5   Collapse data and fitted fragility functions, conditioned on spectral accelerations at different periods. Symbols indicate counted fractions of collapse from the dynamic analyses, and lines indicate fitted fragility functions.

For the primary calculation of interest the results from Figure A-4 and Figure A-5 are combined with the hazard curves for the corresponding conditioning S_a to compute the annual rate of exceeding a given MIDR level as follows:

$$\lambda\left(MIDR > y\right) = \int P\left(MIDR > y \mid S_a\left(T^*\right) = x\right) \mid d\lambda\left(S_a\left(T^*\right) > x\right) \mid \qquad \text{(A-3)}$$

where $d\lambda\left(S_a\left(T^*\right) > x\right)$ is the derivative of the hazard curve for $S_a(T^*)$, $P\left(MIDR > y \mid S_a\left(T^*\right) = x\right)$ is the probability of MIDR exceeding y given a ground motion with $S_a\left(T^*\right) = x$, and $\lambda\left(MIDR > y\right)$ is the rate of MIDR exceeding y. The calculation in Equation A-3 is often referred to as the first step of the "PEER Integral," (Cornell and Krawinkler, 2000), a "drift hazard" calculation (Krawinkler and Miranda, 2004), or a "time-based assessment" (ATC, 2011).

When implemented numerically, the continuous integral of Equation A-3 is replaced with a summation over a discrete set of considered $S_a(T^*)$ amplitudes, as follows:

$$\lambda\left(MIDR > y\right) = \sum_{i=1}^{n} P\left(MIDR > y \mid S_a\left(T^*\right) = x_i\right) \lambda\left(S_a\left(T^*\right) = x_i\right) \qquad \text{(A-4)}$$

where n is the number of considered $S_a(T^*)$ amplitudes, and $\lambda\left(S_a\left(T^*\right) > x_i\right)$ is the rate of observing $S_a(T^*)$ amplitudes in some small range represented by the discrete amplitude x_i. Here $\lambda\left(S_a\left(T^*\right) > x_i\right)$ is computed from the hazard curve $\lambda\left(S_a\left(T^*\right) > x\right)$ via finite differences as follows:

$$\lambda\left(S_a\left(T^*\right)=x_i\right)=\frac{\lambda\left(S_a\left(T^*\right)>x_{i-1}\right)-\lambda\left(S_a\left(T^*\right)>x_{i+1}\right)}{2} \qquad \text{(A-5)}$$

where the x_i are sorted in increasing order (from the smallest considered value at x_1 to the largest at x_n) and where slight adjustments are made to the formula at the minimum and maximum values to account for endpoints.

For the results shown here, the probability of MIDR > y was obtained by assuming a lognormal distribution for the non-collapse MIDR results at a given $S_a(T^*)$, and estimating the mean and standard deviation of the log of MIDR at each $S_a(T^*)$ level from the structural analysis data illustrated in Figure A-4; the means and standard deviations were smoothed across $S_a(T^*)$ levels, to reduce the small sample size variability in these estimates (mean lnMIDR was modeled as linearly varying with lnS_a and the standard deviation of lnMIDR was modeled as constant—these models are used to compute the fitted distributions illustrated in Figure A-4). The probability of collapse data from Figure A-5 was considered by counting the fraction of collapses at each $S_a(T^*)$ level, and then using a maximum likelihood approach to fit a lognormal fragility function to those data, as documented at the following website: http://www.stanford.edu/~bakerjw/fragility.html. The probability of MIDR > y was then computed by assuming that all collapse cases exceed y, and fitting a lognormal distribution to the non-collapse MIDRs, so that the prediction is given by

$$P\left(MIDR>y\mid S_a\left(T^*\right)=x_i\right)=P\left(C\right)+\left(1-P\left(C\right)\right)\left(1-\Phi\left(\frac{\ln y-\mu_{\ln MIDR}}{\beta_{\ln MIDR}}\right)\right) \qquad \text{(A-6)}$$

where $P(C)$ is the probability of collapse given $S_a(T^*) = x_i$ estimated from the collapse fragility function and $\mu_{\ln MIDR}$ and $\beta_{\ln MIDR}$ are the mean and standard deviation, respectively, of lnMIDR values given $S_a(T^*) = x_i$. This procedure has been proposed elsewhere (e.g., Shome and Cornell, 1999) and is commonly used for calculations of this type.

Using this approach, Equation A-4 was evaluated using the four sets of ground motion hazard curves, ground motions, and resulting structural responses associated with each of the considered T^* values. The resulting drift hazard curves are shown in Figure A-6. The predictions of the rates of exceeding a given MIDR are very consistent regardless of the conditioning period (except for the case of T^*=0.45s when MIDR > 0.02, which will be discussed later).
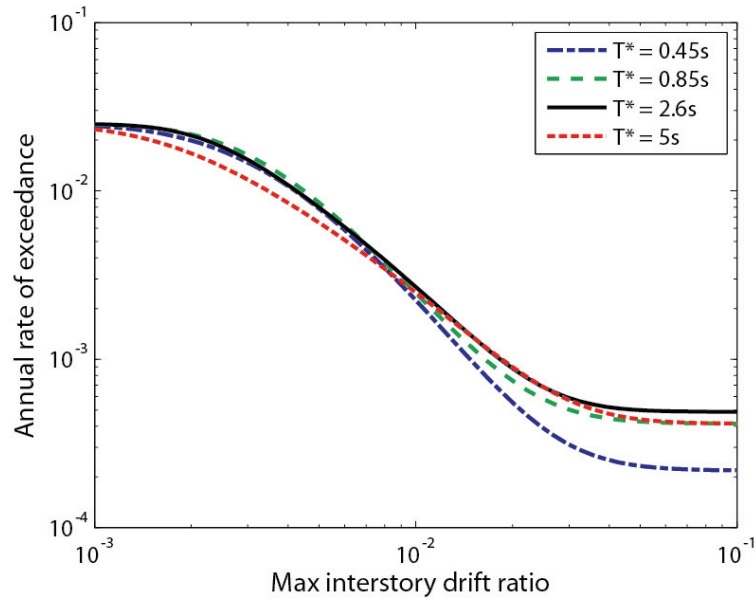
Figure A-6   Drift hazard curves obtained using hazard curves and ground
             motions with four different conditioning periods.

A.3.4   Hazard Consistency of Ground Motion Response Spectra

The relative consistency of results in Figure A-6 may be surprising at first, so the
data underlying these results are more closely examined. In Figure A-7, the response
spectra of all ground motions selected and scaled to match $S_a(2.6s)$ and $S_a(0.85s)$
targets at all amplitudes are plotted; the shapes of the spectra are "pinched" at 0.85s
and 2.6s in Figure A-7a and Figure A-7b, respectively, since only ten $S_a(T^*)$
amplitudes were used here. At other periods, the spectra are more varied, as the
amplitudes at other periods have variability even when $S_a(T^*)$ is known with
certainty. But these ground motions were selected to maintain proper conditional
means and variances, ensuring that the distributions of spectra at all periods are still
consistent with all known hazard information for the site being considered (and it is a
problem with this consistency that leads to the problematic $T^* = 0.45s$ results as is
discussed below). It is difficult to see this consistency visually in Figure A-7,
because there are 40 ground motions at each $S_a(T^*) = x_i$ amplitude, while the real site
will have many more low-amplitude ground motions than high-amplitude motions
(and Equation A-4 accounts for this in the drift hazard computation by incorporating
weights on each x_i level from the hazard curve).
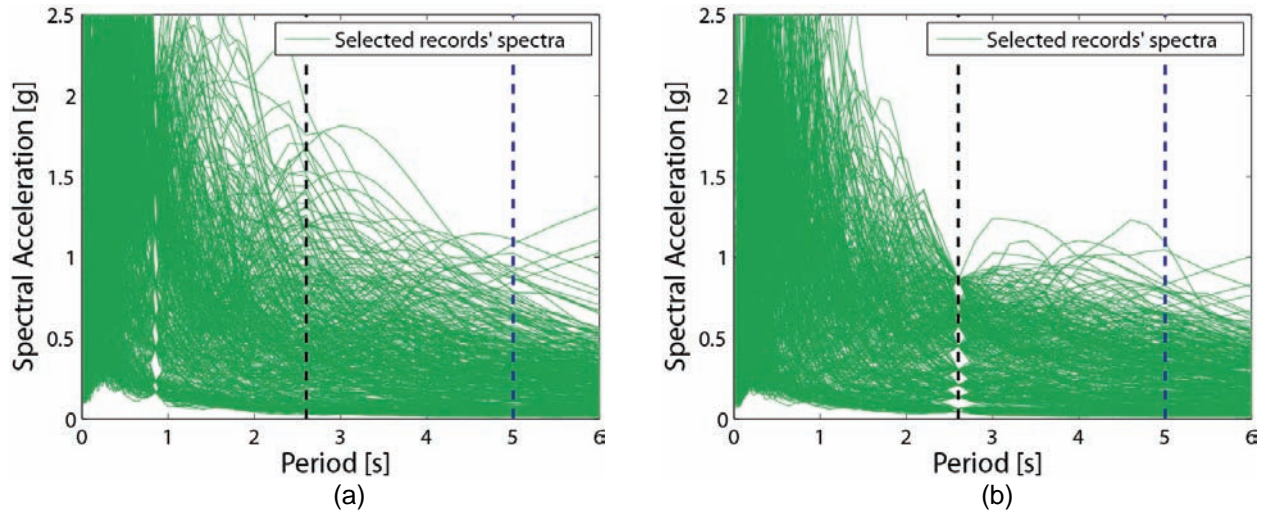
Figure A-7   Plots showing: (a) response spectra of ground motions selected using T^* = 0.85s; and (b) response spectra of ground motions selected using T^* = 2.6s.

To make a quantitative comparison of the two sets of response spectra, the rate of exceeding a given x_i amplitude at any arbitrary period x_i, implied by the ground motions selected conditional on $S_a(T^*)$, is computing using an equation very similar to Equation A-4:

$$\lambda\left(S_a(T) > y\right) = \sum_{i=1}^{n} P\left(S_a(T) > y \mid S_a(T^*) = x_i\right) \lambda\left(S_a(T^*) = x_i\right) \qquad \text{(A-7)}$$

where $P\left(S_a(T) > y \mid S_a(T^*) = x_i\right)$ is the probability that a ground motion in the selected record set has S_a at period T greater than y, given that $S_a(T^*) = x_i$. Here this probability is estimated as simply the fraction of the 40 ground motions with $S_a(T^*) = x_i$ that have $S_a(T) > y$.

Figure A-8a shows the computed rate of ground motions with $S_a(2.6s) > y$ for each set of selected motions (the two in Figure A-7 plus the sets selected based on T^* = 0.45s and T^* = 5.0s). Also shown for reference is the "direct hazard curve" for $S_a(2.6s)$ obtained from seismic hazard analysis. Ideally the selected ground motions would be consistent with this direct hazard curve. The ground motions selected using T^* = 2.6s have a stepped plot in Figure A-8a, due to the ten discrete $S_a(2.6s)$ amplitudes that were considered when selecting motions and the fact that $P\left(S_a(T) > y \mid S_a(T^*) = x_i\right)$ is equal to either 0 or 1 when T and T^* are equal. The ground motions with other T^* values have smoother curves, but all of the curves are in good general agreement, indicating that even though the other sets of ground motions did not scale ground motions to match $S_a(2.6s)$, they have the proper distribution of $S_a(2.6s)$ as specified by the hazard curve at that period. Thus, if $S_a(2.6s)$ is a good predictor of structural response, then the ground motions selected to match $S_a(0.85s)$ will still do a good job of capturing the distribution of structural response values that might be observed for the given site and structure considered.

The same goes for other periods as well, where the ground motion sets are also consistent (e.g., for this structure, spectral values at periods near 5 s appear to be the most important for prediction of large MIDRs). A similar plot is shown in Figure A-8b for the rate of exceeding $S_a(5s)$; in this case the ground motions with $T^* = 5s$ have the stepped curve, and the other T^* cases are smooth. Again the curves are in relatively good agreement with the true ground motion hazard curve, except for the case of $T^* = 0.45s$ at high amplitudes. This lack of agreement appears to explain the discrepancy of the $T^* = 0.45s$ drift hazard results in Figure A-6, as will be discussed below.

(a)   (b)
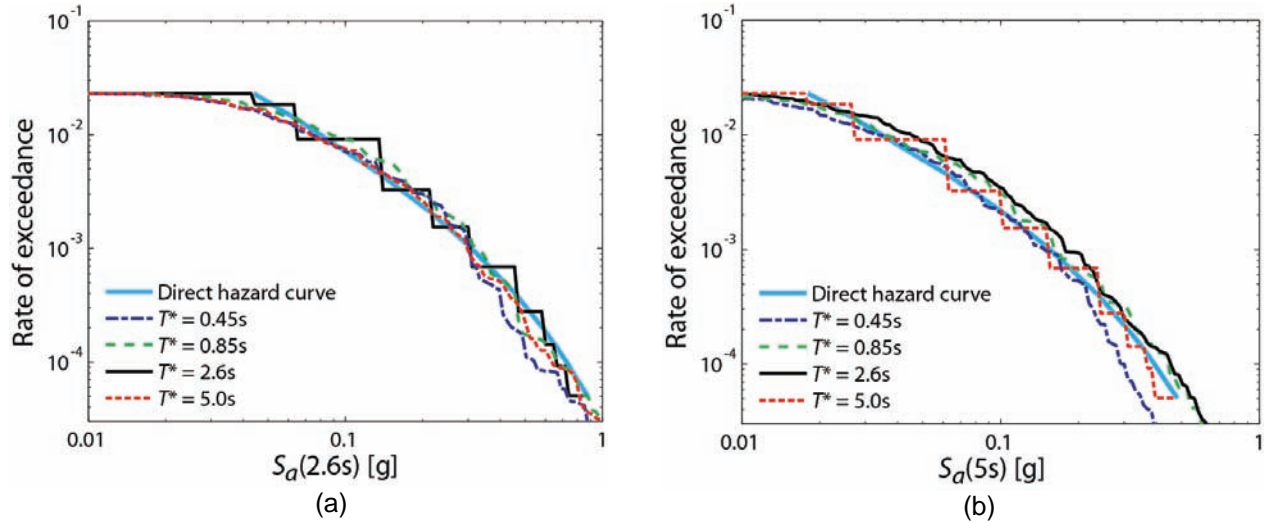
Figure A-8   Plots showing: (a) rate of $S_a(2.6s) > y$ implied by each of the selected ground motion sets, plus the original ground motion hazard curve for reference; and (b) rate of $S_a(5s) > y$ implied by each of the selected ground motion sets, plus the original ground motion hazard curve for reference.

The analysis of Figure A-8 can be taken further by looking at pairs of $S_a(T)$ values in these sets of selected ground motions. Figure A-9a shows scatter plots of the spectral values at 0.85s and 2.6s for the sets of motions selected using $T^* = 0.85s$ and $T^* = 2.6s$. The ground motions selected and scaled to match $S_a(0.85s)$ targets show up as horizontal stripes located at vertical heights corresponding to the ten $S_a(0.85s)$ amplitudes considered here; similarly, the $S_a(2.6s)$ ground motions show up as vertical stripes. If the selection and scaling were done properly, both sets of motions should represent the true joint distribution of $S_a(0.85s)$ and $S_a(2.6s)$ associated with ground motions occurring at the example site. It is again not possible to judge this consistency visually using Figure A-9a, because the selected ground motions need to be weighted by their rates of occurrence (determined via the hazard curve for the conditioning period). Figure A-9b shows contours of probability density for $S_a(0.85s)$ and $S_a(2.6s)$, estimated using kernel smoothing on the data in Figure A-9a and weighing each record by its corresponding rate of $S_a(T^*)$ occurrence. Figure A-9b illustrates that the agreement between the two ground motion sets is not good for small $S_a(0.85s)$ and $S_a(2.6s)$ values in the lower left corner of the plot, where the

selected ground motions poorly cover this range; that is acceptable, however, as ground motions in that region produce small MIDR values and thus the poor sampling was intentional (i.e., only relatively rare S_a amplitudes are considered here). The more important upper right corner of Figure A-9b shows better agreement between the two ground motion sets. Ideal ground motion sets should show perfect agreement in these contours, but the finite number of ground motions and S_a amplitudes considered here limit the ability to perfectly represent the joint distribution at all S_a periods. Given this limitation, selecting ground motions by conditioning at a "good" $T*$ is a useful approach, as it ensures that at least the distribution of S_a at this important period will be represented correctly.

(a)   (b)
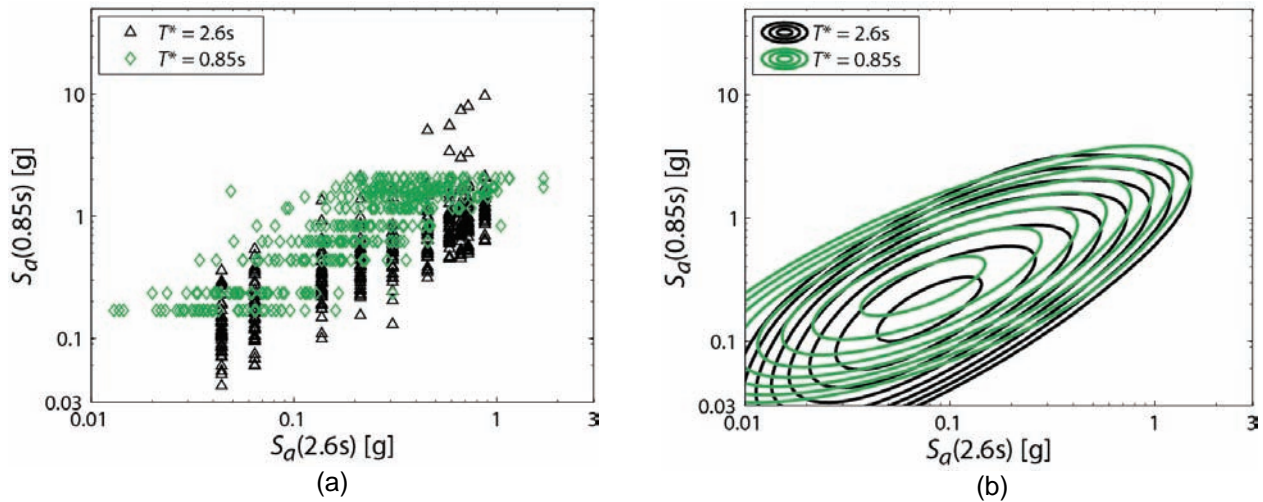
Figure A-9   Plots showing: (a) $S_a(2.6s)$ and $S_a(0.85s)$ values from the record sets selected by conditioning on $S_a(2.6s)$ or $S_a(0.85s)$; and (b) estimated contours of $S_a(2.6s)$ and $S_a(0.85s)$ values, obtained from the data in (a).

These calculations are related to two other topics in seismic reliability, so two notes here may be of interest. First, there is a connection between the choice of conditioning period $T*$ and the choice of a sampling distribution, as the S_a ground motion hazard curves are taken as the target distribution and represented by sampling from stratified values of $S_a(T*)$ (similar to the concept of Importance Sampling methods (e.g., Fishman, 2006)). A poor sampling distribution does not produce wrong answers, but it is less efficient as many of the "samples" (i.e., ground motions) are of less interest than they would have been if a good $T*$ had been chosen. Second, in principle the exact distribution of $S_a(0.85s)$ and $S_a(2.6s)$ associated with ground motions at this site can be calculated using Vector PSHA (Bazzurro and Cornell, 2002). No software is available in this case, however, to repeat the hazard calculation for this example site using the same seismic source model and ground motion prediction models as are used by the USGS, so here the consistency of alternate ground motion sets is checked to judge the accuracy of the selection procedure, rather than comparing the results to a "true" Vector PSHA answer.

A.4　Refinement of Target Conditional Spectra for Ground Motion Selection

While Figure A-6 showed very good agreement in drift hazard results among three of the conditioning periods, the results using $T^* = 0.45$s were not in close agreement with the others. The results in Figures A-6 and A-8 indicate that the discrepancies in this case relate to collapse predictions and the high-amplitude S_a values at long periods associated with ground motions causing collapse. These results will be studied more carefully in this section.

First, it is noted that for the $T^* = 0.45$s case, the collapse fragility function in Figure A-5 was relatively poorly constrained, as even the highest considered $S_a(0.45$s$)$ amplitude produced only 11 collapses out of 40 analyses. Further structural analyses at higher $S_a(0.45$s$)$ amplitudes were performed for this case to confirm that this was not the source of the discrepancy in drift hazard, and it was confirmed that this was not the problem (Lin, 2012).

The more important problem with the $S_a(0.45$s$)$ ground motions is apparent in Figure A-8, which indicated that the $T^* = 0.45$s ground motions were somewhat deficient in large-amplitudes at $S_a(5$ s$)$, which might lead to underestimation of collapses. This deficiency is due to an approximation in the implementation of Equation A-1 and Equation A-2 used for computing the target Conditional Spectra. Here only the mean magnitude and distance from hazard disaggregation are used for computing these targets, while typical disaggregation results indicate that a particular $S_a(T^*)$ amplitude is generally caused by more than a single magnitude/distance pair. To understand the impact of these multiple magnitudes and distances, Figure A-10 shows a disaggregation for $S_a(0.5$s$)$ at the example site (with available data at the closest period to the $T^* = 0.45$s case of interest). The mean magnitude and distance from this disaggregation are 7.5 and 10 km, respectively (with a mean ε of 1.3). The Conditional Spectrum associated with this mean magnitude, distance and ε is shown in Figure A-11a. But there are non-negligible contributions in Figure A-10 from earthquakes at a distance of 10 km for magnitudes ranging from 7 to 8 (these are all events on the nearby San Andreas fault). Figure A-11b shows the resulting conditional spectra for three magnitude values over this range. The mean shapes of the three spectra differ, because the frequency content of ground motions associated with these varying earthquake scenarios will differ. The variability of these spectra indicates that when the multiple magnitudes and distances associated with a given disaggregation are taken into account, the variability of the spectrum at periods other than T^* is increased relative to the approximate case using only a single mean magnitude and distance. A similar increase in variability also results from making predictions using multiple ground motion prediction models (consistent with the use of multiple models in the hazard calculations) rather than just a single model.
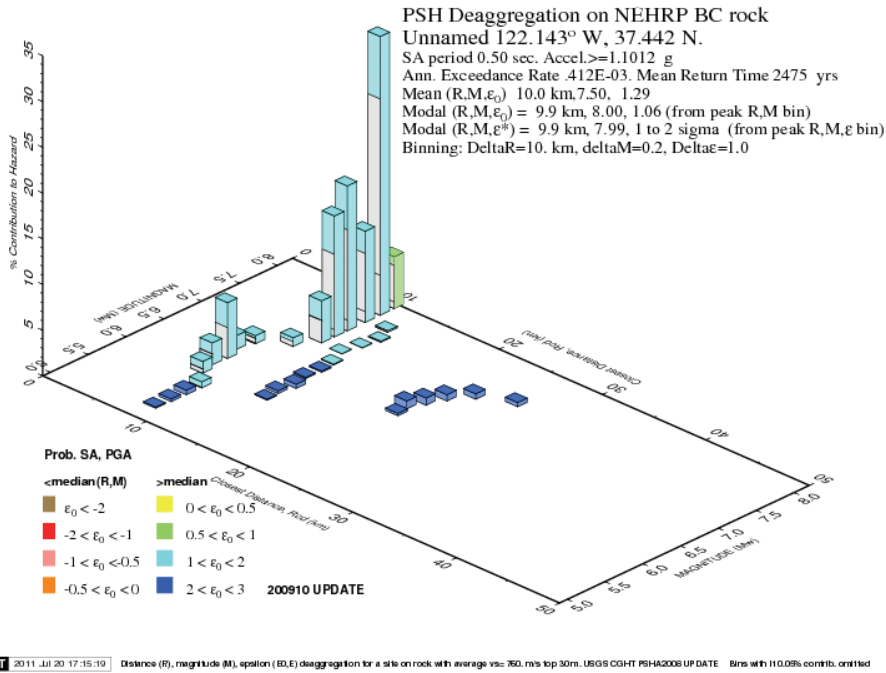
Figure A-10   Disaggregation for S_a(0.5s) = 1.1g (the amplitude with 2% in 50 years probability of exceedance) for the example site (USGS, 2008).
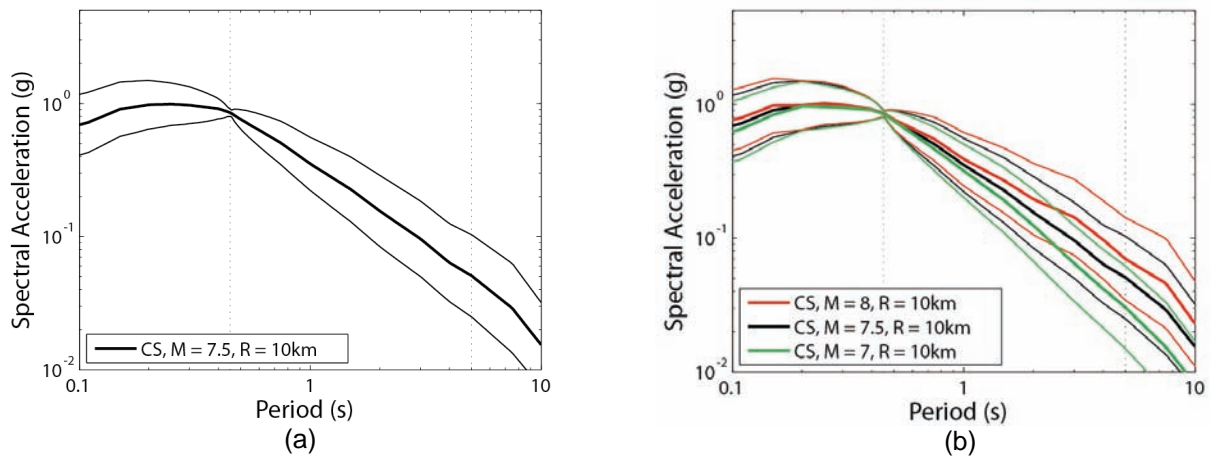
Figure A-11   Plots showing: (a) Conditional Spectrum given S_a(0.45s) = 1.1g, using mean magnitude and distance from Figure A-10; and (b) Conditional Spectrum given S_a(0.45s) = 1.1g, using three magnitude and distance pairs showing significant contributions to hazard in Figure A-10.

The increased variability from these factors can be captured formally in the conditional standard deviation computation, as documented elsewhere (Lin et al., 2011). The mean conditional spectrum may also in principle be affected by this

approximation, but this does not appear to be as significant of a practical issue in many cases. Figure A-12 shows approximate and exact results for the example site considered here, at a short and long conditioning period, as presented in Lin et al. (2011). Those results indicate that, for this particular site, the approximations used here are very accurate for the 1 s conditioning period, but that conditional standard deviations are underestimated by the approximation for the 0.2 s conditioning period case. As the underestimation of conditional standard deviation is most prominent at periods far from the conditioning period (as seen in Figure A-12 and more generally in Lin et al., 2011), it is perhaps not surprising that the conditional standard deviations at $S_a(5s)$ for the $T^* = 0.45s$ case is underestimated, resulting in a lack of high-amplitude $S_a(5s)$ values in those ground motions.
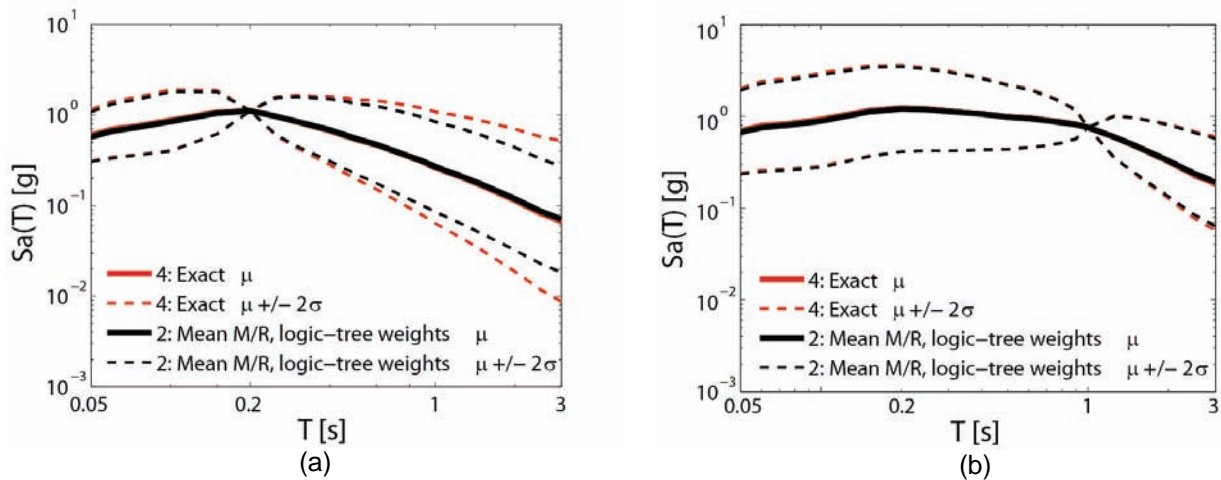
Figure A-12   Exact and approximate conditional spectrum for the example site, given $S_a(T^*)$ with 2% probability of exceedance in 50 years. Exact results are denoted "4: Exact" and approximate results are denoted "2: Mean M/R, logic tree weights" in the legend: (a) Conditional Spectrum using $T^* = 0.2s$; (b) Conditional Spectrum using $T^* = 1s$. Results from Lin et al. (2011).

Ideally the exact Conditional Spectrum calculations would be used for all results presented in this appendix, but those calculations are rather cumbersome and not feasible for practical applications (although automated tools for such calculations should be available in the near future).

Since the exact Conditional Spectra cannot be calculated, it can be approximately corrected by inflating the approximate standard deviations by a constant. Several values for the inflation constant (from 0% to 50%) were considered, and the 10% value was chosen because it resulted in S_a distributions from the resulting selected ground motions that most closely matched the numerical hazard curves at a range of periods of interest. The same inflation factor was applied at all periods for a given spectrum, and was used for all $S_a(T^*)$ levels. With an appropriate conditional standard deviation, the ground motions should match the corresponding target hazard curves as described above. No adjustment is made to the approximate mean spectra,

as experience shows them to be similar to exact mean spectra in most cases. Depending upon the site and conditioning period of interest, the inflation factor may vary but this approach is simple and suitable for addressing the primary questions of interest in this study.

In the results above, the ground motions selected using $T^* = 0.85$s, 2.6s, and 5s showed good agreement with corresponding ground motion hazard curves, so no adjustments were made in those cases. For the case of $T^* = 0.45$s, the conditional standard deviations were inflated by 10% and ground motions were reselected to match this new target. The spectra of the selected ground motions with $T^* = 0.45$s are plotted at four periods versus the corresponding ground motion hazard curves in Figure A-13. The spectra from the original ground motions are shown in Figure A-13a, and the new motions with a 10% larger standard deviation are shown in Figure A-13b.

Note again the stepped curve for the ground motions at 0.45s, due to the ten discrete $S_a(0.45$s$)$ amplitudes that were considered when selecting these motions. The curves in Figure A-13a are in relatively good agreement with the true ground motion hazard curve, except for the case of $S_a(5$s$)$ at high amplitudes, and $S_a(2.6$s$)$ to a lesser extent. With a conditional standard deviation inflated by 10% for the Figure A-13b motions, the curves at 5 s and 2.6s are in better agreement, demonstrating improved consistency with the known hazard information. The resulting collapse fragility functions are shown in Figure A-14. The inflated conditional standard deviation resolves the deficiency in high-amplitude S_a values, and therefore results in a higher probability of collapse for a given $S_a(0.45$s$)$ amplitude.

(a)   (b)
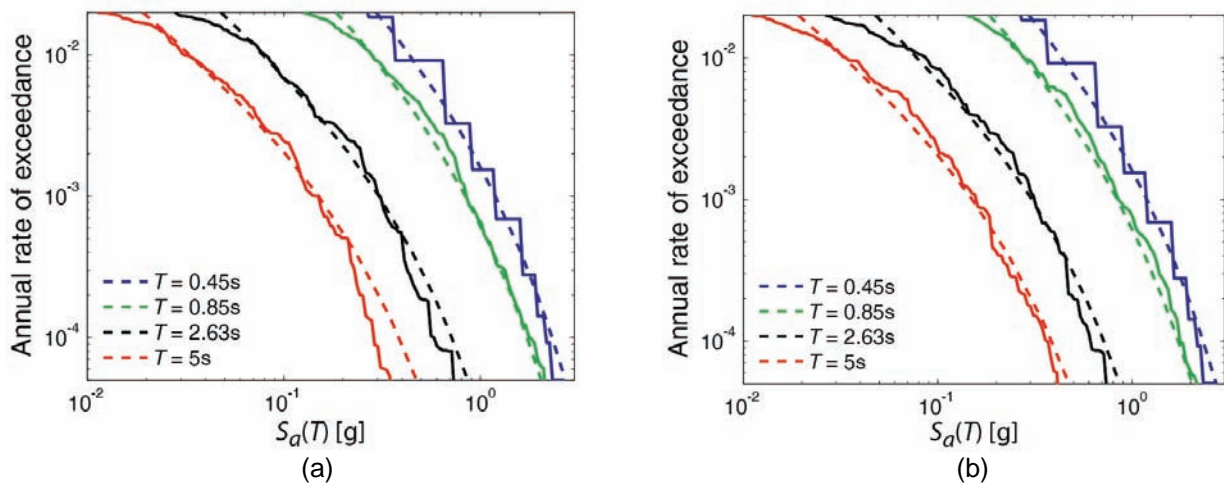
Figure A-13   Comparison of selected ground motion spectra at four periods (in solid lines) versus corresponding ground motion hazard curves (in dashed lines): (a) ground motions selected with $T^* = 0.45$s and using basic approximate Conditional Spectra; (b) ground motions selected with $T^* = 0.45$s and using approximate Conditional Spectra with conditional standard deviations inflated by 10%.
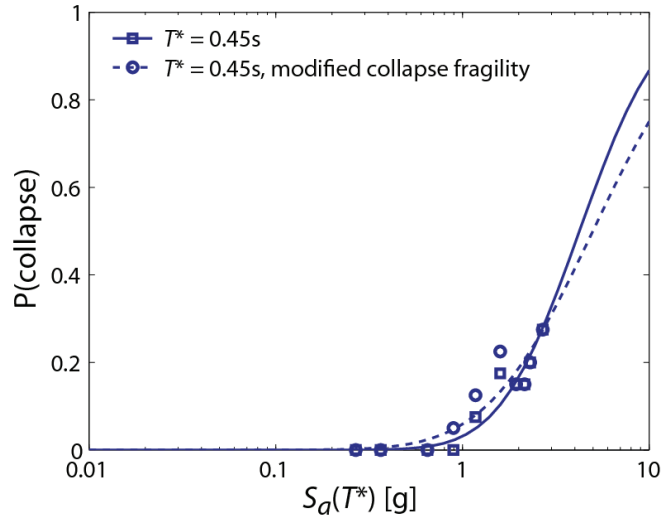
Figure A-14   Collapse fragility function conditioned on $S_a(0.45s)$, and the modified data (with an inflated conditional standard deviation).

The drift hazard curve was recomputed using these new motions and is compared to the original drift hazard curve for $T^* = 0.45s$ in Figure A-15a. The new drift hazard curve is also compared to the previous drift hazard curves using other conditioning periods in Figure A-15b, and the agreement among these four curves is very good. This suggests that if ground motions are selected carefully with appropriate conditional standard deviations to match the true hazard curves, the MIDR drift hazard would be in good agreement regardless of the choice of conditioning periods.
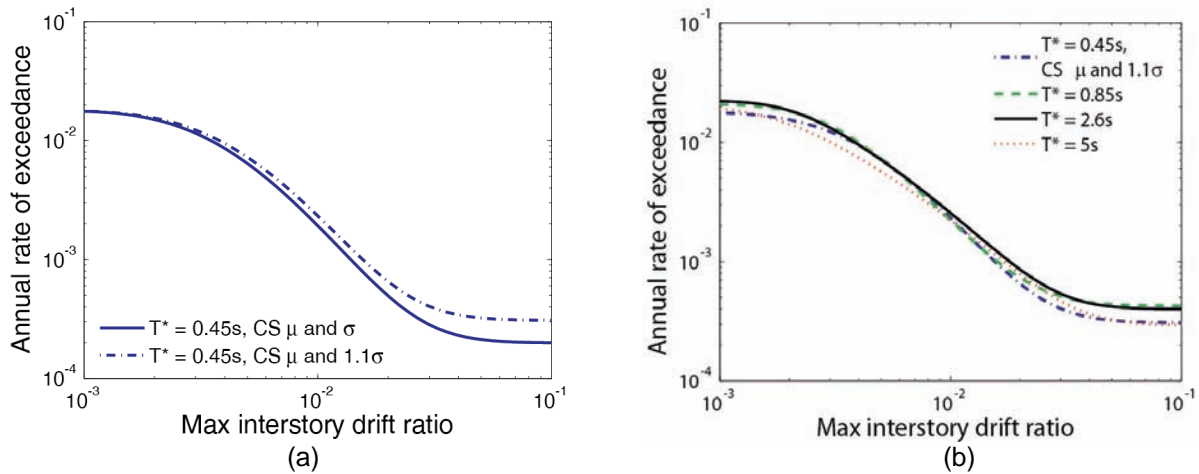
Figure A-15   Plots showing: (a) drift hazard curves obtained from ground motions with a basic conditional standard deviation and inflated conditional standard deviations for the case of $S_a(0.45s)$; and (b) drift hazard curves obtained with four choices of T^*, using an inflated conditional standard deviation for the case of $S_a(0.45s)$.

From these analyses, the following observations can be made: First, the Conditional Spectrum approach should in principle provide hazard-consistent ground motions and thus make resulting structural reliability calculations invariant to the choice of

conditioning period. This was not quite true in the initial results shown here, because the approximate way in which the Conditional Spectrum is typically computed can create a discrepancy between selected ground motions and ground motion hazard. If this is corrected, via adjustment of the conditional spectrum standard deviations, to ensure greater ground motion hazard consistency, then the structural reliability ("drift hazard") results become consistent. This observation is further verified by analysis from 11 additional buildings in Lin (2012) and discussed further in Section A.8.

Despite this refinement, only spectral values are considered here – not other ground motion properties that in some cases may be relevant to structural response (e.g., velocity pulses, duration). If non-spectral ground motion parameters are also deemed important for predicting the engineering demand parameter of interest, the approach above can be generalized to account for those parameters (Bradley, 2010), though some practical limitations may remain in terms of models for predicted values of, and correlations between, these additional parameters.

A.5   Comparison to Results from Other Target Spectra

For comparison with the results presented above, the drift hazard calculation procedure is repeated using additional sets of ground motions: sets selected to match the Conditional Mean Spectrum only (i.e., not accounting for spectrum variability), and sets selected to match the Uniform Hazard Spectrum (UHS) at each $S_a(T^*)$ level. Examples of these spectra are shown in Figure A-16. Spectra of ground motions selected to match the CMS are shown in Figure A-16a, illustrating the reduced variability of these ground motions' spectra relative to the CS ground motions' spectra (see Figure A-3b for comparison). Spectra of ground motions selected to match the UHS are also shown in Figure A-16b, with the CMS also shown for reference to illustrate that these motions are in general stronger than the CMS spectra at periods other than the conditioning period. For both of these target spectra, new ground motions were selected to match the target spectra at each amplitude, dynamic analyses were performed, and the results were used to compute $P\big(MIDR > y \mid S_a\big(T^*\big) = x\big)$ and repeat the drift hazard calculation of Equation A-4.
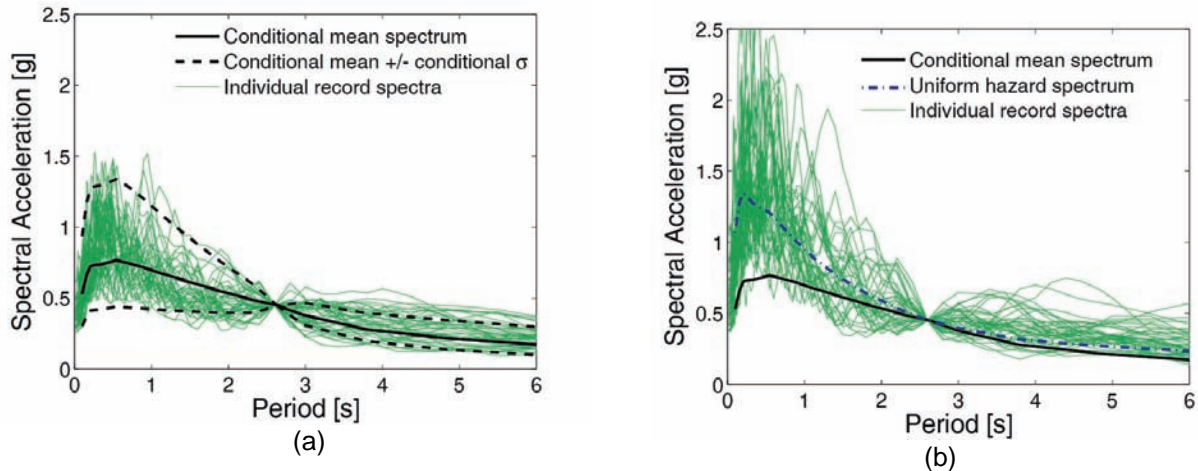
Figure A-16   Target spectra and spectra of selected ground motions with S_a(2.6s) having a 2% probability of exceedance in 50 years: (a) Conditional Mean Spectrum target, and (b) Uniform Hazard Spectrum target.

Drift hazard results from the UHS and CMS ground motions, using T^*= 2.6s are shown in Figure A-17, in comparison with the CS results from above. In this case, the rate of exceeding large MIDR levels is overestimated when ground motions are selected to match UHS; this finding is consistent with previous observations that use of the UHS as a target spectrum leads to conservative estimates of structural response. The CMS ground motions produce comparable estimates to the CS motions in this case.
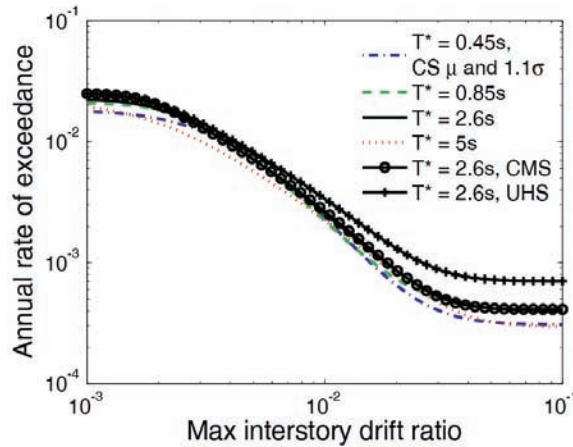
Figure A-17   Drift hazard curves obtained from ground motions selected to match Conditional Spectra (using four conditioning periods), Conditional Mean Spectra, and Uniform Hazard Spectra.

Figure A-18 shows the distributions of response spectra from these two new sets of ground motions. The CMS spectra at short periods (seen in Figure A-18a) are deficient at high amplitudes relative to the target hazard curves, since variability in the spectra are omitted here; the spectra are (somewhat surprisingly) high at 5 s,

which likely explains why the drift hazard results are not low relative to CS-based results. The UHS spectra in Figure A-18b are relatively higher at all periods, and especially at 5 s, which explains the high predicted rates of collapse in Figure A-17; they are still slightly low at short periods, because the ground motions have little spectral variability and this somewhat offsets the high mean values of the UHS at those periods.
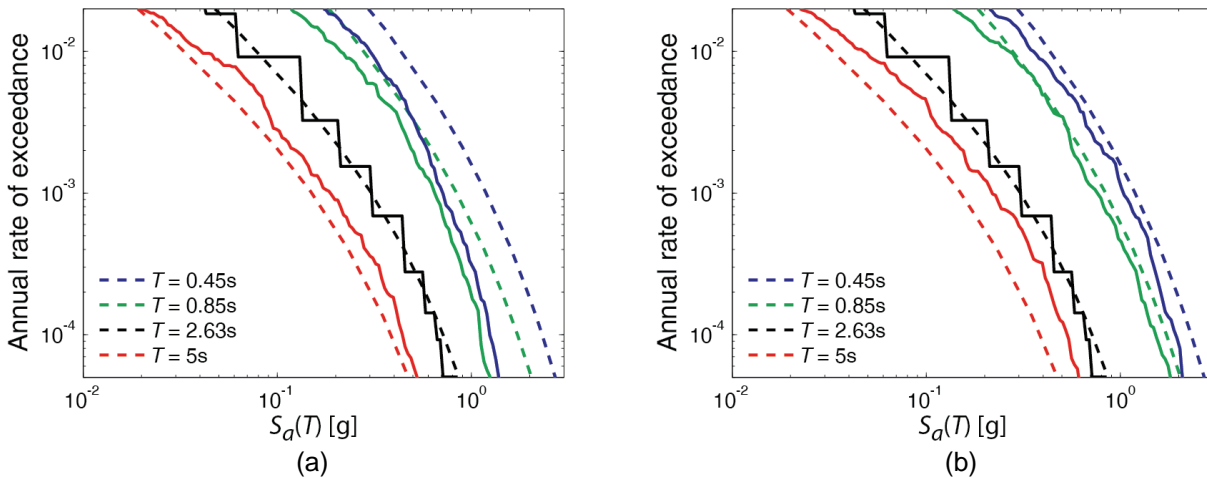
Figure A-18   Comparison of selected ground motion spectra at 4 periods (in solid lines) versus corresponding ground motion hazard curves (in dashed lines): (a) ground motions selected to match Conditional Mean Spectra with $T^* = 2.6$s; and (b) ground motions selected to match Uniform Hazard Spectra with $T^* = 2.6$s.

For a second set of comparisons, Figure A-19 shows CMS and UHS drift hazard results, but this time using a conditioning period of $T^* = 0.45$s. The UHS results are still high relative to CS results, and are comparable to the Figure A-17 results, since the UHS target is not affected by conditioning period and thus the selected ground motions are similar regardless of conditioning period. The CMS results, however, are very low relative to the other results. The reason for this is apparent in Figure A-20, which shows the distribution of response spectra from these two sets of ground motions. The CMS spectra are extremely deficient in high-amplitude S_a's at $T = 2.6$s and 5s, meaning that there are few ground motions in the selected set that are capable of causing collapse of this structure.
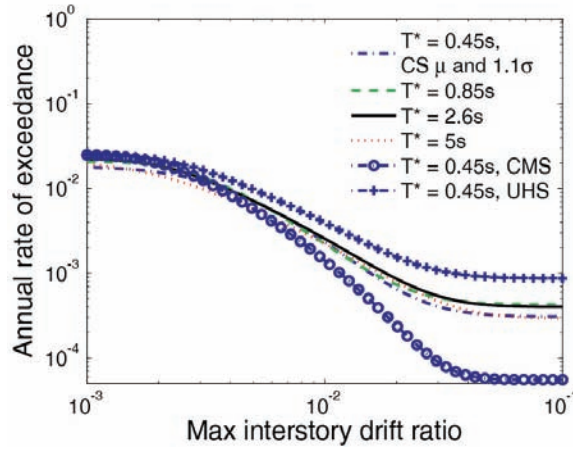
Figure A-19   Drift hazard curves obtained from ground motions selected to match Conditional Spectra (using four conditioning periods), Conditional Mean Spectra, and Uniform Hazard Spectra.

(a)   (b)
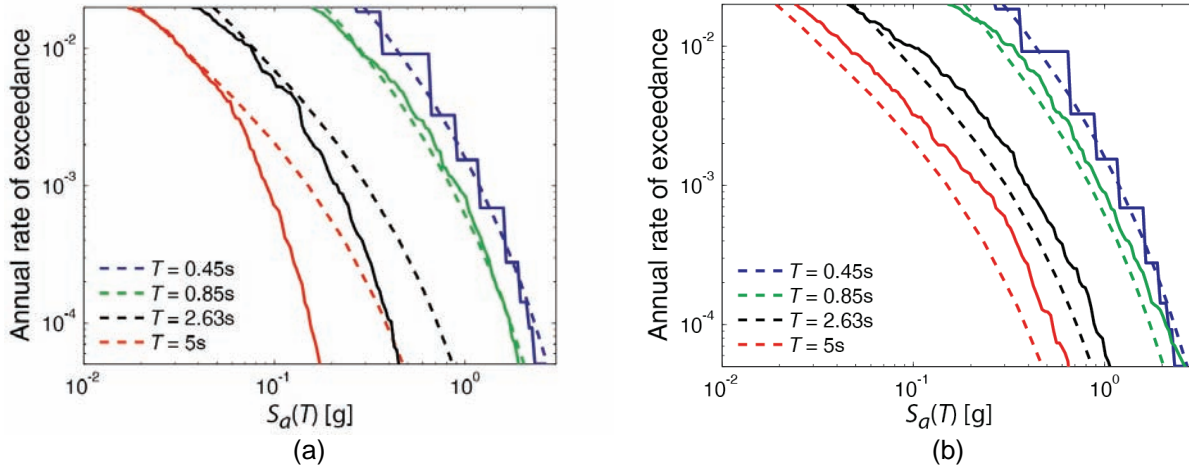
Figure A-20   Comparison of selected ground motion spectra at 4 periods (in solid lines) versus corresponding ground motion hazard curves (in dashed lines): (a) ground motions selected to match Conditional Mean Spectra with $T^* = 0.45$s; (b) ground motions selected to match Uniform Hazard Spectra with $T^* = 0.45$s.

Taken together, the results of this section indicate that selecting and scaling ground motions to match a UHS will typically result in conservative drift hazard results, while matching a CMS will often result in unconservative results due to the omission of spectral variability at periods other than the conditioning period (although the unconservatism may not be significant if S_a at the conditioning period is a good predictor of the engineering demand parameter of interest). These trends are consistent with intuition and past observations regarding the use of these targets, and are also explained by examination of the response spectra of ground motions selected and scaled to match these targets. A few additional results of this type are presented in Lin (2012) to further illustrate the generality of these trends.

A.6 Prediction of Alternate Engineering Demand Parameters

To help illustrate the generality of the above results, time-based assessment calculations were performed for peak floor accelerations (PFA) as well. Peak floor accelerations (maximum acceleration observed over all floors, over the duration of shaking) are often observed at upper stories of the example building and are sensitive to excitation of higher modes of the building, so they are not highly correlated with maximum interstory drift ratios (which are more closely related to first-mode response).

Using the same sets of Conditional Spectrum ground motions, time-based assessments were performed and example results are shown in Figure A-21. Some adjustments of conditional standard deviations were again needed in order to ensure hazard consistency of the short-period spectral accelerations when the conditioning period was first-mode or longer (because these short-period spectra are important for PFA). Once appropriate conditional standard deviations were determined for each conditioning period, the resulting time-based assessment results are very consistent from case to case.
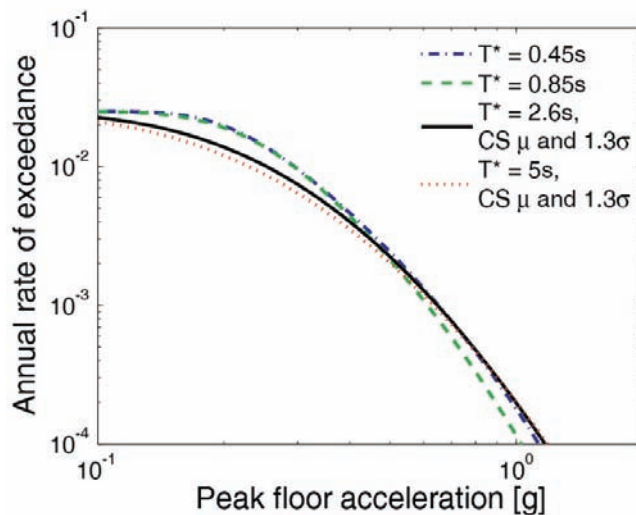
Figure A-21   Rates of exceedance of peak floor accelerations, as computed using time-based assessments with four conditioning periods. Inflated conditional standard deviations were used when $T^* = 2.6s$ and 5s to ensure hazard consistency, as noted in the legend.

Similar results are shown in Figure A-22 for interstory drift ratio and floor accelerations observed on the 15th story of the structure (rather than the maximum across all stories). These upper-floor drifts and accelerations are again more sensitive to higher modes than to maximum interstory drift ratio across all stories, and are used to illustrate prediction of single-story response parameters that are often of interest in loss assessment calculations. Figure A-22 illustrates that these predictions are also consistent when differing conditioning periods are considered.
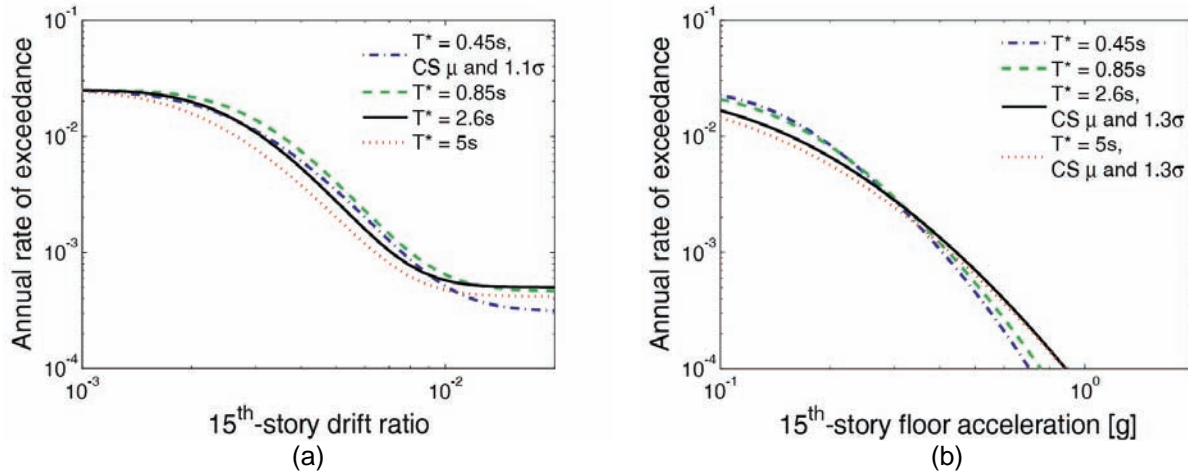
Figure A-22   Rates of exceedance of drift ratios and floor accelerations on the 15th story of the building.

The results in this section again indicate the consistency of time-based assessments across conditioning periods, though they also illustrate the importance of ensuring hazard consistency of the response spectra at periods related to the structural response parameter of interest (or more generally, hazard consistency of any ground motion intensity measure of interest). For prediction of floor accelerations, more attention is needed to be paid to short-period spectra than in the above MIDR calculations, given the higher-mode sensitivity of these structural response parameters.

A.7   Structural Analysis Results from an Intensity-Based Assessment Perspective

Figure A-4 briefly noted that the mean MIDR results for an $S_a(T^*)$ amplitude with a given return period varied depending upon the choice of T^*. This section examines those results in more detail.

Figure A-23 shows the estimated median MIDR and PFA results from the dynamic analyses of the 20-story building discussed above. Here, rather than combining the distributions of the engineering demand parameters of interest with the hazard curve in a time-based assessment calculation, the median responses observed at each ground motion intensity level are examined directly. It is not meaningful to directly compare the amplitudes of spectral values at differing periods, so in this figure the return period associated with each $S_a(T^*)$ value considered is plotted, rather than its amplitude. For each of the four T^* values considered above, the median MIDR and PFA associated with each amplitude is plotted. Also plotted for reference are comparable median values from ground motions scaled to the UHS (in that case, the return period is the return period of any single spectral ordinate on the UHS). Counted medians are plotted here, to avoid dealing with collapse results separately.

In Figure A-23a, medians are not reported at intensities where more than 50% of ground motions caused collapse.
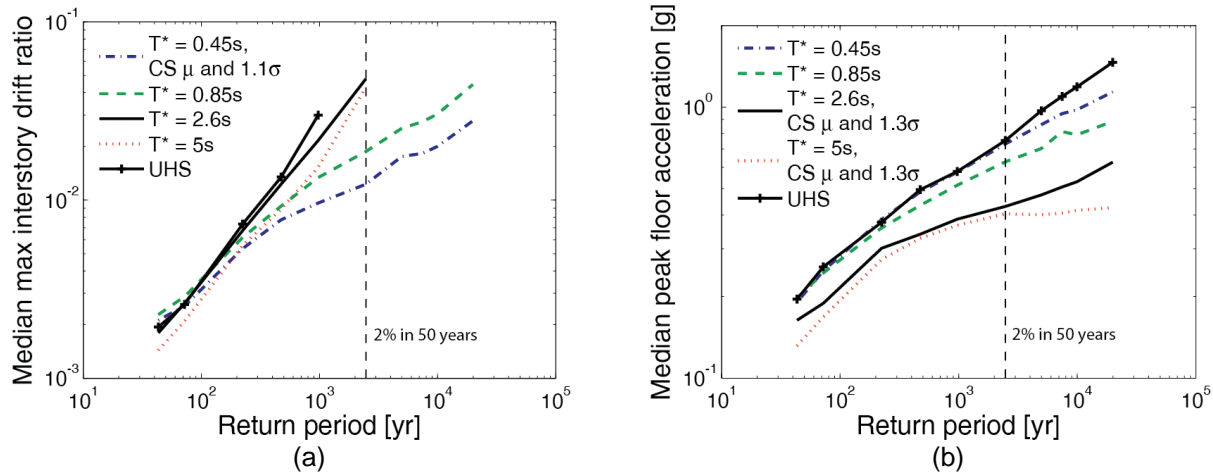
Figure A-23   Median maximum interstory drift ratio and peak floor acceleration from dynamic analysis of the 20-story building, obtained from ground motions matched to Conditional Spectra with four conditioning periods and to Uniform Hazard Spectra. Median results are plotted versus the return period of the spectral acceleration amplitude at the specified conditioning period.

Several observations can be made from Figure A-23. First, the UHS-matched ground motions almost always produce larger median responses than the CS-matched ground motions with an equivalent return period, as expected. The differences are sometimes not large relative to the CS ground motions at a specific conditioning period. The second observation is that the CS conditioning period associated with the largest median response is not constant over all cases considered. For the MIDR results in Figure A-23a, the S_a at the first-mode period produces the largest medians at a given return period, consistent with intuition that MIDRs would be dominated by first-mode elastic response and thus a spectrum peaked at the first-mode period would produce the largest MIDRs. For the PFA results in Figure A-23b, the conditioning periods associated with large responses are much shorter. The third-mode elastic period produces the highest median values, with the second-mode period producing nearly as large of values and the longer periods producing much lower values; this is consistent with PFA's being a higher-mode driven response parameter.

These observations have important implications for building-code-type intensity-based checks. If future codes allow use of Conditional Spectra or Conditional Mean Spectra in place of a Uniform Hazard Spectrum, the average values of responses computed in those checks may be reduced even if the target return period of the ground motion is unchanged due to the eliminated conservatism of the UHS target. The level of reduction depends upon the extent to which the response parameter of interest is associated with spectral values at multiple periods; structures that behave

like elastic single-degree-of-freedom oscillators are sensitive only to spectral acceleration at a single period and thus the responses from CS-matched or UHS-matched motions conditioned on that period will be identical. Conversely, structural response parameters sensitive to multiple modes of excitation, or to significant nonlinearity (such as collapse, where the structure's effective period lengthens) may experience reduced responses from CS-matched motions relative to UHS-matched motions with the same intensity at the conditioning period.

A.8   Analysis of Additional Structures

To verify the above observations more generally, eleven additional structures were analyzed using the same procedure with ground motions selected to match Conditional Spectra. Perimeter frame and space frame structures with heights from 1 to 20 stories, all originally designed during the development of the FEMA P-695 report (2009a), were considered. Summary information regarding these structures is provided in Table A-1. Maximum interstory drift ratio and peak floor acceleration predictions were considered, in both time-based and intensity-based assessment procedures. All structures were located at the same Palo Alto site used above, and spectral accelerations with the same exceedance probabilities were considered.

Table A-1   Summary Information for Buildings Studied

Building #	FEMA P-695 Building #	Space or Perimeter Frame	Number of Stories	Significant Modal Periods (s)
1	1020	Perimeter	20	2.6, 0.85, 0.45
2	1013	Perimeter	12	2.0, 0.68, 0.39
3	1011	Perimeter	8	1.7, 0.58, 0.33
4	1008	Perimeter	4	0.91, 0.29, 0.17
5	2064	Perimeter	2	0.63, 0.18
6	2069	Perimeter	1	0.68
7	1021	Space	20	2.5, 0.92, 0.54
8	1014	Space	12	2.2, 0.78, 0.45
9	1012	Space	8	1.8, 0.64, 0.36
10	1003	Space	4	1.1, 0.33, 0.17
11	1001	Space	2	0.6, 0.17
12	2061	Space	1	0.42

Note: The "FEMA P-695 building #" field refers to the building number in the FEMA P-695 report corresponding to the model used here. The "Significant modal periods" column lists the first three modal periods if available, or fewer if the structure does not have that many elastic modes of vibration.

Conditioning periods for Conditional Spectra were T_1, T_2, T_3, and $2T_1$ (except in the case of the very short structures, where T_2 and T_3 were not considered in some cases). For each conditioning period and spectral amplitude, forty recorded ground motions were selected and scaled such that their spectra matched the target mean and standard deviations computed using Equations A-1 and A-2. Additional sets of ground motions were selected in some cases to match a CS with an inflated conditional standard deviation, as was done above with the $T^*= 0.45$s case.

In all analysis cases, consistency of time-based assessment results across conditioning periods was again observed, while intensity-based assessment results varied as the conditioning period varied, for a given structure. These additional results are provided in Lin (2012) and provide further empirical confirmation of the findings described in detail above.

A.9   Conclusions

This appendix has presented a study on the sensitivity of time-based assessments to the choice of conditioning period when the Conditional Spectrum is used as a target for ground motion selection and scaling. Results shown here focused on time-based assessments of the rate of exceeding various levels of maximum interstory drift in a structure, though other engineering demand parameters were also considered, and intensity-based assessment results were also presented and discussed. The structure used is a 20-story concrete frame structure assumed to be located in Palo Alto, California, using a structural model with strength and stiffness deterioration that is believed to reasonably capture the responses up to the point of dynamic-instability collapse.

The time-based assessment was performed several times, using ground motions selected and scaled to match Conditional Spectra, where the conditioning period used for these calculations was varied from 0.45 to 5.0 seconds (i.e., the third-mode structural period up to twice the first-mode period). For each case, the drift hazard results were similar. The similarity of the results stems from the fact that the careful record selection ensures that the distributions of response spectra at all periods are nominally comparable, so the distribution of resulting maximum interstory drifts should also be comparable (to the extent that response spectra describe the relationship between the ground motions and structural responses). Seen in this light, choosing a conditioning period is equivalent to choosing a sampling distribution in an importance sampling reliability analysis—a good sampling distribution will produce precise reliability estimates using small amounts of data, while a poor sampling distribution reduces efficiency but does not necessarily result in a biased prediction.

From these results, it is observed that if the analysis goal is to perform time-based assessment, then one should be able to compute an accurate drift hazard curve using

any conditioning period, as long as careful ground motion selection ensures proper representation of spectral values and other ground motion parameters of interest. Here "proper representation" refers to consistency with the site ground motion hazard curves at all relevant periods, and this is achieved by using the Conditional Spectrum approach to determine target response spectra for the selected ground motions. The reproducibility of the drift hazard curves with varying conditional periods results from the fact that the ground motion intensity measure used to link the ground motion hazard and the structural response is not an inherent physical part of the seismic reliability problem considered; it is only a useful link to decouple the hazard and structural analysis. If this link is maintained carefully then one should get a consistent answer (the correct answer) for the drift hazard curve in every case. The consistency in drift hazard achieved here is in contrast to some previous speculation on this topic, because this study utilizes the recently developed Conditional Spectra for ground motion selection, and uses the first available algorithm for selecting ground motions to match this CS target.

One practical challenge associated with these findings is that selecting ground motions that are truly consistent with ground motion hazard at all periods requires the use of an exact target Conditional Spectrum (i.e., one that accounts for multiple causal magnitudes and distances associated with a given S_a amplitude, and for multiple ground motion prediction models); practical computation of this Conditional Spectrum target, however, typically considers only a single ground motion prediction model and only the mean magnitude and distance from disaggregation. Because computation of the exact Conditional Spectrum target is very difficult in practice, here the approximate Conditional Spectrum is used and its conditional standard deviation is adjusted until consistency of the selected ground motion spectra with corresponding ground motion hazard at periods important to the problem being studied have been achieved. This adjustment is not needed in many cases, but in some cases it is needed and greatly improves the results.

Choice of a "good" conditioning period serves several useful purposes. In the context of predicting the full drift hazard curve, choice of a good conditioning period helps because the spectral accelerations at the conditioning period will be a good predictor of structural response; this makes any inaccuracies in representing spectral values at other periods to have a less severe impact on the resulting drift hazard predictions. Additionally, use of a good conditioning period reduces the variability in structural responses and thus reduces the number of dynamic analyses that are required to accurately estimate distributions of structural response. Luco and Cornell (2007) referred to these two properties as "sufficiency" and "efficiency," respectively. Those concepts are taken further here, acknowledging that there is no intensity measure with perfect efficiency and sufficiency, and so performing careful ground motion selection to compensate for shortcomings that are inherent in any

intensity measure. Nonetheless, the only consideration is spectral values, not other ground motion properties, such as velocity pulses not fully captured in the spectral acceleration values, and duration. If non-spectral ground motion parameters were also deemed important for predicting the engineering demand parameter of interest, the approach above can be generalized to account for those parameters in addition to spectral parameters (Bradley, 2010).

An important issue regarding conditioning period arises when the purpose of the performance assessment is to compute the mean or median response associated with an $S_a(T^*)$ having a specified probability of exceedance (e.g., for a building-code-type check). In this case, the response prediction will always change depending upon the choice of conditioning period. This comes from the fact that the choice of intensity measure is an inherent part of the problem statement, and so in this case changing the intensity measure changes the question that is being asked. Resolution of this issue is not obvious, but likely lies in identifying a performance check that, when passed, confirms satisfactory reliability of the structural system.

Additional results of the type shown above were produced for 11 additional structures and are available in Lin (2012) and provide further empirical confirmation of these findings. Those results support the observations made here, and collectively provide a slightly more complete picture of the relationship between careful ground motion selection and robust structural response results.

A.10 Recommended Future Work

The above results provide a more detailed understanding of the effect of conditioning period on structural analysis results obtained from ground motions selected and scaled to match a conditional spectrum target. The results, however, also highlight topics where future work is needed. A few key topics are noted here.

A.10.1 *Computation of Exact Conditional Spectra Targets*

This work identified the potential importance of computing exact rather than approximate Conditional Spectra (specifically, the need to compute an exact conditional standard deviation that accounts for the increased spectral variability resulting from contributions of multiple earthquake scenarios and multiple ground motion prediction models to prediction of exceedance of the target spectral amplitude). The exact calculations are feasible but inconvenient, and so automated tools for performing this calculation would be valuable for users hoping to benefit from this new target spectrum. The US Geological Survey and commercial PSHA software developers have recently begun providing exact calculations of Conditional Mean Spectra for user-specified sites. Expansion of those tools to compute exact conditional standard deviations as well would be a useful extension.

A.10.2   Implications for Analysis of 3-D Structural Models

The results above were obtained by analyzing 2-D structural models subjected to a single component of ground motion, and so some thought is needed to translate these observations into conclusions for 3-D structural models subjected to multicomponent ground motions. For time-based assessments, the findings above provide some reassurance that time-based assessments can be robustly performed for 3-D structural models as well, and the results should in principle be independent of the conditioning period and the choice of response spectra definition (i.e., arbitrary component, geometric mean, or maximum component) so long as the ground motions are scaled to a target consistent with that specified by a hazard curve for spectral acceleration defined in the same way, and so long as the spectral values at other periods and for other definitions are consistent with target conditional distributions, given the conditioning spectral amplitude. This conclusion is reached by taking the above analysis of spectral accelerations at multiple periods, and extending it to spectral accelerations at multiple orientations. This thinking is also consistent with earlier research on this topic (e.g., Baker and Cornell, 2006b).

A.10.3   Target Analysis Scenarios for Intensity-Based Assessments

For intensity-based assessments, the results above indicate that mean values or distributions of engineering demand parameters conditioned on S_a at a single period T^* will in general be smaller than corresponding values conditional on a Uniform Hazard Spectrum (when the $S_a(T^*)$ has the same return period as the UHS). Because the Uniform Hazard Spectrum is a quite conservative target, it is straightforward to argue that intensity-based assessments should perhaps not be conditioned on a UHS target (as is done, for example, in many of the code applications discussed in Chapter 3). If one switches to conditioning on $S_a(T^*)$ (and considers the accompanying CMS or CS to compute defensible spectral targets at other periods), then the question of choice of T^* arises, because the results will vary with varying T^*. One option is to simply specify a T^* (e.g., the first-model period of the structure) and define the intensity-based assessment as conditional on that period. Another option would be to specify multiple values of T^*, and require the structure to perform acceptably for the intensity-based assessment in each T^* case.

The results above show that both of these options would result in lower engineering demand parameters compared to those from a UHS-based assessment. But the results from the two alternate options differ from each other (and again it is emphasized that the first option will produce different results depending upon the choice of T^*). Resolution of this issue is not straightforward, as changing the target analysis scenario is equivalent to changing the question being asked, and there is no clear consensus on what exactly the question being asked is in most code documents that use intensity-based assessments. If the question is, "what is the average engineering

demand parameter given ground motions with a target UHS?", then by definition the only correct answer is the answer obtained from using a target UHS for selecting and scaling ground motions. If that is not the intended question being asked (which may be the case given the problematic nature of the UHS target), then one must carefully articulate what exactly the question is. In the case of ASCE/SEI 7-10, *Minimum Design Loads for Buildings and Other Structures* (ASCE, 2010), the stated objective of the design requirements is to achieve building designs that have less than a 1% probability of collapse in 50 years, and the intensity-based assessment (and corresponding acceptance criteria) are implicitly intended to indicate whether this objective is likely to be achieved; no detailed study has been performed, however, to determine an intensity-based assessment that it is a good indicator of whether the collapse risk objective has been achieved. Results of the type presented above would be useful in identifying intensity-based assessment procedures that are indicative of time-based seismic performance metrics.

At the present moment, specifying checks at multiple conditional spectra may be the best option for an immediate refinement to a code check, as it is the more conservative of the above two options, while still allowing the analyst to avoid the conservatism of the UHS. A multiple-spectrum check would also be consistent with some other design guidelines that have adopted concepts for target spectra that represent individual earthquake scenarios rather than uniform hazard spectra (Department of Energy, 1996; USNRC, 2007; and ASCE, 2005). While a multiple-spectrum check is likely the most practical incremental change to present practice, a check requiring only a single target spectrum should not yet be dismissed completely before the analysis objective and corresponding acceptance criteria are evaluated more carefully.

Appendix B
Response-Spectrum Matching

B.1   Introduction

This appendix summarizes two studies that were carried out on the topic of response-spectrum matching (referred to as spectrum matching). Section B.2 presents a follow-on study to that of the Pacific Earthquake Engineering Research Center Ground Motion Selection and Modification (PEER GMSM) Program, summarized in *Evaluation of Ground Motion Selection and Modification Methods: Predicting Median Interstory Drift Response of Buildings* (Haselton et al., 2009). Two of the structural models considered in that program are reanalyzed here, using suites of ground motions selected, scaled and spectrum matched using the RspMatch2005 software developed by Hancock et al. (2006), over different period ranges and damping values. The results of these analyses are compared with those of Haselton et al. and quantitative recommendations for the use of spectrum matching in response-history analysis are drawn.

Section B.3 investigates the effectiveness of spectrum matching records that contain a velocity pulse. Velocity pulses are a particular example of a nonstationary feature of a ground motion history that ideally the RspMatch2005 algorithm should be able to preserve. This study quantitatively assesses several approaches that may be used for preserving velocity pulses in spectrum matching using RspMatch2005.

Although all results in this section were developed using the program RspMatch2005, the issues addressed will apply to ground motions developed using different software, as well. At the very least, it is suggested that the methodology presented herein is an appropriate framework in which to assess these issues, and other programs could be readily compared against the RspMatch2005 results in this section.

B.2   Effect of Response-Spectrum Matching on PEER GMSM Study Results

B.2.1 Background and Existing Literature

B.2.1.1 Effect of Spectrum Matching on Structural Analysis Results

A number of publications have investigated the use of spectrum-matched ground motions for nonlinear response-history analyses. In some cases, the conclusions from these studies differed considerably from one another, and it has been difficult for the potential end-user of spectrum-matched ground motions to assess whether they are appropriate for a given analysis application. A principal point of controversy is

whether spectrum-matched motions lead to unconservatively biased estimates of the median (or mean) response. For the most part, inconsistency on this issue is related to benchmarks that were used to assess bias, the target spectrum used for spectrum matching, and the ground motions and structural analysis models used.

As discussed previously, spectrum-matched motions cannot be used if the full distribution of structural response needs to be calculated. The advantage of using spectrum matching is that the dispersion among analyses is reduced, allowing a stable estimate of the median response using fewer ground motions. However, reducing the dispersion on the input also means that a realistic dispersion on the output is not possible to obtain. In any case, even if unmatched records are used, the typical number of ground motions used in design office applications (often seven) are insufficient to obtain robust estimates of the distribution of response (Buratti et al., 2011; Jayaram et al., 2011.)

As mentioned above, several studies have identified an unconservative bias when comparing the inelastic response of structures subjected to spectrum-matched motions (Carballo and Cornell, 2000; Bazzurro and Luco, 2006; Huang et al., 2008b). The study of Iervolino et al. (2010) also noted a small bias, although concluded that it was not statistically significant. A point in common to all these studies is that the benchmark was taken as the inelastic response of the same structural model to a suite of unmatched ground motions. In each case, the median spectrum for the unmatched motions was a close match of the target spectrum, but the dispersion in this set was significantly greater. Carballo and Cornell (2000) noted that inelastic response is nonlinearly related to the intensity of the input motions, and that intensities higher than the target spectrum produced disproportionately larger inelastic demand than the lower demand produced by lower intensities. Therefore, the median inelastic response from a suite of records with more variable spectra would be skewed towards higher values – an effect which is not present when records are spectrum matched to tightly fit the target spectrum.

As noted in Appendix A and Jayaram et al. (2011), an appropriate amount of dispersion in a suite of ground motions should reflect the variance in the conditional spectrum, conditioned on an appropriate structural period. The studies cited above all assumed that the variation in the ground motion set used as a baseline was the best available estimate of the "true" response, and therefore that the lower inelastic demand produced by the spectrum-matched motions indicated unconservative bias. In light of developments in the PEER GMSM study and the work of Jayaram et al. (2011), it is important to repeat these studies with a benchmark that better reflects the dispersion appropriate for a scenario of magnitude, distance, and spectral acceleration at a given period.

Two studies that have explored a similar objective to the present work were published by Hancock et al. (2008) and Heo et al. (2011). In each of these publications, a more rigorous benchmark was defined by performing regression analysis on the results of many response-history analyses – in the former case, regression relationships were defined in terms of seismological parameters such as magnitude and distance, while, in the latter case, spectral response ordinates were used, similar to the PEER GMSM "point of comparison." When comparing with this benchmark, neither study found the bias identified by previous researchers.

The studies differed in the target spectrum used for matching. Hancock et al. (2008) used two scenario response spectra, from the median and median-plus-one-sigma response from a ground motion prediction equation. Heo et al. (2011) matched records to the ASCE/SEI 7-05, *Minimum Design Loads for Buildings and Other Structures* (ASCE, 2006), design spectrum – effectively a Uniform Hazard Spectrum (UHS). Neither of these studies, therefore, investigated the same objective as the PEER GMSM study, in which the scenario was represented in terms of a single spectral acceleration value, and relevant seismological parameters – appropriate when a probabilistic seismic hazard analysis (PSHA) and disaggregation have been carried out, or disaggregation results have been obtained from the USGS website. The present study, therefore, aims to extend the PEER GMSM work to spectrum-matched motions, making use of the structural models and benchmark results that have been employed therein.

It is worth noting that the study by Bazzurro and Luco (2006) and part of the study by Huang et al. (2008b) used near-fault motions, both unmodified and as seeds to spectrum matching. It is likely that several of these records contained velocity pulses before matching, and that some of these pulses would have been removed by spectrum matching to a smooth target (see Section B.3). This would have amplified the difference between the unmatched and matched records observed by the authors.

B.2.1.2 Assessing Adequacy of Spectrum-Matched Ground Motions

Spectrum matching can introduce varying amounts of artificial modification to seed records, and therefore, not all spectrum-matched motions are equally valid. Since the objective of modifying real recorded ground motions is to retain the non-stationary characteristics of the seed record, large artificial adjustments could be seen as unacceptable.

Apart from qualitative recommendations in the RspMatch2005 documentation (Hancock et al., 2006) and the anecdotal suggestion to select appropriate seed ground motions to ensure that required changes are minimal (Grant et al., 2008), there are no quantitative studies investigating the effect that large changes can have on nonlinear structural response prediction. In practice, spectrum-matched motions are generally assessed by visually comparing the traces of acceleration, velocity, displacement, and

possibly Arias Intensity, before and after matching, and making a judgment as to whether introduced changes should be considered significant. Arias Intensity is often cited as being a measure of the ground motion energy content. However, this is only true in the sense it was derived by Arias (1970), who integrated input energy demand over an infinite, evenly-spaced frequency range. For application to a single structural model, for which the response is governed by a relatively narrow range of frequencies, the change in Arias Intensity does not seem to be the most reasonable measure of how much the structural demand imposed by the ground motion is affected by the matching process.

Commonly, more ground motions are generated than required, and the "best" are selected for analysis – again, selected by visually comparing changes to the signal in the time domain. Records that do not converge are discarded in favor of those that do. While this seems a reasonable procedure, there is the potential for this filtering to introduce bias into structural analysis results, if there is a systematic reason that some ground motions are changed more than others. For example, anecdotally it seems that records of longer duration may converge more easily in RspMatch2005, and may also be modified less by the process. This makes some intuitive sense, as a longer record may have less correlation between the times at which peaks occur, and therefore, RspMatch2005 would alter different portions of the record for matching spectral ordinates at different periods. The longer duration records that pass through this screening may bias the demand for duration-sensitive structures. This potential for bias needs further exploration – both for ground motions containing velocity pulses, and those without.

B.2.2 Objectives of Study

This study seeks to assess the accuracy and precision of nonlinear response-history analysis results carried out with spectrum-matched ground motions. The earthquake scenarios are defined as in the PEER GMSM work, and are therefore given in terms of magnitude, distance and a single response spectral ordinate at the fundamental period of each structure. This reflects the practical situation where a PSHA and a disaggregation have been carried out, and allows construction of a Conditional Mean Spectrum (CMS) for selection, scaling, and matching of ground motions.

B.2.3 Description of Structural Models

Two models from the PEER GMSM study were used – the 12- and 20-story reinforced concrete special moment frames, referred to as Building B and Building C, respectively. These models were selected to allow comparison with the PEER GMSM work, and because a high-level point of comparison had been developed as part of that work that could also serve as a benchmark for the results of this work (see Section B.2.5). The special moment frames were designed as part of the ATC-63 project, which produced the FEMA P-695, *Quantification of Building Seismic*

Performance Factors (FEMA, 2009) report following design requirements of IBC 2003, *International Building Code* (ICC, 2003), ASCE/SEI 7-02, *Minimum Design Loads for Buildings and Other Structures* (ASCE, 2002), and ACI 318-02, *Building Code Requirements for Structural Concrete* (ACI, 2002).

The fundamental periods, T_1, for Buildings B and C are 2.01 seconds and 2.63 seconds, respectively.

B.2.4 Description of Earthquake Scenario and Ground Motions

Two earthquake scenarios from the PEER GMSM study were used. The following descriptions are taken from that study:

1. "M7.0 scenario": A magnitude-7 earthquake occurring on a strike-slip fault, at a site that is 10 km from the fault rupture on soil with $V_{s,30}$ of 400 m/s (shear wave velocity for the top 30 m of the soil profile). The ground motion for this scenario is also constrained to have a spectral acceleration demand at the building's first-mode period, $S_a(T_1)$, that is two standard deviations above the median predicted value (using the Campbell and Bozorgnia 2008 ground motion prediction equation). This type of ground motion event is also often referred to as a "+2ε motion." This scenario is used for both Buildings B and C.

2. "M7.5 scenario": This is the same as the magnitude-7 scenario but is a magnitude-7.5 event, and the ground motion has an $S_a(T_1)$ value that is only one standard deviation above the median predicted value (i.e., a "+1ε motion"). This scenario is used only for Building C.

In the PEER GMSM study, ground motions were provided for each selection and scaling method in four suites containing seven ground motions each, for a total of 28 ground motions. In this study, where ground motions were taken from the PEER GMSM work, either unmodified or as seeds for spectrum matching, all 28 ground motions were considered as a single suite. This allowed the comparison of accuracy and precision among the different selection and matching methods to be carried out more readily. In addition, for some comparisons, records were developed using the method of Jayaram et al. (2011), in which the variance associated with the conditional spectrum is taken into account. These ground motions are more variable than those produced using other methods, and therefore, 40 ground motions were developed using this methodology.

Table B-1 lists a summary of the ground motion suites used in this study. Suites are designated by a label, with "U" referring to unmatched motions, and "M" referring to matched motions. The main suite of initial seed ground motions are referred to as Suite U1, and are the same as those referred to as "Method 300" in the PEER GMSM study. They were selected and linearly scaled to minimize the sum of the squared errors between the logarithms of the spectral ordinates, and the logarithms of the

spectral ordinates of the target conditional mean spectrum. This was evaluated at 20 logarithmically-spaced period values, between $0.2T_1$ and $2.0T_1$. This objective in ground motion selection ensures that the required changes to the spectra of seed motions are small, and therefore, ideally that the changes to the ground motions are also minimized.

Table B-1   Summary of Ground Motion Suites

Suite	Selection	Target Spectrum	Period Range	Damping Value(s)
		Unmatched Motions		
U1	28 x PEER GMSM Method 300			
U2	28 x PEER GMSM Method 100			
U3	40 x Jayaram et al. (2011)			
		Spectrum-Matched Motions		
M1	Same as U1	CMS	$0.2T_1$–$2.0T_1$	5%
M2	Same as U1	UHS	$0.2T_1$–$2.0T_1$	5%
M3	Same as U1	CMS	$0.2T_1$–$3.0T_1$	5%
M4	Same as U1	CMS	$0.2T1$–$2.0T_1$	5%, 20%
M5	Same as U1	CMS	$0.2T_1$–$3.0T_1$	5%, 20%
M6	Same as U2	CMS	$0.2T_1$–$2.0T_1$	5%
M7	Same as U2	CMS	$0.2T_1$–$3.0T_1$	5%
M8	Same as U2	CMS	$0.2T_1$–$2.0T_1$	5%, 20%
M9	Same as U3	CMS	$0.2T_1$–$3.0T_1$	5%
M10	Same as U1	CM+σ	$0.2T_1$–$3.0T_1$	5%

Acceleration histories for all the ground motions from suites U1 and M1 (before and after matching) for Building C with Scenario M7 are shown in Figures B-1 and B-2.

Spectrum matching was carried out using the program RspMatch2005. Default parameters suggested in the RspMatch2005 documentation were used, including the recommended 40 matching periods per order of magnitude interval, and a matching tolerance of 5% (i.e., ±5% error on the output record response spectrum, compared with the target spectrum). In several cases, it was not possible to achieve convergence with this tolerance, although generally the match was reasonable over almost the entire period range, and the average mismatch was small. The RspMatch2005 documentation recommends performing matching in multiple sweeps, successively incorporating longer periods into the matching process to better preserve the non-stationary content in the seed ground motions. In all the analyses reported in this chapter, two period sweeps were used.
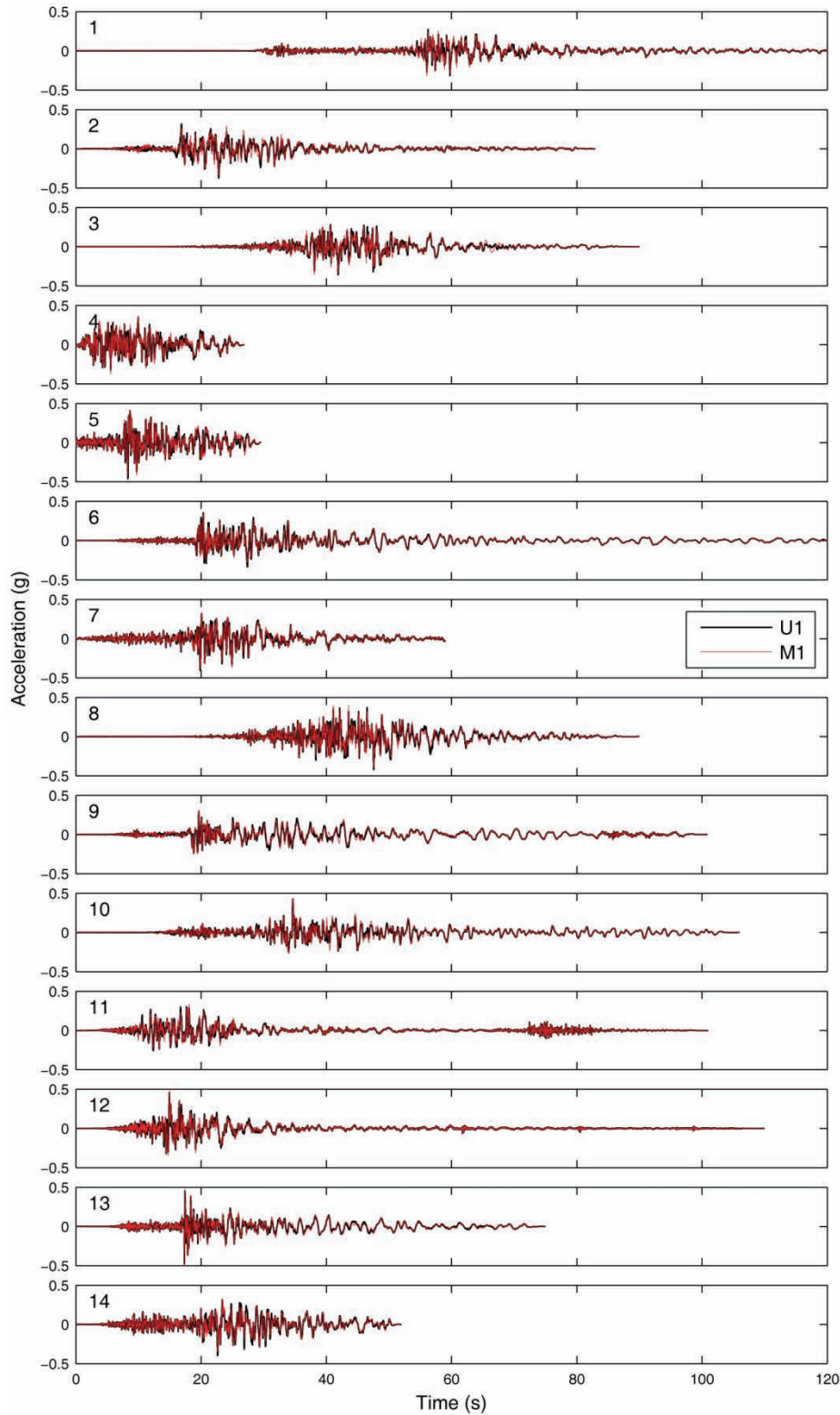
Figure B-1   Acceleration histories before (Suite U1) and after (Suite M1) spectrum matching for Building C, Scenario M7. Ground motions 1–14.
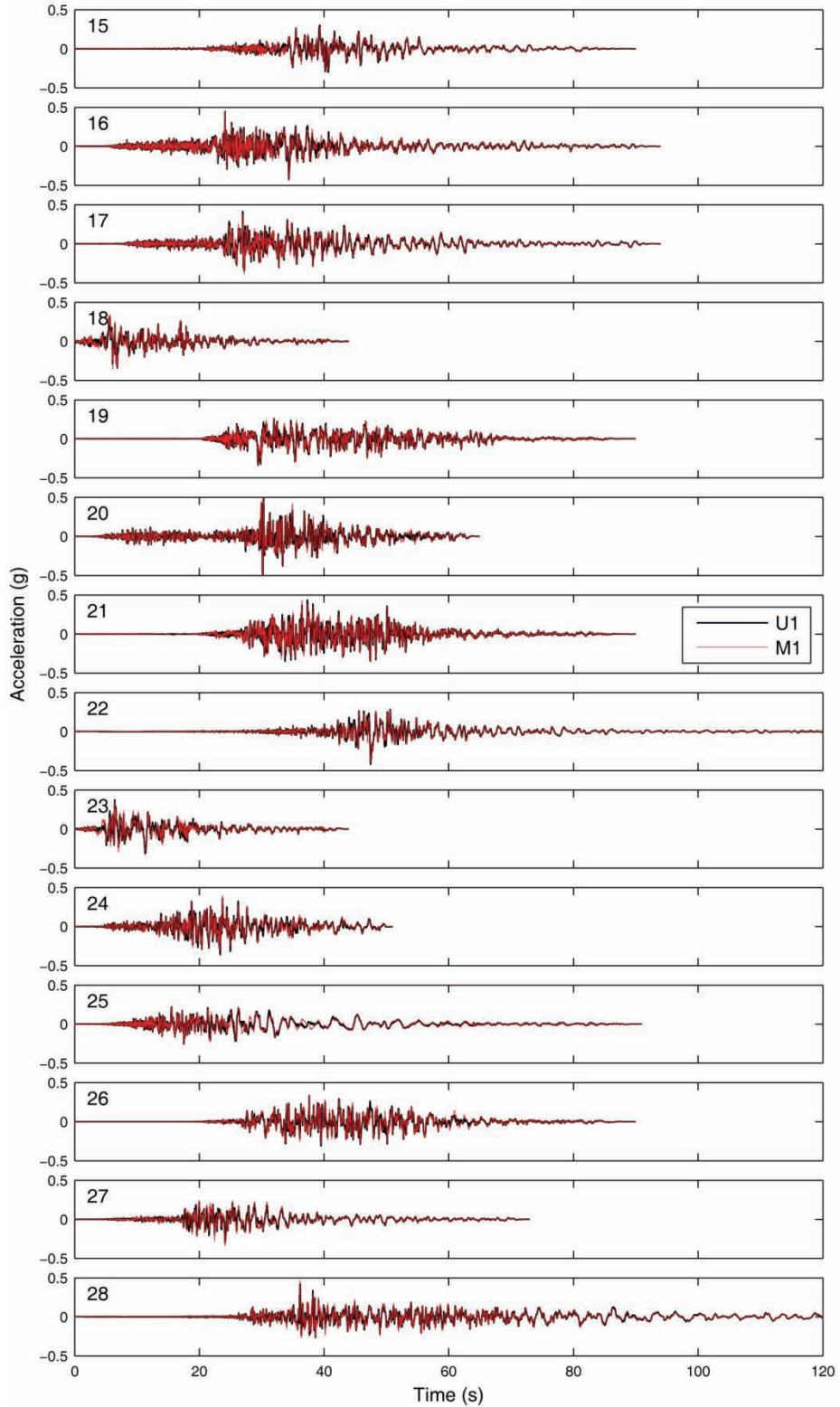
Figure B-2   Acceleration histories before (Suite U1) and after (Suite M1)
                  spectrum matching for Building C, Scenario M7. Ground motions 15–
                  28.

Initially, and except where otherwise noted, ground motions were spectrum matched over a period range between $0.2T_1$ and $2.0T_1$, and for a damping ratio of 5%. This is wider than the period range of $0.2T_1$ to $1.5T_1$ given in ASCE/SEI 7 for selection and scaling of ground motions, but is consistent with the PEER GMSM Method 300 record selection, and is also the range given in Eurocode 8 for selection and scaling (CEN, 2004). The damping value of 5% is consistent with the ASCE/SEI 7 representation of seismic demand, although Hancock et al. (2008) have shown that matching to multiple damping values can reduce the dispersion of dynamic analysis results.

Since the CMS is different for each model and scenario, different ground motions are selected, scaled and matched for each. Note that the suites based on Method 100 from the PEER GMSM work (Suites U2, M6, M7, and M8) were only developed for the Building C, M7 scenario model, and therefore, spectra and analysis results are only shown for this model.

Response spectra (5%-damped) for the unmatched motions (Suites U1, U2 and U3) are shown in Figures B-3 through B-5, along with the CMS for each building model and scenario. The records in Suite U1 (Figure B-3) provide, on average, a reasonable initial match to the target CMS across the range of periods considered in their selection (from $0.2T_1$ to $2.0T_1$). The records in Suite U3 (Figure B-5) were selected to include the dispersion in the conditional target spectrum using the method of Jayaram et al. (2011), and are compared with both the conditional mean spectrum and the $\pm 1\sigma$ bounds on the conditional spectrum. Note that Suite U1, selected to be as close as possible to the CMS, has significantly less dispersion than Suite U3. Suite U2 (for Building C, Scenario M7 only) was selected based on magnitude and distance bands, and scaled to the spectral acceleration at the fundamental period only; since ε was not considered in their selection, at other periods, the record spectra tend to be higher than the CMS, and the dispersion on the spectra is large.
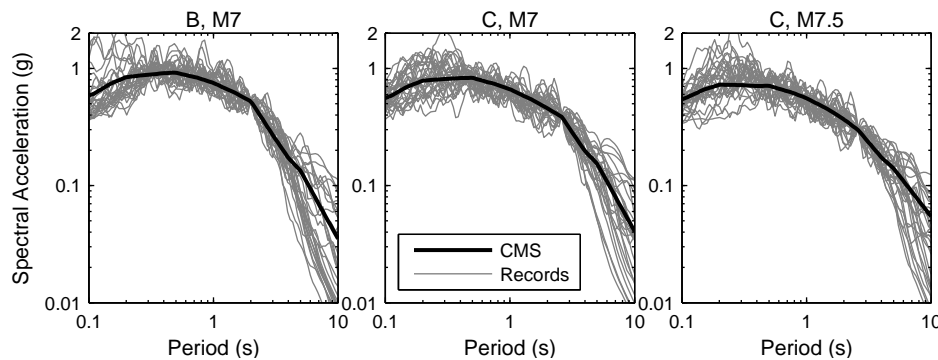
Figure B-3   Response spectra for Suite U1.
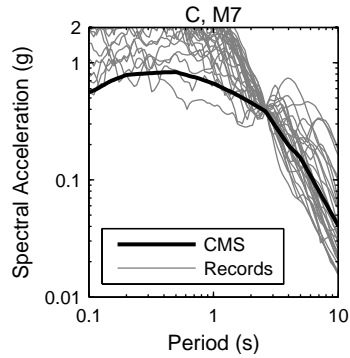
Figure B-4   Response spectra for Suite U2 (Building C, Scenario M7 only).
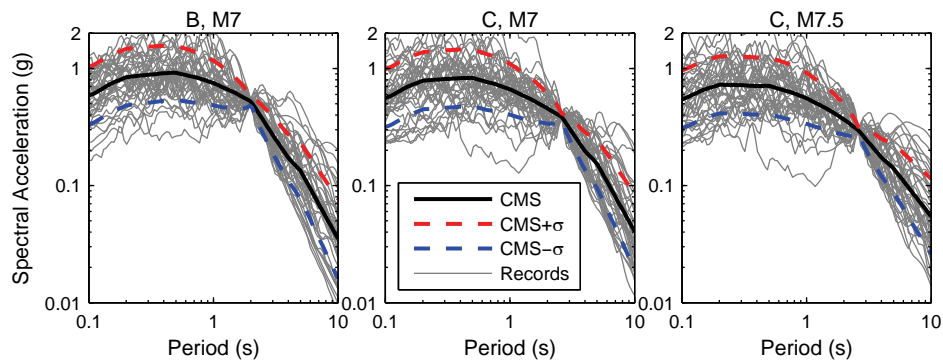
Figure B-5   Response spectra for Suite U3.

Response spectra for one set of matched motions (Suite M1) are compared with the target spectrum in Figure B-6. The ground motions are the same as those in Figure B-3, following spectrum matching to the CMS across the period range $0.2T_1$ to $2.0T_1$, for damping of 5% only. The matched period range is shown unshaded in the plot (i.e., shaded periods were not controlled in the matching process). The records are closely matched to the target spectrum (within the 5% input tolerance) over the period range of matching, but retain a similar level of dispersion for periods outside this range.
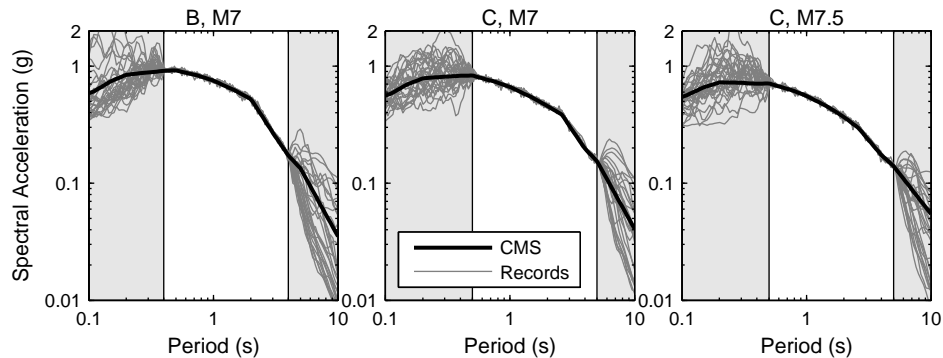
Figure B-6   Response spectra for Suite M1 (matched to Conditional Mean Spectrum, $0.2T_1$ to $2.0T_1$, 5% damping).

Following an initial study with these period and damping values (Suite M1), described in the following, it was found that the variation still present in the spectral ordinates outside this period range had an effect on the prediction of the engineering demand parameters considered (see below). Furthermore, Hancock et al. (2008) suggest that spectral ordinates with higher damping values may be a suitable proxy for the prediction of inelastic response, and therefore that spectrum matching should be carried out at multiple damping values. It was found that spectral ordinates at periods of $3.0T_1$ were correlated with first-mode dominated demand parameters, as were spectral ordinates at T_1 with damping of 20%. Spectral ordinates at periods of $0.02T_1$ were correlated with higher-mode dominated demand parameters. With the objective of improving estimates of maximum interstory drift (also referred to as maximum story drift), the period range for spectrum matching was extended out to $3.0T_1$ in Suites M3, M5, M7, M9 and M10. Furthermore, a target 20%-damped spectrum was developed (by taking the median of the 20%-damped spectra in Suite U1), and matching was carried out to both the 5%-damped and 20%-damped target spectra in suites M4, M5 and M8. The option of extending the matching to shorter periods was not pursued here, although could be valuable for predicting higher mode dominated quantities, provided that convergence can still be achieved with the matching software.

B.2.5 Structural Analysis Results

Analyses were carried out for Buildings B and C with Scenario M7, and Building C with Scenario M7.5 (except for the analyses for Suites U2, M6, M7, and M8, for which only Building C with M7 scenario was considered). Since a different target spectrum is appropriate for each, different seed records and target spectra were used.

Structural results are presented in terms of maximum interstory drift ratios (MIDR) over all levels in each building model and peak floor acceleration at roof level (PFA). A third engineering demand parameter – secondary floor response spectral ordinates for the roof level and a period of 1.0 seconds (FSa) – was also considered; results for FSa are not presented here, but conclusions were broadly similar to those for PFA. The MIDR quantity is expected to be primarily first-mode controlled, while PFA and FSa involve larger contributions from higher modes. In each of the figures in this section, circular markers show the results from each analysis in the suite, and horizontal lines mark the median (50th percentile) and counted 16th and 84th percentiles. Collapses are plotted separately, and if the counted 84th percentile is in the collapse range, this is not plotted.

Point of comparison benchmarks were only available from the PEER GMSM study for MIDR. The methodology for developing these point of comparison benchmarks involves carrying out hundreds of response-history analyses on the same structural model used here, and developing a regression model to predict the MIDR response in

terms of important ground motion parameters (such as spectral ordinates at several periods). Then PEER NGA ground motion prediction equations are used to develop distributions for these ground motion parameters, which are convolved with the MIDR regression relationships to estimate median MIDR for the scenarios defined in Section B.2.4.

The points of comparison are shown as a grey horizontal line on each of the figures in this section, and are considered the best estimate of the "true" MIDR response for the purposes of this study (see further discussion in Haselton et al. (2009)). For the other two response quantities considered, the median value from 40 records selected and scaled using the method of Jayaram et al. (2011) is taken as the point of comparison. It is recognized that this is not as robust as the PEER GMSM points of comparison for MIDR. However, the favorable comparison for the median of these analyses with the MIDR point of comparison and the rigorous approach used to develop this suite of records gives confidence that this is the most appropriate point of comparison, in lieu of a more detailed derivation such as in Haselton et al. (2009).

For Building C with M7.5 scenario, the PEER GMSM report was not conclusive and listed two estimates, 0.0148 and 0.016, while the results for the Jayaram et al. (2011) records reported a median value of 0.0155, which is between the two values reported, although marginally closer to the higher of the two. Thus, it is not possible to select between the two point of comparison values with any confidence on the basis of this comparison. For the remainder of this study, however, the higher value of 0.016 is used as the point of comparison for this scenario.

B.2.5.1 Results for Unmatched Ground Motions

Figures B-7 and B-8 show the MIDR and PFA results for Suites U1 and U3 for each structure and scenario considered. The results for Suite U1 are identical to those reported in Haselton et al. (2009) (referred to as Method 300). As could be expected, the results from Suite U3 exhibit significantly more dispersion in the output, and therefore, more structural collapses. The median MIDR results are similar across the three building model and earthquake scenario combinations, although for Building B, Suite U1 results are slightly lower than the point of comparison, while Suite U3 results are nearly identical to the point of comparison. This result, along with the other buildings/scenarios, validates the use of the Jayaram et al. method as a point of comparison for the other response quantities in the remainder of this study. Note that the counted 84th percentile response for Building B with M7 scenario, and Building C with M7.5 scenario, is in the collapse range.

For the other two response quantities, the median result from Suite U1 (Method 300) gives a reasonable match of the adopted point of comparison, although for Building C with M7 scenario, the PFA (and FSa, not shown) are biased low.
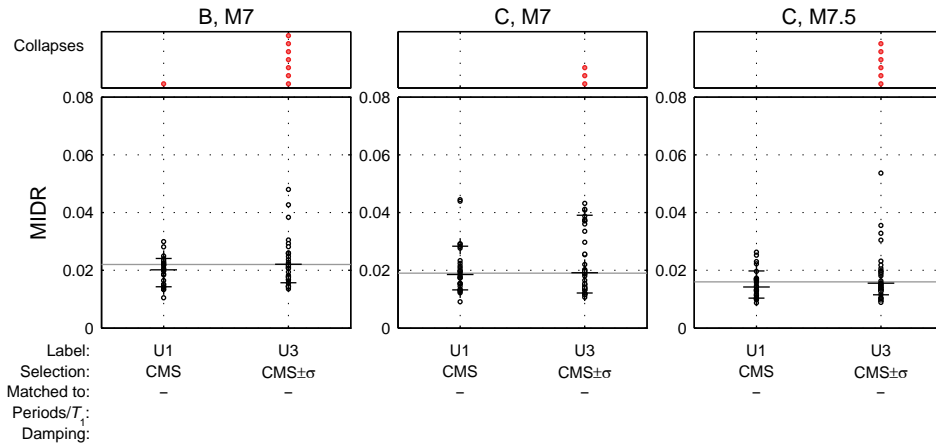
Figure B-7   Comparison of maximum interstory drift ratios for Suites U1 and U3.
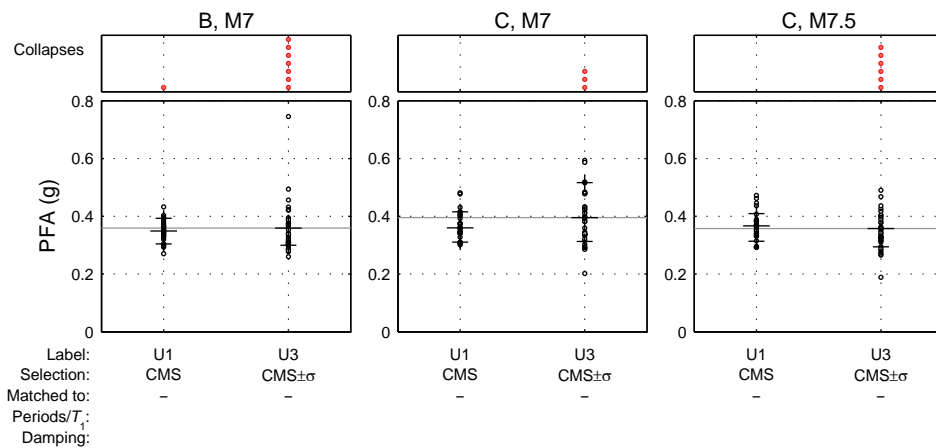
Figure B-8   Comparison of peak floor accelerations for Suites U1 and U3.

B.2.5.2 Results for Spectrum-Matched Records with Default Parameters

The ground motions from Suite U1 were spectrum matched to the target spectrum with 5%-damped CMS, over a period range of $0.2T_1$ to $2.0T_1$, with other parameters as described in Section B.2.4. The spectra of the resulting ground motions from this suite were compared with the target CMS spectra in Figure B-6. The dispersion of the original seed records (Figure B-3) was relatively low, but the spectrum matching process results in spectra that are all within a small tolerance (in this case 5%) of the target spectrum, provided that they can be made to converge. The shaded period range on Figure B-6 marks the limits of the spectrum matching, beyond which significant dispersion still remains in the records.

Some studies on spectrum matching (e.g., Heo et al., 2011) have used a UHS as a target, and indeed this is probably more common in practical application. It has also been argued that matching to the UHS, which is generally higher than the CMS across most of the period range for positive ε values, may counteract the unconservative bias that some authors (Guyader and Iwan, 2006; Miranda and Ruiz

Garcia, 2002) have identified. On the other hand, the amount by which the UHS exceeds the CMS depends on the value of ε, and therefore, even if reasonable results are obtained matching to the UHS for one scenario (e.g., Heo et al., 2011), this conclusion may not hold generally for other values, e.g., $\varepsilon = 0$.

Nevertheless, the same initial seed records (Suite U1 as seeds) were also matched to the UHS for each of the scenarios, assumed to be represented by a constant ε above the median of the ground motion prediction equation. Since the records were originally selected to provide a close match to the CMS, and no additional linear scaling of the records was carried out prior to matching, the spectral ordinates of the records were generally increased by the matching process. Spectral ordinates outside the matched period range were generally lower than the UHS target, particularly for the M7, $\varepsilon = 2$ scenario, where the difference between the CMS and the UHS is largest.

Results from these two new sets of records are compared with the unmatched Suite U1 records, for MIDR in Figure B-9, and PFA in Figure B-10. For the MIDR results, the records matched to the CMS are comparable in median to the unmatched records, although in all three scenarios there is a small reduction, consistent with the hypothesis that reducing the dispersion of the input reduces the median response. There is not a significant benefit in reducing the dispersion of the output using these default parameters for spectrum matching over the unmatched records. It should be noted that the unmatched seed records generally showed a relatively close match to the target spectrum to begin with. If the dispersion is divided into a component due to the variation in the input spectra and a component due to the variable structural response given this spectral shape, only the first portion of this would be amenable to reduction by spectrum matching.

Label:	U1	M1	M2		U1	M1	M2		U1	M1	M2
Selection:	CMS	CMS	CMS		CMS	CMS	CMS		CMS	CMS	CMS
Matched to:	–	CMS	UHS		–	CMS	UHS		–	CMS	UHS
Periods/T_1:		0.2–2.0	0.2–2.0			0.2–2.0	0.2–2.0			0.2–2.0	0.2–2.0
Damping:		5%	5%			5%	5%			5%	5%
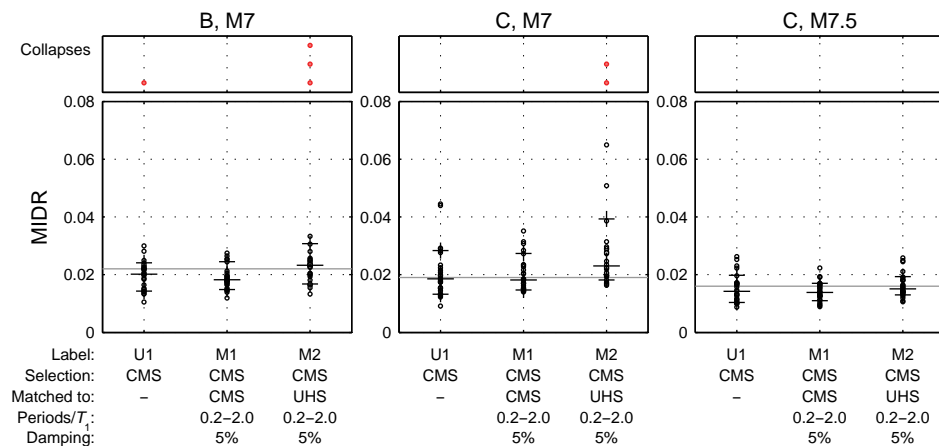
Figure B-9   Comparison of maximum interstory drift ratios showing Suite U1 (unmatched), Suite M1 (matched to Conditional Mean Spectrum), and Suite M2 (matched to Uniform Hazard Spectrum).

The records matched to the UHS show slightly higher median MIDR results, and result in more collapses than either of the other two sets. For Building B with Scenario M7, matching to the UHS does counteract the slightly negative bias observed for the other two sets, whereas for the Building C models, the median MIDR is either conservatively biased (for the M7 scenario) or almost perfectly matching the point of comparison (for the M7.5 scenario). The difference between matching to the CMS and UHS only appears to be significant (for MIDR) for the $\varepsilon = 2$ cases (M7 scenario), and not for the $\varepsilon = 1$ case (M7.5 scenario).

Results for PFA shows broadly similar trends for the records matched to the CMS. For the records matched to the UHS, there is a noticeable increase in the median PFA, even for the M7.5 scenario.
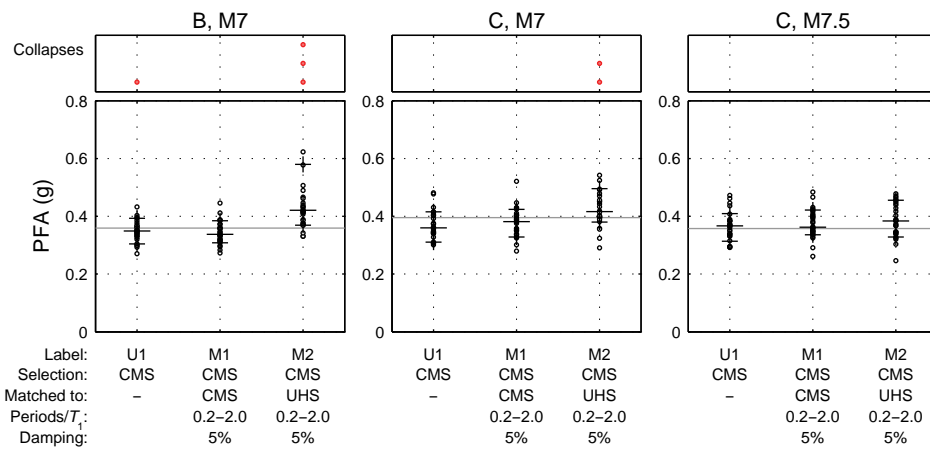
Figure B-10   Comparison of peak floor acceleration showing Suite U1 (unmatched), Suite M1 (matched to Conditional Mean Spectrum), and Suite M2 (matched to Uniform Hazard Spectrum).

Results from the next two subsections suggest that for records with a poor initial match to the target spectrum, a longer period range should be considered for spectrum matching. Suite U1 records used as seeds here for the matching process were selected and scaled to be a good initial match of the CMS, and not the UHS to which they were subsequently spectrum matched, meaning that the spectra for records matched to the UHS are generally lower than the target spectrum outside the $0.2T_1$ to $2.0T_1$ period range considered in the matching. Therefore, if anything, the results presented here for the UHS-matched records are likely to be lower than would be obtained if either a new set of initial seed records were used, initially selected and scaled to the UHS, or matching was carried out over a longer period range.

B.2.5.3 Effect of Period Range and Damping Values of Spectrum Matching

This subsection investigates the effect of matching ground motions over a wider period range, and for an additional damping ratio of 20%. To motivate this, simple linear regression was performed on the natural logarithms of spectral ordinates at

$0.02T_1$ and $3.0T_1$, and at the fundamental period, T_1, for damping of 20%. Statistically significant relationships were found for MIDR vs. $S_a(3T_1, 5\%)$ and $S_a(T_1, 20\%)$, and PFA vs. $S_a(0.02T_1, 5\%)$.

These conclusions were based on a limited amount of data (28 analyses), and if more analyses were carried out, the other relationships may be proved statistically significant. However, this does suggest that to reduce the dispersion of the results further from that shown in the previous subsection, it would be valuable to widen the period range for spectrum matching from at least $0.02T_1$ to $3T_1$, and to consider matching also a 20%-damped target spectrum. The upper limit on the period range and the 20%-damped spectrum are important for reducing the dispersion on first-mode dominated response quantities such as MIDR, while the lower limit on the period range is important for the higher-mode dominated quantities like PFA.

It becomes increasingly difficult to obtain convergence with RspMatch2005 as the period range is increased, and more damping values are targeted. Therefore, for the purpose of this section, only the modifications relating to improving the MIDR were considered, that is increasing the upper period limit to $3T_1$, and matching a target 20%-damped spectrum. Since the 20% damping ordinates are not included in the scenario considered here (and would not normally be available from the results of PSHA), the target spectrum for 20% damping was taken as the median 20%-damped spectrum from the 28 ground motions in Suite U1. In practical applications, the 5%-damped spectrum would need to be adjusted using factors from either standards such as ASCE/SEI 7, or relationships from literature (e.g., Stafford et al., 2008).

Three separate matching exercises were carried out here: (1) the upper period limit was increased to $3T_1$, with damping of 5% only; (2) the upper period limit remained at $2T_1$, and matching was carried out to both the 5%- and 20%-damped target spectra; and (3) both upper period limit was increased and 5% and 20% spectra were matched. As before, Suite U1 records were used as seeds.

The results for these new suites, M3, M4, and M5, are compared with the results for the unmatched seed records in Figures B-11 and B-12, which may be compared with the earlier results for the default matching parameters (Figures B-9 and B-10). For MIDR, the median results are similar to before, although a slight negative bias has been introduced for Building C with Scenario M7, for the two suites where the period range has been extended. The negative bias on Building B results has also been preserved. The dispersion is generally decreased, although the lower bound dispersion is limited by the potential for inelastic response to be predicted by elastic spectral ordinates. Results for Building C with Scenario M7.5 show the benefit of extending the period range and matching to higher damping values.
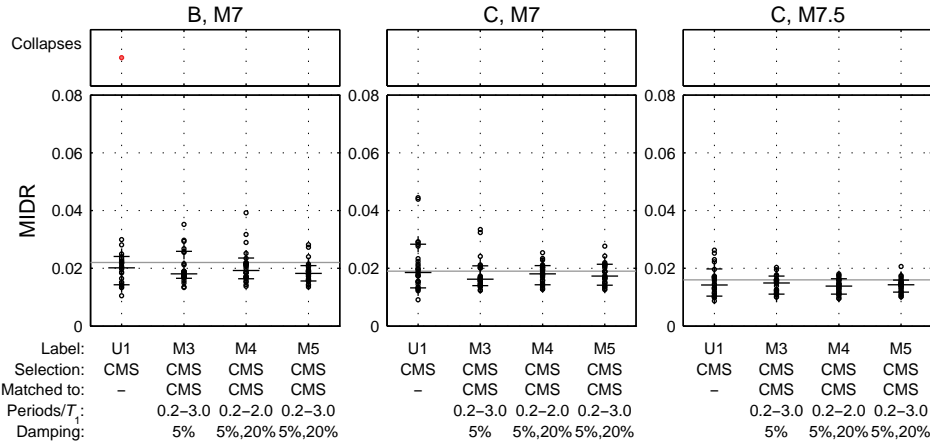
Figure B-11   Comparison of maximum interstory drift ratios showing Suite U1 (unmatched), Suite M3, Suite M4, and Suite M5 (matched to Conditional Mean Spectrum with different period range and damping assumptions).
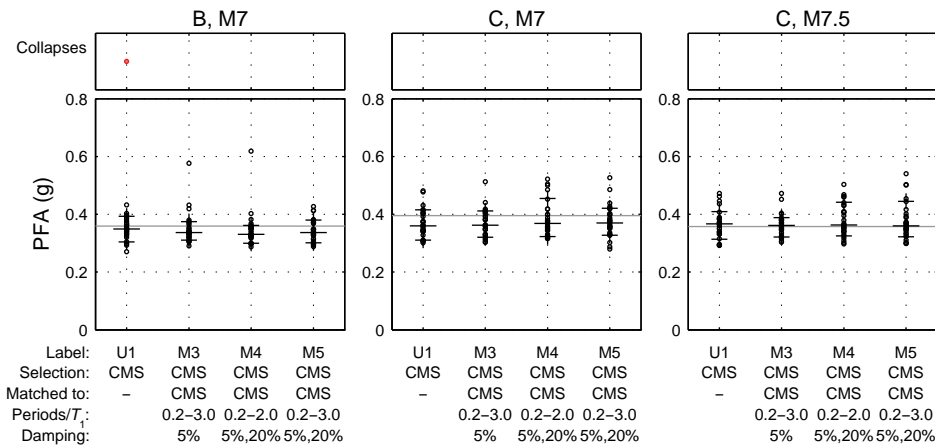
Figure B-12   Comparison of peak floor accelerations showing Suite U1 (unmatched), Suite M3, Suite M4, and Suite M5 (matched to Conditional Mean Spectrum with different period range and damping assumptions).

As could be expected, the PFA results are not significantly improved. The regression relationships derived previously did not show a significant dependence of PFA on either the spectral ordinates at $3T_1$, nor on the 20%-damped ordinate at T_1. It is expected that matching to lower periods may improve this result.

B.2.5.4 Effect of Initial Seed Motions

The ground motions from Suite U1 exhibit relatively little dispersion compared to other methodologies considered in that study, and therefore, the comparisons in the previous section do not show the full benefit of spectrum matching at reducing this dispersion. To further illustrate this, Suite U2 ground motions, selected with Method 100 in the PEER GMSM report, are considered in this subsection. These ground motions were selected based on a close match of scenario magnitude and distance,

and scaled such that their spectral acceleration at the fundamental period of the structure, $S_a(T_1)$, was equal to the target value. Only Building C with M7 scenario is considered in this subsection.

Since ε is not considered in the selection, the spectra for records in this set are on average higher than the target CMS at periods lower and higher than the fundamental period. In practice, the ground motions selected by Method 100 would typically be scaled to provide a better match of the spectrum over the full period range prior to spectrum matching, but in this case the original scale factors from the PEER GMSM study were maintained.

The ground motions were spectrum matched to the CMS target spectrum, initially with the default parameters and period range noted in Section B.2.4, and then successively considering the wider period range of the previous subsection, $0.2T_1$ to $3.0T_1$, and matching to 5%- and 20%-damped target spectra. In the latter case, the 20%-damped target spectrum was taken from the mean 20%-damped target spectrum for the unmatched Suite U1 ground motions (i.e., the same target considered in the previous section). Problems with convergence meant that it was not possible to consider both the wider period range and multiple damping levels as in the previous subsection.

Results for the three suites of spectrum-matched ground motions (Suites M6, M7, and M8) for the engineering demand parameters considered (MIDR and PFA) are compared with the results for the unmatched records in Figures B-13 and B-14. It is first worth noting that, as in the PEER GMSM study, the Suite U2 ground motions produce median MIDR estimates that are significantly higher than the point of comparison. This observation also applies for PFA.

The MIDR results are significantly improved by the spectrum matching, particularly for the two latter suites of records – with either the increased period range or two damping targets. In each case, the median MIDR is very close to the point of comparison, and the dispersion has been reduced significantly. Thus, spectrum matching out to a longer period range offers improvement of the median and reduction of the dispersion, where the spectral ordinates outside the matched period limits are on average higher than the target spectrum.

In the previous subsection, the records had been selected and scaled to be close to the target spectrum across the full range, and therefore, even at unmatched periods, the match was reasonable. Therefore, spectrum matching was mainly used to reduce the dispersion rather than to improve median estimates.
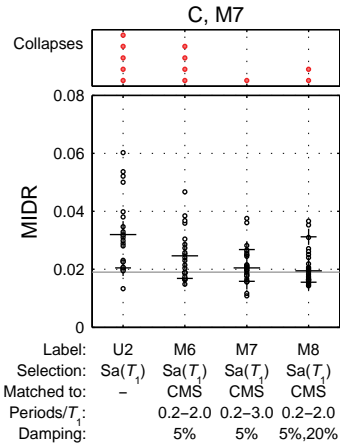
Figure B-13   Comparison of maximum interstory drift ratios showing Suite U2 (unmatched), Suite M6, Suite M7, and Suite M8 (matched to Conditional Mean Spectrum with different period range and damping ranges).
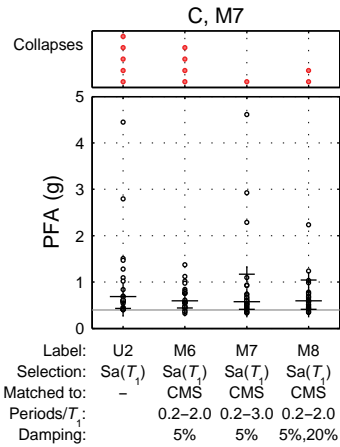
Figure B-14   Comparison of peak floor accelerations showing Suite U2 (unmatched), Suite M6, Suite M7, and Suite M8 (matched to Conditional Mean Spectrum with different period range and damping ranges).

PFA results are improved only slightly by spectrum matching, and are generally higher than the point of comparison. Based on the results of the previous subsection, this could presumably be improved by extending the period range of spectrum matching to lower periods (say $0.02T_1$).

B.2.5.5 Consideration of Dispersion in Spectrum Matching

Two sets of results are considered in this subsection, both related to the treatment of dispersion in spectrum matching, although otherwise unrelated. The first set of results are based on spectrum matching the ground motions from the method of Jayaram et al. (2011), for which the unmatched records were considered earlier, and referred to as Suite U3. This provides an interesting comparison with the results for

Suite U1, for which the initial dispersion had been minimized by the selection method used.

The second set of results are for the Suite U1 ground motions matched to the 84th percentile of the Conditional Spectrum (see Appendix A), abbreviated here as "CM+σ." The objective was to determine whether spectrum-matched ground motions could be used to estimate the distribution of an engineering demand parameter, and not just median values. Hancock et al. (2008) carried out a similar study, selecting and matching ground motions to an 84th-percentile target spectrum. However, in their case, this percentile value was based on the uncertainty in the ground motion prediction equation (i.e., they considered $\varepsilon = 1$ across the full period range), and not the uncertainty on the conditional spectrum, discussed in Appendix A.

Results for these two sets of ground motions are shown, along with the results for the unmatched Jayaram et al. (2011) records, in Figures B-15 and B-16 for engineering demand parameters MIDR and PFA. As in previous subsections, the results from ground motions matched to the CMS generally provide a good median estimate of the point of comparison for each of the parameters considered, and, in this case, reduce the dispersion of the results considerably.
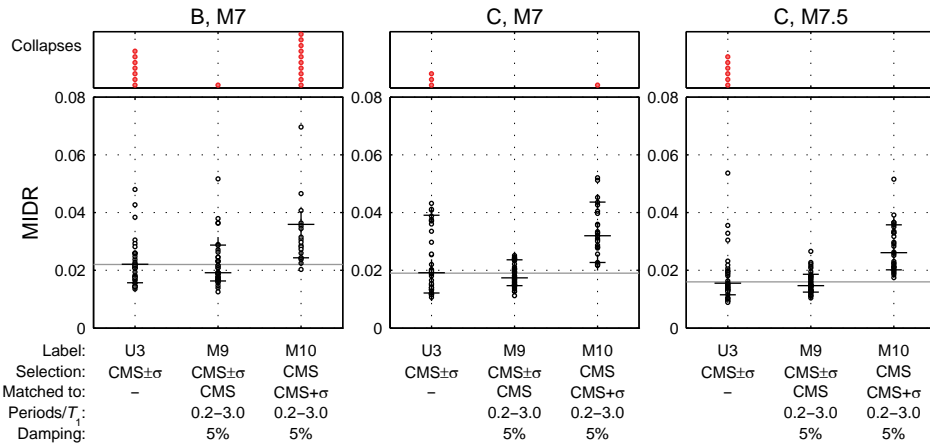
Figure B-15   Comparison of maximum interstory drift ratios showing Suite U3 (unmatched), Suite M9 (Suite U3 matched to Conditional Mean Spectrum), and Suite M10 (Suite U1 matched to Conditional Mean-Plus-One-Sigma Spectrum).
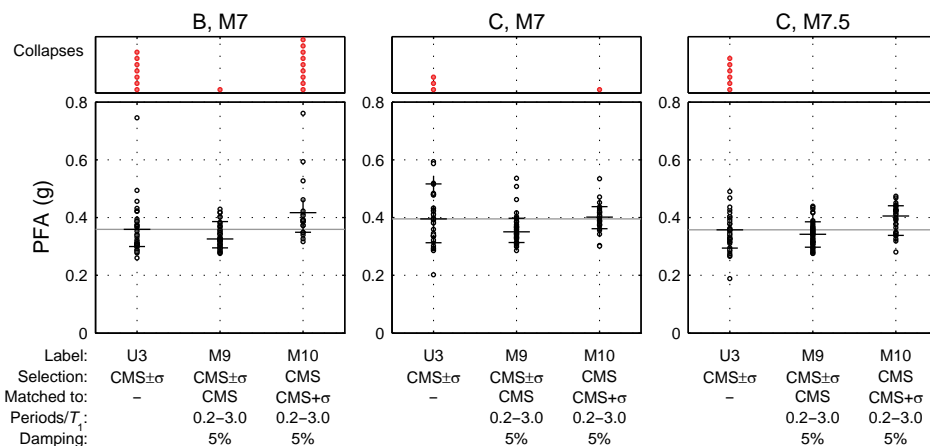
Figure B-16   Comparison of peak floor accelerations showing Suite U3
(unmatched), Suite M9 (Suite U3 matched to Conditional Mean
Spectrum), and Suite M10 (Suite U1 matched to Conditional Mean-
Plus-One-Sigma Spectrum).

In this case, it is assumed that the 40 records in Suite U3 for each scenario give a reasonable estimate of not just the median response, but also the distribution of response. For the ground motions matched to the CM+σ spectrum, the appropriate comparison is between the median of the matched motions and the 84th percentile of the unmatched motions. Unfortunately, the probability of collapse for Building B with Scenario M7, and Building C with Scenario M7.5, estimated from the unmatched records is sufficiently high (17.5% and 15%, respectively) that the counted 84th percentile results cannot be calculated (loosely speaking, the 84th percentile result is a collapse), and therefore, the comparison cannot be carried out. On the other hand, this suggests that the median result for the matched motions should also indicate collapse, which is not the case in the analyses carried out. Building C with M7 scenario, for which the 84th percentile estimate from the Suite U3 records is available, shows mixed results from this comparison. The 84th percentile MIDR value from the unmatched records is approximately double the point of comparison median estimate (3.9% vs. 1.9%). The median from the records matched to the CM+σ spectrum is 3.2%.

The discrepancy between these results could reflect a real difficulty with accurately estimating the 84th percentile response using ground motions spectrum matched to the CM+σ spectrum, or could be a problem with the point of comparison used. The number of 40 ground motions was selected for the Jayaram et al. method to obtain a robust estimation of the median, and more ground motions could be required to also obtain an accurate point of comparison for the whole distribution, including 84th percentile.

The dispersion in the estimation of engineering demand parameters from nonlinear response-history analysis is a combination of dispersion in the input spectrum (taken

into account in these analyses by explicitly matching to a higher percentile) and dispersion in nonlinear structural demand given an elastic spectrum (not taken into account here). An upper bound estimate for the latter portion of the dispersion (for this structural model) can be obtained from the "best" results in Figure B-12, for which the standard deviation of the ln(MIDR) values is around 0.20. The standard deviation in the input spectrum is different at different periods, but the effect of its variation can be judged by comparing the median from the CM+σ spectrum-matched results (3.2%) to the median from the CMS-matched results (1.6%). The implied standard deviation is ln(3.2/1.6) = 0.69. These standard deviations may be combined with the square root of the sum of the squares (SRSS) combination to give a total standard deviation of 0.72. This would give a best estimate for the 84th percentile of exp(0.72) $\times$ 1.6% = 3.3%. Therefore, this is not enough to explain the discrepancy in the 84th percentile prediction.

B.2.6   Assessing Adequacy of Spectrum-Matched Motions

In the studies reported in the previous section, no attempt was made to distinguish "acceptable" ground motions from "non-acceptable" ones, in terms of the amount of artificial modification introduced by the spectrum matching process. Partly, this is due to the concern that selection of a subset of ground motions from a bigger set may introduce bias to estimates of structural response, if the selection is not random or has a tendency to pick more or less demanding motions. For example, consider a ground motion with significant energy concentrated into a single pulse (such as the pulse-type motions discussed further in Section B.2). It is likely that peak response will occur at approximately the same time for all vibration periods (and, if relevant, damping values) of interest. Therefore, there is significant correlation between the artificial adjustments introduced by spectrum matching. In addition, convergence may be difficult to achieve. By contrast, for a long duration ground motion with different frequency content in different portions of the signal, it is easier for the program to modify spectral ordinates with different periods independently, and therefore, convergence may be rapid. Although this example is illustrative only, it shows that selecting ground motions simply because they converge or require minimal adjustment could feasibly introduce bias.

The usual justification for rejecting spectrum-matched motions that were significantly modified by the matching process is that they no longer exhibit "realistic" characteristics of actual recorded ground motions. Indeed, the algorithm is designed to introduce minimal artificial change to the non-stationary characteristics of the original signal, and allowing large modifications does defeat the purpose somewhat. There are two main ways in which spectrum-matched motions may be considered "unrealistic":

1. Their response spectra are smooth, whereas real recorded ground motions have more jagged spectra.

2. Their acceleration, velocity and displacement response is at least partially made up of artificial wavelet adjustments, whose functional form is related to their effectiveness in the spectrum matching algorithm more than to the physical nature of seismic signals (notwithstanding the efforts of Hancock et al. (2006), and Al Atik and Abrahamson (2010), to develop wavelets that do not lead to velocity and displacement drift when added to a signal).

The former reason is perhaps compelling, although it should also be noted that the jaggedness of a suite of real ground motions decreases as ground motion databases become larger, giving more real records to pick from. Each ground motion in the database may be considered a single realization of a random process, in the same way that Jayaram et al. (2011) generate a new random target for each ground motion they select. If a million random response spectra are needed to be simulated consistently with the statistical model of Jayaram et al. (2011), then selecting a few with the closest match to a smooth target spectrum would give much smoother spectra than those shown in Figure B-3 (Suite U1).

A more reasonable concern about spectral shape smoothing may be made when spectrum matching is used on records that did not provide a reasonable initial match of the target spectrum, potentially leading to a sharp gradient in the spectra of the matched records just outside the period range considered in the matching. For this reason, it is suggested that ground motions should be initially selected and scaled to minimize the initial discrepancy between the initial response spectrum and the target spectrum (Grant et al., 2008). Even if this selection only takes into account the periods considered in the matching, the suite of ground motions selected will, on the average, match the target spectrum outside this range – at least if the target is appropriate (see, for example, Figure B-6).

The second reason noted above for why spectrum-matched motions may be considered "unrealistic" is the focus of this section. In practice, engineers will often plot the acceleration, velocity and displacement of the unmatched and matched motions versus time, and qualitatively compare the changes that have been introduced. It is also common to compare the Arias Intensity (Arias, 1970; Husid, 1973) before and after matching, and to reject ground motions with large changes (Hancock et al., 2006). Apart from possible biases that may be introduced through this pruning process, noted above, this also introduces subjectivity, as different practitioners will have different standards for what changes may be considered acceptable.

Regardless of the reasons that spectrum-matched motions may be considered unrealistic, their effectiveness should be judged on their use in response-history analysis, and whether or not they lead to accurate and precise estimates of the "true"

structural response. Accuracy in this context refers to a lack of a systematic conservative or unconservative bias in prediction of response; precision refers to a relatively low dispersion in results, to allow confident estimates of the mean. Even a clearly unrealistic matched ground motion (say when the initial seed motion is scaled to a small fraction of the target spectrum, and therefore, the spectrum matching process essentially creates a fully artificial signal) should be considered acceptable, if its use in response-history analysis does not produce any discernable bias in the estimation of any engineering demand parameters of interest. In this sense, spectrum matching could be considered a "means to an end" – even if the actual ground shaking the structural model is subjected to does not represent a physically realizable process, if this cannot be determined by observing the output it should be considered irrelevant.

Before investigating further whether large changes in spectrum matching introduce bias, it is worth noting a few final points:

- The idea of spectrum matching is to modify a seed record such that its spectrum closely matches a target spectrum over a range of periods. That is, the intensity of the ground motion (as measured through its elastic response spectral ordinates) was in some way not appropriate, and spectrum matching is designed to fix this. Therefore, other measures of ground motion intensity may have also changed. If they were not, it would be possible to conclude that spectrum matching was cosmetic only, and not useful for generating ground motions with reasonable demand on nonlinear systems.

- Linear scaling, i.e., multiplying the whole signal by a constant scaling factor, is routinely used, as it helps to compensate for relatively few earthquake recordings of intensity comparable to code demand levels. Many studies have investigated whether linear scaling introduces bias, and the conclusion appears to be that large scaling is permissible provided that spectral shape is taken into account (Baker, 2007a). Scaling a motion by a factor of 2, say, changes the peak ground acceleration (and many other scalar intensity measures) by a factor of 2, and the Arias Intensity by a factor of 4. Arguably, any measure of acceptable change to a ground motion should take into account that large linear scaling is considered permissible. In this study, the initial seed motion (against which any changes are measured) is always taken as the linearly scaled motion, immediately prior to spectrum matching.

- Artificial wavelet adjustments (as in RspMatch2005) to a ground motion are not necessarily unrealistic. In fact, the main use of wavelet analysis is in the wavelet transform, which allows decomposition of any time series into a number of wavelet functions, subject to certain criteria on the signal itself and the choice of wavelet basis (e.g., Mallat, 1999). Therefore, any ground acceleration history may be considered to be a large number of wavelet adjustments to a zero initial

signal. Similarly, the wavelet-transform-based matching algorithms discussed previously can be considered an extension of linear scaling, in that the original wavelet components of the signal are scaled separately. Of course, the frequency and phase characteristics of wavelet decompositions of real ground motions may not match those of spectrum-matched motions, but it does offer a sense in which wavelet adjustments may be considered "realistic."

With this motivation, the change measured in spectrum matching will be discussed in the next subsection. A useful measure of change will be one which offers some predictive power in assessing whether bias will be introduced to the results of nonlinear response-history analysis. Only changes to an original seed motion are investigated, and not absolute measures of ground motion intensity. For example, whether or not peak ground velocity (PGV) is a good predictor of nonlinear response is not considered, as presumably this conclusion will apply regardless of whether spectrum matching has been carried out. Therefore, if other parameters like PGV are important, they should be considered in the initial ground motion selection – whether spectrum matching is to be carried out or not.

B.2.6.1 Measuring Changes Introduced By Spectrum Matching

In this subsection, a number of scalar measures of change are introduced, to quantify the adjustment made by spectrum matching to the initial seed ground motion. The measures are summarized and described in Table B-2. Scalar measures are preferred, as they allow robust quantitative acceptance criteria to be developed based on regression analysis on results of structural analysis. It is recognized, however, that scalar measures can miss features that visual comparisons of ground motion histories over time can make evident.

It is worth simply noting, however, that it is common for parameters based on acceleration (for example Arias Intensity) can be changed significantly by the matching process, while parameters based on velocity or displacement are hardly affected, or vice versa.

The parameters referred to as "maximum difference in normalized peak parameters" in Table B-2 compare the build-up over time of cumulative squared quantities, normalized with respect to their final values. The relative change parameters are taken as the absolute maximum value of the difference between the normalized curves. The cumulative squared velocity (CSV) build-up over time is shown along with the normalized CSV versus time in Figure B-17, and the $\max(\Delta CSV_{norm})$ measure is identified as the maximum difference between the curves in the latter plot. Note that, in this case, the difference in final CSV values is relatively small (12%), but the maximum normalized difference parameter illustrates the difference in the time over which the cumulative squared velocity builds up. A similar measure was

used by Anderson (2004) for comparing physics-based (synthetically-generated) records with real recorded ground motions.

Table B-2   Summary of Measures of Change Considered in this Study

Type	Parameter	Description
Peak ground motion parameters	ΔPGA	Ratio of peak ground acceleration in matched ground motion to seed motion
	ΔPGV	Ratio of peak ground velocity
	ΔPGD	Ratio of peak ground displacement
Cumulative squared ground motion parameters	ΔAI	Ratio of final value of Arias Intensity
	ΔCSV	Ratio of final value of cumulative squared velocity
	ΔCSD	Ratio of final value of cumulative squared displacement
Max difference in normalized peak parameters	$\max(\Delta AI_{norm})$	Maximum difference over time of Arias Intensity normalized with respect to final value, between matched ground motion and seed motion
	$\max(\Delta CSV_{norm})$	Maximum difference over time of cumulative squared velocity normalized with respect to final value
	$\max(\Delta CSD_{norm})$	Maximum difference over time of cumulative squared displacement normalized with respect to final value
Input energy and integral parameters	$\Delta IE(T_1)$	Ratio of input energy (per unit mass) at fundamental period of structure
	$\Delta \int IE(T)\,dT$	Ratio of input energy (per unit mass) integrated over periods between 1 and 2 times fundamental period
	$\Delta \int IE(\omega)\,d\omega$	Ratio of input energy (per unit mass) integrated over natural frequencies between 0.5 and 1 times fundamental frequency

(a)

(b)
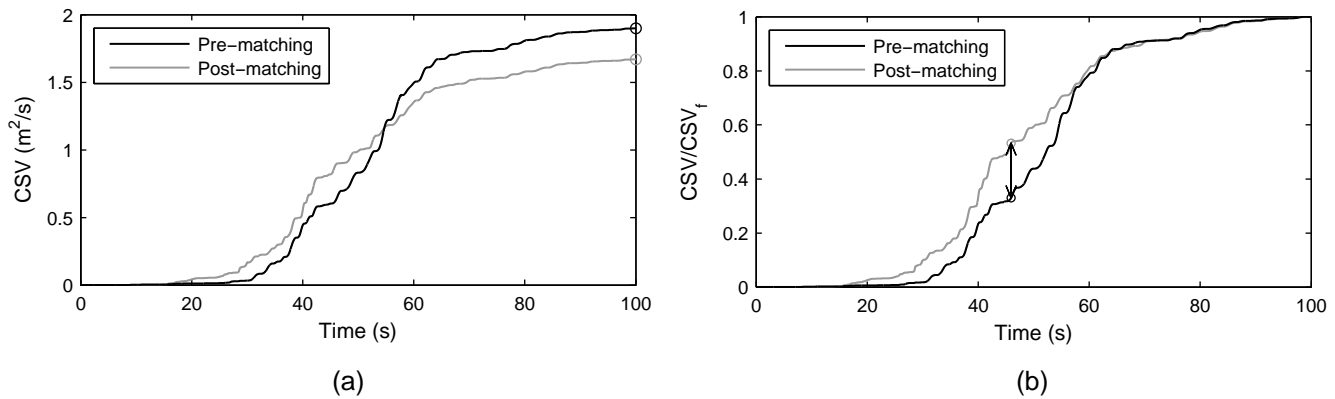
Figure B-17   Plots showing: (a) example cumulative squared velocity history, pre- and post-matching; $\Delta I = 0.880$; (b) example normalized cumulative squared velocity history, pre- and post-matching; $\max(\Delta CSV_{norm}) = 0.203$.

In the current context, these measures have the advantage that they are insensitive to initial scaling of the ground motions. As noted in the previous section, linear scaling of ground motions is usually considered to be acceptable, and yet all of the other

measures of change that have been discussed would indicate changes proportional to the scaling factor (for peak ground motion measures) or to the scaling factor squared (for cumulative squared parameters). Unlike other measures, the maximum normalized difference parameters are not defined as a ratio, but by an absolute difference. The example in Figure B-17b shows that the difference may take values between zero (for two identical signals or signals differing only by a constant linear scaling) and one.

The final set of parameters considered relate to the energy that the ground motion imparts to a single degree of freedom system. Arias Intensity (AI) was originally derived by Arias (1970) based on energy considerations where he showed that the expression for Arias Intensity as a scalar multiple of the cumulative squared acceleration could be obtained by integrating the input energy per unit mass to single-degree-of-freedom (SDOF) systems with zero damping over evenly spaced frequencies from zero to infinity. For damped systems, there is an extra constant term in front of the integral, which is close to unity for typically small levels of damping.

Arias Intensity is often cited as a measure of the energy content of a ground motion signal, although from the derivation referred to above, it is clear that this is true only in the specific sense of an infinite range of uniformly spaced frequencies. For a specific application, such as deciding whether or not artificial modifications to a ground motion will affect the nonlinear response of a particular structure, it is perhaps less relevant. Therefore, the first energy-based parameter introduced here is the input energy per unit mass for a 5%-damped SDOF system with a vibration period equal to the fundamental period of the structure considered. Input energy is defined as the energy in the SDOF system (kinetic and potential energy plus total damping energy dissipated) at the end of the ground motion, consistent with Arias' definition, and not as the peak value of energy during the time series as used by some other authors (e.g., Uang and Bertero, 1990).

Input energy per unit mass, IE, as a function of period for the example ground motion is shown in the left panel of Figure B-18, both before and after scaling. In this particular example, the IE at the fundamental period of the structure (2.63 seconds) is hardly changed by the spectrum matching; at other periods, it is much more significantly affected (e.g., almost a factor of 3 reduction at a period of 5 seconds). In the following, the relative input energy, $\Delta IE(T_1)$, is defined as the ratio of $IE(T_1)$ for the post-matched to the pre-matched motion.
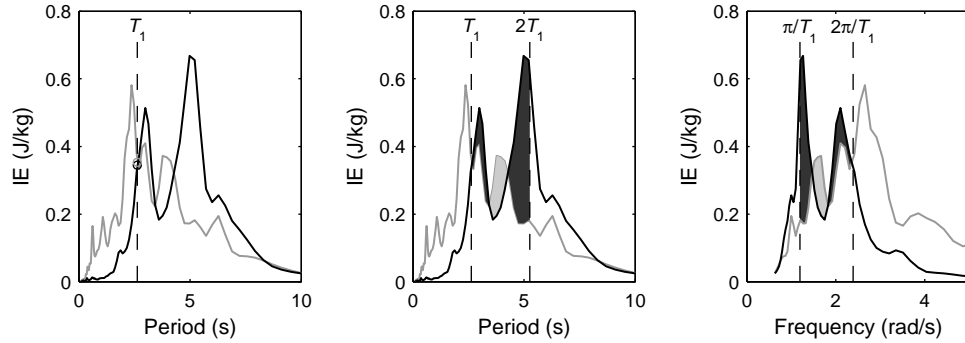
Figure B-18   Example input energy spectra, pre- and post-matching; showing (left) ordinate at T_1, (middle) integration over periods between T_1 and $2T_1$, (right) integration over frequencies between $2\pi/T_1$ and π/T_1. Darker shading shows range where original record input energy greater than matched record; lighter shading shows the opposite. $\Delta IE(T_1) = 1.02$; $\Delta\int IE(T)\,dT = 0.717$; $\Delta\int IE(\omega)\,d\omega = 0.805$.

For nonlinear systems, period elongation will mean that the energy imparted by the ground motion is not fully described by a single ordinate of the input energy spectrum shown in Figure B-18. Two integral parameters are defined here – the integral of IE over periods between T_1 and $2T_1$, and the integral of IE over natural frequencies between π/T_1 and $2\pi/T_1$. The relative integral input energies, $\Delta\int IE(T)\,dT$ and $\Delta\int IE(\omega)\,d\omega$, are then the ratio of these integrals for the post-matched to the pre-matched motion. This calculation is illustrated schematically in the middle and right panels of Figure B-18, for period and frequency, respectively. If the difference (rather than the ratio) was considered, this would be given by the lighter shaded area (where the energy for the spectrum-matched motion is greater than for the original) minus the darker shaded area (where the opposite applies). Because a ratio is used here, this graphical explanation does not hold, but it does help to illustrate the concept. Note that if the darker area is equal to the lighter area, the integrals will be identical over this period range, and therefore, the ratio used here would be one.

A final comment about Figure B-18 is that the right panel of the plot (IE against frequency) also illustrates why the Arias Intensity is significantly higher for the example spectrum-matched ground motion (141% higher). Recall that the AI is proportional to the area under the IE versus frequency from zero to infinity. Although the axis has been cut off at 5 rad/s, it is clear that most of the additional "input energy content" of the ground motion is for frequencies greater than $2\pi/T_1$. This may be relevant for higher-mode structural response, but is less relevant for engineering demand parameters dominated by the fundamental mode. Therefore, a strong dependence between output PFA and FSa with AI, but less dependence of MIDR with AI may be expected. The input energy parameters, on the other hand, are specifically related to periods equal to or greater than the fundamental period, and are therefore more relevant to first-mode-dominated demand parameters.

B.2.6.2 Effect of Changes on Structural Response

In this section, the effect of changes to ground motions by spectrum matching is investigated by evaluating bias in structural response calculations versus the measures of change introduced in the previous section. The aim is to determine if numerical acceptability criteria can be established for limiting the amount of artificial change that is introduced to a ground motion based on a quantifiable dependence of response estimates. Therefore, only measures of change are investigated, and not raw absolute intensity measures such as PGA, PGV, or spectral ordinates. The latter can be of particular interest for determining an appropriate period range for spectrum matching, but this is not the aim of this section. The effect of other intensity measures on structural response is also interesting, but it is expected that any dependencies would hold for both spectrum-matched and unmatched ground motions, and therefore should be taken into account in seed record selection.

For each of the 12 change parameters (refer to Table B-2), three engineering demand parameters (MIDR, PFA, and FSa) and building/earthquake scenarios, results were plotted, and linear regression analysis was carried out. For the change parameters defined by a ratio (all except the maximum difference in normalized cumulative squared parameters), least-squares regression was carried out on the following relationship:

$$\log_{10}\left(\frac{\text{EDP}}{\text{EDP}_{\text{POC}}}\right) = b_0 + b_1 \log_{10}\left(CP\right) \tag{B-1}$$

where EDP is the engineering demand parameter, EDP_{POC} is its value according to the point of comparison, CP is the change parameter, and b_0 and b_1 are regression constants. Normalizing with respect to the point of comparison estimates allows quantitative comparisons to be made between EDPs and different building models and scenarios.

For the change parameters based on a difference (the normalized cumulative squared parameters), the regression was carried out on the following relationship:

$$\log_{10}\left(\frac{\text{EDP}}{\text{EDP}_{\text{POC}}}\right) = b_0 + b_1\left(CP\right) \tag{B-2}$$

Not all ground motions from Section B.2.5 were used in the regression analyses. Suites of motions were selected for which the median estimates of the EDP both before and after spectrum matching were approximately equal to the points of comparison. The objective was to see if any of the outliers in the data could be attributed to large changes to the ground motions introduced by spectrum matching. Results such as those where initial seed motions were significantly higher than the target spectrum over much of the period range would have skewed the regression

towards large reductions in ground motion intensity, rather than considering reductions and increases equally. Therefore, all the ground motion suites from the Suite U1 records matched to the CMS were used (Suites M1, M3, M4, M5), along with the Jayaram et al. (2011) records, matched to the CMS (Suite M9). The latter were mostly included as there was more dispersion in the initial suite of records (albeit centered on the CMS), and therefore, larger changes were introduced by spectrum matching.

Linear regression was carried out for each of the three EDPs versus each of the change measures listed in Table B-2, for the three building model and earthquake scenario combinations considered. Figure B-19 shows a typical example of the regression results, for input energy at the fundamental period versus MIDR, normalized with respect to the point of comparison prediction. Note that the regression lines have been extrapolated to the edges of each plot solely for comparing the relationships visually; it is recognized that they should not be extrapolated beyond the extent of the data in practical use. The only building collapse (for Building B with Scenario M7) is shown separately – although a single example is not of any statistical significance, it is also interesting to see if this collapse can be attributed to any changes introduced by spectrum matching. The collapse point is not included in the regression analyses.

The results in this figure (and other figures) do not seem to show any strong correlations between engineering demand parameters and measures of change. For many of the change measures considered, the bulk of the data is clustered around 1, indicating relatively small change (at least for the parameters based on the ratio of post- to pre-matched intensity measures). As a consequence, many of the more extreme points, in terms of a poor estimation of point of comparison response, are actually for relatively small amounts of change, suggesting that possibly the artificial adjustments to these motions is not to blame for the outlying response.
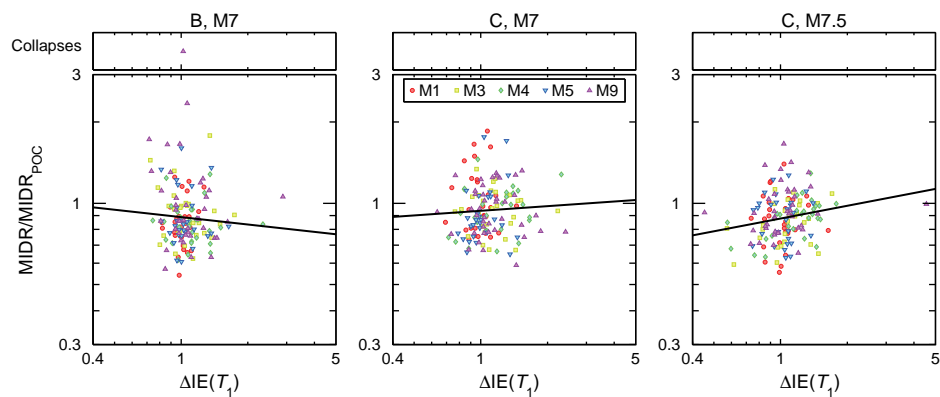
Figure B-19   Example regression analysis for results of MIDR versus $\Delta IE(T_1)$.

It is of anecdotal interest (although not of any statistical significance) to point out in Figure B-19 that for Building C with Scenario M7.5 the most extreme difference in input energy (with the matched motion around 4.5 times the unmatched motion) gives a nearly perfect prediction of the point of comparison. On the other hand, a case for Building B with Scenario M7, has almost zero change in input energy, but is the one example of building collapse in the dataset used here.

Statistical data from the regression analyses are reported in Table B-3 and Table B-4, showing R^2 values and p-values for the two-sided test of the null hypothesis that b_1 is significantly different from zero. The null hypothesis is rejected at the 5% level in the cases shown in bold face. It should be noted that when carrying out exploratory regression analysis in this manner on over 100 combinations of engineering demand and change parameters, some of these null hypotheses are expected to be rejected by chance alone. In this particular application, similar trends (same slope of regression relationship) and statistical significance are expected to apply across all building models and earthquake scenarios. This does not appear to hold for any of the combinations of engineering demand and change parameters.

Table B-3 R^2 **for Regression Relationships**

Building Scenario	MIDR B, M7	MIDR C, M7	MIDR C, M7.5	PFA B, M7	PFA C, M7	PFA C, M7.5	FSa B, M7	FSa C, M7	FSa C, M7.5
ΔPGA	0.015	0.000	0.025	0.001	0.019	0.012	0.007	0.003	0.000
ΔPGV	0.000	0.000	0.042	0.020	0.007	0.009	0.004	0.002	0.000
ΔPGD	0.001	0.001	0.005	0.076	0.004	0.009	0.016	0.000	0.003
ΔAI	0.000	0.000	0.023	0.000	0.034	0.007	0.013	0.000	0.001
ΔCSV	0.014	0.001	0.006	0.094	0.001	0.002	0.006	0.002	0.004
ΔCSD	0.003	0.005	0.002	0.072	0.008	0.001	0.014	0.000	0.002
$\max(\Delta AI_{norm})$	0.009	0.005	0.010	0.030	0.013	0.068	0.024	0.005	0.015
$\max(\Delta CSV_{norm})$	0.009	0.023	0.001	0.013	0.001	0.036	0.007	0.005	0.013
$\max(\Delta CSD_{norm})$	0.008	0.020	0.001	0.043	0.000	0.001	0.007	0.001	0.024
$\Delta IE(T_1)$	0.006	0.003	0.038	0.032	0.005	0.006	0.002	0.000	0.006
$\Delta\int IE(T)\,dT$	0.001	0.003	0.000	0.043	0.001	0.005	0.001	0.001	0.006
$\Delta\int IE(\omega)\,d\omega$	0.001	0.000	0.003	0.030	0.001	0.000	0.000	0.000	0.004

One notable observation from Table B-4 is that the regression relationships for PFA for Building B with M7 scenario in terms of most of the change parameters are statistically significant. From further analysis of the data, it became evident that there were two significant outliers that were overly influential in the regression analysis. Removing these two points and repeating the regression increases the p-

values to greater than 5% for all of the change parameters. Although one must be careful in eliminating data on the basis of extreme values, relationships derived under the significant influence of two data points (out of a total of 152) should be treated with due skepticism.

Table B-4 Two-Sided *p* Value for Regression Relationships (Bold Values Significant at 95% Level)

Building Scenario	MIDR			PFA			FSa		
	B, M7	C, M7	C, M7.5	B, M7	C, M7	C, M7.5	B, M7	C, M7	C, M7.5
ΔPGA	0.14	0.83	**0.05**	0.70	0.09	0.18	0.30	0.48	0.85
ΔPGV	0.82	0.87	**0.01**	0.08	0.30	0.25	0.43	0.63	0.95
ΔPGD	0.72	0.68	0.39	**0.00**	0.43	0.24	0.12	0.95	0.53
ΔAI	0.97	0.98	0.06	0.87	**0.02**	0.31	0.17	0.93	0.66
ΔCSV	0.15	0.76	0.33	**0.00**	0.77	0.63	0.35	0.55	0.44
ΔCSD	0.54	0.40	0.60	**0.00**	0.27	0.65	0.14	0.90	0.56
max(ΔAI$_{norm}$)	0.26	0.38	0.23	**0.03**	0.16	**0.00**	0.06	0.38	0.13
max(ΔCSV$_{norm}$)	0.26	0.07	0.74	0.16	0.71	**0.02**	0.29	0.41	0.16
max(ΔCSD$_{norm}$)	0.28	0.08	0.75	**0.01**	0.86	0.66	0.31	0.68	0.06
ΔIE(T_1)	0.36	0.48	**0.02**	**0.03**	0.38	0.34	0.59	0.94	0.35
Δ∫IE(T) dT	0.71	0.54	0.90	**0.01**	0.72	0.39	0.75	0.79	0.33
Δ∫IE(ω) dω	0.79	0.80	0.52	**0.03**	0.71	0.90	0.98	0.86	0.43

Although in most cases it is not possible to reject the null hypothesis (that there is no linear correlation between the change and engineering demand parameters), this of course does not mean that the conclusion is that the opposite is true (that there is no correlation). On the other hand, even if a strong correlation exists, this may not be particularly relevant if the slope of the relationship is small. The slope of each regression line, b_1, is given in Table B-5. The constant term, b_0, is not given, as it relates to overall bias in the prediction of point of comparison response, which has already been investigated in previous sections, and does not relate to the dependence of the response on the change parameters.

The steepest slope for those parameters that follow Equation B-1 is 0.196 (MIDR versus ΔPGV), while the steepest for those that follow Equation B-2 is 0.271 (PFA versus max(ΔAI$_{norm}$)). For a ±10% change in MIDR parameter, the former would require ΔPGV values less than around 0.6 or greater than 1.6, which applies for very few of the data in the suites considered. A ±10% change in PFA for the latter case would require max(ΔAI$_{norm}$) greater than 0.15, which does hold for a portion of the data.

Table B-5   Regression Parameter b_1 for Regression Relationships

Building Scenario	MIDR B, M7	MIDR C, M7	MIDR C, M7.5	PFA B, M7	PFA C, M7	PFA C, M7.5	FSa B, M7	FSa C, M7	FSa C, M7.5
ΔPGA	-0.128	0.018	0.129	-0.017	0.085	0.060	0.053	0.051	0.013
ΔPGV	0.023	0.012	0.196	0.092	0.049	0.061	-0.048	0.033	0.005
ΔPGD	0.014	-0.015	0.030	0.069	0.018	0.028	-0.037	-0.002	-0.023
ΔAI	0.003	0.001	0.116	0.006	0.096	0.044	0.060	0.006	-0.028
ΔCSV	0.092	-0.015	0.043	0.119	-0.009	0.014	-0.034	-0.026	-0.035
ΔCSD	0.012	-0.014	0.009	0.032	0.011	0.005	-0.016	-0.002	-0.010
max(ΔAI$_{norm}$)	0.161	-0.108	0.151	-0.153	-0.106	-0.271	-0.159	0.095	-0.196
max(ΔCSV$_{norm}$)	0.114	-0.165	0.027	0.072	-0.020	-0.128	-0.062	0.065	-0.117
max(ΔCSD$_{norm}$)	0.062	-0.087	0.015	0.073	0.005	-0.014	-0.034	-0.018	-0.093
ΔIE(T_1)	-0.091	0.057	0.157	0.111	-0.043	-0.043	-0.032	0.006	0.064
$\Delta\int$IE(T) dT	0.022	-0.030	-0.006	0.077	-0.011	-0.028	-0.011	-0.012	-0.048
$\Delta\int$IE(ω) dω	0.017	-0.014	0.037	0.071	-0.013	-0.005	-0.001	-0.009	-0.046

Recognizing that the b_1 values are uncertain, a reasonably conservative range of allowable values for each of the change parameters can be constructed by using the steepest value from the 95% confidence interval for b_1. This reflects both the uncertainty in the regressed relationship, and the dependence between the change and engineering demand parameters. Based on this steepest slope, the range of values of the change parameter within which the change in the engineering demand parameter is less than ±10% can be calculated. Note that this does not mean that the value of the engineering demand parameter is within 10% of the point of comparison value, but just that the measured change does not influence its value by more than 10% (with 95% confidence). For each building and earthquake scenario, these lower/upper bound values of the change parameters are capped at the minimum and maximum values of the change parameter that were used in the regression analysis (i.e., do not extrapolate beyond the data).

As mentioned earlier, fairly consistent trends across various buildings and scenarios can be generally expected, even if each model will be sensitive to various characteristics of the ground motions. Therefore, for the purpose of developing simple ranges of allowable parameters, the arithmetic mean of the lower and upper bounds over the three buildings and scenarios can be taken. Finally, since an estimate of the values of multiple engineering demand parameters is desired, the worst case over each of the engineering demand parameters can be considered.

The results of this process are reported in Table B-6 in terms of lower and upper bound values that could be considered permissible for spectrum matching. It should be emphasized that these calculations were based on data that for the most part were not shown to be statistically significant. On the other hand, the 95th percentile slope was used to estimate a maximum likely dependence of structural response on these measures of change, based on the limited data used here. The main lesson to draw from Table B-6 is that relatively large changes can be made to ground motions with spectrum matching without significantly biasing structural analysis results. The most restrictive criteria are probably the limits based on $\max(\Delta AI_{norm})$, $\max(\Delta CSV_{norm})$ and $\max(\Delta CSD_{norm})$, which may be the most relevant scalar quantities to check when assessing the quality of the spectrum matching process. The limits tentatively suggested in Table B-6 should only be used in conjunction with a careful selection of seed ground motions.

Table B-6   Conservative Upper- and Lower-Bound Values for Measures of Change Introduced by Spectrum Matching

Parameter	Lower Bound	Upper Bound
ΔPGA	0.4	1.9
ΔPGV	0.5	1.7
ΔPGD	0.5	3.8
ΔAI	0.4	2.0
ΔCSV	0.4	2.7
ΔCSD	0.4	7.1
$\max(\Delta AI_{norm})$	0.0	0.2
$\max(\Delta CSV_{norm})$	0.0	0.2
$\max(\Delta CSD_{norm})$	0.0	0.4
$\Delta IE(T_i)$	0.6	1.9
$\Delta \int IE(T)\,dT$	0.4	2.3
$\Delta \int IE(\omega)\,d\omega$	0.5	2.2

B.2.6.3   Measures of Change Applied to Horizontal Components of Unmatched Records in PEER NGA Database

The position adopted in the previous sections is that changes to a seed record by the spectrum matching process are only unacceptable if they produce a significant bias on structural response. Different measures of change introduced by matching were explored. Anderson (2004) also made use of similar measures of comparison between two ground motion histories, albeit for the purpose of comparing synthetically-generated (physics-based) records with real recorded ground motions. To identify acceptable limits for these measures of change, differences between two horizontal components of a number of real recorded ground motions were calculated.

If two components may be considered statistically independent realizations of the same stochastic process, then this provides an estimate of the real variation in the process, for a given earthquake scenario.

In the present context, the value of such a comparison is more tenuous, as there is no real sense in which two components of a recorded ground motion can be considered analogous to a pre- and post-matching record. Nevertheless, for many applications, engineers would consider two components of a recorded accelerogram equally acceptable for response-history analysis, at least in the absence of any directivity effects and after correcting for differences in elastic response spectra. Therefore, such a comparison may provide useful lower bounds to acceptable limits to measured changes introduced by the matching process. Clearly, there will be record-to-record variation in such measures. Therefore, the measures of change for a large number of records are calculated: those contained in the PEER NGA database (Chiou et al., 2008) and report the median, and 16th and 84th percentile values for each of the measures in Table B-7. The calculation uses a random component of each record as a baseline for the relative comparison. For example, the first line of the table indicates that for 68% of the ground motions in the PEER NGA database, the PGA of the first component is between 74% and 135% of the PGA of the second component (1st and 2nd assigned randomly).

Table B-7   Measures of Change Calculated Between Ground Motion Components in PEER NGA Database

Parameter	16th percentile	50th percentile	84th percentile
ΔPGA	0.74	1.00	1.35
ΔPGV	0.71	1.01	1.43
ΔPGD	0.61	1.00	1.66
ΔAI	0.72	1.01	1.42
ΔCSV	0.59	1.00	1.74
ΔCSD	0.45	1.00	2.41
$\max(\Delta AI_{norm})$	0.09	0.15	0.24
$\max(\Delta CSV_{norm})$	0.13	0.20	0.32
$\max(\Delta CSD_{norm})$	0.16	0.25	0.40
$\Delta IE(T_1)$	0.47	1.00	2.13
$\Delta\int IE(T)\,dT$	0.51	1.00	1.96
$\Delta\int IE(\omega)\,d\omega$	0.51	1.00	1.95

It is interesting to note that the 16th and 84th percentile values shown in Table B-7 are broadly similar to the limits adopted in Table B-6, although for most parameters, the range was slightly wider in the spectrum-matched records in Table B-6. Of course,

the comparison is affected by the adopted confidence interval for the data in Table B-8 and the percentile values reported in Table B-7. Nevertheless, it provides a useful check on the results reported in the previous subsection.

B.3   Effect of Response-Spectrum Matching on Velocity Pulses

B.3.1 Introduction

Response-spectrum matching ideally preserves the nonstationary characteristics of the initial seed ground motion, while modifying the elastic response spectrum to match a target spectrum. The algorithm used in the RspMatch software (Lilhanand and Tseng, 1988, Abrahamson, 1992), for example, uses adjustments to the acceleration that are relatively localized in both time and frequency, with the aim of minimizing the overall modification to the acceleration history (as well as ideally minimizing other measures of change, discussed in the previous section). The algorithm and the software implementation permit the user to select the wavelet family that is used for the adjustment; spectrum matching using wavelets that are in some way representative of portions of real acceleration histories is more likely to produce reasonable output. For example, the original implementation by Lilhanand and Tseng (1988) used impulse functions for the acceleration increment, while later versions (Hancock et al., 2006; Al Atik and Abrahamson, 2010) adopted acceleration wavelets that did not lead to velocity or displacement drift when integrated.

Other sections of this report, in particular Appendix C, discuss the need to consider velocity pulses in the development of ground motions in the near-fault region. Ground motions containing pulses exhibit higher elastic spectral demand at structural periods in the vicinity of the period of the pulse (Shahi and Baker, 2011), and to the extent that elastic spectral demand is a good estimator of peak inelastic structural response, this effect can be taken into account with an appropriate target spectrum for matching. Records containing velocity pulses, however, are known to lead to disproportionately large nonlinear response (e.g., Alavi and Krawinkler, 2001; Mavroeidis et al., 2004, Akkar et al., 2005). It would be reasonable to conclude that a record matched to an appropriate target spectrum and containing a velocity pulse with the appropriate characteristics would impose an appropriate level of demand on inelastic systems.

This section is concerned with the preservation of a velocity pulse in the initial seed motion after spectrum matching. In this study, the objective is to preserve the original pulse characteristics, and not to use spectrum matching to create a new velocity pulse or modify the period or amplitude of an existing pulse. Therefore, the procedure adopted here is to select records with a velocity pulse closest in period to the desired pulse period, linearly scale to attain the target spectral demand at the pulse period, and use spectrum matching to adjust the elastic response spectrum at other periods.

B.3.2 Response-Spectrum Matching of Ground Motions to a Target Spectrum Incorporating a Narrow-Band Adjustment for Near-Fault Pulses

The first situation considered here is when matching is carried out to a target spectrum that contains a narrow-band amplification to take into account the expected presence of velocity pulses. "Narrow-band" is used in this context to refer to adjustments that explicitly account for the expected pulse period, T_p, and apply adjustments to spectral accelerations centered (approximately) on this period (Somerville et al., 2004). In this study, the adjustment proposed by Shahi and Baker (2011) is used. "Broadband" adjustments, by contrast, are those which amplify a wider range of periods to take into account the potential effects of pulses with a range of possible periods. Examples are the adjustments proposed by (Somerville et al., 1997, and Abrahamson, 2000), as well as a uniform hazard spectrum determined by PSHA that takes into account narrow-band adjustments for a wide range of possible periods (Shahi and Baker, 2011).

An appropriate target spectrum would take into account the effects of both the correlation of ε values for different structural periods (Baker and Cornell, 2006a), and the narrow-band adjustment to the response spectrum due to the presence of velocity pulses (Shahi and Baker, 2011). Disaggregation of PSHA with a proper account for the possible effect of velocity pulses (Shahi and Baker, 2011) would allow the analyst to determine the portion of the observed ε that is attributable to pulses with different periods, and the portion that is due to the incorporation of the uncertainty on the ground motion prediction equation (see Appendix A).

For the purpose of the study in this section, the effect of ε (the component of uncertainty related to the ground motion prediction equation) is ignored. The target spectrum for matching is taken as the median value from the Campbell and Bozorgnia (2008) ground motion prediction equation, with $M_w = 7.5$ and $R_{jb} = 10$ km, amplified by the narrow-band amplification of Shahi and Baker (2011). Pulse periods of 5.45s and 3.11s were considered, corresponding to the median and median-minus-one-standard-deviation values from the Shahi and Baker (2011) prediction equation with $M_w = 7.5$. The target spectra are illustrated by the dashed (red) lines in Figure B-20, B-21a and b. Note from the figures that the peak amplification to the response spectrum is centered at periods slightly lower than the pulse period.

Figure B-20   Comparison of target spectrum incorporating narrow-band adjustment for T_p = 5.45s velocity pulse with record spectra (a) before and (b) after matching. Unshaded period range was considered in matching.
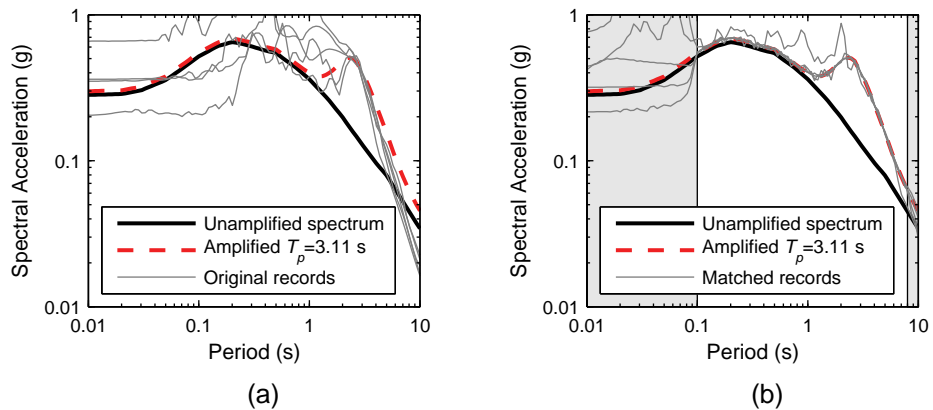
Figure B-21   Comparison of target spectrum incorporating narrow-band adjustment for T_p = 3.11s velocity pulse with record spectra (a) before and (b) after matching. Unshaded period range was considered in matching.

Ground motions were selected from the PEER NGA database from the fault-normal component of those identified by Baker (2007b) as containing a pulse. Only records with a maximum usable period greater than 8 seconds were considered. For each target spectrum, all records with pulse period within ±10% of the scenario pulse period were used – a total of 8 and 5 records for the 5.45 and 3.11 second pulse periods, respectively, were available satisfying these criteria. Prior to matching, ground motions were linearly scaled to provide a close initial match of the target spectrum over a period range within 20% of the pulse period. Initial response spectra of the selected records, after linear scaling, are compared with the target spectra in Figure B-20a and Figure 21a for the two scenarios. Other information about the selected ground motions is provided in Table B-8, including scale factors ("Scale1") adopted.

Spectrum matching was carried out on the 5%-damped target only, between periods of 0.1 and 8.0 seconds. All other input parameters to RspMatch2005 were as in Section B.2. Response spectra from the matched records are compared with the target spectra in Figures B-20b and 21b.

As in previous examples, the effectiveness of the RspMatch2005 algorithm at providing a close match of a target spectrum over a wide period range is apparent from Figures B-20b and 21b (the exception is Set 2, Record #2, which is the outlying spectrum in Figure B-21b, for which RspMatch2005 did not converge using the default parameters). However, as noted previously, the elastic response spectrum is not a complete measure of the inelastic demand imposed by ground motions containing velocity pulses. The algorithm of Baker (2007b) is therefore used to identify the presence of pulses in the matched records, and to evaluate their characteristics. Table B-9 compares the following properties of the unmatched and matched ground motions: pulse indicator (PI), pulse period (T_p) and peak ground velocity (PGV).

Table B-8 **Ground Motions Containing Velocity Pulses Selected for Spectrum Matching Study**

Record #	Event	Year	Station	Scale 1	Scale 2	Scale 3
Set 1. Records selected and scaled for T_p = 5.45 seconds						
1	Imperial Valley-06	1979	El Centro Array #3	2.94	1.99	1.68
2	Imperial Valley-06	1979	El Centro Array #8	1.91	1.28	1.42
3	Imperial Valley-06	1979	El Centro Differential Array	2.08	1.44	1.16
4	Landers	1992	Lucerne	1.04	0.70	0.49
5	Kocaeli, Turkey	1999	Gebze	2.03	1.36	1.33
6	Chi-Chi, Taiwan	1999	TCU036	1.28	0.88	1.11
7	Chi-Chi, Taiwan	1999	TCU065	0.62	0.41	0.54
8	Chi-Chi, Taiwan	1999	TCU075	1.10	0.74	0.78
Set 2. Records selected and scaled for T_p = 3.11 seconds						
1	Imperial Valley-06	1979	EC Meloland Overpass FF	0.93	0.49	0.60
2	Cape Mendocino	1992	Petrolia	1.79	0.94	0.84
3	Northridge-01	1994	Sylmar - Olive View Med FF	0.89	0.47	0.56
4	Chi-Chi, Taiwan	1999	TAP003	2.23	1.16	2.09
5	Chi-Chi, Taiwan-03	1999	CHY024	1.93	1.02	2.09

Table B-9 Characteristics of Ground Motions and Velocity Pulses Before and After Spectrum Matching to Narrow-Band Adjusted Target Spectrum

Record #	Pulse Indicator		PGV (cm/s)		T_P (s)		Verdict
	Before	After	Before	After	Before	After	
Set 1. Records selected and scaled for $T_P = 5.45$ seconds							
1	1.00	1.00	121	84	5.24	4.92	Accept
2	1.00	0.91	93	94	5.39	7.50	Reject
3	1.00	0.99	124	91	5.86	5.77	Accept
4	1.00	0.34	146	103	5.10	7.04	Reject
5	1.00	0.98	105	80	5.87	7.33	Reject
6	1.00	1.00	80	79	5.40	5.12	Accept
7	0.96	1.00	79	85	5.74	5.88	Accept
8	1.00	1.00	97	85	5.15	5.40	Accept
Set 2. Records selected and scaled for $T_P = 3.11$ seconds							
1	1.00	0.38	107	72	3.35	4.75	Reject
2	0.92	0.00	147	75	3.00	5.39	Reject
3	1.00	0.98	109	106	3.11	3.74	Reject
4	0.99	1.00	74	85	3.41	3.86	Accept
5	1.00	0.99	64	83	3.19	3.26	Accept

As noted in the discussion of ground motions without velocity pulses (Section B.2.6), a spectrum-matched record should not be solely dismissed on the basis of large changes to ground motion intensity measures or other characteristics, unless this is expected to bias structural response calculations. However, in this case the specific objective is to retain the characteristics of pulses in the original seed record. On this basis, Record #4 in Set 1, and Records #2 and #3 in Set 2 should be rejected, as their pulse indicator after matching is below the threshold of 0.85, taken to indicate the presence of a velocity pulse by Baker (2007b). For the first of these, an extracted portion of the ground velocity history comprising the velocity pulse, before and after spectrum matching, is shown in Figure B-22 (column labeled "Set 1, #4"). The plots show the total velocity (top), the extracted velocity pulse (middle) and the residual motion (bottom). In this case, the extracted pulse is not significantly altered, although is slightly reduced in amplitude. The pulse indicator is decreased from 1.00 to 0.34, however, as significant long-period energy has been added to the rest of the signal (not evident from the portion shown in Figure B-22).

Figure B-22   Example portions of ground velocity histories for spectrum matching
             to narrow-band amplification study; total velocity (top plots),
             extracted pulse (middle) and residual (bottom).

Records #2 and #5 of Set 1 are also rejected – although they retain a pulse in the matched record according to the pulse indicator, the pulse period is increased by 38% and 25%, respectively, which means that the final records no longer satisfy the original scenario of a pulse period close to 5.45 seconds. Figure B-22 shows the ground velocity histories for the second of these (in the column labeled "Set 1, #5"). In this case, certain features of the velocity pulse have been retained, but the first half cycle of the pulse has been reduced, and the overall period of the pulse has been elongated.

Finally, although it is not obvious from the pulse indicator and pulse period, Figure B-22 shows that Record #3 in Set 2 has also been significantly altered. The matching process has reduced the presence of the original velocity pulse, and created a new pulse with similar period, earlier in the signal. Unusually, the extracted pulse shows a non-zero initial velocity; although not obvious from Figure B-22 the total velocity history does start at zero, but ramps up very quickly. This record is rejected on the basis that the "real" pulse has been removed, and the artificial one has potentially unrealistic characteristics.

The remaining seven ground motions were considered acceptable, in that the main characteristics of the original record were retained following matching. Two examples, Set 1, Record #8, and Set 2, Record #5, are shown in Figure B-22. In these cases, there is very little change to either the extracted velocity pulse or the overall signal. The final pulse periods of these two examples are also closest to the target pulse periods of 5.45s and 3.11s, for Sets 1 and 2, respectively.

It is interesting to note that the PGV for some of the "accepted" records in Table B-9, has been modified by up to a third. Although PGV can be an important intensity

measure for ground motions containing velocity pulses, a large change in PGV to indicate an inappropriately matched motion is not considered. In fact, the predictive equation for PGV of Bray and Rodriguez-Marek (2004) gives a median value of 69 cm/s and a median-plus-sigma value of 112 cm/s for the present scenario ($M_w = 7.5$, $R_{jb} = 10$ km, soil site). Therefore, the large reduction in PGV in Set 1, Records #1 and #3, in particular, can be seen as a correction to a more reasonable value for this scenario.

It should also be noted that convergence and quality of spectrum matching with RspMatch2005 can be somewhat sensitive to the program options selected, at least for certain seed motions. The matching process was repeated with four sweeps of periods (0.1s-0.3s; 0.1s-0.9s; 0.1s-2.7s; 0.1s-8.0s), which improved Record #4 of Set 1, but had neutral or negative effect on the other records. This was also repeated (for Set 1 only) using wavelets with a decreasing number of cycles (10, 8, 6 and 4) in each successive sweep, on the hypothesis that the longer period pulses would be modified less by wavelets with a comparable number of cycles. However, this was unsuccessful, and worsened the results for all ground motions.

In summary, a small number of spectrum-matched ground motions containing velocity pulses for two scenarios were developed: pulse periods of 5.45s and 3.11s, and both with $M_w = 7.5$ and $R_{jb} = 10$ km. Through inspection of the pulse characteristics using the method of Baker (2007b), almost half of the initial pool of records were rejected. The technique of selecting from a pool of more or less successfully matched records has the potential for introducing bias, if there is a systematic reason why some records are preserved better than others, as discussed in Section B.2.1.

B.3.3   *Response-Spectrum Matching of Ground Motions to a Target Spectrum Incorporating a Broadband Adjustment for Near-Fault Pulses*

In many practical applications where pulse-type ground motions are relevant, the target response spectrum takes into account the possible presence of velocity pulses by applying an amplification across a broad range of periods. For example, the method of Somerville et al. (1997), later modified by Abrahamson (2000), applies a correction for periods of 0.5 second and above. The uniform hazard spectrum produced by a probabilistic seismic hazard analysis incorporating the effect of pulses averages the amplification for different possible pulse periods (Shahi and Baker, 2011), and therefore it too may be considered a broadband amplification of the uniform hazard spectrum if pulses were not taken into account. The latter has the benefit that a disaggregation may be used to back-calculate the pulse periods that are of most relevance for a given structural period.

A problem with matching an individual pulse-type ground motion to a broadband-amplified target spectrum is that the ground motion will have a single pulse period which will generally amplify the response spectrum over a narrow period range. It is difficult to modify the record in such a way that the pulse is preserved in the velocity history, but that the spectrum is smoothed to match the target. In this section, an initial study is carried out to see if the pulses can be preserved, at least for some input seed records.

The same median spectrum as in the previous section was used (for $M_w = 7.5$, $R_{jb} = 10$ km), but with a broadband amplification applied from Somerville et al. (1997), as modified by Abrahamson (2000). The target spectrum is shown in Figure B-23a. The ground motions described in Table B-8 were again used as input, but rescaled such that the response spectrum around the pulse period was equal to the target spectrum (scale factors "Scale2" in Table B-8). Spectra for a subset of the original records (see below) are compared with the target spectrum in Figure B-23a. The same target spectrum was used for both sets of ground motions (those selected initially for pulse periods close to 5.45 seconds and 3.11 seconds).

Several strategies were attempted for matching the records with RspMatch2005. Initially, the same method as before was used – matching using default parameters over the full period range between 0.1 seconds and 8.0 seconds. Carrying out the pulse extraction process of Baker (2007b) before and after matching, the pulse was preserved in only two of the ground motions from the Set 1 (Records #7 and #8), and none of those in the Set 2. In all other cases, the additional long period content added by the spectrum matching smoothed out the velocity pulse. The pulse indicator still suggested the presence of pulses in around half of these, but the extracted pulse period was increased by up to 200%.
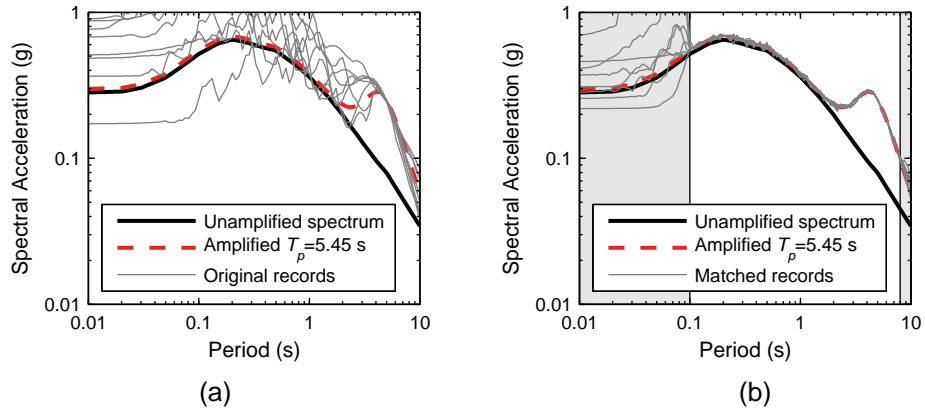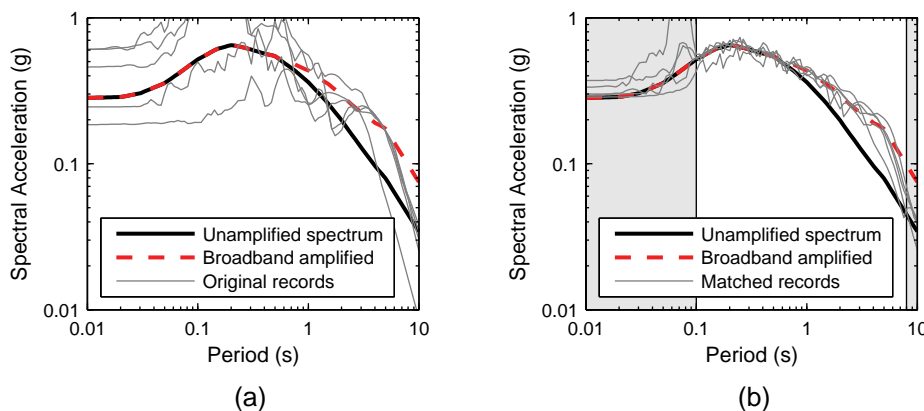

Figure B-23   Comparison of target spectrum incorporating broadband adjustment for velocity pulses with record spectra: (a) before and (b) after matching. Unshaded period range was considered in matching. Only "accepted" records in Table B-9 are shown.

Variants on the default approach were also attempted – including matching over different period ranges and initially scaling up the seed records to match the longer period content (but overestimate the target spectrum at the pulse period). In all cases, Set 1 Records #7 and #8 were successfully matched retaining the velocity pulses, and all other ground motions were modified excessively.

An approach that met with slightly more success involved the following steps for each ground motion:

1. Extract the velocity pulse using the method of Baker (2007b).

2. Calculate the response spectrum for the original ground motion ("total") and for the residual motion after the pulse has been extracted ("residual").

3. Determine a new target spectrum by scaling the original target by the ratio of the residual spectrum to the total spectrum.

4. Run RspMatch2005 with the residual ground motion as the seed record, matching to the modified target spectrum.

5. Add the extracted velocity pulse (from Step 2) to the output of RspMatch2005.

The original extracted velocity pulse is therefore unmodified by this procedure, as it is extracted from the original seed and added back in after spectrum matching. Of course, if additional long period content is added in the matching, this could replace the highest energy wavelets that made up the original extracted pulse in the identification method of Baker (2007b).

The addition of the pulse at the end of the procedure also means that the final resulting response spectrum is not necessarily a good match of the original target spectrum. The success of this procedure relies upon the modified spectrum determined in Step 3. Scaling the original target spectrum by the ratio of the residual to the target spectra assumes that the effect of the pulse on the response spectrum is multiplicative, and that this ratio will be preserved when the residual motion is modified in the matching. There is no physical reason for this to be expected to apply generally, and therefore, both the pulse characteristics and the match to the original spectrum need to be checked at the end of the procedure. Other modified target spectra in Step 3 were evaluated, but the adopted approach gave the most consistent results.

The procedure described above gave acceptable results for 5 out of 13 of the seed ground motions – Set 1, #1, 2, 3 and 8, and Set 2, #1. For the other Set 1 motions (with pulse periods around 5.45 seconds), the pulse was generally preserved intact, but the final match to the target spectrum was poor. For the other Set 2 motions (pulse periods around 3.11 seconds), the pulse was significantly modified by long period content added by the spectrum matching. Figure B-23b shows the response

spectra for the subset of matched motions that were considered acceptable, compared with the original target spectrum. In general, the match to the target spectrum across the considered period range is good, although it is slightly low for periods greater than the pulse period. The spectral demand for periods greater than the pulse period is essentially dominated completely by the demand produced by the pulse, and is insensitive to the reduced target adopted for matching the residual ground motion. Therefore, it is not possible to obtain a better match for these longer periods using the method described here.

Figure B-24 shows the velocity histories (total, extracted pulse, and residual) for the five ground motions considered "acceptable" in Table B-10. As before, when the spectrum matching successfully preserves the velocity pulses, the change to the velocity histories is very small. Table B-10 also summarizes the pre- and post-matching characteristics of the extracted velocity pulses, for the records that were considered "acceptable" only.

In summary, one can conclude that in general it is more difficult to preserve velocity pulses when spectrum matching to a smooth target with a broadband adjustment for pulses. It is possible to improve the results slightly by first extracting the velocity pulse from the record using the method of Baker (2007b), matching the residual motion to a modified target spectrum, then adding the pulse back onto the matched motion.
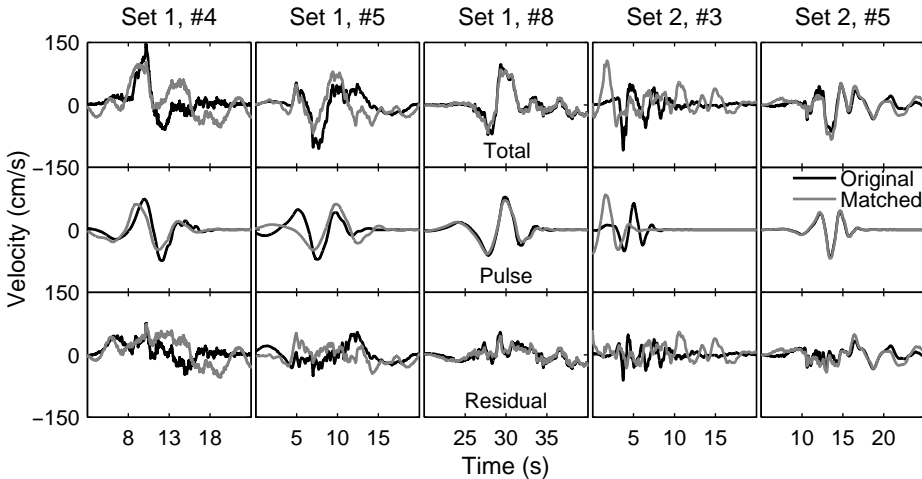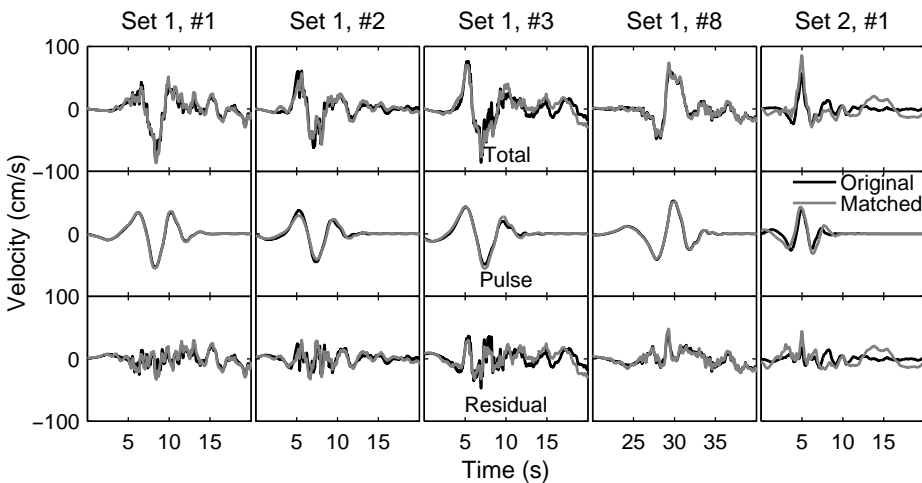

Figure B-24   Example portions of ground velocity histories for spectrum matching to broadband amplification study; total velocity (top), extracted pulse (middle) and residual (bottom).

Table B-10 Characteristics of Ground Motions and Velocity Pulses Before and After Spectrum Matching to Broadband Adjusted Target Spectrum (Accepted Records Only)

Record #	Pulse Indicator		PGV (cm/s)		T_p (s)		Verdict
	Before	After	Before	After	Before	After	
Set 1. Records selected and scaled for T_p = 5.45 seconds							
1	1.00	1.00	82	87	5.24	5.29	Accept
2	1.00	1.00	62	57	5.39	5.61	Accept
3	1.00	1.00	86	77	5.86	5.99	Accept
8	1.00	0.99	65	74	5.15	5.28	Accept
Set 2. Records selected and scaled for T_p = 3.11 seconds							
1	1.00	0.99	56	85	3.35	4.05	Accept

B.3.4 Response-Spectrum Matching of Pulse-Type Ground Motions to a Target Spectrum not Incorporating Adjustment for Near-Fault Pulses

An alternative scenario that may also be of practical relevance is when a target spectrum not incorporating any adjustment for near-fault pulses is available, but pulse-type ground motions are required for the analysis. In this case, a narrow-band or broadband adjustment, as described in the previous sections, could be applied, and used as the basis for matching. Alternatively, the scenario spectrum could be considered the appropriate target for the residual ground motion, following extraction of the velocity pulse by the method of Baker (2007b). Following matching, the velocity pulse could be added back on to the matched residual ground motion. In this case, spectrum matching is not used to obtain a close fit to a target spectrum, as the final spectrum of the record would be expected to be higher than the original target spectrum across a range of periods about the pulse period. Here, spectrum matching is used to obtain a consistent spectral demand across all periods, independently of the presence of a pulse, for consistency with a seismic hazard analysis that has not incorporated any effect of pulses.

For this study, the median unamplified spectrum (shown in Figures B-25 and B-26) was used as the target spectrum for matching. The same 13 seed motions from Table B-8 were used. Since the target spectrum no longer represents an appropriate target for initial scaling, at least around the pulse period (as it does not take into account the presence of pulses), the ground motions were scaled to a constant PGV = 69 cm/s, from the Bray and Rodriguez-Marek (2004) predictive equation discussed earlier (scale factor "Scale3" in Table B-8). As in the previous section, for each ground motion, the velocity pulse was extracted, the residual motion was matched to the target spectrum, and then the velocity pulse was added back in.

In this case, there is no approximation involved in defining a target spectrum for the residual motion, as this is the desired target spectrum. This does mean, however, that the final record spectra will show some dispersion, particularly at periods around the pulse period. The final record spectra are compared with both the target spectrum for matching (i.e., the median spectrum not taking into account pulses) and the narrow-band amplified spectrum described in Section B.2.2 in Figures B-25b and Figure B-26b, for pulse periods of T_p= 5.45s and 3.11s, respectively. Outside the range of pulse periods (where the median spectrum and narrow-band amplified spectrum are similar), the records are well-matched to the target spectrum. Close to the pulse period, the fact that the pulses have been added back into the record means that the record spectrum is increased with respect to the original unamplified target. On average, obtaining the narrow-band amplified target, also shown in the figures, is expected. For the 13 ground motions considered here, the record spectra average is a bit low compared to the narrow-band amplified spectrum, although this appears to be the fault of the initial scaling to PGV, which means the initial spectra were low with respect to this amplified target initially. The goal here was to use a linear scaling method that did not require derivation of the narrow-band amplification, but, when available, this would be a more appropriate method for initial scaling (i.e., "Scale1" rather than "Scale3" from Table B-8).
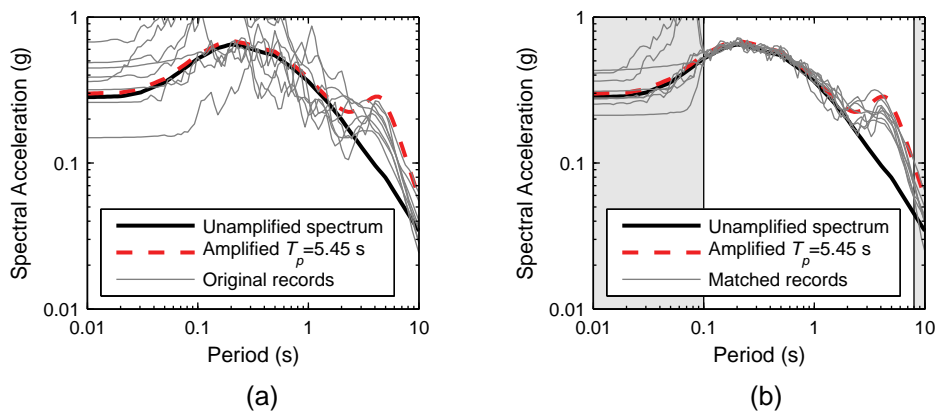
Figure B-25   Comparison of target spectrum unamplified for velocity pulses and spectrum with narrow-band adjustment for T_p= 5.45s velocity pulse with record spectra: (a) before and (b) after matching. Unshaded period range was considered in matching.
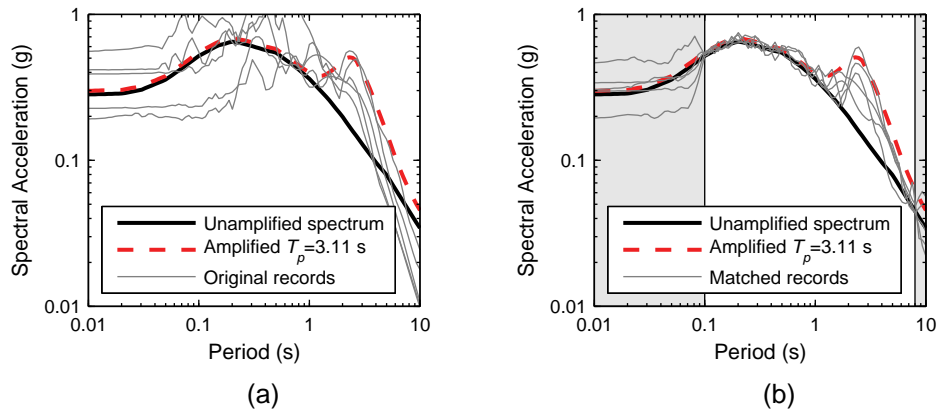
Figure B-26   Comparison of target spectrum unamplified for velocity pulses and spectrum with narrow-band adjustment for T_p = 3.11s velocity pulse with record spectra: (a) before and (b) after matching. Unshaded period range was considered in matching.

As before, the characteristics of the velocity pulses before and after matching in Table B-11 are compared. In this case, six out of eight of the first set of records, and three out of five of the second set are considered acceptable, on the basis of these characteristics alone.

Portions of velocity histories are also shown in Figure B-26. Set 1, #4 and #6, and Set 2, #1, are shown as examples of matched ground motions that were rejected on the basis of the lengthened pulse period in Table B-11. Recall that the pulse period indicated by Baker's (2007b) extraction method is based on a pseudo-period approach, since pulses do not have a non-ambiguous period definition in the same way that sine waves do. In this case, arguably the rejection of these records on the basis of this pseudo-period is severe, as the pulse characteristics are at least approximately preserved following matching. For example, Table B-11 shows that Set 1, #8 exhibited a 45% increase in the pulse period following matching, but the velocity histories for the extracted pulse are very similar. In these cases, an alternative definition of pulse period, such as that of Bray and Rodriguez-Marek (2004), may be a more reliable indicator of the preservation of pulse characteristics after spectrum matching. The other two ground motions in Figure B-27 (Set 1, #8 and Set 2, #5) are examples of records that were accepted in Table B-11, and show very little change of the velocity histories, particularly for the extracted pulses.

Table B-11 Characteristics of Ground Motions and Velocity Pulses Before and After Spectrum Matching to Unamplified Target Spectrum

Record #	Pulse Indicator		PGV (cm/s)		T_p (s)		Verdict
	Before	After	Before	After	Before	After	
Set 1. Records selected and scaled for T_p = 5.45 seconds							
1	1.00	1.00	69	72	5.24	5.76	Accept
2	1.00	1.00	69	72	5.39	5.22	Accept
3	1.00	1.00	69	73	5.86	6.06	Accept
4	1.00	1.00	69	104	5.10	6.34	Reject
5	1.00	1.00	69	67	5.87	5.15	Accept
6	1.00	1.00	69	67	5.40	7.80	Reject
7	0.96	1.00	69	66	5.74	5.46	Accept
8	1.00	0.98	69	67	5.15	5.27	Accept
Set 2. Records selected and scaled for T_p = 3.11 seconds							
1	1.00	1.00	69	80	3.35	4.94	Reject
2	0.92	0.97	69	68	3.00	3.71	Accept
3	1.00	0.00	69	50	3.11	13.89	Reject
4	0.99	1.00	69	74	3.41	3.65	Accept
5	1.00	0.99	69	87	3.19	3.22	Accept
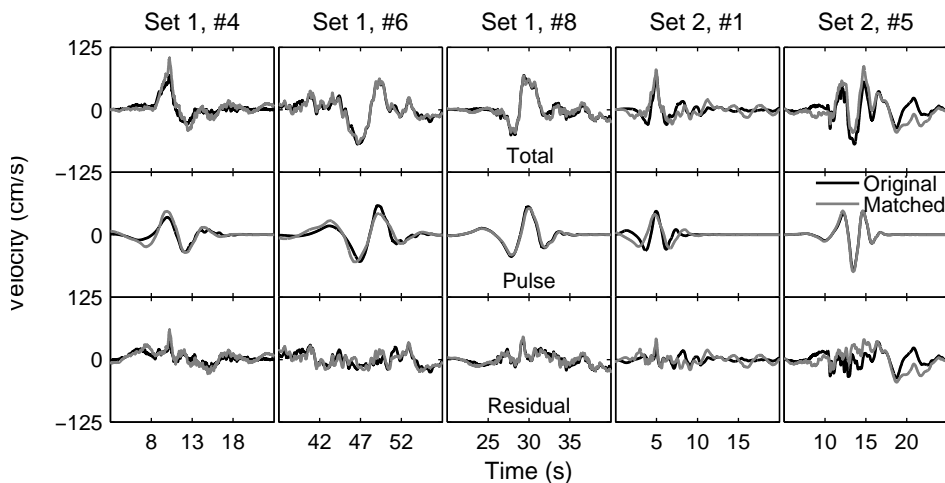
Figure B-27   Example portions of ground velocity histories for spectrum matching to unamplified amplification study; total velocity (top), extracted pulse (middle) and residual (bottom).

Appendix C
Near-Fault Earthquake Ground Motions

C.1   Introduction

This appendix presents additional information on the study of near-fault earthquake ground motions.

Earthquake ground motions recorded at small site-to-source distances can have significantly different characteristics than those recorded at larger distances. Sites in the near-fault region (assumed herein to be site-to-source distance less than 20 km) may experience shaking described as forward directivity (rupture towards the site) or backward directivity (rupture away from the site). Significant double-sided pulses in the velocity-time series are often observed in the forward-directivity (FD) case. These intense pulse-type ground motions can adversely affect the seismic performance of structures. Other near-fault phenomena can produce significant pulses in the velocity-time series as well. Additionally, there are cases when rupture occurs towards a site and intense FD pulse motions do not occur. In this study, recorded ground motions in the near-fault region are classified as FD pulse, pulse, and non-pulse motions, and recommendations are made regarding how to include pulse-type motions in the selection of design ground motions for projects sited in the near-fault region.

C.2   Overview

In the near-fault region, rupture of a fault towards a site can produce pulse-type motions in which much of the seismic energy is concentrated in one or two intense cycles in the velocity-time series. The characteristics of near-fault pulse motions are substantially different from those of ordinary ground motions. This study provides insights regarding the selection of design ground motions in the near-fault region so that the contribution of pulse-type motions is properly accounted for in the process. Conventional good practices, such as selecting design motions that best represent the governing earthquake magnitude and distance, should be followed.

This study answers the questions of how many pulse-type motions to select when in the near-fault region and how best to select these pulse-type motions. The proposed procedure is used with the results of a PSHA to estimate the appropriate number of pulse motions to use and how best to select the pulse motions. The epsilon of the seismic design parameter and distance are good indicators of the proportion of pulse motions to select as part of a suite of design ground motions.

A model was developed to estimate the number of ground motion records within a suite of ground motions that should be selected to represent the proper contribution of pulse motions to the seismic hazard for cases in which the fundamental period of the structure, T, is at least 0.7 seconds. The proportion of pulse motions as a function of the epsilon, ε, of the design ground motion parameter i.e., $S_a(T)$ at the selected seismic hazard level and closest distance from the site to the source (R in km) is:

$$Proportion\ of\ Pulse\ Motions = \frac{\exp(0.905 - 0.188R + 1.337\varepsilon)}{1 + \exp(0.905 - 0.188R + 1.337\varepsilon)}$$

For example, for the case wherein $R = 10$ km and $\varepsilon = 1$ for the 5% damped spectral acceleration at the structural period of $T = 3$s, the proportion of ground motions that should be pulse motions is estimated to be 0.59, which indicates that four records of a suite of seven total records should be pulse motions. Seed pulse-type motions records should be selected from the records provided in Table C-2 that cover the period range of interest of the structure being analyzed. A pair of scaled pulse motions should have its maximum component oriented within ±30° of the fault-normal orientation in the near-fault region.

C.3   State-of-the-Practice and Current Gaps in Knowledge

C.3.1 Forward-Directivity Effects

To account for near-fault, forward-directivity effects on earthquake ground motions used in design, two approaches have been developed:

1. The response-spectrum approach characterizes the FD motion through response spectral amplification factors; and

2. The time-domain approach characterizes the FD motion through its velocity-time history, with its peak ground velocity, predominant pulse period, and number of significant velocity pulses.

C.3.1.1 Response-Spectrum Approach

Somerville et al. (1997) take into account near-fault FD effects in design by modifying acceleration response spectra with empirically based spectra amplification factors that are determined based on the geometric relationship between the site and the ruptured fault but independent of site condition and ground motion intensity. Geometric conditions leading to FD were identified from the predicted ratio of fault-normal to fault-parallel spectral acceleration at a period of 3 seconds. A ratio larger than one was used to identify FD motions.

The Abrahamson (2000) paper is an update of the Somerville et al. (1997) model to make it applicable to a probabilistic seismic hazard analysis and to decrease the maximum effects of FD on acceleration response spectra for strike-slip events. The paper restates the primary two rupture directivity effects: (1) a change in strength of shaking of the average horizontal component of motion; and (2) the systematic

differences in the strength of shaking on the two horizontal components oriented perpendicular and parallel to the strike of the fault. The author also highlights important contributions from the Somerville et al. (1997) model, which comprises two period-dependent response spectral scaling factors that may be applied to horizontal ground motion prediction equations. The first factor accounts for the change in shaking intensity in the average horizontal component of motion due to near-fault rupture directivity effects. The second factor reflects the directional nature of the shaking intensity using two ratios: fault-normal and fault-parallel components versus the average component.

C.3.1.2 Time Domain Approach

Bray and Rodriguez-Marek (2004), Rodriguez-Marek and Bray (2006), and Bray et al. (2009) simplify the characterization of near-fault FD motions by using only the peak ground velocity (PGV), approximate period of the dominant pulse, T_v, and the number of significant cycles of pulse motions, N, of the fault-normal component of FD motions. Importantly, they bring in the effects of local soil conditions on these velocity-based ground motion parameters. Their primary findings are:

- The PGV of the motion computed at the top of the soil is generally larger than the PGV of the rock input motion, with the exception of input motions with large intensities and short pulse periods. The largest amplification of PGV for the very stiff soil profile (Site C) occurs for input motions with short pulse periods, whereas the largest amplification of PGV for the stiff soil profile (Site D) occurs at intermediate periods.

- The period, T_v, of the FD pulse at a soil site systematically increases with increasing soil depth or increasing rock input motion intensity. The dynamic stiffness of the soil profile also affects the amplitude and period of the pulse observed at the ground surface.

- Lower magnitude earthquakes may result in velocity pulses with lower periods, which may produce more damage in short-period structures than larger-magnitude events.

- Empirical relationships cannot be used at this time to predict the number of significant cycles, N, because it depends on details for the rupture mechanism that cannot be known a priori. In developing design ground motions for use in projects, it is recommended to select records that have only one or two significant cycles of motion. If simulated or modified ground motion records that have a large number of significant cycles of motion in their velocity time history were to be used, it would be unreasonable. Likewise, it would be unnecessarily conservative to use high intensity FD pulse motions with long durations of strong shaking.

C.3.2 Recent Developments

In a study that compliments and extends a previous study by Beyer and Bommer (2006), Watson-Lamprey and Boore (2007) examine the relation between different measures of horizontal ground motion components. Widely used PEER NGA relations provide orientation-independent geometric-means of spectral accelerations recorded in two orthogonal horizontal directions (GMRotI50) as defined by Boore et al. (2006). However, at times the horizontal component of ground motion with the maximum possible spectral acceleration (MaxRot) is desired. It had been believed that in the near-fault region the strike-normal (SN) component had the largest spectral acceleration values in the long period range, but this is not always the case. The authors develop conversion factors for different spectral acceleration measures for horizontal components of ground motions, including those in the near-fault region. They found that these conversion factors are distance, magnitude, and radiation pattern dependent.

From the extensive data made available through the PEER NGA project, Huang et al. (2008a) investigated the relationships between MMgm (maximum –minimum geometric-mean), SN (strike-normal) and SP (strike-parallel), actual record GMRotI50, and NGA-predicted GMRotI50 spectral demand for the period range of 0 to 4 seconds in the near-fault region. They found:

- Maximum demand is best represented for periods of at least two seconds or greater and closest site-to-fault distances less than 3 to 5 km.

- In the period range from 0 to 4 seconds, the ratio of maximum demand to the NGA-predicted GMRotI50 ranges from 1.2 to 1.3 and the median of the ratio of the maximum spectral demand to MMgm ranges from 1.2 to 1.45.

- In the short-period range, the NGA-predicted GMRotI50 overestimates MMgm and GMRotI50 in a median sense, because they used total residuals and ignored the correlation of the residuals through the event term. In the long period range NGA-predicted GMRotI50 estimates geometric-mean demand with less than 10% error in a median sense.

- In the near-fault region, the median of the ratio of maximum spectral demand to the average NGA-predicted GMRotI50 (GMRotI50_ave) is dependent on period and the Somerville et al. (1997) directivity parameters.

- This study developed scale factors to transform GMRotI50_ave to maximum demand in the near-fault region for average directivity, forward directivity, and worst-case directivity. At periods of 0.2, 1.0, and 3.0 seconds, the scale factors for average directivity are (0.9, 1.3, 1.4), for forward directivity are (1.2, 1.5, 1.7), and for worst-case directivity are (1.2, 1.5, and 2.0).

Spudich and Chiou (2008) present correction factors that predict directivity-induced variations of spectral acceleration that are about half of the strike-slip variations predicted by Somerville et al. (1997), which reduces the record-to-record sigma by

between 2 and 20% at periods of 5 seconds or greater. These directivity correction factors can be applied to the ground motion prediction relations of Abrahamson and Silva, Boore and Atkinson, Campbell and Bozorgnia, and Chiou and Youngs. Maps of the predicted directivity effects also reveal important spatial differences. The isochrone directivity resembles the predictions of Somerville et al. (1997) for the vertical dipping strike-slip fault but predicts much narrower zones of amplification in the forward (south) direction and a small deamplification in the backward (north) direction. The isochrone directivity also resembles the pattern predicted by Somerville et al. (1997) for the reverse event, but has a more gradual and natural transition going from the hanging wall or footwall zones to the neutral zones.

Baker (2007b), Tothong et al. (2007), and Shahi and Baker (2011) have employed a wavelet transform procedure to identify pulse-type signals in a ground motion time history so it can be extracted to classify pulse-type motions in a quantitative manner. The proposed procedure is based solely on objective signal-processing techniques. By also considering source-site geometry, earthquake magnitude, and distance, the probability of observing a pulse as a function of these and other parameters can be obtained. This type of approach lends itself to incorporation within robust probabilistic seismic hazard analysis (PSHA) that considers near-fault pulse motions. Through disaggregation of the PSHA, the appropriate number of pulse-type ground motions in a suite of design ground motions for a project in the near-fault region can be estimated. Shahi and Baker (2011) recommend selecting pulse-type near-fault motions with pulse periods that capture the distribution found through the disaggregation of the seismic hazard at the site.

C.3.3   Fling-Step Effects

Fling-step results from the permanent ground displacement resulting from surface faulting and tectonic warping associated with surface faulting. The ground displacement occurs during strong shaking, and thus it affects the characteristics of ground motions. Fling-step effects have received less attention than FD effects. Fling step is generally characterized by a monotonic step in the displacement time history in the direction of fault slip, which leads to a one-sided velocity pulse. The magnitude of the displacement step is estimated using empirical relations such as Wells and Coppersmith (1994) and Petersen et al. (2011). The shape of the discrete step in permanent displacement is often assumed to be in the form of a hyperbolic tangent function.

C.3.4   Gaps in the Current Knowledge

There are several significant gaps in the profession's current knowledge regarding near-fault motions that include forward directivity or fling step. They include:

1. There is still much debate regarding the characteristics of near-fault ground motions that are most important in producing high seismic demands on engineered systems. Thus, there are no widely accepted criteria for evaluating the selection of near-fault motions for engineering design.

2. There are relatively few recorded FD ground motions. With a limited number of records, empirically based models are poorly constrained and contain significant uncertainties. Potentially important effects such as site effects are difficult to investigate. With the passage of time, additional near-fault ground motions will become available, and each new set of data could potentially lead to significant changes in the profession's understanding of near-fault motions.

3. With few recordings, simulations are often employed to gain insight. However, these simulations are not well calibrated and details of the fault rupture mechanism (e.g., location and characteristics of asperities and nonuniform slip distributions along the ruptured fault plane) are difficult to discern and predict in future events. Near-fault FD motions also produce significant material nonlinearity, however, seismic site response analyses are often performed in the frequency domain using equivalent-linear material characterization that do not account for soil failure at larger strains. Fully nonlinear seismic site response analyses may be employed, but these analyses are more complex. Thus, uncertainty remains high. The development of additional, updated predictive models for capturing near-fault effects is desirable.

4. The use of a suite of spectrum-compatible motions that includes FD pulse motions in design introduces significant difficulties. For example, forcing FD pulse motions to have acceleration response spectra that match a rounded target spectrum can lead to unreasonable changes in the modified record's velocity time history or pulse motions that contain unrealistically high spectral accelerations across a wide range of frequencies. The concept of Conditional Mean Spectrum (CMS) by Baker and Cornell (2006b) offers a useful framework for selecting and modifying near-fault FD motions in a manner that avoids the problems by attempting to make modified FD pulse motions fit to a broad uniform hazard spectrum.

5. Seismic site response analyses are often performed considering unidirectional shaking, where only the larger fault-normal component of a FD motion is employed. However, there are combinations of fault-parallel and fault-normal motions due to bi-directional shaking that produce greater material nonlinearity than that shown when just performing analyses using the larger fault-normal component.

6. Additional work is warranted to explore the importance of fling-step effects on the seismic performance of engineered systems. If shown to be important, additional work would then be required to develop robust methods for incorporating fling step into design ground motions.

C.4 Scope of Study

The primary objectives of this study are:

1. Develop a database of pulse-type motions that include the effects of forward-directivity that could be used by engineers to select pulse-type motions for use in

dynamic analyses in the near-fault region. The creation of the pulse-motion database includes the development of a pulse-motion classification scheme.

2. Develop a procedure using the results of a traditional PSHA for estimating the appropriate number of pulse motions that should be used within a suite of design earthquake ground motions.

3. Given the number of pulse motions, provide guidance regarding the selection of "seed" pulse motions for use in engineering analysis and design.

These objectives are addressed in turn in the remaining part of this appendix.

C.5   Classification of Near-Fault Pulse Motions

FD pulse motions and other pulse motions that cannot be explained by the phenomenon of forward directivity differ from non-pulse ("ordinary") ground motions through their intense, compact signal in the velocity-time series. Most of the energy in a pulse motion is concentrated in one or two intense cycles in the velocity-time series. To distinguish FD pulse and other pulse motions from ordinary ground motions in the near-fault region, a classification scheme was developed to identify early-arriving, high-intensity, two-sided velocity pulses.

All ground motion data were obtained from the 2005 PEER NGA flatfile used to develop the NGA ground motion prediction equations (Chiou et al., 2008). This study only considered records with moment magnitudes greater than or equal to 6.0 and closest source-to-site distances, R_{RUP}, out to 30 km to provide data within and just beyond the near-fault region. Distance is an independent parameter of the model developed in this study and therefore the exact distance cut-off used is not a major concern as long as it is well beyond the range of primary interest (i.e., 0 to around 20 km). A magnitude cut-off of 6.0 was selected for several reasons. As code-based design ground motions are less likely to be governed by events with magnitudes less than around 6, developing the model for magnitudes greater than 6 makes it applicable to the range of primary interest. Furthermore, events with magnitudes lower than 6 are less likely to produce substantial forward directivity and there is also precedent in the use of magnitude cut-offs of around 6.0 from previous studies (e.g., Somerville et al., 1997). Caution should be used when attempting to apply the model to magnitudes that fall outside the range of 6.0 to around 8.0.

Ground motions that were missing acceleration-time series for one horizontal component, had unknown horizontal component orientations, or were not used in Abrahamson and Silva (2008) were removed from the database for this study. The Kobe 1995, Port Island (0 m) record (NGA# 1114) was removed as it was influenced by liquefaction. The Landers 1992, Lucerne (NGA# 879) record had two horizontal components which were slightly non-orthogonal (85 degrees) but for this study they were treated as orthogonal. In total 29 motions were excluded due to the reasons mentioned. The resulting ground motion database shown in Table C-1 contained 390 records from 35 earthquakes.

Table C-1   List of NGA Records Used in Study

NGA #	Earthquake Name	Station Name	NGA #	Earthquake Name	Station Name
28	Parkfield	Cholame - Shandon Array #12	232	Mammoth Lakes-01	Mammoth Lakes H. S.
30	Parkfield	Cholame - Shandon Array #5	265	Victoria, Mexico	Cerro Prieto
31	Parkfield	Cholame - Shandon Array #8	266	Victoria, Mexico	Chihuahua
33	Parkfield	Temblor pre-1969	269	Victoria, Mexico	Victoria Hospital Sotano
57	San Fernando	Castaic - Old Ridge Route	284	Irpinia, Italy-01	Auletta
68	San Fernando	LA - Hollywood Stor FF	285	Irpinia, Italy-01	Bagnoli Irpinio
70	San Fernando	Lake Hughes #1	286	Irpinia, Italy-01	Bisaccia
71	San Fernando	Lake Hughes #12	288	Irpinia, Italy-01	Brienza
72	San Fernando	Lake Hughes #4	289	Irpinia, Italy-01	Calitri
73	San Fernando	Lake Hughes #9	290	Irpinia, Italy-01	Mercato San Severino
77	San Fernando	Pacoima Dam (upper left abut)	292	Irpinia, Italy-01	Sturno
78	San Fernando	Palmdale Fire Station	295	Irpinia, Italy-02	Auletta
88	San Fernando	Santa Felita Dam (Outlet)	296	Irpinia, Italy-02	Bagnoli Irpinio
95	Managua, Nicaragua-01	Managua, ESSO	297	Irpinia, Italy-02	Bisaccia
125	Friuli, Italy-01	Tolmezzo	300	Irpinia, Italy-02	Calitri
126	Gazli, USSR	Karakyr	302	Irpinia, Italy-02	Rionero In Vulture
138	Tabas, Iran	Boshrooyeh	303	Irpinia, Italy-02	Sturno
139	Tabas, Iran	Dayhook	322	Coalinga-01	Cantua Creek School
143	Tabas, Iran	Tabas	336	Coalinga-01	Parkfield - Fault Zone 11
158	Imperial Valley-06	Aeropuerto Mexicali	337	Coalinga-01	Parkfield - Fault Zone 12
159	Imperial Valley-06	Agrarias	338	Coalinga-01	Parkfield - Fault Zone 14
160	Imperial Valley-06	Bonds Corner	339	Coalinga-01	Parkfield - Fault Zone 15
161	Imperial Valley-06	Brawley Airport	340	Coalinga-01	Parkfield - Fault Zone 16
162	Imperial Valley-06	Calexico Fire Station	346	Coalinga-01	Parkfield - Fault Zone 8
163	Imperial Valley-06	Calipatria Fire Station	359	Coalinga-01	Parkfield - Vineyard Cany 1E
164	Imperial Valley-06	Cerro Prieto	360	Coalinga-01	Parkfield - Vineyard Cany 1W
165	Imperial Valley-06	Chihuahua	368	Coalinga-01	Pleasant Valley P.P. - yard
167	Imperial Valley-06	Compuertas	369	Coalinga-01	Slack Canyon
169	Imperial Valley-06	Delta	447	Morgan Hill	Agnews State Hospital
170	Imperial Valley-06	EC County Center FF	448	Morgan Hill	Anderson Dam (Downstream)
171	Imperial Valley-06	EC Meloland Overpass FF	450	Morgan Hill	Corralitos
172	Imperial Valley-06	El Centro Array #1	451	Morgan Hill	Coyote Lake Dam (SW Abut)
173	Imperial Valley-06	El Centro Array #10	454	Morgan Hill	Gilroy - Gavilan Coll.
174	Imperial Valley-06	El Centro Array #11	455	Morgan Hill	Gilroy Array #1
175	Imperial Valley-06	El Centro Array #12	456	Morgan Hill	Gilroy Array #2
176	Imperial Valley-06	El Centro Array #13	457	Morgan Hill	Gilroy Array #3
178	Imperial Valley-06	El Centro Array #3	458	Morgan Hill	Gilroy Array #4
179	Imperial Valley-06	El Centro Array #4	459	Morgan Hill	Gilroy Array #6
180	Imperial Valley-06	El Centro Array #5	460	Morgan Hill	Gilroy Array #7
181	Imperial Valley-06	El Centro Array #6	461	Morgan Hill	Halls Valley
182	Imperial Valley-06	El Centro Array #7	463	Morgan Hill	Hollister Diff Array #1
183	Imperial Valley-06	El Centro Array #8	464	Morgan Hill	Hollister Diff Array #3
184	Imperial Valley-06	El Centro Differential Array	465	Morgan Hill	Hollister Diff Array #4
185	Imperial Valley-06	Holtville Post Office	466	Morgan Hill	Hollister Diff Array #5
187	Imperial Valley-06	Parachute Test Site	467	Morgan Hill	Hollister Diff. Array
189	Imperial Valley-06	SAHOP Casa Flores	470	Morgan Hill	San Juan Bautista, 24 Polk St
190	Imperial Valley-06	Superstition Mtn Camera	495	Nahanni, Canada	Site 1
192	Imperial Valley-06	Westmorland Fire Sta	496	Nahanni, Canada	Site 2
230	Mammoth Lakes-01	Convict Creek	497	Nahanni, Canada	Site 3
231	Mammoth Lakes-01	Long Valley Dam (Upr L Abut)	514	N. Palm Springs	Cabazon

Table C-1   List of NGA Records Used in Study (continued)

NGA #	Earthquake Name	Station Name	NGA #	Earthquake Name	Station Name
516	N. Palm Springs	Cranston Forest Station	801	Loma Prieta	San Jose - Santa Teresa Hills
517	N. Palm Springs	Desert Hot Springs	802	Loma Prieta	Saratoga - Aloha Ave
518	N. Palm Springs	Fun Valley	803	Loma Prieta	Saratoga - W Valley Coll.
521	N. Palm Springs	Hurkey Creek Park	806	Loma Prieta	Sunnyvale - Colton Ave.
524	N. Palm Springs	Joshua Tree	809	Loma Prieta	UCSC
527	N. Palm Springs	Morongo Valley	810	Loma Prieta	UCSC Lick Observatory
529	N. Palm Springs	North Palm Springs	811	Loma Prieta	WAHO
530	N. Palm Springs	Palm Springs Airport	815	Griva, Greece	Kilkis
534	N. Palm Springs	San Jacinto - Soboba	821	Erzican, Turkey	Erzincan
537	N. Palm Springs	Silent Valley - Poppet Flat	825	Cape Mendocino	Cape Mendocino
540	N. Palm Springs	Whitewater Trout Farm	827	Cape Mendocino	Fortuna - Fortuna Blvd
548	Chalfant Valley-02	Benton	828	Cape Mendocino	Petrolia
549	Chalfant Valley-02	Bishop - LADWP South St	829	Cape Mendocino	Rio Dell Overpass - FF
550	Chalfant Valley-02	Bishop - Paradise Lodge	830	Cape Mendocino	Shelter Cove Airport
552	Chalfant Valley-02	Lake Crowley - Shehorn Res.	850	Landers	Desert Hot Springs
553	Chalfant Valley-02	Long Valley Dam (Downst)	864	Landers	Joshua Tree
554	Chalfant Valley-02	Long Valley Dam (L Abut)	879	Landers	Lucerne
558	Chalfant Valley-02	Zack Brothers Ranch	880	Landers	Mission Creek Fault
587	New Zealand-02	Matahina Dam	881	Landers	Morongo Valley
718	Superstition Hills-01	Wildlife Liquef. Array	882	Landers	North Palm Springs
719	Superstition Hills-02	Brawley Airport	900	Landers	Yermo Fire Station
720	Superstition Hills-02	Calipatria Fire Station	949	Northridge-01	Arleta - Nordhoff Fire Sta
721	Superstition Hills-02	El Centro Imp. Co. Cent	952	Northridge-01	Beverly Hills - 12520 Mulhol
722	Superstition Hills-02	Kornbloom Road (temp)	953	Northridge-01	Beverly Hills - 14145 Mulhol
723	Superstition Hills-02	Parachute Test Site	954	Northridge-01	Big Tujunga, Angeles Nat F
724	Superstition Hills-02	Plaster City	957	Northridge-01	Burbank - Howard Rd.
725	Superstition Hills-02	Poe Road (temp)	959	Northridge-01	Canoga Park - Topanga Can
726	Superstition Hills-02	Salton Sea Wildlife Refuge	960	Northridge-01	Canyon Country - W Lost Cany
727	Superstition Hills-02	Superstition Mtn Camera	963	Northridge-01	Castaic - Old Ridge Route
728	Superstition Hills-02	Westmorland Fire Sta	974	Northridge-01	Glendale - Las Palmas
729	Superstition Hills-02	Wildlife Liquef. Array	978	Northridge-01	Hollywood - Willoughby Ave
737	Loma Prieta	Agnews State Hospital	983	Northridge-01	Jensen Filter Plant Generator
739	Loma Prieta	Anderson Dam (Downstream)	985	Northridge-01	LA - Baldwin Hills
740	Loma Prieta	Anderson Dam (L Abut)	986	Northridge-01	LA - Brentwood VA Hospital
741	Loma Prieta	BRAN	987	Northridge-01	LA - Centinela St
752	Loma Prieta	Capitola	988	Northridge-01	LA - Century City CC North
753	Loma Prieta	Corralitos	989	Northridge-01	LA - Chalon Rd
754	Loma Prieta	Coyote Lake Dam (Downst)	993	Northridge-01	LA - Fletcher Dr
755	Loma Prieta	Coyote Lake Dam (SW Abut)	994	Northridge-01	LA - Griffith Park Observatory
763	Loma Prieta	Gilroy - Gavilan Coll.	995	Northridge-01	LA - Hollywood Stor FF
764	Loma Prieta	Gilroy - Historic Bldg.	996	Northridge-01	LA - N Faring Rd
765	Loma Prieta	Gilroy Array #1	998	Northridge-01	LA - N Westmoreland
766	Loma Prieta	Gilroy Array #2	1003	Northridge-01	LA - Saturn St
767	Loma Prieta	Gilroy Array #3	1004	Northridge-01	LA - Sepulveda VA Hospital
768	Loma Prieta	Gilroy Array #4	1006	Northridge-01	LA - UCLA Grounds
769	Loma Prieta	Gilroy Array #6	1008	Northridge-01	LA - W 15th St
770	Loma Prieta	Gilroy Array #7	1009	Northridge-01	LA - Wadsworth VA Hospital North
776	Loma Prieta	Hollister - South & Pine	1010	Northridge-01	LA - Wadsworth VA Hospital South
778	Loma Prieta	Hollister Diff. Array	1011	Northridge-01	LA - Wonderland Ave
779	Loma Prieta	LGPC	1012	Northridge-01	LA 00

Table C-1   List of NGA Records Used in Study (continued)

NGA #	Earthquake Name	Station Name	NGA #	Earthquake Name	Station Name
1013	Northridge-01	LA Dam	1197	Chi-Chi, Taiwan	CHY028
1016	Northridge-01	La Crescenta - New York	1198	Chi-Chi, Taiwan	CHY029
1020	Northridge-01	Lake Hughes #12A	1201	Chi-Chi, Taiwan	CHY034
1023	Northridge-01	Lake Hughes #9	1202	Chi-Chi, Taiwan	CHY035
1039	Northridge-01	Moorpark - Fire Sta	1203	Chi-Chi, Taiwan	CHY036
1042	Northridge-01	N Hollywood - Coldwater Can	1205	Chi-Chi, Taiwan	CHY041
1044	Northridge-01	Newhall - Fire Sta	1206	Chi-Chi, Taiwan	CHY042
1045	Northridge-01	Newhall - W Pico Canyon Rd.	1208	Chi-Chi, Taiwan	CHY046
1048	Northridge-01	Northridge - 17645 Saticoy St	1209	Chi-Chi, Taiwan	CHY047
1049	Northridge-01	Pacific Palisades - Sunset	1227	Chi-Chi, Taiwan	CHY074
1050	Northridge-01	Pacoima Dam (downstr)	1231	Chi-Chi, Taiwan	CHY080
1051	Northridge-01	Pacoima Dam (upper left)	1234	Chi-Chi, Taiwan	CHY086
1052	Northridge-01	Pacoima Kagel Canyon	1235	Chi-Chi, Taiwan	CHY087
1063	Northridge-01	Rinaldi Receiving Sta	1238	Chi-Chi, Taiwan	CHY092
1077	Northridge-01	Santa Monica City Hall	1244	Chi-Chi, Taiwan	CHY101
1078	Northridge-01	Santa Susana Ground	1246	Chi-Chi, Taiwan	CHY104
1080	Northridge-01	Simi Valley - Katherine Rd	1476	Chi-Chi, Taiwan	TCU029
1082	Northridge-01	Sun Valley - Roscoe Blvd	1480	Chi-Chi, Taiwan	TCU036
1083	Northridge-01	Sunland - Mt Gleason Ave	1481	Chi-Chi, Taiwan	TCU038
1084	Northridge-01	Sylmar - Converter Sta	1482	Chi-Chi, Taiwan	TCU039
1085	Northridge-01	Sylmar - Converter Sta East	1483	Chi-Chi, Taiwan	TCU040
1086	Northridge-01	Sylmar - Olive View Med FF	1484	Chi-Chi, Taiwan	TCU042
1087	Northridge-01	Tarzana - Cedar Hill A	1485	Chi-Chi, Taiwan	TCU045
1089	Northridge-01	Topanga - Fire Sta	1486	Chi-Chi, Taiwan	TCU046
1091	Northridge-01	Vasquez Rocks Park	1488	Chi-Chi, Taiwan	TCU048
1100	Kobe, Japan	Abeno	1489	Chi-Chi, Taiwan	TCU049
1101	Kobe, Japan	Amagasaki	1490	Chi-Chi, Taiwan	TCU050
1104	Kobe, Japan	Fukushima	1491	Chi-Chi, Taiwan	TCU051
1106	Kobe, Japan	KJMA	1492	Chi-Chi, Taiwan	TCU052
1107	Kobe, Japan	Kakogawa	1493	Chi-Chi, Taiwan	TCU053
1108	Kobe, Japan	Kobe University	1494	Chi-Chi, Taiwan	TCU054
1110	Kobe, Japan	Morigawachi	1495	Chi-Chi, Taiwan	TCU055
1111	Kobe, Japan	Nishi-Akashi	1496	Chi-Chi, Taiwan	TCU056
1113	Kobe, Japan	OSAJ	1497	Chi-Chi, Taiwan	TCU057
1115	Kobe, Japan	Sakai	1498	Chi-Chi, Taiwan	TCU059
1116	Kobe, Japan	Shin-Osaka	1499	Chi-Chi, Taiwan	TCU060
1119	Kobe, Japan	Takarazuka	1500	Chi-Chi, Taiwan	TCU061
1120	Kobe, Japan	Takatori	1501	Chi-Chi, Taiwan	TCU063
1121	Kobe, Japan	Yae	1502	Chi-Chi, Taiwan	TCU064
1141	Dinar, Turkey	Dinar	1503	Chi-Chi, Taiwan	TCU065
1148	Kocaeli, Turkey	Arcelik	1504	Chi-Chi, Taiwan	TCU067
1158	Kocaeli, Turkey	Duzce	1505	Chi-Chi, Taiwan	TCU068
1165	Kocaeli, Turkey	Izmit	1506	Chi-Chi, Taiwan	TCU070
1176	Kocaeli, Turkey	Yarimca	1507	Chi-Chi, Taiwan	TCU071
1180	Chi-Chi, Taiwan	CHY002	1508	Chi-Chi, Taiwan	TCU072
1182	Chi-Chi, Taiwan	CHY006	1509	Chi-Chi, Taiwan	TCU074
1184	Chi-Chi, Taiwan	CHY010	1510	Chi-Chi, Taiwan	TCU075
1193	Chi-Chi, Taiwan	CHY024	1511	Chi-Chi, Taiwan	TCU076
1194	Chi-Chi, Taiwan	CHY025	1512	Chi-Chi, Taiwan	TCU078
1195	Chi-Chi, Taiwan	CHY026	1513	Chi-Chi, Taiwan	TCU079

Table C-1   List of NGA Records Used in Study (continued)

NGA #	Earthquake Name	Station Name	NGA #	Earthquake Name	Station Name
1515	Chi-Chi, Taiwan	TCU082	2495	Chi-Chi, Taiwan-03	CHY080
1517	Chi-Chi, Taiwan	TCU084	2507	Chi-Chi, Taiwan-03	CHY101
1519	Chi-Chi, Taiwan	TCU087	2618	Chi-Chi, Taiwan-03	TCU065
1520	Chi-Chi, Taiwan	TCU088	2619	Chi-Chi, Taiwan-03	TCU067
1521	Chi-Chi, Taiwan	TCU089	2622	Chi-Chi, Taiwan-03	TCU071
1527	Chi-Chi, Taiwan	TCU100	2623	Chi-Chi, Taiwan-03	TCU072
1528	Chi-Chi, Taiwan	TCU101	2624	Chi-Chi, Taiwan-03	TCU073
1529	Chi-Chi, Taiwan	TCU102	2625	Chi-Chi, Taiwan-03	TCU074
1530	Chi-Chi, Taiwan	TCU103	2626	Chi-Chi, Taiwan-03	TCU075
1531	Chi-Chi, Taiwan	TCU104	2627	Chi-Chi, Taiwan-03	TCU076
1532	Chi-Chi, Taiwan	TCU105	2628	Chi-Chi, Taiwan-03	TCU078
1533	Chi-Chi, Taiwan	TCU106	2629	Chi-Chi, Taiwan-03	TCU079
1534	Chi-Chi, Taiwan	TCU107	2632	Chi-Chi, Taiwan-03	TCU084
1535	Chi-Chi, Taiwan	TCU109	2635	Chi-Chi, Taiwan-03	TCU089
1536	Chi-Chi, Taiwan	TCU110	2650	Chi-Chi, Taiwan-03	TCU116
1537	Chi-Chi, Taiwan	TCU111	2654	Chi-Chi, Taiwan-03	TCU120
1538	Chi-Chi, Taiwan	TCU112	2655	Chi-Chi, Taiwan-03	TCU122
1540	Chi-Chi, Taiwan	TCU115	2658	Chi-Chi, Taiwan-03	TCU129
1541	Chi-Chi, Taiwan	TCU116	2661	Chi-Chi, Taiwan-03	TCU138
1542	Chi-Chi, Taiwan	TCU117	2699	Chi-Chi, Taiwan-04	CHY024
1543	Chi-Chi, Taiwan	TCU118	2700	Chi-Chi, Taiwan-04	CHY025
1545	Chi-Chi, Taiwan	TCU120	2703	Chi-Chi, Taiwan-04	CHY028
1546	Chi-Chi, Taiwan	TCU122	2704	Chi-Chi, Taiwan-04	CHY029
1547	Chi-Chi, Taiwan	TCU123	2708	Chi-Chi, Taiwan-04	CHY034
1548	Chi-Chi, Taiwan	TCU128	2709	Chi-Chi, Taiwan-04	CHY035
1549	Chi-Chi, Taiwan	TCU129	2734	Chi-Chi, Taiwan-04	CHY074
1550	Chi-Chi, Taiwan	TCU136	2739	Chi-Chi, Taiwan-04	CHY080
1551	Chi-Chi, Taiwan	TCU138	2752	Chi-Chi, Taiwan-04	CHY101
1553	Chi-Chi, Taiwan	TCU141	2871	Chi-Chi, Taiwan-04	TCU084
1602	Duzce, Turkey	Bolu	2873	Chi-Chi, Taiwan-04	TCU089
1605	Duzce, Turkey	Duzce	2888	Chi-Chi, Taiwan-04	TCU116
1611	Duzce, Turkey	Lamont 1058	2893	Chi-Chi, Taiwan-04	TCU122
1612	Duzce, Turkey	Lamont 1059	3300	Chi-Chi, Taiwan-06	CHY074
1613	Duzce, Turkey	Lamont 1060	3467	Chi-Chi, Taiwan-06	TCU065
1614	Duzce, Turkey	Lamont 1061	3468	Chi-Chi, Taiwan-06	TCU067
1615	Duzce, Turkey	Lamont 1062	3470	Chi-Chi, Taiwan-06	TCU072
1616	Duzce, Turkey	Lamont 362	3471	Chi-Chi, Taiwan-06	TCU075
1617	Duzce, Turkey	Lamont 375	3472	Chi-Chi, Taiwan-06	TCU076
1618	Duzce, Turkey	Lamont 531	3473	Chi-Chi, Taiwan-06	TCU078
1787	Hector Mine	Hector	3474	Chi-Chi, Taiwan-06	TCU079
2114	Denali, Alaska	TAPS Pump Station #10	3475	Chi-Chi, Taiwan-06	TCU080
2457	Chi-Chi, Taiwan-03	CHY024	3505	Chi-Chi, Taiwan-06	TCU125
2458	Chi-Chi, Taiwan-03	CHY025	3507	Chi-Chi, Taiwan-06	TCU129
2461	Chi-Chi, Taiwan-03	CHY028	3548	Loma Prieta	Los Gatos - Lexington Dam
2490	Chi-Chi, Taiwan-03	CHY074	3549	Northridge-01	Monte Nido Fire Station

As an initial step, each record was rotated through all orientations at 1 degree increments. At each 1 degree increment the PGV of the two orthogonal components

---

was calculated. The maximum PGV of all orientations is called max PGV in this study. The maximum ratio of the two PGVs from the orthogonal components in all orientations is termed max PGV ratio in this study. The orientations corresponding to each of these maximums were also retained.

To focus on the characteristics of the velocity-time series near the period of the most significant velocity pulse, each motion was filtered using a low-pass, 3-pole, causal Butterworth filter. As the pulses in this study had a range of periods it was found that using a constant frequency cutoff for all records yielded undesirable results. To address this issue a different cutoff frequency for each record was determined using the following steps:

1. The pseudo-spectral velocity at 5% damping of the record rotated to the maximum PGV ratio was calculated at period increments of 0.05 second for a range of periods from 0.5 to 6.0 seconds. If the maximum usable period from the NGA flatfile was less than 6 seconds the range used was 0.5 to the maximum usable period.

2. The median spectral velocity was estimated using the equally weighted NGA models of Abrahamson and Silva (2008), Boore and Atkinson (2008), Campbell and Bozorgnia (2008) and Chiou and Youngs (2008). Linear interpolation was used to estimate the median prediction at 0.05 second increments.

3. The period at which the ratio of the spectral velocity of the record to the median estimate from the NGA models was largest was used as an estimate of the pulse period.

4. Filtering was performed on the acceleration time series using a corner period of one-third the estimated pulse period. Several other ratios were tested but it was found that one-third was most appropriate.

5. For 12 of the 390 records, the corner period was adjusted when it was clear that the method described above provided undesirable results.

This process is illustrated through an example shown in Figure C-1 using the Imperial Valley 1979, Brawley Airport record. The dashed line shows the spectral velocity of the record rotated to the orientation of the maximum PGV ratio. The dotted line shows the median spectral velocity from the NGA models. The scale for these two velocity spectra is shown to the right of the plot. The solid line is the ratio between the two spectral velocities and reaches its maximum at a period of 4.65 seconds. A corner period of 4.65/3=1.55 seconds (or a frequency of 0.645 Hz) is then used to filter the acceleration-time series. The filtered motion and unfiltered motion for Brawley Airport are presented in Figure C-2.
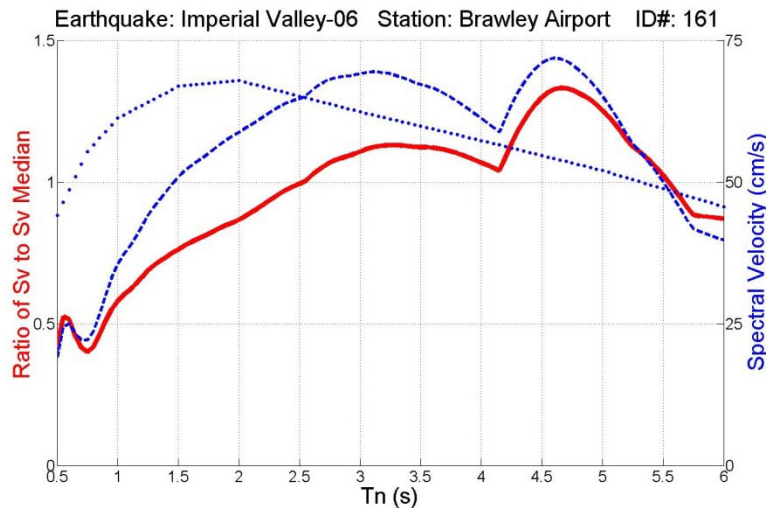
Figure C-1   Illustration of corner period calculation for Imperial Valley 1979, Brawley Airport.

The filtered acceleration-time series were integrated to velocity and then rotated through all possible orientations while an algorithm developed in MATLAB identified the largest peak to peak velocity (PPV) pulse at each 1 degree increment. The basic steps used by the algorithm to identify the PPV pulse and other parameters were:

1. Identify the zero crossings of the filtered velocity-time series and identify the peak velocity of each "half cycle" between each pair of zero crossings. A half cycle was considered significant if its maximum value was greater than 25% of the first approximation of the PPV. The first approximation of the PPV was the maximum ("positive") velocity minus the minimum velocity ("negative") of the entire record.

2. The PPV was then calculated as the maximum difference between the peaks of adjacent significant half cycles.

3. The cumulative squared velocity at a given time in the velocity-time series is the sum of the squared velocity of all preceding time steps. The normalized cumulative squared velocity (NCSV) at a given time is the cumulative squared velocity at that time divided by the cumulative squared velocity at the end of the record.

4. The NCSV at the time of the first zero crossing associated with the PPV cycle and the NCSV at the time of the last zero crossing associated with the PPV cycle were obtained. The difference between these two is termed the NCSV difference for the remainder of this study. The PPV cycle is always two adjacent half cycles.

5. The number of significant half cycles associated with the PPV cycle was calculated. A half cycle is considered to be associated with the PPV cycle if there is not a gap of time between the two half cycles greater than the difference

between the two zero crossings of the adjacent half cycle associated with the PPV pulse.

An example of the process is illustrated in Figure C-2 which shows the case for the orientation that maximizes the PPV. The PPV of the filtered motion is around 55 cm/s. The NCSV is shown with its scale on the right side of the plot. At the first zero crossing associated with the PPV cycle the NCSV is nearly zero and at the last zero crossing associated with the PPV cycle the NCSV is 64%. The number of cycles associated with the PPV pulse is 1 (two half cycles). There is an additional half cycle with a peak at around 17 seconds with sufficiently large velocity to be considered a significant cycle but the elapsed time between the adjacent zero crossings is too large for it to be associated with the PPV cycle.
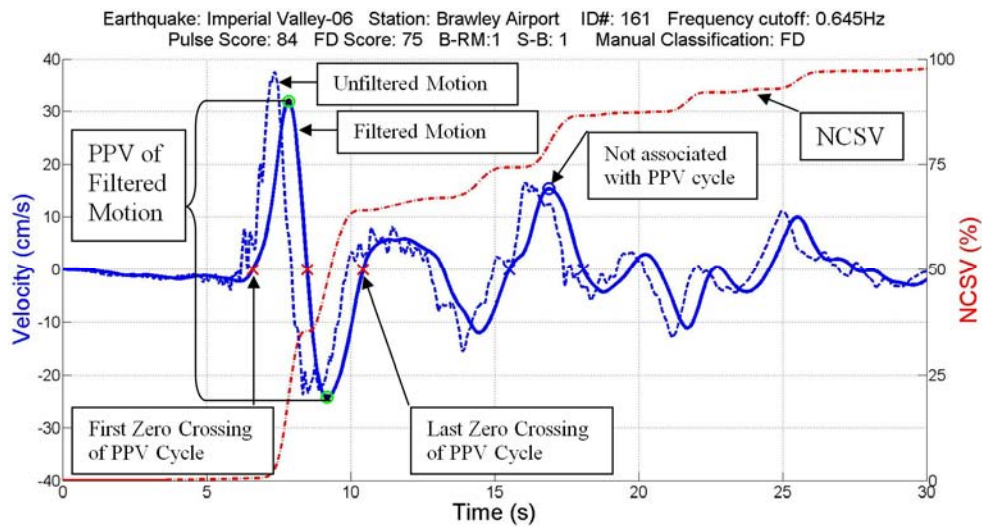
Figure C-2   Illustration of key definitions used in algorithm.

The NCSV difference is a good indicator of the pulse-type qualities of a motion. Motions where a large portion of the NCSV is associated with a single cycle are more pulse-type than motions where the NCSV is more evenly distributed and does not rise rapidly over a short time. This is apparent in the rapid increase of the NCSV during the pulse in Figure C-3a compared to the gradual increase shown in Figure C-3b. A second indicator of a pulse-type motion is a low number of significant cycles associated with the PPV pulse. The significant pulses associated with the PPV pulse can provide a better indicator of the pulse-type nature of a record than the total number of significant pulses because in some cases a second sub event (e.g., Kobe 1995) can cause additional pulses that are separated from the PPV pulse.

To classify motions as pulses or non-pulses, a weighting scheme was developed that considered the NCSV difference as well as the number of significant cycles. The weighting system assigned a score to each motion for both these parameters, with a higher score indicating a more pulse-type motion. A motion scored 100% in the NCSV category if the NCSV difference was greater than 0.7. Motions that had an NCSV difference less than 0.5 scored 0%. For motions between 0.7 and 0.5 the score

transitioned linearly between 100% and 0%. For the example of Brawley Airport, there was a NCSV difference of 0.635 and therefore this motion scored a 68% in the NCSV category. In the number of significant cycles category, motions with 1.5 significant cycles or less scored 100%, motions with 2 cycles scored 50%, and motions with 2.5 significant cycles or more scored 0%. In the case of Brawley Airport, there was one significant cycle and thus the motion scored 100% in this category. The total score was calculated with each of the two categories weighted 50%, thus the overall pulse score for Brawley Airport is 84%. Motions that scored above 60% were considered pulses.

(a)   (b)
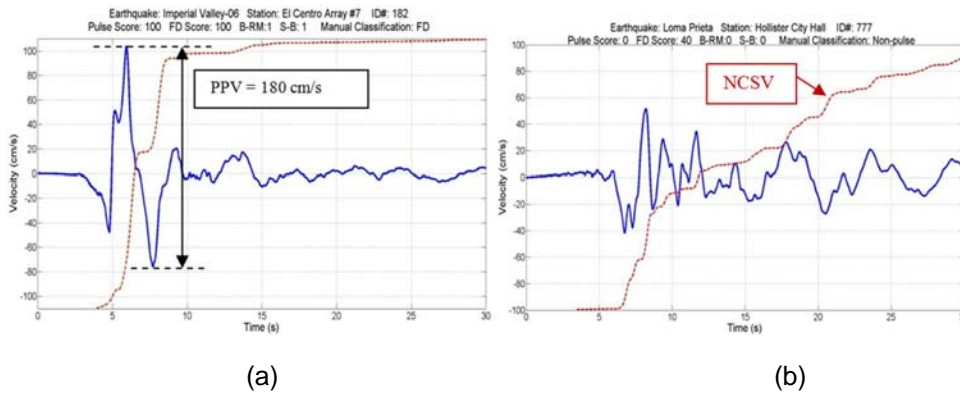
Figure C-3   Plots showing: (a) near-fault FD pulse motion with PPV and NCSV shown (Imperial Valley 1979, El Centro Array #7, USGS = Site C, R = 0.6 km, Fault Strike = 323 degrees); (b) near-fault non-pulse motion (Loma Prieta 1989, Hollister City Hall, USGS = Site C, R = 27.6 km, Fault Strike = 128 degrees).

The scoring system described was in part developed by using the existing classifications of Shahi and Baker (2011) and Bray and Rodriguez-Marek (2004) to "train" the scoring scheme. For example, consider Figure C-4 which shows the proportion of motions classified as pulses by Shahi and Baker (2011) or forward directivity by Bray and Rodriguez-Marek (2004) as a function of NCSV difference. The data shown were grouped into bins by NCSV, and for each bin the proportion of motions that were classified as pulses were tabulated. As the NCSV difference increased, it was more likely that a given motion had been classified as a pulse. A logistic regression, which is appropriate for binomial data, was also used and yielded a similar trend as seen in Figure C-4. Figure C-5 shows a similar plot using the number of significant cycles associated with the PPV pulse. As the number of significant cycles increased for a given motion, it was less likely to have been classified as a pulse in the existing classifications. Several alternate parameters were considered that could be used to classify pulses but it was found that in this case a relatively simple combination of NCSV and number of significant pulses worked well. The specific cut-offs and weights of individual categories were also calibrated in part by using these previous classifications.

The tapering of the score from 100% to 0% in an individual category is superior to using a single cut-off because in general there is not a clear cut-off and picking one is subjective. Choosing a specific taper scheme is also subjective but it acknowledges that there is not a clean cut-off and there is uncertainty in the classification. By combining several relevant factors into the final pulse score, the classification is more robust than using any single factor alone. Ultimately, a cut-off is needed to categorize the database of motions into pulse and non-pulse but by using the scoring system described, the performance was much improved compared to using individual cut-offs on NCSV difference or number of significant pulses.
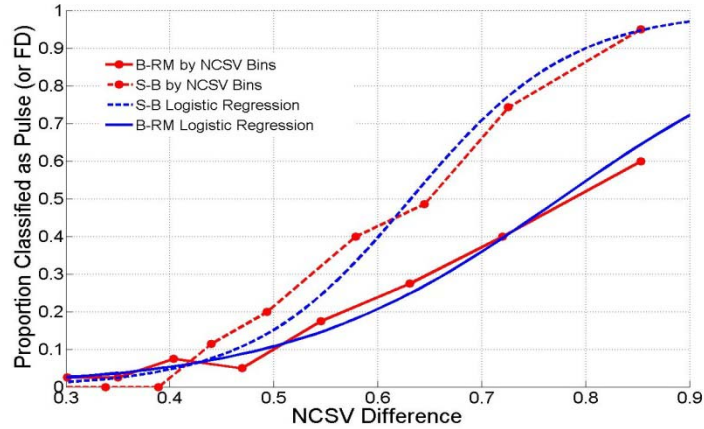
Figure C-4   Proportion of ground motions classified as pulses by Shahi and Baker (2011) or forward directivity by Bray and Rodriguez-Marek (2004) as a function of NCSV difference.
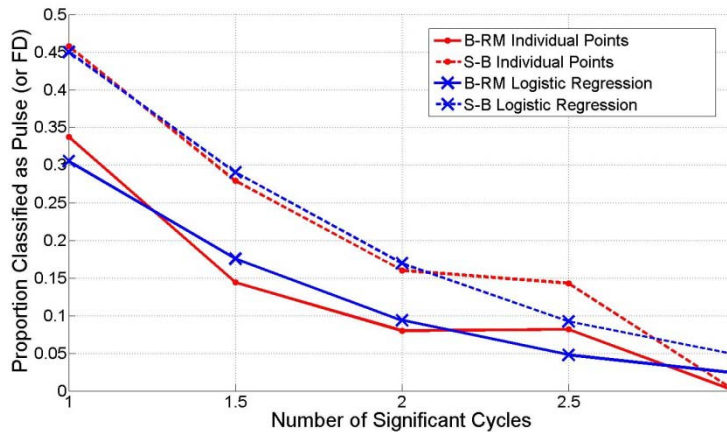
Figure C-5   Proportion of ground motions classified as pulses by Shahi and Baker (2011) or forward directivity by Bray and Rodriguez-Marek (2004) as a function of number of significant cycles.

The classification scheme was supplemented with a subjective evaluation because it was realized that nuances of a record were not always captured by an automated classification scheme. Of the 390 motions in the database, 97 received pulse scores greater than 60. In total seven motions with pulse scores less than 60 were manually added to the pulse category and 16 motions with pulse scores greater than 60 were removed from the pulse category. This brought the total number of motions

classified as pulses to 88. Thirty motions were considered to be questionable as to whether they were pulse-type; for this study, the questionable motions were considered to be non-pulse motions.

To quantify the number of pulse motions that could potentially be explained by forward directivity, a second scoring system was developed. A main parameter indicating that a pulse was likely caused by forward directivity was the Isochrone Directivity Predictor (IDP) proposed by Spudich and Chiou (2008). The IDP takes into account rupture and site geometry to describe the expected forward-directivity amplification of the spectral acceleration from NGA ground motion prediction equations as a function of period, closest distance (R_{RUP}), and magnitude. Higher IDP values indicate higher expected amplification due to directivity. Although it depends on the period, magnitude, distance, and the particular NGA model used, IDP values of around 1.5 mark the transition from backward-directivity deamplification to forward-directivity amplification. A second parameter used in the FD score is the PGV ratio as researchers such as Somerville et al. (1997) have noted that forward-directivity motions tend to have high ratios of PGV in the fault-normal to fault-parallel direction due to the superposition of SH waves that cause directivity. The final parameter used in the FD score is the orientation of the maximum PPV pulse. Again, due to the physical processes that lead to forward directivity, the pulse is expected to be near the fault-normal orientation. The scoring scheme was similar to that used for pulses and used a linear transition between the two values listed below for each parameter:

1. Value of IDP: 100% score for IDP > 2, 0% score for IDP < 1.5. Weighted as 60% of the FD score.

2. Value of the maximum PGV ratio: 100% score for PGV ratio > 2.2, 0% score for PGV ratio < 1.7. Weighted as 25% of the FD score.

3. Deviation of the orientation of the PPV pulse from fault-normal direction: 100% score for deviation < 30 degrees, 0% score for deviation > 50 degrees. Weighted as 15% of the FD score.

Of the 88 motions classified as pulses, 54 motions received FD scores greater than 60% and are likely to have been caused by forward directivity. These motions will be referred to as FD pulses. The remaining 34 motions that had been previously classified as pulses received FD scores lower than 60% and in this study were considered unlikely to be caused by forward-directivity. Thus, of the 88 pulse motions, the majority were likely to be caused by forward directivity. Although the model in this study did not distinguish between these two categories of pulses, this distinction could become important in the future. For example, the NGA-West-2 models may incorporate directivity and thus reduce the epsilon of the FD pulse motions, but this should have little effect on non-FD pulse epsilons necessitating a distinction.

The period of each pulse motion was estimated using a method similar to that employed to estimate the period of the pulse for use in the filtering process. The only modification is that the motion is rotated to the max PPV orientation prior to calculating the spectral velocities. The period of the pulse is the period at which the ratio of the spectral velocity of the PPV pulse to the median spectral velocity of the NGA models is maximized. Several other methods of identifying the period were also tested. These methods included using the period associated with the maximum spectral velocity, the ratio of the spectral velocity of the two orthogonal components, or the zero crossings of the pulse in the velocity-time series. However, these alternate methods did not prove to be as robust.

C.6   Near-Fault Pulse Motions Database

The identified FD pulse and pulse motions with their key characteristics are provided in Table C-2 where the pulse motions are grouped by the period of the predominant pulse in the velocity-time series. The colors in the last column (Pulse Period *sec.*) identify the two period bins that were established and show the overlap. FD pulse and pulse ground motion records should be selected from the motions listed in the table that cover the period range of interest of the structure being analyzed. Plots of each pulse motion rotated to the max PPV pulse orientation (and the orthogonal component) are included at the end of this appendix to facilitate the selection of appropriate motions. Alternate classifications such as those proposed by Bray and Rodriguez-Marek (2004) and Shahi and Baker (2011) could also be used.

C.7   Number of Forward-Directivity Pulse and Pulse Ground Motions

An investigation into the occurrence of pulse motions found that pulse motions are more likely to occur when the design ground motions parameter at the selected seismic hazard level is due to a high epsilon value (e.g., the disaggregation of the seismic hazard indicated that the design spectral acceleration at the period of the structure results from an epsilon value greater than one). Additionally, this effect depends greatly on source-to-site distance, with the likelihood of pulse motions occurring increasing significantly as the source-to-site distance decreases. These effects can be observed in Figure C-6.

The contours in Figure C-6 were created by calculating the proportion of pulses in overlapping bins. The process was carried out using overlapping bins of size 5 km in distance by 1 unit of epsilon. To create overlapping bins, the bin positions were shifted by increments of 1 km in distance and 0.1 in ε. For each bin the proportion of pulse motions was calculated along with the mean distance and mean epsilon of the events within the bin. These data were then interpolated to a regularly spaced grid and contours were plotted. The limited data necessitated the use of fairly large bins to obtain a reasonable estimate of the proportion, and the exact locations of these contours depend on how the data were binned. However, the overall trend remains consistent regardless of the exact binning procedure.

Table C-2   Near-Fault FD Pulse and Pulse Ground Motions

NGA #[1]	Earthquake	Station	M_w	Closest Distance km	Max PGV cm/s	PGV of Orth. Comp. cm/s	PPV[2] cm/s	PPV Azimuth deg.	Pulse Period sec.	
1003	Northridge-01	LA - Saturn St	6.7	27.0	40	31	74	94	0.5	
496	Nahanni, Canada	Site 2	6.8	4.9	35	24	55	165	0.6	
461	Morgan Hill	Halls Valley	6.2	3.5	40	12	67	46	0.6	
1051	Northridge-01	Pacoima Dam (upper left)	6.7	7.0	107	50	169	35	0.8	
451	Morgan Hill	Coyote Lake Dam (SW Abut)	6.2	0.5	81	55	128	104	0.8	
1004	Northridge-01	LA - Sepulveda VA Hospital	6.7	8.4	78	75	148	88	0.8	
3473	Chi-Chi, Taiwan-06	TCU078	6.3	11.5	34	28	51	1	0.8	
2627	Chi-Chi, Taiwan-03	TCU076	6.2	14.7	62	18	92	99	0.9	
3475	Chi-Chi, Taiwan-06	TCU080	6.3	10.2	41	19	72	45	0.9	
1602	Duzce, Turkey	Bolu	7.1	12.0	64	59	120	90	0.9	
2626	Chi-Chi, Taiwan-03	TCU075	6.2	19.7	26	9	44	108	1.0	
3548	Loma Prieta	Los Gatos - Lexington Dam	6.9	5.0	101	29	175	50	1.1	
359	Coalinga-01	Parkfield - Vineyard Cany 1E	6.4	26.4	29	22	55	116	1.1	
1063	Northridge-01	Rinaldi Receiving Sta	6.7	6.5	167	62	252	23	1.1	
1084	Northridge-01	Sylmar - Converter Sta	6.7	5.4	133	87	207	163	1.1	
459	Morgan Hill	Gilroy Array #6	6.2	9.9	38	8	60	79	1.2	
529	N. Palm Springs	North Palm Springs	6.1	4.0	74	31	98	24	1.2	
77	San Fernando	Pacoima Dam (up. left abut)	6.6	1.8	119	40	159	2	1.2	
722	Superstition Hills-02	Kornbloom Road (temp)	6.5	18.5	36	10	51	145	1.2	
285	Irpinia, Italy-01	Bagnoli Irpinio	6.9	8.2	33	20	54	60	1.3	
2618	Chi-Chi, Taiwan-03	TCU065	6.2	26.1	35	17	56	120	1.4	
763	Loma Prieta	Gilroy - Gavilan Coll.	6.9	10.0	31	26	44	92	1.4	
765	Loma Prieta	Gilroy Array #1	6.9	9.6	39	29	47	87	1.4	
764	Loma Prieta	Gilroy - Historic Bldg.	6.9	11.0	42	24	69	148	1.5	
766	Loma Prieta	Gilroy Array #2	6.9	11.1	46	25	78	67	1.5	
517	N. Palm Springs	Desert Hot Springs	6.1	6.8	31	18	42	175	1.6	
1119	Kobe, Japan	Takarazuka	6.9	0.3	90	61	140	56	1.6	
1085	Northridge-01	Sylmar - Converter Sta East	6.7	5.2	118	76	157	164	1.7	
723	Superstition Hills-02	Parachute Test Site	6.5	1.0	116	44	200	63	1.9	
1182	Chi-Chi, Taiwan	CHY006	7.6	9.8	66	41	107	105	1.9	
2114	Denali, Alaska	TAPS Pump Station #10	7.9	2.7	147	66	187	74	1.9	
159	Imperial Valley-06	Agrarias	6.5	0.7	54	20	74	50	1.9	
767	Loma Prieta	Gilroy Array #3	6.9	12.8	50	37	72	86	2.0	
1013	Northridge-01	LA Dam	6.7	5.9	77	42	108	30	2.1	
821	Erzican, Turkey	Erzincan	6.7	4.4	96	46	144	24	2.4	
1045	Northridge-01	Newhall - W Pico Canyon Rd.	6.7	5.5	94	63	176	58	2.4	
1086	Northridge-01	Sylmar - Olive View Med FF	6.7	5.3	132	73	160	15	2.5	
1529	Chi-Chi, Taiwan	TCU102	7.6	1.5	118	73	181	76	2.7	
2658	Chi-Chi, Taiwan-03	TCU129	6.2	12.8	40	13	60	94	2.7	
828	Cape Mendocino	Petrolia	7.0	8.2	98	42	115	108	2.7	
171	Imperial Valley-06	EC Meloland Overpass FF	6.5	0.1	115	29	150	63	2.9	
292	Irpinia, Italy-01	Sturno	6.9	10.8	52	32	97	94	3.0	
1050	Northridge-01	Pacoima Dam (downstr)	6.7	7.0	51	24	33	48	3.2	
178	Imperial Valley-06	El Centro Array #3	6.5	12.9	55	30	70	118	3.3	
181	Imperial Valley-06	El Centro Array #6	6.5	1.4	117	61	201	76	3.5	
182	Imperial Valley-06	El Centro Array #7	6.5	0.6	109	52	154	65	3.5	
170	Imperial Valley-06	EC County Center FF	6.5	7.3	69	37	92	81	3.6	
180	Imperial Valley-06	El Centro Array #5	6.5	4.0	93	55	142	52	3.8	
1158	Kocaeli, Turkey	Duzce	7.5	15.4	62	50	100	14	3.8	

Table C-2   Near-Fault FD Pulse and Pulse Ground Motions (continued)

NGA #[1]	Earthquake	Station	M_w	Closest Distance km	Max PGV cm/s	PGV of Orth. Comp. cm/s	PPV[2] cm/s	PPV Azimuth deg.	Pulse Period sec.	
779	Loma Prieta	LGPC	6.9	3.9	109	45	167	11	3.9	
1511	Chi-Chi, Taiwan	TCU076	7.6	2.8	89	39	103	132	3.9	
825	Cape Mendocino	Cape Mendocino	7.0	7.0	131	39	145	4	4.0	
1176	Kocaeli, Turkey	Yarimca	7.5	4.8	73	48	139	16	4.1	
879	Landers	Lucerne	7.3	2.2	147	33	173	74	4.3	
179	Imperial Valley-06	El Centro Array #4	6.5	7.1	82	61	131	48	4.4	
185	Imperial Valley-06	Holtville Post Office	6.5	7.7	69	25	92	97	4.4	
1165	Kocaeli, Turkey	Izmit	7.5	7.2	30	22	50	86	4.4	
1519	Chi-Chi, Taiwan	TCU087	7.6	7.0	54	43	87	122	4.5	
1510	Chi-Chi, Taiwan	TCU075	7.6	0.9	89	38	147	93	4.6	
1476	Chi-Chi, Taiwan	TCU029	7.6	28.1	66	39	118	152	4.7	
161	Imperial Valley-06	Brawley Airport	6.5	10.4	45	35	56	60	4.7	
1548	Chi-Chi, Taiwan	TCU128	7.6	13.2	80	54	145	132	4.8	
1244	Chi-Chi, Taiwan	CHY101	7.6	10.0	115	70	173	11	4.9	
1480	Chi-Chi, Taiwan	TCU036	7.6	19.8	69	42	121	120	5.1	
143	Tabas, Iran	Tabas	7.4	2.1	123	106	189	180	5.2	
1483	Chi-Chi, Taiwan	TCU040	7.6	22.1	55	45	95	105	5.6	
183	Imperial Valley-06	El Centro Array #8	6.5	3.9	70	44	87	82	5.9	
184	Imperial Valley-06	El Centro Differential Array	6.5	5.1	71	41	107	80	5.9	
173	Imperial Valley-06	El Centro Array #10	6.5	6.2	52	44	69	68	6.0	
802	Loma Prieta	Saratoga - Aloha Ave	6.9	8.5	56	42	70	48	6.0	
803	Loma Prieta	Saratoga - W Valley Coll.	6.9	9.3	75	54	79	69	6.0	
900	Landers	Yermo Fire Station	7.3	23.6	57	17	72	64	6.0	
1148	Kocaeli, Turkey	Arcelik	7.5	13.5	43	12	58	72	6.0	
1481	Chi-Chi, Taiwan	TCU038	7.6	25.4	52	45	87	110	6.0	
1485	Chi-Chi, Taiwan	TCU045	7.6	26.0	47	36	56	81	6.0	
1486	Chi-Chi, Taiwan	TCU046	7.6	16.7	45	26	62	102	6.0	
1489	Chi-Chi, Taiwan	TCU049	7.6	3.8	66	52	81	155	6.0	
1491	Chi-Chi, Taiwan	TCU051	7.6	7.7	49	39	71	112	6.0	
1492	Chi-Chi, Taiwan	TCU052	7.6	0.7	179	83	283	114	6.0	
1493	Chi-Chi, Taiwan	TCU053	7.6	6.0	49	45	77	44	6.0	
1494	Chi-Chi, Taiwan	TCU054	7.6	5.3	62	37	82	115	6.0	
1501	Chi-Chi, Taiwan	TCU063	7.6	9.8	85	51	139	158	6.0	
1505	Chi-Chi, Taiwan	TCU068	7.6	0.3	296	110	464	152	6.0	
1515	Chi-Chi, Taiwan	TCU082	7.6	5.2	69	41	92	61	6.0	
1528	Chi-Chi, Taiwan	TCU101	7.6	2.1	68	53	97	51	6.0	
1530	Chi-Chi, Taiwan	TCU103	7.6	6.1	62	28	101	81	6.0	
1549	Chi-Chi, Taiwan	TCU129	7.6	1.8	61	34	84	117	6.0	
1550	Chi-Chi, Taiwan	TCU136	7.6	8.3	61	37	99	40	6.0	

Notes: 1) Bold NGA record numbers indicate motion was classified as a FD pulse.
2) The PPV is the peak to peak velocity from the filtered record.
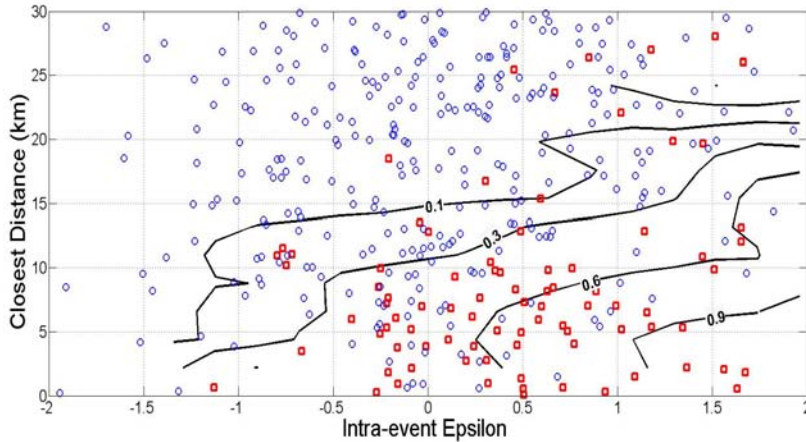
Figure C-6   Contours of proportion of FD pulse and pulse motions as a function of closest distance and intra-event epsilon of the record's PGV based on the Abrahamson and Silva (2008) NGA model. Contours of 0.1, 0.3, 0.6 and 0.9 are shown superimposed on a scatter plot of the 390 motions with red squares indicating motions classified as FD pulse or pulse and blue circles indicating non-pulse motions.

Intra-event epsilon of PGV from Abrahamson and Silva (2008) was used to develop the initial model, but the final model was adjusted to use total epsilon. This was accomplished by normalizing the intra-event residual by the total standard deviation rather than the intra-event standard deviation to obtain an estimate of the mean total epsilon for random event terms for future earthquakes. This total epsilon is consistent with the total epsilon used by the engineer in practice. Therefore, the following relationships can be used directly with total epsilon.

A model was developed to capture the dependence of the proportion of pulse motions on epsilon and distance, and it is displayed in Figure C-7 for select distances. The resulting relationship from a logistic regression of the proportion of FD pulse and pulse motions as a function of the epsilon, ε, of the design ground motion parameter, which is typically spectral acceleration at the period of the structure at the design seismic hazard level, and closest distance from the site to the source, R, is:

$$Proportion\,of\,Pulse\,Motions = \frac{\exp(0.905 - 0.188R + 1.337\varepsilon)}{1 + \exp(0.905 - 0.188R + 1.337\varepsilon)}$$

This relationship may be used by the engineer to estimate the number of ground motion records within a suite of ground motions that should be selected from the provided table of pulse motions to represent the proper contribution of pulse motions to the seismic hazard. For example, for the case wherein $R = 10$ km and $\varepsilon = 1.5$ for the 5% damped spectral acceleration at the structural period of 1.2 seconds, the proportion of ground motions that should be FD pulse and pulse motions is 0.74. Thus, for this case, 5 records (i.e., $0.74 \times 7 = 5.2$) of a suite of 7 records should be FD-pulse and pulse motions. Alternatively, the number of pulse-type ground motions can be estimated by another procedure, such as that proposed by Shahi and Baker

(2011), which estimates the number of pulse-type ground motions in a suite of design ground motions through a relationship that captures the probability of observing a pulse-type motion at a site based on the disaggregation of the hazard as a function of pulse period.
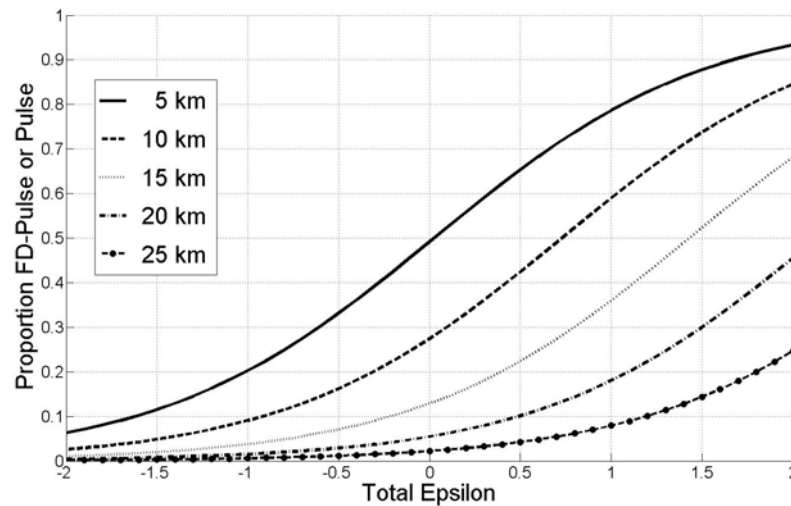
Figure C-7   Proposed model for capturing proportion of FD pulse and pulse motions as a function of the seismic hazards controlling epsilon and distance.

Figure C-8 shows the classifications of Bray and Rodriguez-Marek (2004) and Shahi and Baker (2011) as a function of epsilon for distance bins of 0-10 and 10-20 km. It is important to note that the exact position of the curves depends on how the data were binned in terms of epsilon and distance. However, the overall trend is not sensitive to the binning. The trend in Figure C-8 is similar to that of the proposed model shown in Figure C-7. This is not surprising because all three classification systems have substantial overlap in the motions considered to be pulses. This overlap is reassuring considering the different approaches taken in these classification methods. The method of Shahi and Baker (2011) is largely quantitative, which has advantages including repeatability rapid application to large data sets. The classification of Bray and Rodriguez-Marek (2004) is largely qualitative. It is based on manual classification that could be argued to take a holistic approach by considering many additional factors and nuances not captured by an algorithm. However, it has disadvantages in repeatability and human bias and inconsistencies. In this study, an attempt is made to strike a balance between the advantages and disadvantages of a largely quantitative method and a largely qualitative method. The Bray and Rodriguez-Marek (2004) curves fall below those of Shahi and Baker (2011) and those proposed in this study because of their stricter classification system that only sought to classify FD motions. The recommended model for this study and Shahi and Baker 2011 included more pulses and therefore the proportions classified as pulses as a function of epsilon and distance are understandably higher.
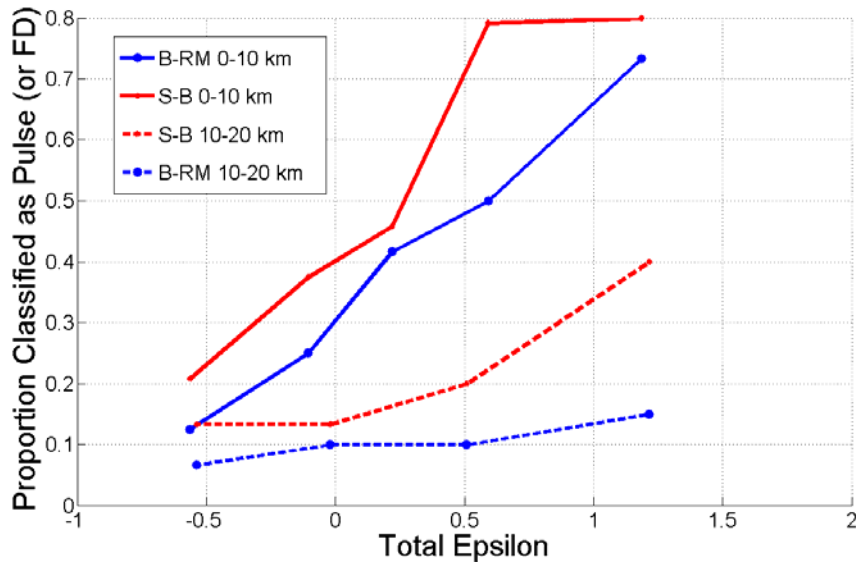
Figure C-8   Proportion classified as pulse by Shahi and Baker (2011) or forward-directivity by Bray and Rodriguez-Marek (2004) as a function of total PGV epsilon.

The model in this study was developed using intra-event epsilon of PGV from Abrahamson and Silva (2008) and then adjusted to be compatible with total PGV epsilon. It is the recommendation of the developers that the PGV epsilon be used if available. If this epsilon is unavailable, the epsilon of the spectral acceleration at the structural period is likely acceptable.

It should be noted that several different model parameters were considered in addition to epsilon and distance. The improvement in model fit with additional parameters was gauged using the term "deviance" which is twice the difference between the maximum possible log-likelihood (i.e., from a model where the data are fit exactly) and the model under consideration. Thus, deviance provides a relative index of fit with lower deviances preferred. A model with only epsilon as the independent parameter had a deviance of 391 and by adding a distance parameter this was greatly reduced to 285. A model using epsilon and magnitude instead of distance had a much higher deviance of 375 and thus it is clear that magnitude is not as important as distance for the ranges of magnitudes and distances used in this study. Adding a magnitude parameter in addition to distance and epsilon only slightly further reduced the deviance from 285 to 279 while using IDP instead of magnitude decreased the deviance from 285 to 272. However, incorporating additional parameters (particularly complicated ones such as IDP) make the application of the model more difficult, and the goal of this study is to provide a relatively simple method that can be applied to the results of a traditional PSHA without excessive additional calculations.

Due to limited data and other considerations, the model was developed using pulses of all periods. This may overestimate the likelihood of the occurrence of pulses when one is only interested in pulses within a certain period range. For example, a pulse with a period of 6 seconds may not have a "pulse-type" effect on a building with a structural period of 1 second. One difficulty in addressing this issue is that there is not a clear transition where a pulse of a given period stops having a "pulse-type" effect on buildings with varying structural periods. For example, a pulse with a period of 3 seconds will have a "pulse-type" effect on structures with periods of around 3 seconds, but it is not clear if will it be "pulse-type" to structures with periods of 2 seconds, 1.5 seconds, etc. A related issue is that the database in this study is dominated by a few well recorded earthquakes, most notably Chi-Chi and its aftershocks which make up nearly a third of the 390 records and the current model gives equal weight to each recording. For these reasons it is difficult to determine the proportion of pulses within specific period ranges. These issues warrant additional investigation in the future.

C.8   Selection of Forward-Directivity Pulse and Pulse Motions

Once the number of FD pulse and pulse motions is determined, these records should be selected from the records listed in Table C-2 that cover the period range of interest of the structure being analyzed. To assist in the selection of motions, plots of the velocity-time series of all pulse motions rotated to the orientation of the max PPV and corresponding orthogonal component are included in Figure C-10, which is at the end of this appendix. FD pulse and pulse motions are provided in period bins of 0.7 to 2.2 seconds (identified by blue column) and 2.2 to 6.0 seconds (identified by red column). The bins include ground motions just outside their nominal period ranges to increase the number of potential records to choose from given the limited number of pulse-type records currently available. The engineer could select from the bin of pulse-type motions that best reflects the period range of interest of the structure being considered. Conventional good practices, such as selecting design motions that best represent the governing earthquake magnitude and distance, should still be followed.

With a limited number of design ground motions in the suite of motions (i.e., a suite of 7 motions is often used in practice and only a portion of these will be pulses), it is important to focus on the period range of interest of the structure. If many ground motions were to be used (e.g., more than 40 or so), then one could develop a more comprehensive suite of motions that captures all key earthquake scenarios including the most likely expected period of the pulse for a range of potential near-fault earthquake scenarios.

Forward-directivity motions have a tendency for the maximum PPV component to be oriented closer to fault normal than fault parallel. As shown in Figure C-9, there is substantial scatter in the orientation of the FD pulses but most fall within 30 degrees of fault normal as indicated by the dashed lines. As expected there is not a clear

pattern to the orientation of the pulses not explained by forward directivity. It should be noted that these results are somewhat biased as the deviation from fault normal was included as a small part (15%) of the FD score. However, if IDP is used as an indicator of forward directivity alone, a similar trend arises. The average deviation from fault normal of all pulse motions with IDP values greater than 2 is around 29 degrees. In contrast, the average deviation of pulse motions with IDP less than 2 is 39 degrees. There is a clear tendency for the FD pulse to be orientated near fault normal on average, but there is uncertainty in the orientation of any single motion.
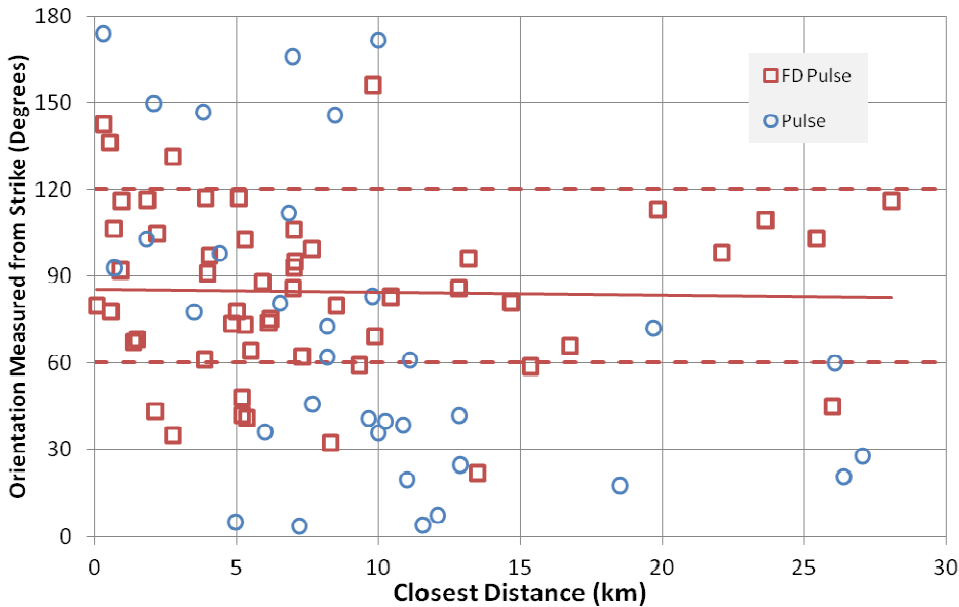
Figure C-9   Orientation of FD pulses and pulses.

If spectrum matching is used, ideally, the motion should be spectrally matched using the concept of a conditional spectrum, because pulse motions contain high spectral ordinates within a narrow period range. Thus, spectral ordinates at other periods are likely to be below spectral acceleration values derived from an equal hazard spectrum. However, traditionally an equal hazard spectrum is used in earthquake engineering design practice, and for this case, it will be necessary to match the target spectrum over the specified period range (e.g., $0.2T$-$1.5T$, where T is the fundamental period of vibration of the structure). "Loose" spectrum matching should be performed for pulse-type motions so that the spectral ordinate at the period of the pulse is not larger than about 15% to 30% of the target spectral ordinate at this period and spectral ordinates at periods away from the period of the pulse are not less than about 10% to 20% of the target spectral values at these periods. Most importantly, the velocity-time series of the matched motion and the seed motion must be inspected to ensure that the nonstationary aspects of the seed motion are preserved in the matching process.

Figure C-10   Velocity-time series of FD pulse and pulse records in max PPV orientation with orthogonal component.

C: Near-Fault Earthquake Ground Motions

Figure C-10   Velocity-time series of FD pulse and pulse records in max PPV orientation with orthogonal component (continued).

Figure C-10   Velocity-time series of FD pulse and pulse records in max PPV orientation with orthogonal component (continued).

Figure C-10   Velocity-time series of FD pulse and pulse records in max PPV orientation with orthogonal component (continued).

Figure C-10   Velocity-time series of FD pulse and pulse records in max PPV orientation with orthogonal component (continued).

C: Near-Fault Earthquake Ground Motions

Figure C-10   Velocity-time series of FD pulse and pulse records in max PPV orientation with orthogonal component (continued).

Figure C-10   Velocity-time series of FD pulse and pulse records in max PPV orientation with orthogonal component (continued).

Figure C-10   Velocity-time series of FD pulse and pulse records in max PPV orientation with orthogonal component (continued).

Figure C-10   Velocity-time series of FD pulse and pulse records in max PPV orientation with orthogonal component (continued).

Figure C-10   Velocity-time series of FD pulse and pulse records in max PPV orientation with orthogonal component (continued).

Appendix D

Key Issues in Ground Motion Selection and Scaling
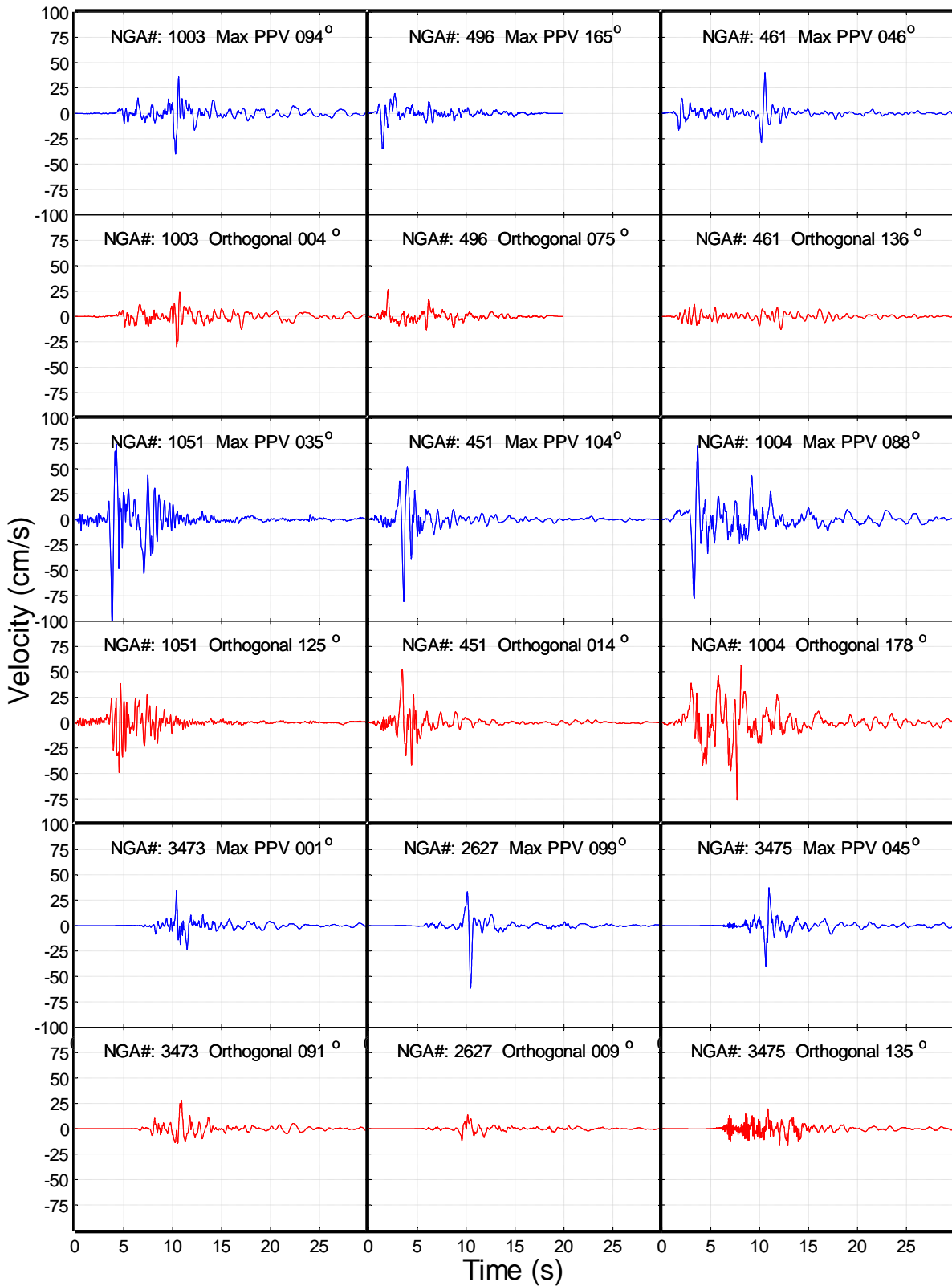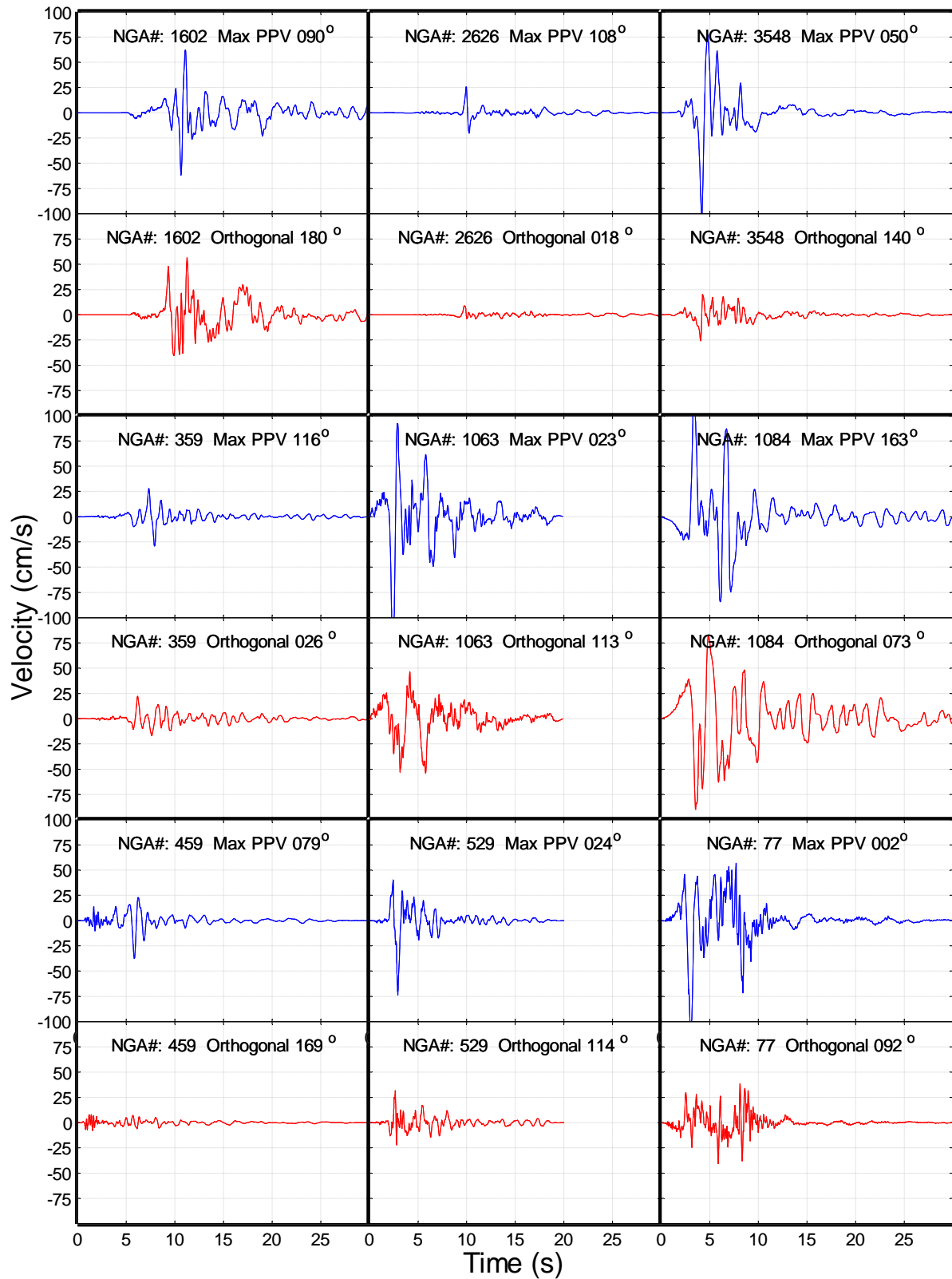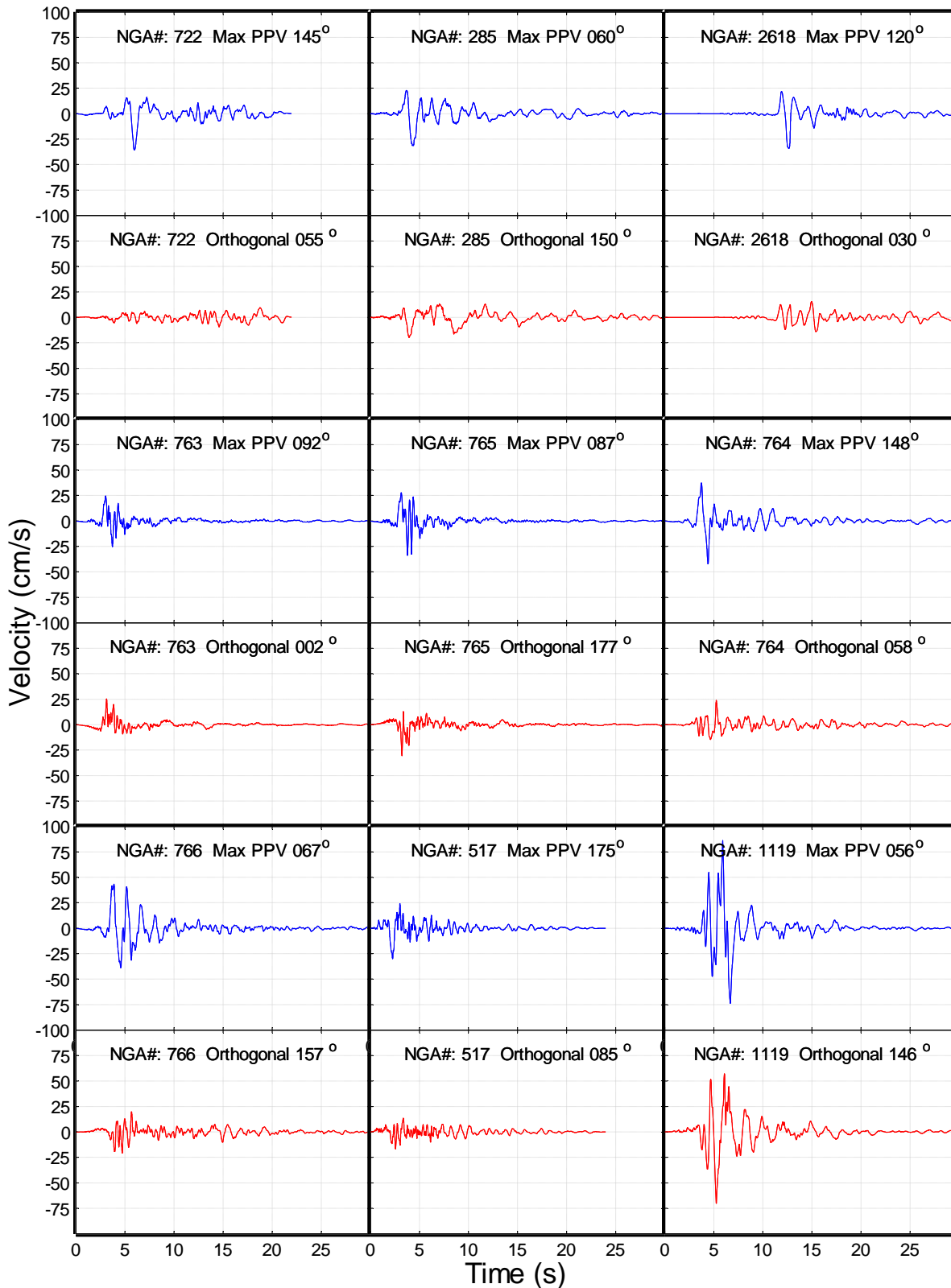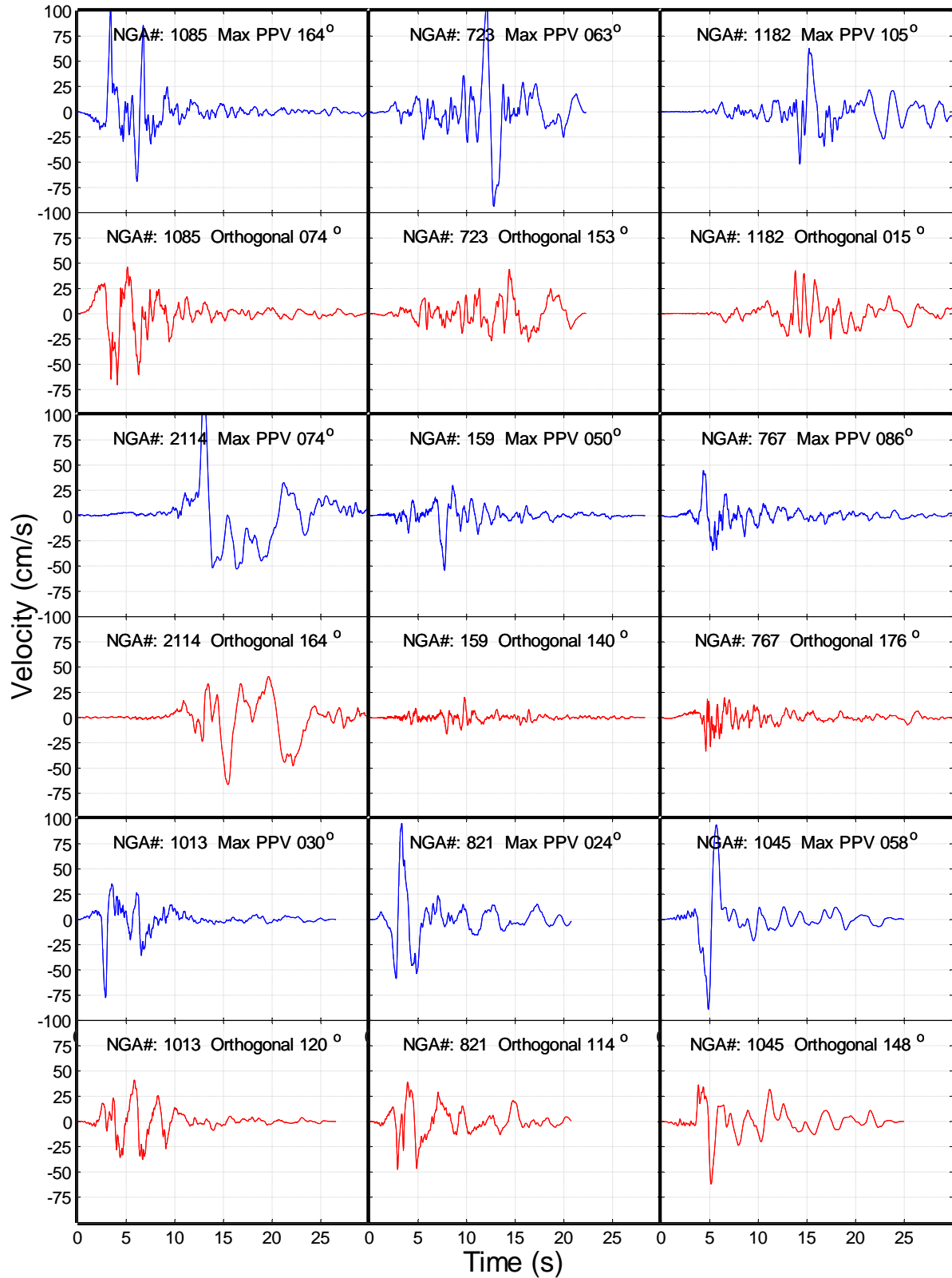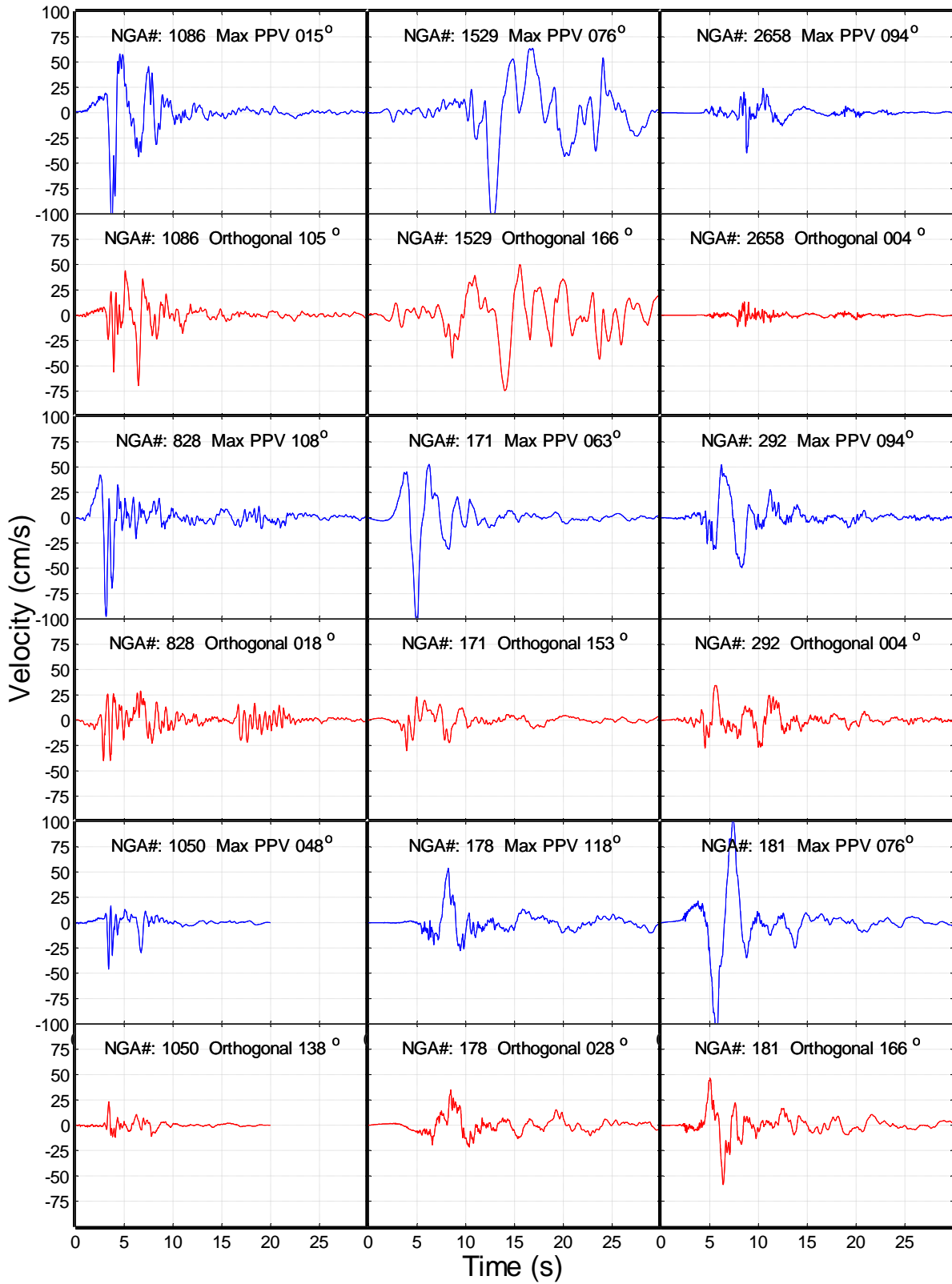
D.1   Introduction

This appendix summarizes the state of the art related to selection and scaling of ground motions for nonlinear response-history analysis of buildings in regions of low, moderate, and high seismic hazard in the United States. In addition, other relevant information, including discussions on site, basin, and basin-edge effects and role of physics-based simulations are presented.

D.2   Characteristics of Ground Motions in Active Crustal Regions

Ground motion characteristics have been most studied in detail for active crustal regions, due largely to the availability of strong-motion recordings of earthquakes in the magnitude-distance range of interest to engineers. The NGA West (Next Generation of Ground motion Attenuation Models for the Western United States) initiative has compiled and characterized ground motion records for shallow (< 25 km) crustal earthquakes in active tectonic regions (Power et al., 2008). The NGA West project compiled 3551 records from 175 shallow crustal earthquakes in active regions around the world, including California, Taiwan, Japan and Europe is available through http://peer.berkeley.edu/nga/. Figure D-1 summarizes the distribution of the records, all of which are available from the online database, by magnitude, distance and site condition. Extensive quality control of record processing, and compilation of meta-data, such as site $V_{s,30}$ and earthquake mechanism, make the NGA West dataset particularly useful.

Teams of ground motion researchers used the records in the database to develop empirical ground motion prediction equations (referred to as NGA West equations) applicable to crustal events in the Western United States (WUS) and similar regions. The NGA West equations were compared to each other by Abrahamson et al. (2008). Figure D-2 shows all ground motion prediction equations for B/C site condition ($V_{s,30}$ = 760 m/s) for 5%-damped peak spectral acceleration (PSA). The plots show the horizontal component independent of rotation angle (GMrotI), after applying corrections to B/C site conditions (based on Boore and Atkinson (2008) site terms) in comparison to the mean and standard deviation of the PSA values (on log scale) within magnitude-distance bins. The closest distance to surface projection of fault rupture, the Joyner-Boore distance, R_{jb}, is used as the distance metric, where the conversion from fault-rupture distance were made where needed using an

approximation for display purposes only, that is, $R_{rup}=R_{jb}$ for $M=7.5$; $R_{rup}=1$ at $R_{jb}=0.1$ for $M=6.5$. The relatively close agreement between the alternative equations suggests consensus on median levels of motions for magnitude-distance ranges that are well sampled in terms of available ground motion data.
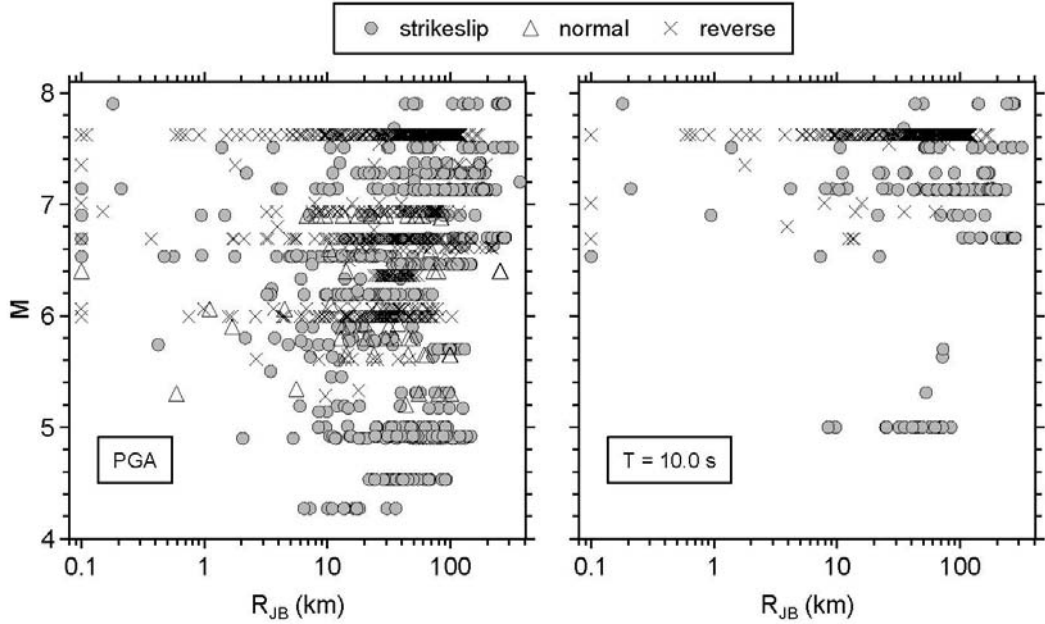
Figure D-1   Distribution of available records from the NGA West database in moment magnitude and Joyner-Boore distance for strikeslip, normal and reverse fault mechanisms (Boore and Atkinson, 2008).

The ready availability of the NGA West database and equations has simplified the ground motion selection process for crustal earthquakes in the WUS. However, there are significant gaps in the understanding of the characteristics of WUS ground motions. For example, the recorded data are relatively sparse at very close distances from the fault and for very large magnitude earthquakes. Thus it is still difficult to find suites of ground motion histories to adequately capture a range of potential near-fault effects such as directivity, differences between fault-normal and fault-parallel motions, and fling-step displacements, though progress has been made in compiling subsets of records displaying such characteristics. These effects are important for sites within a few kilometers of an active fault. There are also few records from very large earthquakes (magnitude greater than 7.5), leaving significant uncertainty in how motions scale with magnitude for earthquakes of magnitude greater than 7. The empirical data appear to suggest that motions for very large earthquakes may actually decrease at very large magnitudes, at short periods (e.g., short-period median motions for magnitude 7.5 at short distances are slightly less than median motions for magnitude 7.0 at similar distances); however the data are too sparse to draw conclusions on this point with any confidence. Thus all NGA West equations use

functional forms that would prevent such "over-saturation" of ground motions at large magnitudes (e.g., Boore and Atkinson, 2008).
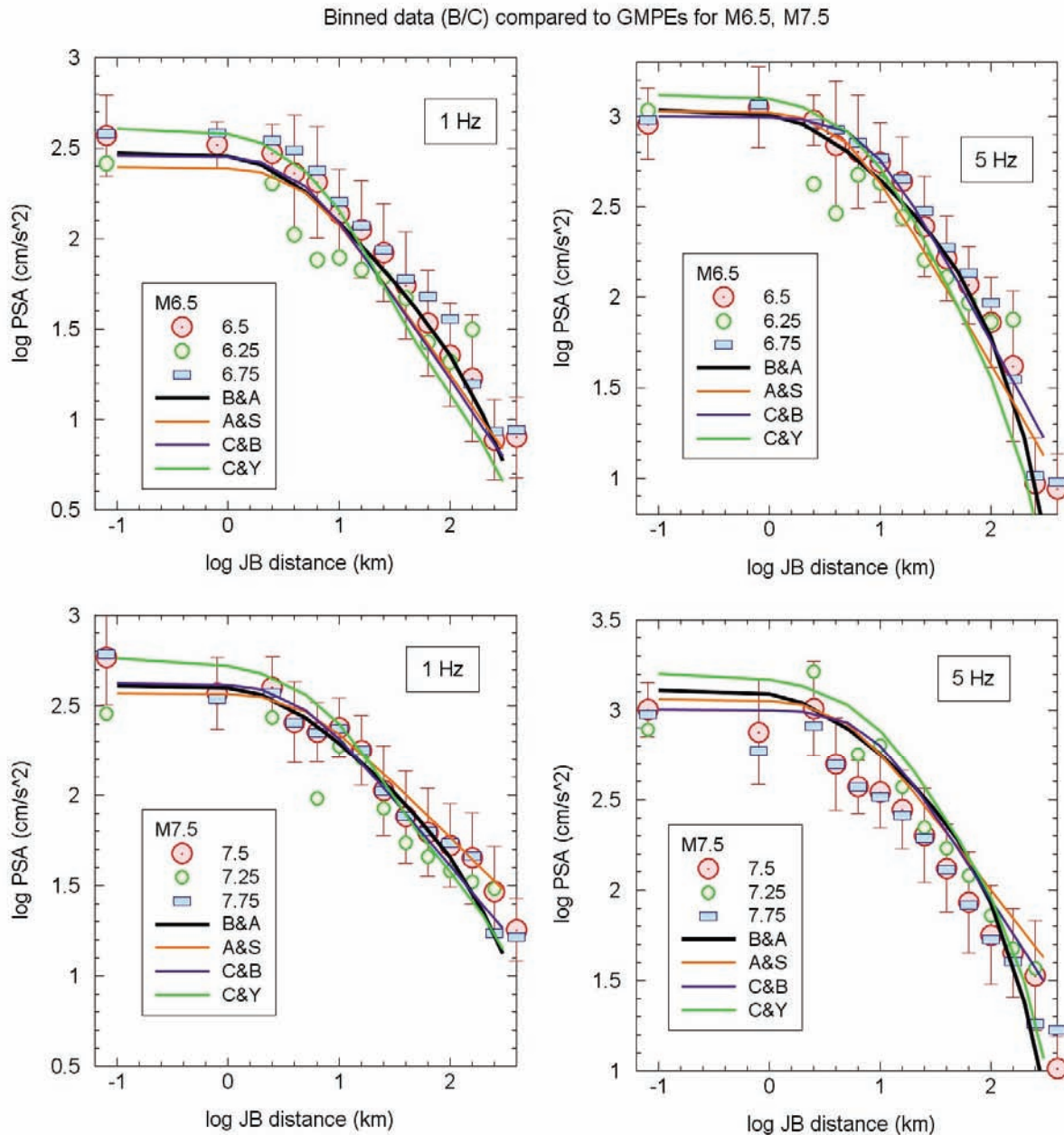
Figure D-2   Predictions of the NGA West equations compared to PSA amplitudes, averaged (geometric mean) and grouped in magnitude-distance bins with error bars showing standard deviation for $M = 7.5$ data. B&A=Boore and Atkinson; A&S=Abrahamson and Silva; C&B=Campbell and Bozorgnia; C&Y=Chiou and Youngs.

Finally, it is known that significant regional differences in ground motions may exist, even within active tectonic regions, due to differences in source processes, attenuation with distance through the regional crustal structure, and systematic

differences in site conditions (even for the same $V_{s,30}$). Yet for practical reasons, and to build a sufficiently large database, the ground motion data from shallow events in all active tectonic regions around the world were combined in the development of the NGA West database and equations. Differences between ground motion in the WUS and Taiwan or Japan for a large crustal earthquake at a given distance are not known. Thus there remain significant gaps in knowledge of ground motion characteristics, even for well-studied active crustal regions, that affect the available choices in ground motions for analysis. For sites where these gaps are important, such as close to active faults, or where the hazard is due to very large events, there may not be sufficient recorded ground motion time series to adequately represent the types of motions for design and assessment of buildings. Simulated motions are useful in these situations.

D.3   Characteristics of Ground Motions in Subduction Regions

Subduction regions face significant hazard from the potential for moderate-to-large earthquakes within the subducting slab (such as the 2000 *M*6.8 Nisqually, Washington earthquake), and for large-to-great earthquakes on the subduction interface (such as the magnitude 9 2011 Tohoku, Japan earthquake). The ground motion characteristics of these types of events in subduction environments may differ significantly from those of typical WUS crustal earthquakes. In-slab events occur at greater depths (typically 50 to 60 km in Western North America) than crustal or interface earthquakes, and have motions that are relatively high at near-source distances but attenuate relatively quickly with distance (e.g., Atkinson and Boore, 2003; Kanno et al., 2006; Zhao et al., 2006; Goda and Atkinson, 2009). Furthermore, due their deep focus, in-slab events do not appear to set up the Moho reflections and refractions and resulting surface-wave trains that can occur with continental earthquakes (Kanno et al., 2006). Focal mechanisms may also differ due to the event type; interface events are thrust mechanism events, whereas in-slab events are most often normal-fault mechanisms, but may also be thrust, and crustal events have a mixture of mechanisms.

Most studies suggest that the major ground motion differences that should be considered among event types, within subduction regions, are those that are directly related to focal depth (e.g., Kanno et al., 2006). Shallow crustal events and shallow interface events within a subduction region appear to have similar source parameters and attenuation characteristics. This observation is evidenced by the similarity of ground motion prediction equations developed for interface events, in comparison to equations developed for crustal events, over most period ranges (e.g., Si and Midoridawa, 1999; Zhao et al., 2006). By contrast, deeper in-slab events have significantly greater short-period amplitudes at near-source distances, and steeper attenuation rates (Atkinson and Boore, 2003; Kanno et al., 2006; Zhao et al., 2006; Goda and Atkinson, 2009). These differences in ground motion characteristics can

be suitably parameterized by using focal depth as a classification variable for ground motion studies, and for selection of appropriate time histories.

Interface events are unique in their potential to have very large magnitudes ($M > 8.5$), due to the large potential rupture area on the subducting interface. Great earthquakes ($M > 8$) produce strong long-period motions that are an important hazard for long-period structures such as high-rise buildings and bridges located in subduction environments such as the Pacific Northwest. The understanding of motions generated by great earthquakes is evolving rapidly, especially with the availability of high quality recordings of great subduction earthquakes in Japan, including the 2011 magnitude 9 Tohoku earthquake and its many aftershocks. These records are an excellent data source for ground motion histories for great subduction earthquakes.

In order to provide a consistent set of equations that illustrates the differences between event types, Zhao et al. (2006) compiled a large database (from Japan and other active regions) and then used a single regression analysis to distinguish the source levels and attenuation from each of the event types. Figure D-3 compares the attenuation characteristics of crustal, in-slab and interface events for an event with magnitude 7.5, based on Zhao's equation and an alternative equation for each event type (Boore and Atkinson (2008) for crustal events, Goda and Atkinson (2009) for interface events, and Atkinson and Boore (2003) for in-slab events). Note that differences between investigators in amplitude levels can be significant, due to differences in the datasets used and the regression methodology. However, the overall trends in the indicated characteristics are fairly clear: the curves for crustal and interface events are similar whereas the in-slab events have higher amplitudes at fault distances less than 100 km, but attenuate more rapidly.

When selecting ground motion records for analysis, it is prudent to choose available records for the type of events that cause the hazard. Thus in subduction regions it may be necessary to select sets of records for representative crustal, in-slab and interface events. In-slab events are distinguished by their deeper focal depths, which may influence their frequency content and attenuation. Interface events may have very large magnitudes ($M > 8$), which will result in long durations with large amplitudes at long periods; interface events will also be distinguished by their thrust focal mechanisms.

GMPEs for B/C, M=7.5
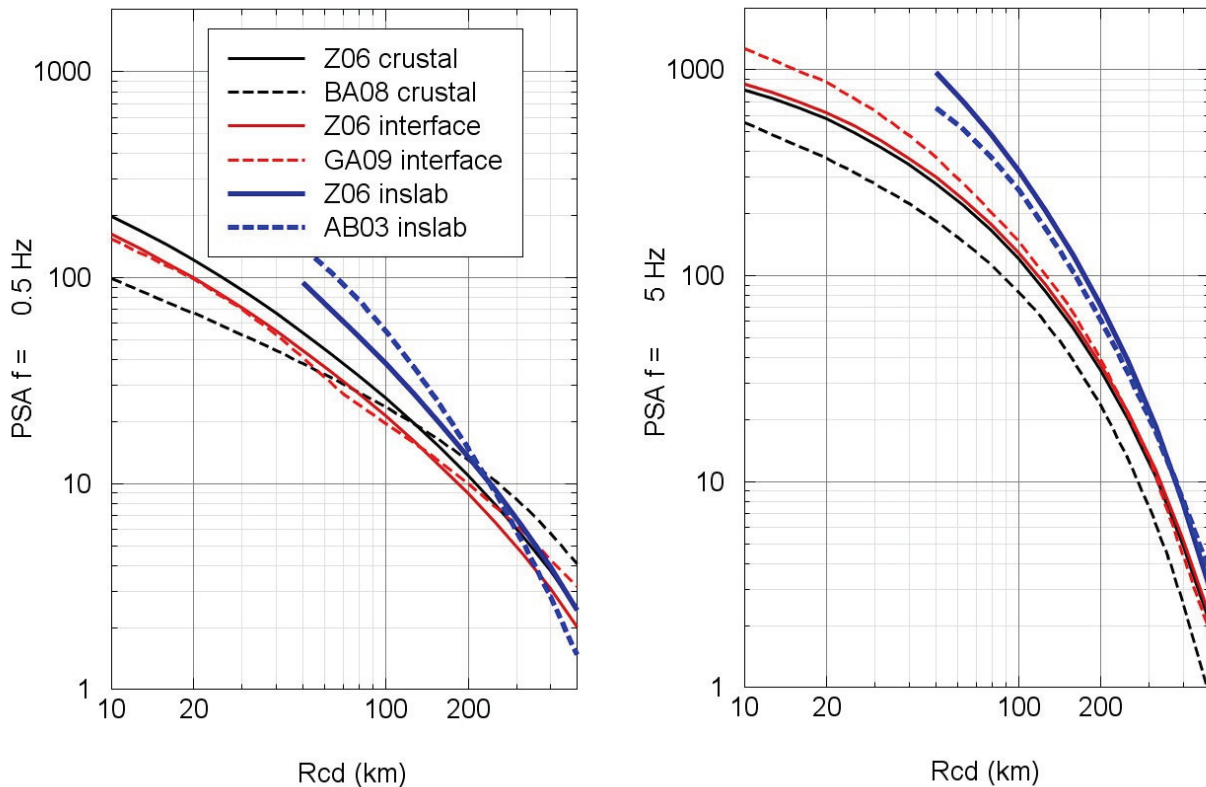
Figure D-3   Comparison of ground motion prediction equations for 5%-damped horizontal peak spectral acceleration for $V_{s,30}$~760m/s versus closest-distance to fault, for $M = 7.5$ events in subduction environments. Z06 crustal = Zhao (2006) with $h = 10$ km; Z06 interface = Zhao (2006) with $h = 20$ km; Z06 inslab = Zhao (2006) with $h = 50$ km; BA08=Boore and Atkinson (2008); GA09=Goda and Atkinson (2009); and AB03=Atkinson and Boore (2003).

D.4   Characteristics of Ground Motions in the Central and Eastern United States

Ground motions for events in the Central and Eastern United States (CEUS) and other stable continental regions are distinguished from their counterparts in the WUS by a shift towards higher frequency content. This shift is particularly prominent in the construction of the Uniform Hazard Spectrum (UHS). This arises due to the compounding of the following factors: (1) low seismicity rates in the CEUS mean that, relative to more active regions, hazard contributions at a given probability level will be coming from smaller magnitudes, and will thus not be as rich in low-frequency energy; (2) CEUS earthquakes tend to be characterized by higher stress drops, a factor of two or more higher than those of active regions (as shown in Kanamori and Anderson (1975), Atkinson and Hanks (1995), Atkinson and Boore (1997), Silva et al. (2002), Campbell (2003), and Atkinson and Wald (2007)), and will thus be rich in high-frequency energy; (3) CEUS high-frequency motions

attenuate relatively slowly due to high Q (Quality factor), and thus high-frequency hazard contributions persist to significant distance; and (4) the reference ground condition for CEUS hazard studies often corresponds to a hard-rock condition, for which high-frequency motions will not be attenuated much by near-surface site effects. The net result is that the target UHS for a CEUS site will have a shape that is shifted towards higher frequencies, relative to a typical WUS site. Ground motion time series in the CEUS must reflect this frequency content.

Relative to more active western sites, the dominant hazard contributions in the CEUS tend to come from somewhat smaller magnitudes, sometimes at slightly greater distances. The dominant magnitudes and distances will depend on the site seismicity, probability level and the frequency band of interest. As a general guide, the high-frequency hazard for CEUS sites at moderate probabilities ($> 10^{-4}$ per annum) may be dominated by events of $M \leq 6$ at distances less than 50 km, while the low-frequency hazard may be dominated by large rare events ($M \geq 7$) at moderate-to-regional distances (e.g., Petersen et al., 2008). Thus these are the types of events for which time histories are often required.

Figure D-4 compares CEUS ground motion spectra for $M5.5$ and $M7.5$ events to those for WUS for a B/C boundary site condition with $V_{s,30}$=760m/s, based on recent ground motion prediction equations. Two CEUS equations are plotted: the empirical equation of Atkinson (2008), as modified by Atkinson and Boore (2011), and a hybrid-empirical model from Pezeshk et al. (2011). The Pezeshk et al. model has been converted to equivalent values for B/C site conditions, in Joyner-Boore distance, for presentation. The WUS equation is the Boore and Atkinson (2008) equation, as modified at low magnitudes by Atkinson and Boore (2011). The figure shows the typical characteristics of eastern motions relative to their western counterparts, namely higher amplitudes at high frequencies, and slower attenuation with distance. The Pezeshk et al. equation also shows a prominent Moho bounce feature (this feature is also in Atkinson and Boore, 1995, 2006, and 2011, not plotted), wherein there is a marked slowing of attenuation in the distance range from 70 km to 130 km as direct waves are joined by post-critical reflections and refractions from the Moho (Burger et al., 1987).
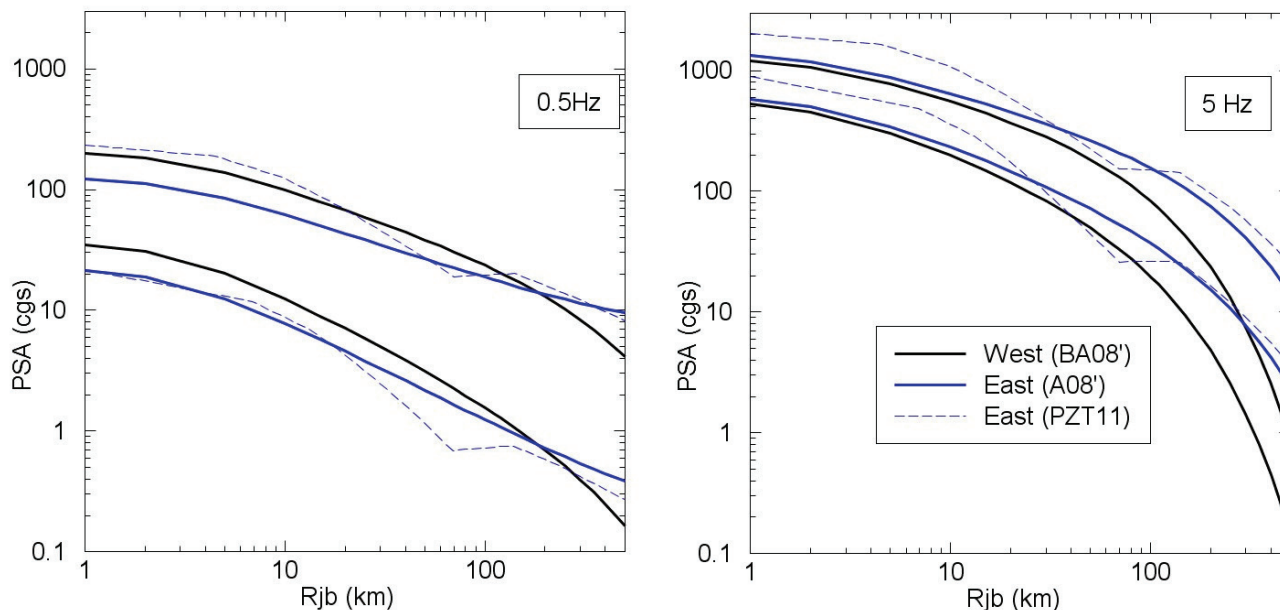
Figure D-4   Comparison of typical ground motion prediction equations for events in the CEUS (A08' from Atkinson and Boore (2011); PZT11, from Pezeshk et al. (2011)) to those for active crustal regions (BA08' from Boore and Atkinson, 2008), for $M = 5.5$ and 7.5, on B/C site conditions versus Joyner-Boore distance.

A major challenge in selecting appropriate records in the magnitude/distance range of interest for CEUS sites arises because there are relatively few records available for CEUS or analog regions, owing to low seismicity rates and sparse instrumentation in mid-plate regions. Records selected from active tectonic regions, such as California, will not have the required high-frequency content, as demonstrated in Figure D-4. This limits the options available for record selection and scaling for the CEUS, as discussed further below.

D.4.1   Linear Scaling of Recorded Motions

As noted previously, the amplitude scaling of recorded motions to match a target spectrum is a traditional approach in the WUS but requires suitable records in terms of magnitude, distance, site condition, and spectral shape. There are insufficient real records for CEUS sites in the required magnitude/distance ranges, and those from more active regions are typically not suitable in terms of site condition and spectral shape. This approach is not reasonable in the CEUS in most cases.

D.4.2   Modification of Real Records Using Spectrum Matching

Al Atik and Abrahamson (2010), Grant et al. (2011), and Hancock et al. (2006) describe the spectrum matching technique, with emphasis on the time domain

approach. Chapter 4 explores some issues associated with spectrum matching. Another technique, which has been used for nuclear power plant applications in the CEUS, involves defining the Fourier amplitude spectrum for a desired magnitude, distance and site condition based on a seismological model and combining it with the Fourier phase spectrum from a real recording (with some limits on the magnitude and distance to ensure a reasonable phase spectrum) to simulate a realistic ground motion history (USNRC, 2001).

The concept of spectrum matching is particularly attractive in the CEUS as it allows the use of real recordings from active regions, but enables the higher frequencies to be supplemented to match CEUS conditions. Since the high frequency motions are largely stochastic in nature (Hanks and McGuire, 1981; Boore, 2003), there are no fundamental problems with adding these components into the records. This procedure was followed in the NUREG/CR 6728 report (USNRC, 2001) to develop a database of CEUS ground motion records. It should be noted that an important step in the evaluation of spectrum-matched records, however obtained, is to compare the initial and resulting histories in acceleration, velocity and displacement, and to make sure that they are reasonable representations of the original time series (i.e., showing physically acceptable changes, without unintended time-domain features). This is arguably the most important step of spectrum matching.

D.4.3   Simulation of Ground Motion Histories

Simulated records are an appealing approach for the development of CEUS histories, as they enable the use of basic knowledge of CEUS source, attenuation and site characteristics to simulate ground motions with appropriate amplitudes and frequency content. There has been some traditional reluctance in the engineering community to accept the use of records that are not recorded. Simulations are a particularly attractive alternative for this region. Kinematic simulation models using the hybrid-broadband technique (e.g., Hartzell et al., 1999; Frankel, 2009; Graves and Pitarka, 2010) have been most widely used in the Western United States, but have also been applied to some applications in the CEUS, particularly in ground motion modeling exercises (Somerville et al., 1990, 2001). Stochastic simulations have also been popular for generic applications in the CEUS and for the development of ground motion prediction equations (e.g., Atkinson and Boore, 1995 and 2006; Toro et al., 1997; Silva et al., 2002; Atkinson et al., 2009; Boore, 2009). Stochastic simulations are attractive in light of the lack of constraints or knowledge of the source parameters and detailed crustal structure that form the deterministic part of the hybrid-broadband simulation models. Studies have indicated that stochastic records can capture the main inelastic response characteristics of systems, despite their simplicity (Atkinson and Goda, 2010). However, the hybrid-broadband approaches offer the opportunity to incorporate more deterministic features of the ground motion time histories, which

is valuable if these aspects can be at least partially constrained by knowledge of the expected source and path conditions.

D.5   Characteristics of Ground Motions in Near-Fault Regions, Considering Rupture Directivity and Velocity Pulses

Near-fault ground motions are different from ordinary (distant) ground motions in that they often contain strong coherent dynamic long period pulses and static ground displacements.

The dynamic motions associated with an earthquake may be dominated by a large long period pulse of motion that occurs on the horizontal component perpendicular to the strike of the fault, caused by rupture directivity effects (Somerville et al., 1997). Near-fault recordings from recent earthquakes indicate that this pulse is a narrow band pulse whose period increases with magnitude, as expected by theory (Somerville et al., 2001). This magnitude dependence of the pulse period causes the response spectrum to have a peak which has a period that increases with magnitude, such that the spectral demand for near-fault ground motions from moderate magnitude earthquakes may exceed that of larger earthquakes at intermediate periods (around 1 second).

The elastic rebound (e.g., Bolt, 1988) also generates static deformation of the ground. The static ground displacements in near-fault ground motions are caused by the relative movement of the two sides of the fault on which the earthquake occurs. The static deformation of the ground consists of a discontinuity in displacement on the fault itself, and a gradual decrease in this displacement away from the fault on either side of the fault. If there is surface faulting, the static displacements are discontinuous across the fault at the ground surface. Even if the fault does not rupture at the surface, there is static deformation of the ground surface due to subsurface faulting. Static ground displacements occur at about the same time as the large dynamic motions, indicating that the static and dynamic displacements need to be treated as coincident events.

D.5.1   Orientation of Dynamic and Static Near-Fault Ground Motions

The top panel of Figure D-5 schematically illustrates the orientations of dynamic and static near-fault ground motions (Somerville, 2002). The strike-slip case is shown in map view, where the fault defines the strike direction. The dynamic motion, rupture directivity pulse, is oriented in the strike-normal direction and the static ground displacement, fling step, is oriented parallel to the fault strike. The dip-slip case is shown in vertical cross section, where the fault defines the dip direction; the strike direction is orthogonal to the page. The rupture directivity pulse is oriented in the direction normal to the fault dip, and has components in both the vertical direction and the horizontal strike normal directions. The static ground displacement is

oriented in the direction parallel to the fault dip, and has components in both the vertical direction and the horizontal strike normal direction.
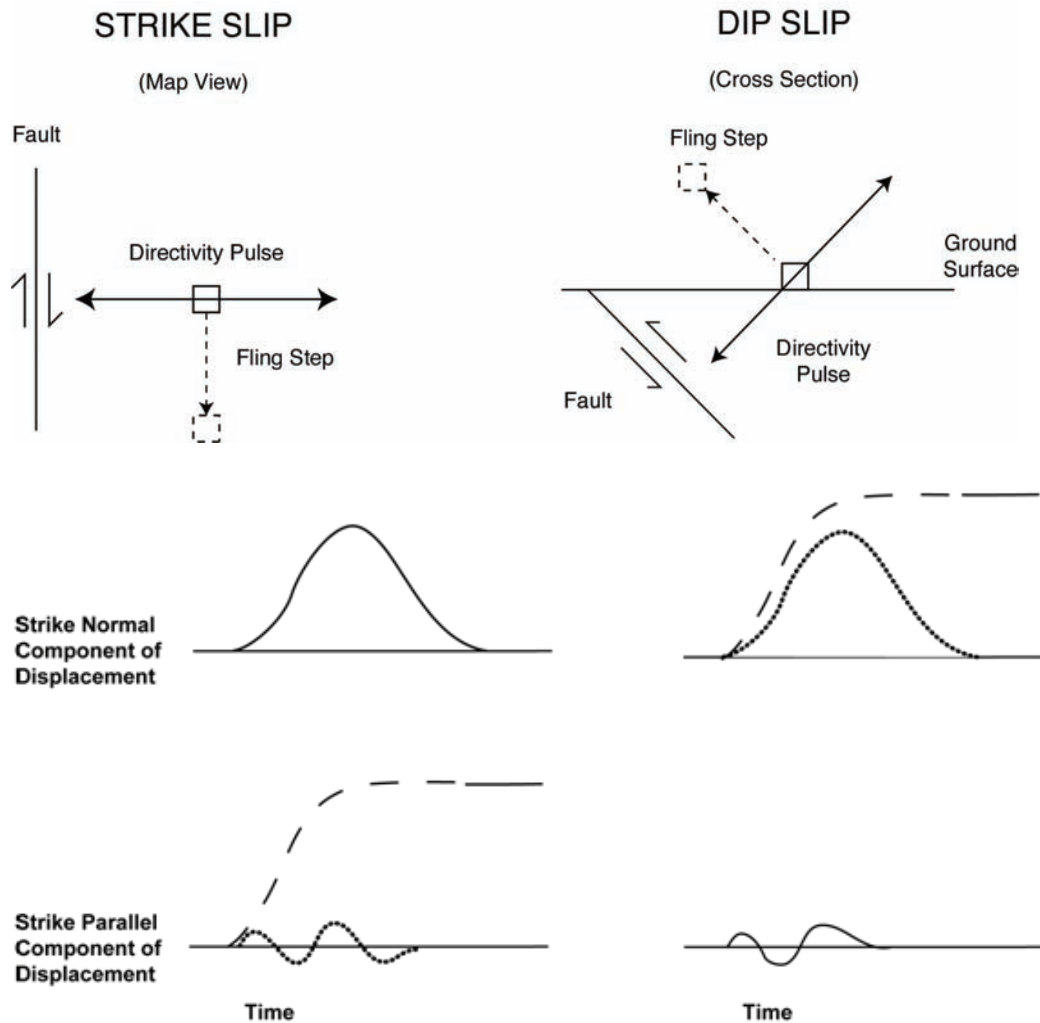
Figure D-5   Top: Schematic orientation of the rupture directivity pulse and fling step for strike-slip (left) and dip-slip (right) faulting. Bottom: Schematic partition of the rupture directivity pulse and fault displacement between strike-normal and strike-parallel components of ground displacement. Waveforms containing static ground displacement are shown as dashed lines; versions of these waveforms with the static ground displacement removed are shown as dotted lines (Somerville, 2002).

The bottom panel of Figure D-5 schematically illustrates the partition of near-fault ground motions into the dynamic ground motion, which is dominated by the rupture directivity pulse, and the static ground displacement. For a strike-slip earthquake, the rupture directivity pulse is partitioned mainly on the strike-normal component, and the static ground displacement is partitioned on the strike-parallel component. If the static ground displacement is removed from the strike-parallel component, very little dynamic motion remains. For a dip-slip earthquake, the dynamic and static displacements occur together on the strike-normal component, and there is little of

either motion on the strike-parallel component. If the static ground displacement is removed from the strike-normal component, a large directivity pulse remains.

There need not be a strong correlation between the static and dynamic components of near-fault ground motion. For example, the 1989 Loma Prieta and 1994 Northridge earthquakes both occurred on faults that did not break the ground surface, so they produced very small static ground displacements, but they did produce strong rupture directivity pulses. For this reason, the dynamic and static ground motions need to be quantified in separate hazard analyses. Once they have been separately quantified, the two components of the hazard can then be combined into a single ground motion time history that contains both dynamic and static ground displacements. The effect of the simultaneous dynamic and static ground motions on the response of a structure can be analyzed using ground motion records that include both the dynamic rupture directivity pulse and the static ground displacement.

D.5.2 Different Fault-Normal and Fault-Parallel Components of Horizontal Dynamic Motions

An earthquake is a shear dislocation that begins at a point on a fault and spreads at a velocity that is almost as large as the shear wave velocity. The propagation of fault rupture toward a site at a velocity close to the shear wave velocity causes most of the seismic energy from the rupture to arrive in a single large pulse of motion that occurs at the beginning of the record (Archuleta and Hartzell, 1981; Somerville et al., 1997). This pulse of motion represents the cumulative effect of almost all of the seismic radiation from the fault. The radiation pattern of the shear dislocation on the fault causes this large pulse of motion to be oriented in the direction perpendicular to the fault plane, causing the fault-normal component of ground motion to be larger than the fault-parallel component at periods longer than about 0.5 second. To accurately characterize near-fault ground motions at distances within about 5 km of the fault, it is therefore necessary to specify separate response spectra and ground motion histories for the fault-normal and fault-parallel components of ground motion.

Somerville et al. (1997) developed a model for the ratio of fault-normal to average horizontal motions caused by rupture directivity effects. They found that this ratio depends primarily on earthquake magnitude and rupture distance, while the dependencies on faulting mechanism and site category were not found to be practically significant. The ratio of fault-normal to average horizontal motions is found to be period-dependent, and becomes significant for periods greater than 0.6 second, indicating a transition from incoherent source radiation and wave propagation conditions at short periods to coherent source radiation and wave propagation conditions at long periods. Somerville et al. (1997) also considered the effects of angle on the polarization (strike angle θ or for strike-slip faulting or zenith-angle ϕ for dip-slip faulting), where the model provides a smooth transition from the

maximum polarization effects (at 0° angle) to the region of no polarization effects (beyond 45°). The Spudich and Chiou (2008) directivity model currently does not address differences between fault-normal and fault-parallel components.

D.5.3 Incidence of the Rupture Directivity Pulse

Forward rupture directivity effects occur when two conditions are met: the rupture front propagates toward the site, and the direction of slip on the fault is aligned with the site. The conditions for generating forward rupture directivity effects are readily met in strike-slip faulting, where the rupture propagates horizontally along strike either unilaterally or bilaterally, and the fault slip direction is oriented horizontally in the direction along the strike of the fault. However, not all near-fault locations experience forward rupture directivity effects in a given event. Backward-directivity effects, which occur when the rupture propagates away from the site, give rise to the opposite effect: long duration motions having low amplitudes at long periods.

The conditions required for forward directivity are also met in dip slip faulting. The alignment of both the rupture direction and the slip direction updip on the fault plane produces rupture directivity effects at sites located around the surface exposure of the fault (or its updip projection if it does not break the surface). Unlike the case for strike-slip faulting, where forward rupture directivity effects occur at all locations along the fault away from the hypocenter, dip slip faulting produces directivity effects on the ground surface that are most concentrated in a limited region updip from the hypocenter.

D.5.4 Duration of Near-Fault Ground Motion Histories

Directivity effects induce systematic spatial variations of duration in near-fault ground motions. In general, the ground motion record is compressed in time in the forward-directivity region, especially on the fault-normal component, while in the backward-directivity region the ground motion record is elongated in time. Engineers tend to question the brief duration of forward directivity motions in the near-fault region that are provided to them for design. This tendency should be resisted, because brief durations are a predictable feature of near-fault ground motions unless there is the potential for multiple rupture episodes on a complex fault system, or there is the potential for basin response to generate long durations.

Somerville et al. (1997) proposed an empirical model using similar directivity predictors as were used in the spectra amplitudes model. The model predicts that, at the locations where maximum directivity effects are obtained, the ground motion duration is about 0.55 times the average duration for both strike-slip and reverse faulting; whereas at locations having the minimum directivity effects, the ground motion duration is about 2.1 times the average duration for dip-slip faulting, and 1.6 times the average duration for strike-slip faulting.

D.5.5 Selection of Ground Motion Records to Represent Near-Fault Effects

In cases where the design response spectrum is derived from a scenario-based deterministic hazard analysis, the static ground displacement can be directly specified from the earthquake source model, and rupture directivity parameters can be derived from the source-site geometry and assumptions about the hypocenter location, and used in conjunction with earthquake magnitude, fault distance, and site conditions to guide the selection of suitable time histories.

In cases where the design response spectrum is derived from probabilistic seismic hazard analysis, the static ground displacement is derived from a probabilistic fault displacement hazard analysis. For the dynamic motions, the selection of suitable ground motion records is based on the disaggregation of the seismic hazard, including the directivity parameters (Table D-1 and Figure D-6) as well as earthquake magnitude, fault distance, and site conditions (Abrahamson, 2000). The disaggregation indicates the contribution that forward rupture directivity makes to the hazard, providing a basis for identifying within a suite of time histories the proportion that should have forward rupture directivity effects.

Several methods have been proposed for identifying and characterizing ground motion time histories that contain rupture directivity pulses. Baker (2007b) analyzed all records within the NGA database and identified fault-normal and fault-parallel records considered to have strong velocity pulses that may be associated with rupture directivity effects. The basic approach followed by Baker was to use wavelet analysis to identify the largest velocity pulses. General criteria that were used by Baker in defining records with pulses due to rupture directivity were: (1) the pulse is large relative to the residual features of the ground motion after the pulse is extracted; (2) the pulse arrives early in the time history, as would be expected for pulses associated with rupture directivity effects; and (3) the absolute velocity amplitudes are large (PGV of record equal to or greater than 30 cm/sec). The same criteria were used by Baker for the fault-strike-parallel component and those results as well as more detailed results and documentation of analyses for both components are contained on the following website: http://stanford.edu/~bakerjw/pulse-classification/.

Table D-1   Summary Table of Rupture Directivity Model Parameters

Parameters	Somerville et al. (1997) and Abrahamson (2000)	Spudich and Chiou (2008)
Functional Form	$f_D = C_1(T) + C_2(T) *X \cos\theta$, for strike-slip (S97) $= C_1(T) + C_2(T) *Y \cos\varphi$ for dip-slip where $C_1(T)$ and $C_2(T)$ are period-dependent constants	where $IDP = CSR_{ri}$ and $a(T)$ and $b(T)$ are period-dependent constants
	$f_D = (C_1(T) + 1.88C_2(T) *X \cos\theta) f_r(R_{rup}) f_M(M)$ for strike-slip, X is capped at 0.4 (A00)	
Magnitude Taper Function	$M = 6.5$-7.5 (S97) (A00)	
Distance Taper Function	$R_{rup} = 0$-50 km (S97) (A00)	
Style of Faulting	Strike-slip and dip-slip	Strike-slip and dip-slip
Site Classification	Any site class	Any site class
Directivity Predictor	$X \cos\theta$ or $Y \cos\varphi$	$IDP = CSR_{ri}$
Length Parameter	X or Y ($Y = d/W$, $X = d/L$)	
Angular Parameter	$\cos\theta$ or $\cos\varphi$	
Zone	Exclusion zone defined for dip-slip fault	Radiation pattern R_{ri}

M: moment magnitude
W: downdip width of rupture
L: strike length of rupture
R_{rup}: closest distance from the site to rupture plane
R_{hypo}: hypocenter distance

D: diagonal distance from hypocenter to the closet point
h: downdip distance from top of the fault to hypocenter.
d: downdip distance from hypocenter to the closet point.
s: along-strike distance from hypocenter to the closest point
θ: azimuth angle
φ: zenith angle

(a)   (b)   (c)
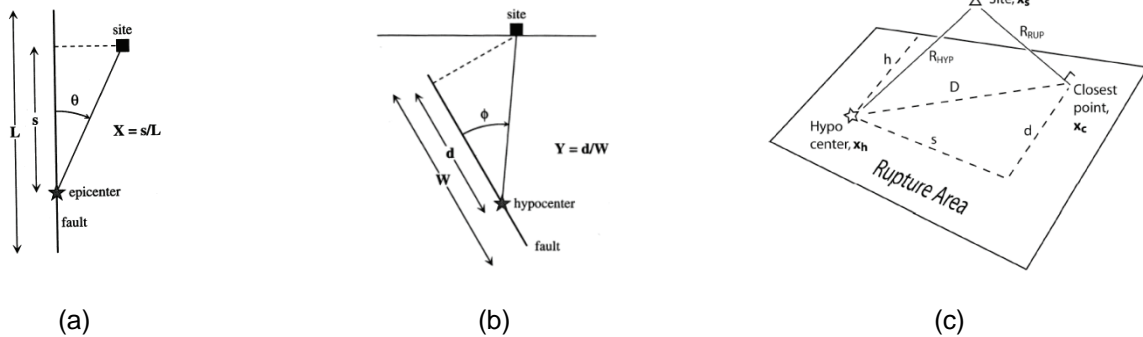
Figure D-6   Summary of rupture directivity model parameters: (a) strike-slip, plane view; (b) dip-slip, vertical view; (c) 3-D view (from U.S. Army Corps of Engineers, 2009).

Somerville et al. (2004), Mavroeidis and Papageorgiou (2003), Bray and Rodriguez-Marek (2004), and Fu and Menun (2004) also prepared lists of near-fault records considered to have directivity pulses. The focus of these researchers was on

identifying pulses on the fault-strike-normal components and only a few fault-strike-parallel pulse records were identified.

Preliminary equations relating the period of the pulse to the earthquake magnitude and the effective velocity of the pulse to the earthquake magnitude and distance have been developed by Somerville et al. (2001), Alavi and Krawinkler (2000) and Rodriguez-Marek (2000). Figure D-7 shows mean correlations of pulse period with magnitude by different investigators (Baker, 2007b; Somerville et al., 2001; Mavroeidis and Papageorgiou, 2003; Bray and Rodriguez-Marek, 2004; and Fu and Menun, 2004). For large surface faulting earthquakes (e.g., the *M*7.6 Chi-Chi earthquake), the value of the pulse period may also be affected the large permanent displacements accompanying the fault rupture and limitations of standard record processing techniques to address the effects of permanent displacements on the velocity time history of a record. At the present time, these effects are not well quantified. Although considerable differences exist between the predictions of different models, all of the correlations show a similar trend for pulse period to increase with earthquake magnitude.
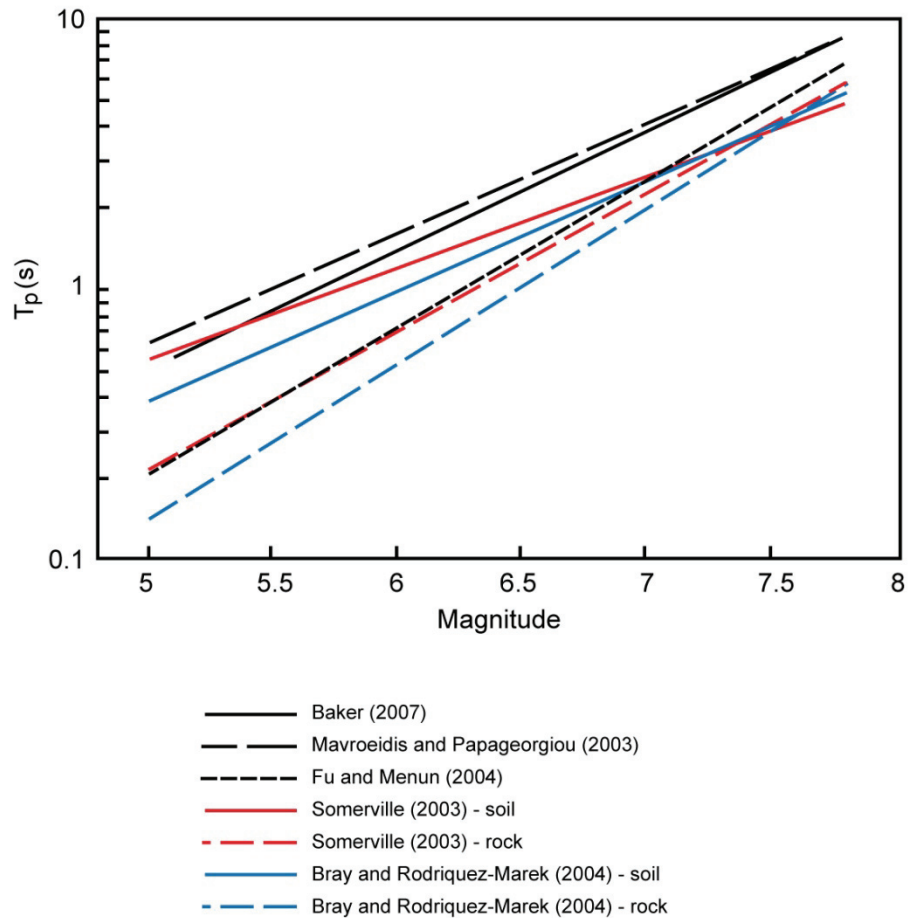
Figure D-7   Correlations of pulse period with earthquake magnitude by various researchers (from U.S. Army Corps of Engineers, 2009).

D.5.6 Archiving Strike-Normal and Strike-Parallel Components of Near-Fault Ground Motions

Figure D-5 demonstrated that near-fault ground velocities and displacements have orientations that are controlled by the geometry of the fault, specifically by the strike, dip, and rake angle (direction of slip) on the fault. Consequently, it is necessary to treat them as vector, rather than scalar, quantities. The simplest method for treating them as vector quantities is to partition them into fault-normal and fault-parallel components. The dynamic and static motions are distinctly different on these two components at all near-fault locations.

Accordingly, near-fault ground motion recordings should be archived in the strike-normal and strike-parallel components, as shown in Figure D-8a. The rotation of the two recorded components North (N) and East (E) into strike-parallel and strike-normal components, SP and SN, is accomplished using the following transformations:

$$SP = N \cos f + E \sin f$$

$$SN = -N \sin f + E \cos f$$

where f is the strike of the fault measured clockwise from North. If the recording orientation is not North and East but rotated clockwise by the angle y, then f would be reduced by y.

Distinct models for the fault-normal and fault-parallel components of near-fault ground motions, derived from appropriately archived recordings and from simulations based on seismological models, are needed for seismic hazard analysis.
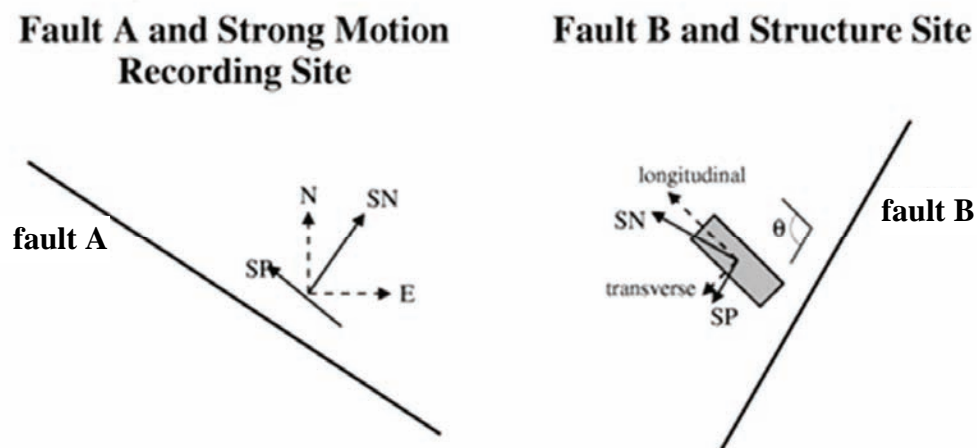
Figure D-8   Strike-normal and strike-parallel components of near-fault ground motions: (a) archiving; (b) application (from Somerville, 2002).

D.5.7 Spectrum Matching of Time Histories to Represent Near-Fault Effects

Unlike ordinary ground motions, near-fault ground motions contain coherent and orientation-dependent effects at intermediate and long period such as rupture directivity pulses and fling steps. For near-fault ground motions, different target spectra should be used for the fault-normal and fault-parallel components. Methods for preserving these features in the process of spectrum matching are being developed as described previously.

D.6   Site Effects, Basin Effects, and Basin-Edge Effects

D.6.1 Site Effects

Site effects can be incorporated in ground motion records in several ways. The simplest is to use a parameter describing the site, such as $V_{s,30}$, as a criterion for selecting recorded or simulated ground motion time histories. Site response analyses provide a means of incorporating more detailed knowledge of the site into the ground motion estimation. Site response analyses also provide a means of modeling the effect of local site conditions for cases where no generalized model exists. The nonlinear properties are often specified in the form of curves that describe the variation of soil shear modulus with shear strain (modulus reduction curves) and by curves that describe the variation of soil damping with shear strain (damping curves). Site response analysis usually involves a time history analysis of a 1-D horizontally layered soil column using nonlinear or equivalent linear methods.

Frequently used computer programs for one-dimensional analysis include the equivalent linear programs SHAKE (Schnabel et al., 1972; Idriss and Sun, 1992), WESHAKE (Sykora et al., 1992), and RASCALS (Silva and Lee, 1987) and the nonlinear programs FLAC (Itasca, 1995), DESRA-2 (Lee and Finn, 1978), MARDES (Chang et al., 1991), SUMDES (Li et al., 1992), D-MOD2 (Matasovic, 2006), DEEPSOIL (Hashash and Park, 2001), TESS (Pyke, 2000), and OpenSees (Yang, 2000; Yang et al., 2003; Mazzoni et al., 2006). If the soil response is highly nonlinear (e.g., high acceleration levels and soft soils), nonlinear programs may be preferable to equivalent linear programs. For analysis of liquefaction effects on site response, computer programs incorporating pore water pressure development, such as DESRA-2, SUMDES, D-MOD2, TESS, DEEPSOIL, and OpenSees, should be used. The output of the analysis is a time history of surface motion.

Two- or three-dimensional models are used in cases where more complex wave propagation effects could be significant, such as sites with highly irregular surface or bedrock topography, high lateral variability in soil conditions, or sedimentary basins (discussed in the following section). In either case, time histories generated in the

analysis are available for use as ground motion histories for the analysis of the structure.

D.6.2 Basin Effects

The site response analyses described above are usually based on horizontally layered models and are focused mainly on the vertical propagation of shear waves. However, irregularities in near surface geology may be better represented by 2-D or 3-D models in which the interaction of body waves with the dipping structure causes the generation and lateral propagation of surface waves (Figure D-9). This effect may be important in sedimentary basins, which consist of alluvial deposits and sedimentary rocks that are geologically younger and have lower seismic wave velocities than the underlying rocks upon which they have been deposited. Basins may be hundred meters to over ten kilometers thick. Ground motions recorded in sedimentary basins are typically stronger at intermediate and long periods than those recorded on comparable surface materials outside basins, and their durations are typically longer. This is significant for seismic hazard evaluation because many urban regions are situated on deep sediment-filled basins.

Conventional criteria for characterizing site response are typically based on the distribution of shear wave velocity with depth in the layer as determined from field measurements. The response of the layer is usually modeled assuming horizontal layering, as illustrated on the left side of Figure D-9. The wave that enters the layer may resonate in the layer but cannot become trapped within the layer. However, in a sedimentary basin with edges, waves can be trapped within the basin. If the wave is propagating in the direction in which the basin is thickening and enters the basin through its edge, it can become trapped within the basin if post-critical incidence angles develop. The resulting total internal reflection at the base of the layer is illustrated at the top right of Figure D-9.

In the lower part of Figure D-9, simple calculations of the basin response are compared with those for the simple horizontal layered model. In each case, a plane wave is incident at an inclined angle from below. The left side of the figure shows the amplification due to impedance contrast effects that occurs on a flat soil layer overlying rock (bottom) relative to the rock response (top). A similar amplification effect is shown for the basin case on the right side of the figure. However, in addition to this amplification, the body wave entering the edge of the basin becomes trapped, generating a surface wave that propagates across the basin. Some of the NGA ground motion models distinguish between sites located on shallow alluvium and those in deep sedimentary basins.

Alternative basin response analysis methods include finite difference (e.g., Graves, 1996), finite element (e.g., Bielak et al., 2003; Yoshimura et al., 2003), and spectral element (e.g., Komatitsch et al., 2004).
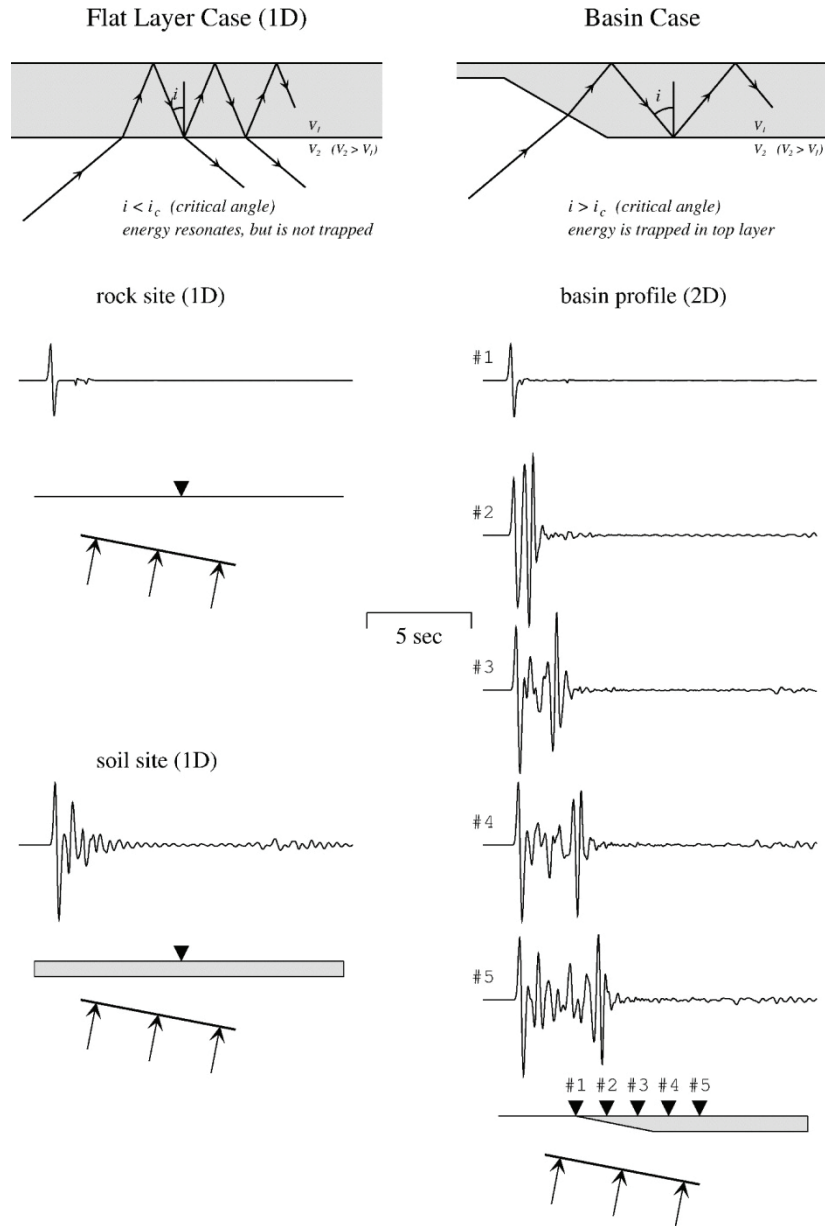
Figure D-9   Schematic diagram showing seismic waves entering a sedimentary layer from below (from Graves, 1993).

The influence of basin response on ground motions at a site is dependent on the location of the earthquake source with respect to the site, and the 3-D geometry of the basin. Broadband ground motion simulations are required to accurately estimate the effect of the basin structure on ground motions at the site. Adjustment factors for basin response were developed through large-scale simulations of basin response in

the Los Angeles region (Day et al., 2008) as part of the NGA West project. These adjustment factors take account of the depth of the basin beneath the site, but do not take account of the specific location of the earthquake source with respect to the site, and the 3-D geometry of the basin. The simulations used in the Day et al. (2008) study were shown to provide reliable estimates of basin ground motions at periods longer than about 2 seconds. At shorter periods, the effect of laterally varying the structure is more stochastic in nature and may not be amenable to estimation using simulation methods unless very detailed information is available about the geological structure at the site.

Realistic simulations in basin response can only be made for basins whose seismic shear wave velocity structure is fairly well known. To date, the most detailed models have been developed for the Los Angeles region (Magistrale et al., 2000). Preliminary models are also available for the San Francisco Bay region (Brocher, 2005), the Puget Trough region (Frankel and Stephenson, 2000; Brocher et al., 2001), and the Portland and Tualatin basins. As part of the PEER Tall Buildings Initiative, ground motion simulations in San Francisco were generated for large scenario earthquakes on the San Andreas and Hayward faults, and in Los Angeles for large scenario earthquakes on the Puente Hills blind thrust fault.

Joyner (2000) developed a model for predicting the amplitudes of basin waves in which there is a dependence on basin depth and distance to the basin edge. Although Somerville et al. (2004) analyzed data from a larger number of basins and found that amplitudes do not have a systematic dependence on distance to the basin edge or the depth of the basin, it seems likely that these parameters nevertheless could influence the waveforms of basin waves. Somerville et al. (2004) found a number of additional features that can influence the ground motion amplitudes, including the depth of the earthquake and the distance of the earthquake from the basin edge. These effects are likely to depend on the location of the earthquake and of the site within the basin, as well as on the basin depth and the distance of the site from the basin edge.

These results indicate the difficulty of identifying simple rules for the selection of ground motions time histories to represent basin effects. In cases where the design ground motions are based on a deterministic earthquake scenario, or where the probabilistic hazard is dominated by a single earthquake source, it may be possible to find ground motion recordings or simulations that contain analogous geometrical conditions such as source location with respect to the basin, location of the site within the basin (including distance from the basin edge), and basin depth.

D.6.3 Basin-Edge Effects

The 1994 Northridge and 1995 Kobe earthquakes showed a basin-edge effect in which large ground motions are generated near the edge of basin having a sharp edge

caused by a basin bounding fault. For example, the largest ground motions in the Los Angeles basin during the Northridge earthquake were recorded just south of the Santa Monica fault. In this region, the basin-edge geology is controlled by the active strand of the westward striking Santa Monica fault. Despite having similar surface geology, sites to the north of the fault (that are closest to the earthquake source) had relatively low amplitudes, whereas more distant sites to the south of the fault had significantly larger amplitudes, with a clear and immediate increase in amplification occurring at the fault scarp. The same pattern was dramatically reflected in the damage distribution indicated by red-tagged buildings, which had a large concentration of damage immediately south of the fault scarp in Santa Monica. The strong correlation of ground motion amplification pattern with the fault location suggests that the underlying basin-edge geology is controlling the ground motion response, and this was confirmed in the 2-D synthetic seismograms (Graves et al., 1998). The large amplification results from constructive interference of direct waves with the basin-edge generated surface waves.

The 1995 Kobe earthquake provided further evidence from recorded strong motion data, supported by wave propagation modeling using basin-edge structures (Pitarka et al., 1998) that ground motions may be particularly large at the edges of fault-controlled basins. Severe damage to buildings due to the Kobe earthquake was observed in a zone about 30 km long and 1 km wide, and offset about 1 km southeast of the fault on which the earthquake occurred. The near-fault ground motions generated by rupture directivity effects in the Kobe earthquake were further amplified by the basin-edge effect. This effect was caused by the constructive interference between direct seismic waves that propagated vertically upward through the basin sediments from below, and seismic waves that diffracted at the basin edge and proceeded laterally into the basin (Pitarka et al., 1998). The basin-edge effect caused a concentration of damage in a narrow zone running parallel to the faults through Kobe and adjacent cities.

In both the Santa Monica and Kobe cases, the basin-edge effect is caused by an abrupt lateral contrast in shear wave velocity caused by faulting. Basin edges that have smooth concave bedrock profiles (such as those not controlled by faulting) are not expected to cause basin-edge effects. Thus we expect that basin-edge effects are not a general feature of basins, but instead are confined to particular kinds of basin edges, especially those controlled by faults. The basin-edge effect is concentrated in a narrow zone extending parallel to the fault on the basin side of the fault. Time histories containing basin-edge effects can be selected from the recordings in basin-edge zone in Santa Monica from the Northridge earthquake and from the Kobe basin-edge zone from the Kobe earthquake.

D.7 Role of Physics-Based Simulations

Comprehensive physics-based ground motion simulation involves simulation of ground motions at a site by modeling the earthquake rupture process on a fault, seismic wave propagation through the earth's crust, and site response (Figure D-10). In some cases, the simulation may be limited to the analysis of the response of a sedimentary basin or the response of a soil column, using input ground motion time histories derived from some other source, such as strong motion recordings. The use of physics-based ground motion simulations is motivated by several considerations.

D.7.1 Lack of Suitable Ground Motion Recordings

At the return periods applicable to seismic building codes, the earthquake shaking hazard in most regions of the United States is associated with larger earthquake magnitudes and closer distances than are available in databases of strong motion recordings. This is particularly true in the Central and Eastern United States, where strong motion recordings are too sparse to provide a basis for developing reliable ground motion prediction equations. Consequently, the development of ground motion prediction equations in the CEUS is based mainly on physics-based ground motion simulations, and it is therefore preferable to use such time histories to represent the seismic hazard estimated from such equations.
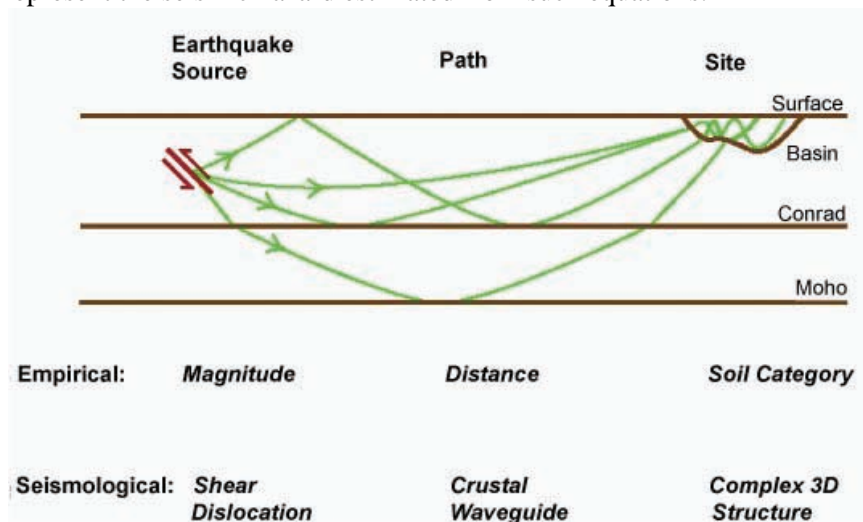
Figure D-10   Schematic diagram of empirical and seismological models of earthquake ground motions (from U.S. Army Corps of Engineers, 2009).

Even in tectonically active regions of the United States, the ground motions that dominate seismic design are from larger earthquake magnitudes than are abundant in the strong motion database. The Pump Station 10 recording of the 2000 Denali, Alaska earthquake is still the only near-fault recording of a magnitude 8 strike-slip earthquake anywhere in the world, yet the seismic hazard in many urban regions in California is dominated by such events. For regions where the hazard is dominated

by thrust earthquakes having magnitudes as large as 7.5, the database consists mainly of recordings from overseas earthquakes such as the 1999 magnitude 7.6 Chi-Chi, Taiwan event, which was associated with large surface faulting with weak short period ground motions and weak rupture directivity effects. These recordings may not provide an optimal representation of events such as a blind thrust earthquake on the Puente Hills Blind Thrust beneath downtown Los Angeles, with its potential for much stronger short-period ground motions and rupture directivity effects.

D.7.2 Intrinsic Advantages of Physics-Based Ground Motion Simulations

As shown previously, the earthquake source is a complex rupture process on a fault. Seismic waves arrive at the site by propagation through a complex waveguide, and complex local geology can have an important influence on the recorded ground motions. Strong motion simulation methods have the advantage of allowing the incorporation of information about earthquake source, seismic wave propagation, and local site characteristics that are specific to the region and to the site in question. These characteristics may include rupture directivity effects, hanging wall/foot wall effects, Moho bounce effects, basin effects, and site effects. Unless strong motion recordings happen to be available at the site, this simulation approach has the potential to generate more accurate representations of the ground motions at the site than are available using ground motion recordings. However, this is contingent upon the use of simulation methods that have the capability to accurately reproduce the characteristics of recorded ground motions in cases where the earthquake source and seismic velocity structure (and hence wave propagation characteristics) are well known, and upon the availability of reliable information about earthquake source and crustal structure characteristics in the site region.

D.7.3 Strong Ground Motion Simulation Methods

The simplest method of strong ground motion simulation is the stochastic method (e.g., Silva et al., 2002; Atkinson et al., 2009; Boore, 2009). In this method, a Fourier spectral model of the ground motion is constructed, starting with a model of the source spectrum. The shape of this spectrum is then modified using factors to represent wave propagation and site effects. The time history is derived by assuming random phase, and distributing the spectral content over a specified duration of motion. The stochastic method is most appropriate at short periods where ground motions display stochastic characteristics. It can model the elastic response spectrum and simple nonlinear response parameters as accurately as more complex models, over a wide period range (e.g., Atkinson et al., 2011). However, the stochastic method does not reliably represent near-fault effects including rupture directivity pulse and the fling step, because it does not have a rigorous basis in theoretical and computational seismology.

The hybrid Green's function method (e.g., Hartzell et al., 1999; Graves and Pitarka, 2010) provides this basis by combining the stochastic method at short periods with a rigorous synthetic seismogram method at intermediate and long periods. The hybrid method uses the elastodynamic representation theorem, which states that the ground motion U(t) can be calculated from the convolution of the slip time function D(t) on the fault with the Green's function G(t) for the appropriate distance and depth, integrated over the fault rupture surface:

$$U(t) = \sum D(t) \times G(t)$$

The earthquake source is represented as a shear dislocation on an extended fault plane. The radiation pattern of the source, and its tendency to become subdued at periods shorter than about 0.5 s, are accurately represented. Wave propagation is represented by Green's functions computed for the seismic velocity structure that contains the fault and the site. These Green's functions contain both body waves and surface waves.

To simulate broadband ground motion histories, the ground motions are computed separately in the short period and long period ranges, and then combined into a single broadband time history (Hartzell et al., 1999). At frequencies below 1 Hz, the methodology is deterministic and contains a theoretically rigorous representation of fault rupture and wave propagation effects that can reproduce recorded ground motion waveforms and amplitudes. At frequencies above 1 Hz, it uses a stochastic representation of source radiation, which is combined with a simplified theoretical representation of wave propagation and scattering effects. The use of different simulation approaches for the different frequency bands is in accord with the seismological observation that source radiation and wave propagation effects tend to become stochastic at frequencies of about 1 Hz and higher.

The hybrid Green's function method has several distinct advantages over the stochastic method at long periods. For example, by using scaling relations for source parameters in conjunction with the elastodynamic representation theorem, it is possible to construct ground motion time histories without resorting to a priori assumptions about the shape of the source spectrum. The Green's functions that are used in this procedure can be calculated from known crustal structure models, and incorporate the effects of crustal structure such as Moho reflections on the attenuation of strong ground motions (Burger et al., 1987). This enables the use of the procedure in regions where recorded ground motion data are sparse or absent. However, the hybrid Green's function method requires the specification of more source and wave propagation parameters than does the stochastic method. If the appropriate parameters are unknown for the site of interest, the potential advantages of the hybrid method to generate more realistic time histories than the stochastic method may not be realizable.

D.7.4 Sources of Simulated Strong Ground Motions

Ground motion simulations containing near-fault rupture directivity effects in the San Francisco Bay region were generated for large scenario earthquakes on the San Andreas and Hayward faults as part of the PEER Tall Buildings Initiative (Graves and Somerville, 2010). In the same program, ground motions containing both rupture directivity effects and basin effects in the Los Angeles region were generated for large scenario earthquakes on the Puente Hills Blind Thrust beneath downtown Los Angeles. Graves et al. (2008) generated ground motion histories containing both rupture directivity effects and basin effects throughout Southern California for large scenario earthquakes on the southern San Andreas Fault as part of the ShakeOut exercise. Simulations of ground motion time histories of the 1994 Northridge earthquake and of larger scenario earthquakes were generated in the SAC 95-03 Report (SAC, 1995).

The USGS has implemented a software feature on its national ground motion mapping website, http://earthquake.usgs.gov/research/hazmaps/, that enables a user of the website to request simulated ground motion histories corresponding to the predominant earthquake source contributors to seismic ground motion hazard at any specific site location in the United States. The dominant contributors are determined through the interactive hazard deaggregation feature on the website. The histories are simulated on-demand using a stochastic point-source simulation method as described on the USGS website.

These ground motion histories are generated using the simplified stochastic procedure and contain realistic representations of short period motions, but they do not contain realistic representations of earthquake source and wave propagation effects, such as near-fault rupture directivity effects, that are contained in more physics-based ground motion simulations. Large suites of ground motion histories were generated for the Central and Eastern United States using more physics-based simulation procedures by Somerville et al. (2001) in the course of generating a ground motion prediction model for those regions.

Glossary

Disaggregation: The decomposition of the seismic hazard at a given site and period into the magnitude/distance pair that is the greatest contributor to the hazard.

Drift hazard curve: A plot of mean annual frequency of exceedance of story drift versus story drift.

Extracted pulse: A velocity pulse (see below) that is extracted by quantitative or qualitative means from the velocity time series of a recorded ground motion.

Fragility function: A plot of probability of exceedance of a damage state (e.g., collapse) versus a demand parameter (e.g., maximum story drift).

Geometric mean spectral acceleration: The square root of the product of horizontal spectral accelerations on orthogonal axes, calculated period by period.

Ground motion hazard curve: A plot of mean annual frequency of exceedance of a spectral quantity (e.g., spectral acceleration at a period, T) versus the spectral quantity.

Ground motion prediction equation: An equation that estimates the distribution of a spectral quantity (e.g., geometric mean spectral acceleration) for a user-specified combination of relevant parameters (e.g., earthquake magnitude, site-to-source distance). Also known as attenuation functions. The equations are based typically on regression analysis of a large set of recorded ground motion data.

Ground motion scaling: Increasing or decreasing the amplitude of earthquake ground motion(s) to match a target spectrum (or spectra).

Intensity-based assessment: The performance of a building for a given intensity of ground motion, where the intensity is defined by a target spectral value at a period or a target spectrum (or spectra).

Maximum direction spectral acceleration: The response spectrum along the strongest axis of shaking.

Mean: For a dataset (e.g., peak story drifts for a specified intensity of shaking), the arithmetic mean is the sum of the values (story drifts) divided by the number of values.

Median: For a dataset, the median is the numerical value separating the higher half of a sample from the lower half and can be computed by arranging the values in the dataset from lowest to highest and selecting the middle value.

Residual story drift (floor displacement): Permanent story drift (floor displacement) after an earthquake.

Response history: The history or time-series of response of a component, floor, story, or building. (Also termed time history in the literature.)

Seed motion: One, two, or three orthogonal recorded components of ground motion to be amplitude scaled and/or modified to match of be consistent with a target spectrum (target spectra).

Spectrum matching: The amplitude scaling and/or frequency modification of a seed ground motion to match a target spectrum over a user-specified period range.

Standard deviation: A measure of the variability in a dataset.

Time-based assessment: The performance of a building over a specified time interval. Performance can be measured in terms of a number of parameters, such as repair cost, business interruption, or casualties.

Velocity pulse: A single-sided or doubled-sided sinusoid in the velocity history of a recorded ground motion. Velocity pulses are a characteristic of some near-fault ground motions.

References

AASHTO, 2010a, *Guide Specifications for Seismic Isolation Design, 3rd Edition,* American Association of State Highway and Transportation Officials, Washington, D.C.

AASHTO, 2010b, *LRFD Bridge Design Specifications*, American Association of State Highway and Transportation Officials, Washington, D.C.

Abrahamson, N.A., 1992, "Non-stationary spectral matching," *Seismological Research Letters*, Vol. 63, No. 1, pp. 30.

Abrahamson, N.A., 2000, "Effects of rupture directivity on probabilistic seismic hazard analysis," *Sixth International Conference on Seismic Zonation*, , Earthquake Engineering Research Institute, Oakland, California.

Abrahamson, N.A. and Al Atik, L., 2010, "Scenario spectra for design ground motions and risk calculation," *Proceedings*, 9th US National and 10th Canadian Conference on Earthquake Engineering, Toronto, Canada.

Abrahamson, N., Atkinson, G., Boore, D., Bozorgnia, Y., Campbell, K., Chiou, B., Idriss, I., Silva, W., and Youngs, R., 2008, "Comparison of the NGA ground-motion relations," *Earthquake Spectra*, Vol. 24, pp. 45-66.

Abrahamson, N.A. and Silva, W.J., 2008, "Summary of the Abrahamson & Silva NGA ground-motion relations," *Earthquake Spectra*, Vol. 24, No. 1, pp. 67-97.

Abrahamson, N.A. and Yunatci, A.A., 2010, "Ground motion occurrence rates for scenario spectra," *Proceedings*, Fifth International Conference on Recent Advances in Geotechnical Earthquake Engineering and Soil Dynamics, San Diego, California, Paper No. 3.18.

ACI, 2002, *Building Code Requirements for Structural Concrete*, ACI 318-02, American Concrete Institute, Farmington Hills, Michigan.

ACI, 2006, *Code Requirements for Nuclear Safety-Related Concrete Structures and Commentary*, ACI 349-06, American Concrete Institute, Farmington Hills, Michigan.

Akkar, S., Yazgan, U., and Gülkan, P., 2005, "Drift estimates in frame buildings subjected to near-fault ground motions," *Journal of Structural Engineering*, Vol. 131, No. 7, pp. 1014-1024.

Al Atik, L. and Abrahamson, N., 2010, "An improved method for nonstationary spectral matching," *Earthquake Spectra*, Vol. 26, No. 3, pp. 601-617.

Alavi, B. and Krawinkler, H., 2000, "Design considerations for near-fault ground motions," *U.S-Japan Workshop on the Effects of Near-Fault Earthquake Shaking*, PEER Report 2000/02, Pacific Earthquake Engineering Research Center, University of California, Berkeley, California.

Anderson, J.G., 2004, "Quantitative measure of the goodness-of-fit of synthetic seismograms," *Proceedings*, 13th World Conference on Earthquake Engineering, Vancouver, Canada.

API, 2008, *Welded Tanks for Oil Storage*, 11th Edition, includes Addendum 1, API Std 650, American Petroleum Institute, Washington, D.C.

Archuleta, R.J. and Hartzell, S.H., 1981, "Effects of fault finiteness on near-source ground motion," *Bulletin of the Seismological Society of America*, Vol. 71, pp. 939-957.

Arias, A., 1970, "A measure of earthquake intensity," *Seismic Design for Nuclear Power Plants*, editor: R. J. Hansen, Cambridge, Massachusetts, pp. 438-483.

ASCE, 2000, *Seismic Analysis of Safety-Related Nuclear Structures and Commentary,* ASCE 4-98, American Society of Civil Engineers, Reston, Virginia.

ASCE, 2002, *Minimum Design Loads for Buildings and Other Structures,* ASCE/SEI 7-02, American Society of Civil Engineers, Reston, Virginia.

ASCE, 2005, *Seismic Design Criteria for Structures, Systems, and Components in Nuclear Facilities,* ASCE/SEI 43-05, American Society of Civil Engineers, Reston, Virginia.

ASCE, 2006, *Minimum Design Loads for Buildings and Other Structures,* ASCE/SEI 7-05, American Society of Civil Engineers, Reston, Virginia.

ASCE, 2007, *Seismic Rehabilitation of Existing Buildings*, ASCE/SEI 41-06, American Society of Civil Engineers, Reston, Virginia.

ASCE, 2010, *Minimum Design Loads for Buildings and Other Structures,* ASCE/SEI 7-10, American Society of Civil Engineers, Reston, Virginia.

ATC, 1995, *Structural Response Modification Factors*, ATC-19 Report, Applied Technology Council, Redwood City, California.

ATC, 2003, *The Missing Piece: Improving Seismic Design and Construction Practices*, ATC-57 Report, Applied Technology Council, Redwood City, California.

ATC, 2011, *Seismic Performance Assessment of Buildings, 90% Draft*, ATC-58-1, Applied Technology Council, Redwood City, California.

Atkinson, G., 2008, "Ground-motion prediction equations for Eastern North America from a referenced empirical approach: implications for epistemic uncertainty," *Bulletin of the Seismological Society of America*, Vol. 98, No. 3, pp. 1304-1318.

Atkinson, G., Assatourians, K., Boore, D., Campbell, K., and Motazedian, D., 2009, "A guide to differences between stochastic point-source and stochastic finite-fault simulations," *Bulletin of the Seismological Society of America*, Vol. 99, pp. 3192-3201.

Atkinson, G. and Boore, D., 1995, "New ground motion relations for eastern North America," *Bulletin of the Seismological Society of America*, Vol. 85, pp. 17-30.

Atkinson, G. and Boore, D., 1997, "Some comparisons of recent ground motion relations," *Seismological Research Letters*, Vol. 68, pp. 24-40.

Atkinson, G. and Boore, D., 2003, "Empirical ground-motion relations for subduction zone earthquakes and their application to Cascadia and other regions," *Bulletin of the Seismological Society of America*, Vol. 93, pp. 1703-1729.

Atkinson, G. and Boore, D., 2006. "Ground motion prediction equations for earthquakes in eastern North America," *Bulletin of the Seismological Society of America*, Vol. 96, pp. 2181-2205.

Atkinson, G. and Boore, D., 2011, "Modifications to existing ground-motion prediction equations in light of new data," *Bulletin of the Seismological Society of America*, Vol. 101, pp. 1121-1135.

Atkinson, G. and Goda, K., 2010, "Ineastic seismic demand of real versus simulated ground-motion records for Cascadia subduction earthquakes," *Bulletin of the Seismological Society of America*, Vol. 100, pp. 102-115.

Atkinson, G., Goda, K., and Assatourians, K., 2011, "Comparison of nonlinear structural responses for accelerograms simulated from the stochastic finite-fault approach versus the hybrid broadband approach," *Bulletin of the Seismological Society of America*, Vol. 101, No. 6, pp. 2967-2980.

Atkinson, G. and Hanks, T., 1995, "A high-frequency magnitude scale," *Bulletin of the Seismological Society of America*, Vol. 85, pp. 825-833.

Atkinson, G. and Wald, D., 2007, "Modified Mercalli Intensity: A surprisingly good measure of ground motion," *Seismological Research Letters*, Vol. 78, pp. 362-368.

Baker, J.W., 2007a, "Measuring bias in structural response caused by ground motion scaling," *Proceedings*, *8th Pacific Conference on Earthquake Engineering*, Nangyang Technological University, Singapore.

Baker, J.W., 2007b, "Quantitative classification of near-fault ground motions using wavelet analysis," *Bulletin of the Seismological Society of America*, Vol. 97, No. 5, pp. 1486-1501.

Baker, J.W., 2011, "The Conditional Mean Spectrum: a tool for ground motion selection," *Journal of Structural Engineering*, Vol. 137, No. 3, pp. 322-331.

Baker, J.W. and Cornell, C.A., 2006a, "Correlation of response spectral values for multicomponent ground motions," *Bulletin of the Seismological Society of America*, Vol. 96, No. 1, pp. 215-227.

Baker, J.W. and Cornell, C.A., 2006b, "Spectral shape, epsilon and record selection," *Earthquake Engineering & Structural Dynamics*, Vol. 35, No. 9, pp. 1077-1095.

Baker, J.W. and Jayaram, N., 2008, "Correlation of spectral acceleration values from NGA ground motions models," *Earthquake Spectra*, Vol. 24, No. 1, pp. 299-317.

Bazzurro, P. and Luco, N., 2006, "Do scaled and spectrum-matched near-source records produce biased nonlinear structural responses?," *Proceedings*, 8th National Conference on Earthquake Engineering, San Francisco, California.

Bertero, V.V., Mahin, S.A., and Herrera, R.A. 1978, "Aseismic design implications of near-fault San Fernando earthquake records," *Earthquake Engineering & Structural Dynamics*, Vol. 6, No. 1, pp. 31-42.

Beyer, K. and Bommer, J.J., 2006, "Relationships between median values and between aleatory variabilities for different definitions of the horizontal component of motion," *Bulletin of the Seismological Society of America*, Vol. 96, No. 4A, pp. 1512-1522.

Bielak, J., Loukakis, K., Hisada, Y., and Yoshimura, C., 2003, "Domain reduction method for three-dimensional earthquake modeling in localized regions, Part I: Theory," *Bulletin of the Seismological Society of America*, Vol. 93, pp. 817-824.

Bolt, B., 1988, *Earthquakes*, W. H. Freeman and Co, New York, New York.

Bommer, J.J., Scott, S.G., and Sarma, S.K., 2000, "Hazard-consistent earthquake scenarios," *Soil Dynamics and Earthquake Engineering*, Vol. 19, pp. 219-231.

Boore, D., 2003, "Prediction of ground motion using the stochastic method," *Pure and Applied Geophysics*, Vol. 160, pp. 635-676.

Boore, D., 2009, "Comparing stochastic point-source and finite-source ground-motion simulations: SMSIM and EXSIM," *Bulletin of the Seismological Society of America*, Vol. 99, pp. 3202-3216.

Boore, D.M., 2010, "Orientation-independent, nongeometric-mean measures of seismic intensity from two horizontal components of motion," *Bulletin of the Seismological Society of America*, Vol. 100, No. 4, pp. 1830-1835.

Boore, D. M. and Atkinson, G., 2008, "Ground-motion prediction equations for the average horizontal component of PGA, PGV, and 5%-damped SA at spectral periods between 0.01 s and 10.0 s," *Earthquake Spectra*, Vol. 24, pp. 99-138.

Boore, D.M., Watson-Lamprey, J., and Abrahamson, N.A., 2006, "Orientation-independent measures of ground motion," *Bulletin of the Seismological Society of America*, Vol. 96, No. 4A, pp. 1502-1511.

Bradley, B.A., 2010, "A generalized conditional intensity measure approach and holistic ground-motion selection," *Earthquake Engineering & Structural Dynamics,* Vol. 39, No. 12, pp. 1321-1342.

Bray, J.D. and Rodriguez-Marek, A., 2004, "Characterization of forward-directivity ground motions in the near-fault region," *Soil Dynamics and Earthquake Engineering*, Vol. 24, No. 11, pp. 815-828.

Bray, J.D., Rodriguez-Marek, A., and Gillie, J.L., 2009, "Design ground motions near active faults," *Bulletin of the New Zealand Society for Earthquake Engineering,* Vol. 42, No. 1.

Brocher, T.M., 2005, *Compressional and Shear Wave Velocity versus Depth in The San Francisco Bay Area, California: Rules for USGS Bay Area Velocity Model 05.0.0*, USGS Open-File Report 2005-1317, U.S. Geological Survey.

Brocher, T.M., Parsons, T., Blakeley, R.J., Christensen, N.I., Fisher, M.A., Wells, R.E., and SHIPS Working Group, 2001, "Upper crustal structure in Puget Lowland, Washington: Results from the 1998 seismic hazards investigation in Puget Sound," *Journal of Geophysical Research*, Vol. 106, No. B7, pp. 13541-13564.

Buratti, N., Stafford, P.J., and Bommer, J.J., 2011, "Earthquake accelerogram selection and scaling procedures for estimating the distribution of structural response," *Journal of Structural Engineering*, Vol. 137, No. 3, pp. 345-357.

Burger, R., Somerville, P., Barker, J., Herrmann, R., and Helmberger, D., 1987, "The effect of crustal structure on strong ground motion attenuation relations in eastern North America," *Bulletin of the Seismological Society of America*, Vol. 77, pp. 420-439.

Campbell, K., 2003, "Prediction of strong-ground motion using the hybrid-empirical method and its use in the development of ground-motion (attenuation) relations in eastern North America," *Bulletin of the Seismological Society of America*, Vol., 93, pp. 1012-1033.

Campbell, K.W. and Bozorgnia, Y., 2008, "NGA ground motion model for the geometric mean horizontal component of PGA, PGV, PGD and 5% damped linear elastic response spectra for periods ranging from 0.01 to 10s," *Earthquake Spectra*, Vol. 24, No. 1, pp. 139-171.

Carballo, J.E. and Cornell, C.A., 2000, *Probabilistic Seismic Demand Analysis: Spectrum Matching and Design*, Report No. RMS-41, Department of Civil and Environmental Engineering, Stanford University, Stanford, California.

CEN, 2004, *Eurocode 8: Design of Structures for Earthquake Resistance, Part 1: General Rules, Seismic Actions and Rules for Buildings*, Comité Européen de Normalisation, Brussels.

Chang, C.-Y., Mok, C.M., Power, M.S., and Tang, Y.K., 1991, *Analysis of Ground Response at Lotung Large-Scale Soil-Structure Interaction Experiment Site*, Report NP-7306-SL, Electric Power Research Institute, Palo Alto, California.

Chiou, B., Darragh, R., Gregor, N., and Silva, W., 2008, "NGA Project strong-motion database," *Earthquake Spectra*, Vol. 24, No. 1, pp. 23-44.

Chiou, B.S.J. and Youngs, R.R., 2008, "Chiou-Youngs NGA ground motion relations for the geometric mean horizontal component of peak and spectral ground motion parameters," *Earthquake Spectra*, Vol. 24, pp. 173-215.

Cornell, C.A, 1968, "Engineering seismic risk analysis," *Bulletin of the Seismological Society of America*, Vol. 58, No. 5, pp. 1583-1606.

CTBUH, 2008, *Recommendations for the Seismic Design of High-Rise Buildings,* Seismic Working Group, Council on Tall Buildings and Urban Habitat, Chicago, Illinois.

Day, S.M., Graves, R., Bielak, J., Dreger, D., Larsen, S., Olsen, K.B., Pitarka, A., and Ramirez-Guzman, L., 2008, "Model for basin effect on long period response spectra," *Earthquake Spectra*, Vol. 24, pp. 257-277.

Department of Energy, 1996, *Guidelines for Use of Probabilistic Seismic Hazard Curves at Department of Energy Sites for Department of Energy Facilities*, DOE-STD-1024-92, Washington, D.C.

Department of Defense, 2004, 2007, 2010, *Seismic Design for Buildings,* United Facilities Criteria 3-310-04.

FEMA, 1997a, *NEHRP Guidelines for the Seismic Rehabilitation of Buildings*, FEMA 273, prepared by Applied Technology Council for Building Seismic Safety Council, Washington, D.C.

FEMA, 1997b, *NEHRP Commentary on the Guidelines for the Seismic Rehabilitation of Buildings*, FEMA 274, prepared by Applied Technology Council for Building Seismic Safety Council, Washington, D.C.

FEMA, 2000, *Prestandard and Commentary for the Seismic Rehabilitation of Buildings*, FEMA 356, prepared by American Society of Civil Engineers for Federal Emergency Management Agency, Washington, D.C.

FEMA, 2005, *Federal Guidelines for Dam Safety: Earthquake Analyses and Design of Dams*, FEMA 65, Interagency Committee on Dam Safety for FEMA, Washington, D.C.

FEMA, 2009, *Quantification of Building Seismic Performance Factors*, FEMA P-695 Report, prepared by Applied Technology Council for Federal Emergency Management Agency, Washington, D.C.

FERC, 2007, *Draft Seismic Design Guidelines and Data Submittal Requirements for LNG Facilities*, Federal Energy Regulatory Commission Office of Energy Projects, Washington, D.C.

Fishman, G.S., 2006, *A First Course in Monte Carlo,* Duxbury Press, Pacific Grove, California.

Frankel, A., 2009, "A constant stress-drop model for producing broadband synthetic seismograms: Comparison with the Next Generation Attenuation Relations," *Bulletin of the Seismological Society of America*, Vol. 99, pp. 664-681.

Fu, Q. and Menun, C., 2004, "Seismic-environment-based simulation of near-fault ground motions," *Proceedings*, 13th World Conference on Earthquake Engineering, Vancouver, Canada.

Goda, K. and Atkinson, G., 2009, "Probabilistic characterization of spatially-correlated response spectra for earthquakes in Japan," *Bulletin of the Seismological Society of America*, Vol. 99, pp. 3003-3020.

Grant, D.N., Greening, P.D., Taylor, M.L., and Ghosh, B., 2008, "Seed record selection for spectral matching with RSPMatch2005," *Proceedings*, 14th World Conference on Earthquake Engineering, Beijing, China.

Grant, D.N., Padilla, D., and Greening, P.D., 2011, "Orientation dependence of earthquake ground motion and structural response," *Protection of Built Environment Against Earthquakes*, editor: M. Dolšek, Springer, 352 p.

Graves, R.W., 1993, "Modeling three-dimensional site response effects in the Marina District Basin, San Francisco, California," *Bulletin of the Seismological Society of America,* Vol. 83, No. 4, pp. 1942-1063.

Graves, R.W., 1996, "Simulating earthquake ground motions in 3D elastic media using staggered-grid finite-differences," *Bulletin of the Seismological Society of America*, Vol. 86, pp. 1091-1106.

Graves, R.W. and Pitarka, A., 2010, "Broadband ground-motion simulation using a hybrid approach," *Bulletin of the Seismological Society of America,* Vol. 100, pp. 2095-2123.

Graves, R.W., Pitarka, A., and Somerville, P.G., 1998, "Ground motion amplification in the Santa Monica area: effects of shallow basin edge structure," *Bulletin of the Seismological Society of America*, Vol. 88, pp. 1224-1242.

Graves, R.W. and Somerville, P.G., 2010, *Simulated Broadband Ground Motion Time Histories for the TBI Project,* report to the Southern California Earthquake Center.

Gulerce, Z. and Abrahamson, N.A., 2010, "Site-specific design spectra for vertical ground motion," *Earthquake Spectra*, Vol. 26, No. 4, pp. 999-1016.

Guyader, A.C. and Iwan, W.D., 2006, "Determining equivalent linear parameters for use in a capacity spectrum method of analysis," *Journal of Structural Engineering*, Vol. 132, No. 1, pp. 59-67.

Hadjian, A.H., 1981, "On the correlation of the components of strong ground motion - Part 2," *Bulletin of the Seismological Society of America*, Vol. 71, No. 4, pp. 1323-1331.

Hancock, J., Bommer, J.J., and Stafford, P.J., 2008, "Numbers of scaled and matched accelerograms required for inelastic dynamic analyses," *Earthquake Engineering & Structural Dynamics*, Vol. 37, No. 14, pp. 1585-1607.

Hancock, J., Watson-Lamprey, J., Abrahamson, N., Bommer, J., Markatis, A., McCoy, E., and Mendis, R., 2006, "An improved method of matching response spectra of recorded earthquake ground motion using wavelets," *Journal of Earthquake Engineering*, Vol. 10, Special Issue 1, pp. 67-89.

Hanks, T. and McGuire, R., 1981, "The character of high-frequency strong ground motion," *Bulletin of the Seismological Society of America*, Vol. 71, pp. 2071-2095.

Hartzell, S., Harmsen, S., Frankel, A., and Larsen, S., 1999, "Calculation of broadband time histories of ground motion: Comparison of methods and validation using strong-ground motion from the 1994 Northridge

earthquake," *Bulletin of the Seismological Society of America*, Vol. 89, pp. 1484-1504.

Haselton, C.B., Baker, J.W., Bozorgnia, Y., Goulet, C.A., Kalkan, E, Luco, N., Shantz, T., Shome, N., Stewart, J.P., Tothong, P., Watson-Lamprey, J., Zareian, F., *Evaluation of Ground Motion Selection and Modification Methods: Predicting Median Interstory Drift Response of Buildings*, PEER Report 2009-01, prepared by the PEER Ground Motion Selection and Modification Working Group, edited by Curt B., Haselton, for the Pacific Earthquake Engineering Research Center, University of California, Berkeley, California.

Hashash, Y.M.A. and Park, D., 2001, "Non-linear one-dimensional seismic ground motion propagation in the Mississippi embayment," *Engineering Geology*, Vol. 62, Nos. 1-3, pp. 185-206.

Heo, Y., Kunnath, S.K., and Abrahamson, N., 2011, "Amplitude-scaled versus spectrum-matched ground motions for seismic performance assessment," *Journal of Structural Engineering*, Vol. 137, No. 3, pp. 278-288.

Howard, J.K., Tracy, C.A., and Burns, R.G., 2005, "Comparing observed and predicted directivity in near-source ground motion," *Earthquake Spectra*, Vol. 21, No. 4, pp. 1063-1092.

Huang, Y., Whittaker, A.S., and Luco, N., 2008a, "Maximum spectral demands in the near-fault region," *Earthquake Spectra*, Vol. 24, No. 1, pp. 319-341.

Huang, Y.-N., Whittaker, A.S., and Luco, N., 2008b, *Performance Assessment of Conventional and Base-Isolated Nuclear Power Plants for Earthquake and Blast Loadings*, Report No. MCEER-08-0019, Multidisciplinary Center for Earthquake Engineering Research (MCEER), University at Buffalo, State University of New York.

Huang, Y.-N., Whittaker, A.S., and Luco, N., 2009, "Orientation of maximum spectral demand in the near-fault region," *Earthquake Spectra*, Vol. 25, No. 3, pp. 707-717.

Huang, Y.-N., Whittaker, A.S., and Luco, N., 2010, *Establishing Maximum Spectral Demand for Performance-Based Earthquake Engineering: Collaborative Research with the University at Buffalo and the USGS,* USGS Technical Report: USGS Award Number 08HQGR0017, U.S. Geological Survey, Reston, Virginia.

Husid, R., 1973, *Terremotos: Análisis Espectral y Características de Acelerogramas como Base del Diseño Sísmico*, Andres Bello, Santiago, Chile.

ICC, 1991, *Uniform Building Code 1991*, International Code Council, Washington, D.C.

ICC, 2003, 2006, *International Building Code,* International Code Council, Washington, D.C.

Idriss, I.M. and Sun, J.I., 1992, *User's Manual for SHAKE91: A Computer Program for Conducting Equivalent Linear Seismic Response Analyses of Horizontally Layered Soil Deposits*, Center for Geotechnical Modeling, Dept. of Civil & Environmental Engineering, University of California, Davis, California.

Iervolino, I., De Luca, F., and Cosenza, E., 2010, "Spectral shape-based assessment of SDOF nonlinear response to real, adjusted and artificial accelerograms," *Engineering Structures*, Vol. 32, No. 9, pp. 2776–2792.

Itasca, 1995, *FLAC (Fast Lagrangian Analysis of Continua)*, Itasca Consulting Group, Inc., Minneapolis, Minnesota.

Jayaram, N., Lin, T., and Baker, J.W., 2011, "A computationally efficient ground-motion selection algorithm for matching a target response spectrum mean and variance," *Earthquake Spectra*, Vol. 27, No. 3, pp. 797-815.

Joyner, W.B., 2000, "Strong motion from surface waves in deep sedimentary basins," *Bulletin of the Seismological Society of America*, Vol. 90, pp. S95-S112.

Kanamori, H. and Anderson, D., 1975, "Theoretical basis of some empirical relations in seismology," *Bulletin of the Seismological Society of America*, Vol. 65, pp. 1073-1095.

Kanno, T., Narita, A., Morikawa, N., Fujiwaru, H., and Fukushima, Y., 2006, "A new attenuation relations for strong ground motion in Japan based on recorded data," *Bulletin of the Seismological Society of America*, Vol. 96, pp. 879-897.

Komatitsch, D., Liu, Q., Tromp, J., Süss, P., Stidham, C., and Shaw, J.H., 2004, "Simulations of ground motion in the Los Angeles basin based upon the spectral-element method," *Bulletin of the Seismological Society of America,* Vol. 94, pp. 187-206.

Kramer, S.L., 1996, *Geotechnical Earthquake Engineering*, Prentice Hall.

Krawinkler H., Medina R., and Alavi, B. 2003, "Seismic drift and ductility demands and their dependence on ground motions," *Engineering Structures*, Vol. 25, No. 5, pp. 637-653.

Lee, M.K.W. and Finn, W.D.L., 1978, *DESRA-2, Dynamic Effective Stress Response Analysis of Soil Deposits with Energy Transmitting Boundary Including Assessment of Liquefaction Potential*, Soil Mechanics Series No. 36, Department of Civil Engineering, University of British Columbia, Vancouver, Canada.

Li, X.S., Wang, Z.L., and Shen, C.K., 1992, *SUMDES, A Nonlinear Procedure for Response Analysis of Horizontally-Layered Sites Subjected to Multi-Directional Earthquake Loading,* Department of Civil Engineering, University of California, Davis, California.

Lilhanand, K. and Tseng, W.S., 1988, "Development and application of realistic earthquake time histories compatible with multiple-damping design spectra," *Proceedings of Ninth World Conference on Earthquake Engineering,* Tokyo, Japan.

Lin, T., 2012, *Advancement of Hazard-Consistent Ground Motion Selection Methodology through Conditional Spectrum and Adaptive Incremental Dynamic Analysis,* PhD Thesis, Department of Civil and Environmental Engineering, Stanford University, Stanford, California.

Lin, T., Harmsen, S.C., Baker, J.W., and Luco, N., 2011, "Conditional spectrum computation incorporating multiple causal earthquakes and ground motion prediction models," *Bulletin of the Seismological Society of America*, (in review).

Magistrale, H., Day, S., Clayton, R., and Graves, R., 2000, "The SCEC Southern California reference three-dimensional seismic velocity model version 2," *Bulletin of the Seismological Society of America*, Vol. 90, pp. S65-S76.

Mahin, S.A. and Bertero, V.V., 1981, "An evaluation of inelastic seismic design spectra," *Journal of the Structural Division*, Vol. 107, No. ST7, pp. 1777-1795.

Mallat, S.G., 1999, *A Wavelet Tour of Signal Processing*, Academic Press, San Diego.

Matasovic, N., 2006, *D-MOD2 – A Computer Program for Seismic Response Analysis of Horizontally Layered Soil Deposits, Earthfill Dams, and Solid Waste Landfills, User's Manual*, GeoMotions, LLC, Lacey, Washington.

Mavroeidis, G.P. and Papageorgiou, A.S., 2003, "A mathematical representation of near-fault ground motions," *Bulletin of the Seismological Society of America*, Vol. 93, No. 3, pp. 1099-1131.

Mavroeidis, G.P., Dong, G., and Papageorgiou, A.S., 2004, "Near-fault ground motions, and the response of elastic and inelastic single-degree-of-freedom (SDOF) systems," *Earthquake Engineering & Structural Dynamics*, Vol. 33, No. 9, pp. 1023-1049.

Mazzoni, S., McKenna, F., Scott, M.H., and Fenves, G.L., 2006, *Open System for Earthquake Engineering Simulation (OpenSees), User Command-Language*

Manual, Pacific Earthquake Engineering Research Center, University of California, Berkeley, California.

McGuire, R., 2004, *Seismic Hazard and Risk Analysis,* EERI Monograph, Earthquake Engineering Research Institute, Oakland, California.

Miranda, E. and Ruiz-García, J., 2002, "Evaluation of approximate methods to estimate maximum inelastic displacement demands," *Earthquake Engineering & Structural Dynamics*, Vol. 31, No. 3, pp. 539-560.

Naeim, F. and Lew, M., 1995, "On the use of design spectrum compatible time histories," *Earthquake Spectra*, Vol. 11, No. 1, pp. 111-127.

NFPA, 2009, *Standard for the Production, Storage, and Handling of Liquefied Natural Gas (LNG)*, NFPA 59A, National Fire Protection Association, Quincy, Massachusetts.

NIST, 2009, *Research Required to Support Full Implementation of Performance-Based Seismic Design*, NIST GCR 09-917-2, prepared by the Building Seismic Safety Council of The National Institute of Building Sciences for the National Institute of Standards and Technology, Gaithersburg, Maryland.

NIST, 2010, *Nonlinear Structural Analysis for Seismic Design: A guide for Practicing Engineers*, NIST GCR 10-917-5, prepared by the NEHRP Consultants Joint Venture for the National Institute of Standards and Technology, Gaithersburg, Maryland.

NIST, 2011, *Soil-Foundation-Structure Interaction for Building Structures*, NIST GCR 11-917-14, 90% draft, prepared by the NEHRP Consultants Joint Venture for the National Institute of Standards and Technology, Gaithersburg, Maryland.

OpenSEES, 2011, *Open System for Earthquake Engineering Simulation,* Pacific Earthquake Engineering Research Center, http://opensees.berkeley.edu. Last accessed Jun. 20, 2011.

PEER, 2009, *Guidelines for Performance-Based Seismic Design of Tall Buildings*, prepared by the Tall Buildings Initiative Guidelines Working Group for the Pacific Earthquake Engineering Research Center, University of California, Berkeley, California.

Petersen, M.D., Dawson, T.E., Chen, R., Cao, T., Wills, C.J., Schwartz, D.P., and Frankel, A.D., 2011, "Fault displacement hazard for strike-slip faults," *Bulletin of the Seismological Society of America,* Vol. 101, No. 2, pp. 805-825.

Pezeshk, S., Zandieh, A., and Tavakoli, B., 2011, "Hybrid empirical ground-motion prediction equations for Eastern North America using NGA models and

updated seismological parameters," *Bulletin of the Seismological Society of America*, Vol. 101, No. 4, pp. 1859-1870.

Pitarka, A., Irikura, K., Iwata, T., and Sekiguchi, H., 1998, "Three-dimensional simulation of the near-fault ground motion for the 1995 Hyogo-ken Nanbu (Kobe), Japan, Earthquake," *Bulletin of the Seismological Society of America*, Vol. 88, pp. 428-440.

Porter, K., Kennedy, R., and Bachman, R., 2007, "Creating fragility functions for performance-based earthquake engineering," *Earthquake Spectra*, Vol. 23, No. 2, pp. 471-489.

Power, M., Chiou, B., Abrahamson, N, Bozorgnia, Y., Shantz, T., and Roblee, C., 2008, "An overview of the NGA project," *Earthquake Spectra*, Vol. 24, pp. 3-21.

Pyke, R.M., 2000, *TESS: A Computer Program for Nonlinear Ground Response Analyses,* TAGA Engineering Systems & Software, Lafayette, California.

Reiter, L., 1990, *Earthquake Hazard Analysis: Issues and insights*, Columbia University Press, New York.

Rodriguez-Marek, A., 2000, *Near Fault Seismic Site Response*, Ph.D. Thesis, Department of Civil and Environmental Engineering, University of California, Berkeley, California.

Rodriguez-Marek, A. and Bray, J.D., 2006, "Seismic site effects for near-fault forward directivity ground motions," *Journal of Geotechnical and Geoenvironmental Engineering*, Vol. 132, No. 12, pp. 1611-1620.

SAC, 1995, *Characterization of Ground Motions during the Northridge Earthquake of January 17, 1994*, Report No. SAC-95-03, prepared by SAC Joint Venture, a partnership of Structural Engineers Association of California, Applied Technology Council, and California Universities for Research in Earthquake Engineering.

Schnabel, P.B., Lysmer, J., and Seed, H.B., 1972, *SHAKE—A Computer Program for Equation Response Analysis of Horizontally Layered Sites,* Report EERC 72-12, Earthquake Engineering Research Center, University of California, Berkeley, California.

Shahi, S.K. and Baker, J.W., 2011, "An empirically calibrated framework for including the effects of near-fault directivity in probabilistic seismic hazard analysis," *Bulletin of the Seismological Society of America*, Vol. 101, No. 2, pp. 742-755.

Shome, N. and Luco, N., 2010, "Loss estimation of multi-mode dominated structures for a scenario of earthquake event," *Proceedings*, 9th US National and 10th Canadian Conference on Earthquake Engineering, Toronto, Canada.

Shome, N., Cornell, C.A., Bazzurro, P., and Carballo, J.E., 1998, "Earthquakes, records, and nonlinear responses," *Earthquake Spectra*, Vol. 14, No. 3, pp. 469-500.

Si, H. and Midorikawa, S., 1999, "New attenuation relationships for peak ground acceleration and velocity considering effects of fault type and site condition," *Journal of Structural and Construction Engineering*, Vol. 523, pp. 63-70.

Silva, W., Gregor, N., and Darragh, R., 2002, *Development of Regional Hard Rock Attenuation Relations for Central and Eastern North America*, Pacific Engineering Report, http://www.Pacificengineering.org. Last accessed Sept. 2010.

Silva, W.J. and Lee, K., 1987, *State-of-the-Art for Assessing Earthquake Hazards in the United States,* Report 24, WES RASCAL Code for Synthesizing Earthquake Ground Motions, Woodward-Clyde Consultants, Walnut Creek, California.

Somerville, P.G., 2002, "Characterizing near fault ground motion for the design and evaluation of bridges," *Third National Seismic Conference & Workshop on Bridges & Highways*, Portland, Oregon.

Somerville, P.G., 2003, "Magnitude scaling of the near fault rupture directivity pulse," *Physics of the Earth and Planetary Interiors*, Vol. 137, pp. 201-212.

Somerville, P.G., Collins, N. Abrahamson, N., Graves, R., and Saikia, C., 2001, *Ground Motion Attenuation Relations for the Central and Eastern United States*, Final Report to the U.S. Geological Survey, Contract No. 99HQGR0098.

Somerville, P.G., Collins, N., Graves, R., and Pitarka, A., 2004, "An engineering ground motion model of basin generated surface waves," *Proceedings*, 14th World Conference on Earthquake Engineering, Vancouver, Canada, Paper No. 515.

Somerville, P.G., Krawinkler, H., and Alavi, B., 1998, "Development of improved ground motion representation and design procedures for near-fault ground motions," *Proceedings*, SMIP98 Seminar on Utilization of Strong Motion Data, Oakland, California, pp. 1-20.

Somerville, P., McLaren, J., Saikia, C., and Helmberger, D., 1990, "The Nov. 25, 1988 Saguenay, Quebec earthquake: Source parameters and the attenuation

of strong ground motion," *Bulletin of the Seismological Society of America*, Vol. 80, pp. 1118-1143.

Somerville, P.G., Smith, N.F., Graves, R.W., and Abrahamson, N.A., 1997, "Modification of empirical strong ground motion attenuation relations to include the amplitude and duration effects of rupture directivity," *Seismological Research Letters*, Vol. 68, No. 1, pp. 199-222.

Somerville, P.G. and Thio, H.K., 2011, "Development of ground motion time histories for seismic design," *Proceedings*, Ninth Pacific Conference on Earthquake Engineering: Building an Earthquake-Resilient Society, Auckland, New Zealand.

Spudich, P. and Chiou, B.S.J., 2008, "Directivity in NGA Earthquake ground motions: analysis using isochrone theory," *Earthquake Spectra*, Vol. 24, No. 1, pp. 279-298.

Sykora, D., Wahl, R., and Wallace, D., 1992, *USACE Geotechnical Earthquake Engineering Software, Report 1 WESHAKE for Personal Computers* (*version 1.0*), Instruction Report.

Toro, G., Abrahamson, N., and Schneider, J., 1997, "Model of strong ground motion in eastern and central North America: Best estimates and uncertainties," *Seismological Research Letters*, Vol. 68, pp. 41-57.

Tothong, P., Cornell C.A., and Baker J.W., 2007, "Explicit directivity-pulse inclusion in probabilistic seismic hazard analysis," *Earthquake Spectra*, Vol. 23, No. 4, pp. 867-891.

USNRC, 1976, *Combining Modal Responses and Spatial Components in Seismic Response Analysis*, Regulatory Guide 1.92, U.S. Nuclear Regulatory Commission Office of Standards Development, Washington, D.C.

USNRC, 2001, *Technical Basis for Revision of Regulatory Guidance on Design Ground Motions: Hazard- and Risk-Consistent Ground Motion Spectra Guidelines,* NUREG/CR-6728 Report, prepared by Risk Engineering Inc. for the U.S. Nuclear Regulatory Commission Office of Nuclear Regulatory Research, Washington, D.C.

USNRC, 2007, *A Performance-Based Approach to Define the Site-Specific Earthquake Ground Motion*, Regulatory Guide 1.208, U.S. Nuclear Regulatory Commission Office of Nuclear Regulatory Research, Washington, D.C.

U.S. Army Corps of Engineers, 2009, *Selection of Design Earthquakes and Associated Ground Motions,* EC 1110-2-6000.

USGS, 2008, *Interactive Deaggregation Tools,* United States Geological Survey, https://geohazards.usgs.gov/deaggint/2008/. Last accessed Jun. 20, 2011.

Vamvatsikos, D. and Cornell, C.A., 2004, "Applied incremental dynamic analysis," *Earthquake Spectra*, Vol. 20, No. 2, pp. 523-553.

Watson-Lamprey, J.A. and Abrahamson, N.A., 2006, "Bias caused by use of spectrum compatible motions," *Eighth U.S. National Conference on Earthquake Engineering*, San Francisco, California.

Watson-Lamprey, J.A. and Boore, D.M., 2007, "Beyond SaGMRotI: Conversion to SaArb, SaSN, and SaMaxRot," *Bulletin of the Seismological Society of America*, Vol. 97, No. 5, pp. 1511-1524.

Wells, D.L. and Coppersmith, K.J., 1994, "Analysis of empirical relationships among magnitude, rupture length, rupture area, and surface displacement," *Bulletin Seismological Society of America*, Vol. 84, pp. 974-1002.

Yang, Z., 2000, *Numerical Modeling of Earthquake Site Response Including Dilation and Liquefaction,* Ph.D. Dissertation, Department of Civil Engineering and Engineering Mechanics, Columbia University, New York, New York.

Yang, Z., Elgamal, A., and Parra, E., 2003, "Computational model for cyclic mobility and associated shear deformation," *Journal of Geotechnical and Geoenvironmental Engineering*, Vol. 129, No. 12, pp. 1119-1127.

Yoshimura, C., Bielak, J., Hisada, Y., and Fernandez, A., 2003, "Domain reduction method for three-dimensional earthquake modeling in localized regions, Part II: Verification and applications," *Bulletin of the Seismological Society of America,* Vol. 93, pp. 825-840.

Zhao, J., Zhang, J., Asano, A., Ohno, Y., Oouchi, T., Takahashi, T., Ogawa, H., Irikura, K., Thio, H., Somerville, P., Fukushima, Y., and Fukushima Y., 2006, "Attenuation relations of strong ground motion in Japan using site classification based on predominant period," *Bulletin of the Seismological Society of America*, Vol. 96, pp. 898-913.

Project Participants

National Institute of Standards and Technology

John (Jack) R. Hayes, Jr.
Engineering Laboratory (MS8604)
National Institute of Standards and Technology
100 Bureau Drive
Gaithersburg, Maryland 20899
www.NEHRP.gov

Kevin K. F. Wong
Engineering Laboratory (MS8604)
National Institute of Standards and Technology
100 Bureau Drive
Gaithersburg, Maryland 20899
www.NEHRP.gov

Steven L. McCabe
Engineering Laboratory (MS8604)
National Institute of Standards and Technology
100 Bureau Drive
Gaithersburg, Maryland 20899
www.NEHRP.gov

NEHRP Consultants Joint Venture

APPLIED TECHNOLOGY COUNCIL
201 Redwood Shores Parkway, Suite 240
Redwood City, California 94065
www.ATCouncil.org

CONSORTIUM OF UNIVERSITIES FOR
RESEARCH IN EARTHQUAKE ENGINEERING
1301 S. 46th Street, Building 420
Richmond, California 94804
www.CUREE.org

Joint Venture Management Committee

James R. Harris
J.R. Harris & Company
1776 Lincoln Street, Suite 1100
Denver, Colorado 80203

Christopher Rojahn
Applied Technology Council
201 Redwood Shores Parkway, Suite 240
Redwood City, California, 94065

Robert Reitherman
Consortium of Universities for Research in
Earthquake Engineering
1301 S. 46th Street, Building 420
Richmond, California 94804

Andrew Whittaker
University at Buffalo
Dept. of Civil, Structural, and Environmental Eng.
212 Ketter Hall
Buffalo, New York 14260

Joint Venture Program Committee

Jon A. Heintz (Program Manager)
Applied Technology Council
201 Redwood Shores Parkway, Suite 240
Redwood City, California 94065

Michael Constantinou
University at Buffalo
Dept. of Civil, Structural, and Environmental Eng.
132 Ketter Hall
Buffalo, New York 14260

C.B. Crouse
URS Corporation
1501 4th Avenue, Suite 1400
Seattle, Washington 98101

William T. Holmes
Rutherford and Chekene
55 Second Street, Suite 600
San Francisco, California 94105

Jack Moehle
University of California, Berkeley
Dept. of Civil and Environmental Engineering
325 Davis Hall, MC 1792
Berkeley, California 94720

James R. Harris (ex-officio)
Andrew Whittaker (ex-officio)

Project Manager

Ayse Hortacsu
Applied Technology Council
201 Redwood Shores Parkway, Suite 240
Redwood City, California, 94065

Project Technical Committee

Andrew Whittaker (Technical Director)
University at Buffalo
Dept. of Civil, Structural, and Environmental Eng.
212 Ketter Hall
Buffalo, New York 14260

Gail M. Atkinson
University of Western Ontario
Dept. of Earth Sciences
London, Ontario N6A 5B7 Canada

Jack W. Baker
Stanford University
Dept. of Civil and Environmental Eng.
473 Via Ortega
Stanford, California 94305

Jonathan Bray
University of California, Berkeley
Dept. of Civil and Environmental Engineering
453 Davis Hall, MC 1710
Berkeley, California 94720

Damian N. Grant
Arup
Advanced Technology + Research
13 Fitzroy Street
London W1T 4BQ
United Kingdom

Ronald O. Hamburger
Simpson Gumpertz and Heger
One Market Street, Suite 600
San Francisco, California 94105

Curt Haselton
California State University, Chico
475 East 10th Avenue
Chico, California 95926

Paul Somerville
URS Corporation
566 El Dorado Street, 2nd Floor
Pasadena, California 91101

Working Group Members

Norman Abrahamson
University of California, Berkeley
Dept. of Civil and Environmental Engineering
435 Davis Hall
Berkeley, California 94720

Ana Luz Acevedo-Cabrera
University of California, Berkeley
Dept. of Civil and Environmental Engineering
435 Davis Hall
Berkeley, California 94720

Riccardo Diaferia
University College London
Civil, Environmental and Geomatic Engineering
Gower Street
London WC1E 6BT
United Kingdom

Connor Hayden
University of California, Berkeley
Dept. of Civil and Environmental Engineering
435 Davis Hall
Berkeley, California 94720

Ting Lin
Stanford University
Dept. of Civil and Environmental Eng.
Blume Earthquake Engineering Center, Room 207
Stanford CA 94305

Project Review Panel

John A. Egan
AMEC Geomatrix
2101 Webster Street, 12th Floor
Oakland, California 94612

Robert P. Kennedy
RPK Structural Mechanics Consulting Inc.
28625 Mountain Meadow Road
Escondido, California 92026

Charles A. Kircher
Kircher & Associates
1121 San Antonio Road, Suite D-202
Palo Alto, California 94303

Nicolas Luco
US Geological Survey
Box 25046 – DFC – MS 966
Denver, Colorado 80225

Robin McGuire
Fugro William Lettis & Associates
4155 Darley Avenue, Suite A
Boulder, Colorado 80305

Jack P. Moehle
University of California Berkeley
Dept. of Civil Engineering
325 Davis Hall, MC 1792
Berkeley, California 94720

Michael Willford
Arup
560 Mission Street, 7th Floor
San Francisco, California 94105

FEMA Representative

Helmut Krawinkler
Stanford University
Dept. of Civil and Environmental Eng.
473 Via Ortega
Stanford, California 94305

Workshop Participants

Ibrahim Almufti
Arup
560 Mission St., Suite 700
San Francisco, California 94105

David Andersen
Defense Nuclear Facilities Safety Board
625 Indiana Ave NW, Suite 700
Washington, D.C. 20004

Russel Berkowitz
Forell/Elsesser Engineers
160 Pine Street, 6th Floor
San Francisco, California 94111

Finley Charney
Virginia Polytechnic Institute
200 Patton Hall, MS 0105
Blacksburg, Virginia 24061

C.B. Crouse
URS Corporation
1501 4th Avenue, Suite 1400
Seattle, Washington 98101

Greg Deierlein
Stanford University
Dept. of Civil and Environmental Eng.
Blume Earthquake Engineering Center, M3037
Stanford, California 94305

Robert D. Hanson
Federal Emergency Management Agency
2926 Saklan Drive
Walnut Creek, California 94595

Jim Harris
J. R. Harris & Company
1775 Sherman Street, Suite 1525
Denver, Colorado 80203

John Hooper
Magnusson Klemencic Associates
1301 Fifth Avenue, Suite 3200
Seattle, Washington 98101

Annie Kammerer
U.S. Nuclear Regulatory Commission
21 Church Street, NRC/RES/DE/SGSEB C5A24M
Rockville, MD 20850

Jeff Kimball
Defense Nuclear Facilities Safety Board
625 Indiana Avenue NW, Suite 700
Washington, D.C. 20004

Michael Mahoney
Federal Emergency Management Agency
500 C Street, SW
Washington, D.C. 20472

Silvia Mazzoni
Degenkolb Engineers
1300 Clay Street, Suite 900
Oakland, California 94612

Andy Merovich
A.T. Merovich & Associates
1950 Addison Street, Suite 205
Berkeley, California 94704

Mark Sinclair
Degenkolb Engineers
1300 Clay Street, Suite 900
Oakland, California 94612

Harold Sprague
Black & Veatch
6601 College Blvd.
Overland Park, Kansas 66211

Jonathan Stewart
University of California, Los Angeles
5731-H Boelter Hall
Los Angeles, California 90095

Mike Valley
Consulting Structural Engineer
124 Columbia Heights
Brooklyn, New York 11201